VALIDATION OF METHODOLOGIES FOR SIZING A HIGH PRESSURE GRINDING ROLL

by

Michael M^{c}Clintock

B.Sc. University of Nevada, Reno, 2011

A THESIS SUBMITTED IN PARTIAL FULFILLMENT OF

THE REQUIREMENTS FOR THE DEGREE OF

MASTER OF APPLIED SCIENCE

in

THE FACULTY OF GRADUATE AND POSTDOCTORAL STUDIES

(Mining Engineering)

THE UNIVERSITY OF BRITISH COLUMBIA

(Vancouver)

October 2018

The following individuals certify that they have read, and recommend to the Faculty of Graduate and Postdoctoral Studies for acceptance, a thesis/dissertation entitled:

Validation of Methodologies for Sizing a High Pressure Grinding Roll

submitted by Michael M^{c}Clintock in partial fulfillment of the requirements for

the degree of Master of Applied Science

in Mining Engineering

Examining Committee:

Dr. Bern Klein
Supervisor

Dr. Sanja Miskovic
Supervisory Committee Member

Dr. Persio Rosario
Supervisory Committee Member

Additional Examiner

Additional Supervisory Committee Members:

Supervisory Committee Member

Supervisory Committee Member

Abstract

Currently, there is no standard recognized bench-scale laboratory test for sizing or modelling a high pressure grinding roll (HPGR) in hard rock mining. As a result, metallurgical studies are prohibitively expensive and not economical for early-stage projects. To be adopted as a standard industry test for the HPGR, a bench scale test must: 1) use the same breakage mechanism as an HPGR, 2) produce results that are reproducible by independent metallurgical laboratories, and 3) apply to full-scale HPGR in a non-proprietary manner for engineering design.

In 2015, the Piston Press test Database Calibrated and Direct Calibration methodologies were developed at the NBK Institute of Mining Engineering at the University of British Columbia. These methodologies can calibrate Piston Press test results to the HPGR performance using a UCS machine to define energy breakage relationships. This thesis developed a multi-stage program for facilitating the transfer of these methodologies to industry. This program formalized Piston Press test into a standard operating procedure by examining the effects of moisture, sample preparation, and material porosity. The results of the program demonstrated the Piston Press test to be reproducible. In addition, the results validated the Piston Press test Database Calibrated and Direct Calibration methodologies for a full-scale HPGR closed circuit.

The program results indicate that an increase of moisture 1.5% to 5% during high-pressure compression breakage results in improved reduction ratio performance and has a negligible effect on the specific energy consumption of the sample. Material porosity was found to be an indicator of ore amenability to high-pressure compression breakage. Duplicate test-work conducted at UBC and at an independent laboratory demonstrated the Piston Press test is

reproducible and can be adapted to varying piston press machine configurations. Both the Database Calibrated and Direct Calibrated methodologies are suitable for simulating full-scale HPGR. The simulation methods developed in this research can be easily applied and adopted by industry.

Lay Summary

The purpose of this research is to validate the Piston Press test as an industry standard bench-scale amenability test for high pressure grinding rolls (HPGR) based on three criteria;

- Piston Press test has similar breakage mechanics as HPGR (previously established, Davaanyam, 2015);
- Piston Press test results are independently reproducible;
- Analysis of results is applicable to full-scale HPGR in a non-proprietary manner.

This thesis successfully validates these criteria. It demonstrates the reproducibility of Piston Press test methodologies by retrofitting an independent lab to reproduce duplicate test results to tests conducted internally at UBC. This comparison, combined with validating the two methodologies against full-scale HPGR, shows the results analysis is straightforward, and non-proprietary for independent engineering consultants to conduct.

Preface

In collaboration with ALS Metallurgy, Tropicana JV, and Köppern Machinery Australia, this research was conducted to develop further and advance the Piston Press test Database Calibrated and Direct Calibration methodologies as an industry standard bench-scale test for HPGR geo-metallurgy studies.

Responsibilities during this research included reviewing Piston Press test procedures, conducting geo-metallurgy for evaluating HPGR comminution, facilitating the transfer of the Piston Press test methodologies to commercial metallurgical laboratories, formalizing the Piston Press test procedures into standard operating procedures, and developing a test program to demonstrate the application and validation of the methodologies on full-scale HPGR. As part of the validation of the Piston Press test Database Calibrated and Direct Calibration methodologies against full-scale HPGR, a sampling program, and respective pilot HPGR test programs were carried out. Additional duties included managing metallurgical programs involving HPGR, and Piston Press testing at the University of British Columbia.

Fisher Wang provided additional support by assisting both in the sample collection at the Tropicana Gold Mine and test-work, as well as applying bi-exponential modelling to compare UBC and ALS duplicate testing for the validation of ALS Metallurgy. Amit Kumar and Santiago Seiler assisted with a portion of test-work presented in Chapter 4 that examined effects of porosity on Piston Press testing.

Table of Contents

List of Tables

List of Figures

List of Symbols

B_{wi} – Bond Ball mill work index, kW/t

C.V. – Correlation of Variance, %

D – Diametre

E_{sp} – Specific energy consumption, kWh/t

F_{50} – Feed size at 50% passing, mm

F_{80} – Feed size at 80% passing, mm

F_{sp} – Specific pressing force for HPGR, N/mm^2

h – hour

L – HPGR roll width

M-dot / ṁ– Specific throughput constant, ts/hm^3

M_s – Mass of solid, g

M_T – Total mass of the pycnometer, water, and solid, g

$P_{50\ S.G.}$ – Product size at 50% passing, mm/mm

P_{80} – Product size at 80% passing, mm

ρ_s – Density of solid, g/cc

ρ_t – True density, g/cc

ρ_R – Relative density, g/cc

ρ_t – True density, g/cc

ρ_T – Density of water at a known own ttemperature, g/cc

Q – HPGR throughput, tonnes/h

RR_{50} – Reduction ratio of the 50% passing size of the feed to the product, mm/mm

RR_{80} – Reduction ratio of the 80% passing size of the feed to the product, mm/mm

S.G. – Specific gravity, g/cc

t – Tonnes (metric)

ton – ton (United States Customary Unit (USCU))

tpd – Tonnes per day

V_T – Total volume of the pycometer, water, and solid, cc

V_v – Volume of void space, % and

W_{Air} – Weight measured dry, g

W_{H2O} – Weight measured in Water, g

W_{pi} – Piston work index, kWh/t

List of Abbreviations

CIL	–	Carbon in Leach
HPGR or HRC		High Pressure Grinding Roll
PEA	–	Preliminary Economic Assessment
SAB	–	SAG Ball mill grinding circuit
SABC	–	SAG, Ball mill, & Pebble grinding circuit
SAG	–	Semi-Autogenous Grinding
SPT	–	Static Piston Test
XRD	–	X-ray Diffraction

Acknowledgments

As I embarked on my Master's candidature, I have gained valuable insights into the industry, giving me the opportunity to explore and develop in my professional career. Specifically, I would like to acknowledge the individuals who have supported me through this time.

I would like to thank my Supervisor, Bern Klein, for his mentorship and guidance, as well as my supervising committee. I would like to recognize the SAG Foundation and NSERC for their financial support. NSERC's financial support allowed the collaboration with industry that took place during this research. Both Tropicana JV, Köppern Australia Machinery, and ALS Metallurgy gave valuable in-kind support. I would like to recognize the following people especially; Andrew Gardula and Dilip Das from Köppern Machinery Australia, Hamid Sheriff, Ian Smith, and Peter Mehrfert from ALS Metallurgy, and Mike Di Trento, and Johan, Viljoen from Tropicana JV.

I want to express my gratitude to Zorig Davaanyam for developing the Piston Press test methodologies from which this research was developed. I would like to thank Stefan Nadolski for his time and advice; his technical knowledge and insight were a great asset to my research. I also want to thank Pius Lo and Aaron Hope for making my time at CMP welcoming, as well as Amit Kumar, Fisher Wang, and Santiago Seiler for their friendship and assistance in this research. I would like to acknowledge my partner Lara, who provided support and encouragement; for which I am truly grateful. Furthermore, I would like to thank my mum for her loving support, my dad for his love of the mineral industry, which was inherited by my brother, my sister, and myself. I would like to express my appreciation to my brother who has encouraged me to challenge and always re-examine problems with a new perspective. Most of all, I would like to acknowledge my greatest champion, my sister, whose guidance in my early life has been instrumental in my professional development.

Dedication

To My Big Sister,

Lisa.

Chapter 1: Executive Summary

The introduction of High Pressure Grinding Rolls (HPGR) into hard rock mining offers significant potential for reducing power costs. High pressure Grinding Rolls comminute feed using countercurrent rolls that are typically operating at pressures above 240 Mpa of pressure. The material is loaded via a hopper that choke feeds the HPGR from above the rolls. By design, HPGR breakage can be characterized as high-pressure slow compression breakage. This quality minimizes energy losses associated with heat and excess friction caused during inter-particle breakage. Numerous benefits are attributed to HPGR including, lower energy consumption, improvements of mineral liberation by micro-fracturing, and the generation of increased fines. Despite these benefits, the hard rock mining industry has been slow to adopt HPGR technology. The purpose of this thesis is to facilitate the adoption of HPGR in the hard rock mining industry. This objective was achieved by formalizing a standard operating procedure of the HPGR bench scale Piston Press test in conjunction with test-work that demonstrated reproducible Piston Press test results by an independent laboratory. Lastly, the bench scale test was validated and modelled against a full-scale HPGR circuit.

The current standard method for sizing HPGR is by pilot testing. Pilot HPGR testing requires a significant sample size of 1-2 tonnes (Davaanyam, 2015) for scoping level, and preliminary economic assessment (PEA) studies. For feasibility level studies, sample requirements can exceed 10 tonnes per ore type. Such large sample requirements can make the assessment of HPGR uneconomical, especially for early-stage projects. Acquiring the sample can exceed the costs of actual HPGR testing. In comparison with competing forms of comminution testing such as for SAG milling, HPGR testing and design is expensive and significantly more challenging.

Presently, the industry relies heavily on bench scale tests during flowsheet development. There are a variety of industry-standard bench-scale tests that are used for alternative comminution technologies including the Bond ball mill index, the Bond crushing work index, and the JK Drop Weight suite of tests. All of these bench-scale tests use different breakage mechanics and therefore have limited use for characterizing ore in terms of HPGR amenability.

To date, there is no recognized industry standard bench-scale test for HPGR amenability. Although attempts have been made to standardize a test, they have been largely unsuccessful at gaining industry acceptance for the following reasons:

- Different breakage mechanics from HPGR mean the test is unable to produce product for downstream metallurgical testing;
- Tests are not seen as independently reproducible, as their procedures are proprietary, and;
- Analysis and application of results is proprietary (viewed as a “black box”) and does not facilitate independent engineering design to allow independent analyses and verification.

Commercial metallurgical laboratories and engineering consulting firms need to be comfortable signing off on HPGR circuit design based on test-work results. More research and development is needed for the industry to be encouraged to adopt a standard bench-scale test for HPGR amenability.

In 2015, Davaanyam proposed three bench-scale test methodologies using an MTS piston press machine to comminute material in a piston steel die at high pressure. The methodologies included:

- Database Calibrated methodology suitable for scoping level and PEA studies;
- Direct Calibration methodology for PEA to feasibility level studies, and;
- Simulation methodology for optimization/dynamic simulation.

To date, these methodologies are validated on more than 170 pilot HPGR tests performed at the University of British Columbia. The Piston Press test Database Calibrated and Direct Calibration methodologies meet certain criteria for industry:

- A bench-scale test must have the same breakage mechanism as HPGR, to produce samples for downstream metallurgical programs and to understand the impact of the HPGR on the entire mill flowsheet (Davaanyam, 2015);
- Piston Press test procedures must be formalized into a standard operating procedure that will assist independent laboratories to understand and adopt the procedures;
- Test results must be easily interpretable and applicable for analysis and design by independent engineering firms and consultants;
- The Piston Press test applied to model full-scale HPGR must be validated and demonstrated in a non-proprietary manner.

1.1 Research Objective

A standard recognized bench-scale test is needed to further increase the adoption of HPGR in the base rock industry. To date, the industry has generally not adopted HPGR bench-scale testing for amenability of HPGR. Formally, proposed tests have failed to meet the following requirements 1) same breakage mechanics of HPGR, 2) is reproducible independently, and 3) can be used to model and predict full-scale performance in a non-proprietary way. Therefore, the research presented in this thesis aims to demonstrate the Piston Press test meets these criteria and should be a standard industry test for HPGR amenability. This objective is achieved by the following research objectives, which demonstrate the Piston Press test Database Calibrated and Direct Calibration methodologies:

- Reviewing and formalizing current Piston Press test procedures into standard operating procedures by examining the effects of moisture, sample preparation, and porosity on the Piston Press test;
- Demonstrating the reproducibility of Piston Press test results by reproducing Piston Press test results at an independent metallurgical laboratory;
- Validating the Piston Press test Database Calibrated and Direct Calibration methodologies against full-scale HPGR by comparing calibrated results to pilot and full-scale HPGR by performing closed circuit simulation.

1.2 Thesis Outline

A lack of an industry-accepted HPGR bench-scale test has hindered the adoption of HPGR. It also has resulted in the requirement of costly HPGR pilot testing that has limited the ability for projects to understand the effects of HPGR on a project comprehensively. As a result, this has put HPGR at a disadvantage to other well-established technologies. A cost-effective bench scale test is needed that uses the same breakage mechanics of HPGR, is independently reproducible and easily adoptable by commercial metallurgical laboratories. Furthermore, the capacity of generating results that can be used by independent engineering firms to model full-scale HPGR in a non-proprietary manner. This thesis is structured to demonstrate that the Piston Press test (Davaanyam, 2015) meets these requirements.

The thesis is structured in the following chapter. The general structure of methodology is presented in Chapter 3 along with the procedural methodology used for conducting Piston Press testing. Detail methodologies are discussed in each respective chapters. Chapter 4 discusses the influence of moisture, sample preparation, and porosity on the Piston Press test. These three variables are examined. Chapter 5 covers the reproducibility of the test by examining duplicate testing at UBC in combination with an independent commercial metallurgical lab. Lastly, Chapter 6 covers full-scale validation of the Piston Press test on full-scale HPGR by conducting and comparing closed circuit simulation of Piston Press testing results against pilot and full-scale HPGR scenarios. Recommendations and conclusions are presented in Chapter 7.

Results from the research presented in this thesis establishes that the Piston Press test is well suited as a bench scale test for HPGR amenability. It shares the same high-pressure breakage mechanics of HPGR. The test is reproducible by commercial metallurgical labs, as duplicate testing showed equivalent results. The research also found the Piston Press test could model full-scale the HPGR performance better than pilot HPGR testing indicated.

Chapter 2: Literature Review

The literature review is designed to understand the requirements and demand for a bench scale amenability test for the HPGR. The literature review includes an overview of the HPGR including the breakage mechanics and design parameters of the HPGR, as well as the current method of sizing the HPGR and associated costs. The literature review also includes alternative bench-scale tests previously proposed by industry along concerning the adoption challenges each test faces.

Overall the literature review found significant benefits for the HPGR including lower energy consumption, improved mineral liberation by the generation of increased fines and micro-fracturing, higher availability, lower wear rates and maintenance, and potential of improving recoveries which offer great opportunities to the industry to improve project economics.

The literature review found a strong market demand for both the HPGR and a respective bench scale test. In addition, the literature review found that most proposed HPGR bench-scale testing is either non-proprietary, use different breakage mechanics or a combination of both. These limitations have resulted in hesitation within the industry in fully adopting the respective amenability bench-scale tests.

The literature review is broken up into the following sections:

- History and background of the HPGR;
- HPGR design and operating parameters, including comminution circuit configuration;
- Breakage mechanics of comminution;

- Current Pilot-plant HPGR testing for sizing HPGR;
- All-in costs associated with the HPGR piloting;
- Piston press test Database Calibrated and Direct Calibration methodologies;
- Alternative bench-scale tests;
- Market demand for lower energy consumption;
- Benefits and disadvantages of HPGR.

2.1 Background and History

The development of the HPGR can be understood by examining the evolution of the roll type crusher mechanism along with the development of high-pressure comminution. Roll type mechanical crushers and grinders have been common throughout history. The earliest versions date back to the 2nd century in China where a rotating stone disk was used to grind red mineral cinnabar against a stone plate (Research Association of the British Paint, 1953). The concept of using high pressure was first introduced in the late 1800's by William Easby from Germany. In 1884, Easby was awarded a patent for high-pressure compaction for a double roll configuration similar to today's HPGR design. The high-pressure compaction compressed fines into granules and flakes. This technology was used for the compaction of coal fines into briquettes (Kurtz & Barduhn, 1960). As a result, coal briquetting grew into a sizable industry both in Europe and the United States by the 1900s (Lynch & Rowland, 2009).

After World War II the cement industry was struggling to meet the increased demand for cement that had resulted from rapid economic growth. Innovative solutions that could increase cement clinker production rates were urgently needed. As a result, the cement industry experimented with varying mill designs. Among these was the Huntington ring roller mill that produced a promising product size of 92% passing 150-micron size from 12 to 15 mm feeds (Eckel & Martin, 1905). By the 1960s, the largest Huntington mills reached capacities of 120 tons per day and were capable of producing 1,500 tons per day of cement clinker; by, 1970, that capacity doubled (Lynch & Rowland, 2009). Although throughput had increased, the industry was still in search of a technology that could produce finished cement from clinker lumps as large as 50 mm. Alternative technologies were explored, and some success was found with rod milling. However, rod charging presented difficulties with reducing operating availability (Lynch & Rowland, 2009).

In the 1970's, Schönert investigated dry grinding circuits in cement plants at the Technical Clausthal University of Technology, Germany (Lynch & Rowland, 2009). Schönert's research ultimately led to a patent for high pressure crushing in 1982 that covered comminution above 50 Mpa of pressure. At this point, no specific mechanical machine had been developed that could comminute at this pressure (Lynch & Rowland, 2009). Naturally, the cement industry was the first to implement this technology. High reduction ratios enabled the HPGR to handle feeds up to 50 mm while delivering a final clinker product below 90 microns. The first commercial installation of the HPGR was in 1985 in the cement industry was with the Dortmund CEMEX cement plant in Germany (CEMEX Deutschland AG, 2005).

After the cement industry's success, the diamond industry adopted the HPGR for crushing kimberlite ore (Casteel, 2005). It was discovered that diamond breakage could be minimized by varying the pressure of the rolls (Nadolski, 2012). Since particle breakage occurred along grain boundaries, diamond liberation could be improved while limiting breakage of diamonds by setting the minimum gap setting to the largest expected diamond (Daniel, 2007). In the 1990's, the HPGR was adopted for fine grinding of iron ore concentrates for the generation of pellet plant feed (Casteel, 2005). Soon after, the hard rock industry evaluated the HPGR for Cyprus Sierrita (Morley C., 2010); however, this trial proved to be unsuccessful as the HPGR suffered from excessive liner wear.

Today, improvements in roll liners have largely resolved the liner wear issues of the 1990s that was responsible for the failure during the HPGR trial at Cyprus Sierrita. It is now common for wear liners to last well beyond the initially designed wear-life. For example, Morenci achieved 7000 operation hours with 75% of the liner's wear life remaining (Herman et al., 2015). Therefore, the HPGR adoption in the mining industry has increased in the wake of these improvements. Some of the most notable installations include Freeport-McMoRan's Cerro Verde, Grassberg, Morenci, and Newmont's Boddington copper-gold porphyry mines, and KHGM's Sierra Gorda copper porphyry mine in northern Chile (commissioned in 2014). The use of the HPGR has begun to be considered in smaller tonne operations. In 2015, Golden Queen Mining Co.'s 12,000 tpd Soledad Mountain Mine was commissioned with an HPGR circuit. To date, the HPGR has been installed across varying commodities including hard rock lithium, copper, and gold.

2.2 HPGR Design

HPGR consists of two counter-rotating cylindrical rolls. One roll is mounted in a fixed position while the other roll is mounted in a floating position that allows the roll to move dynamically in response to changing conditions. Hydraulic pistons support the floating roll and allow horizontal movement of the roll during operation (Schönert, 1988). The HPGR's main operating controls are the specific pressing force and roll speed. Roll speed is controlled using a variable speed drive and is the primary mechanism for adjusting machine throughput. The specific pressing force is defined as the force exerted across the cross-sectional area of the roll and is the primary mechanism for controlling product distribution and specific energy consumption. The distance between rolls is referred to as the gap. The gap will dynamically adjust to maintain the correct specific pressing force between the rolls. The HPGR is operated with a choked feed, which is fed into the HPGR from a hopper situated above the HPGR. Product is discharged and conveyed from under the rolls on to a conveyor belt (Figure 2-1: HPGR Design Components (Napier-Munn et al., 1996).

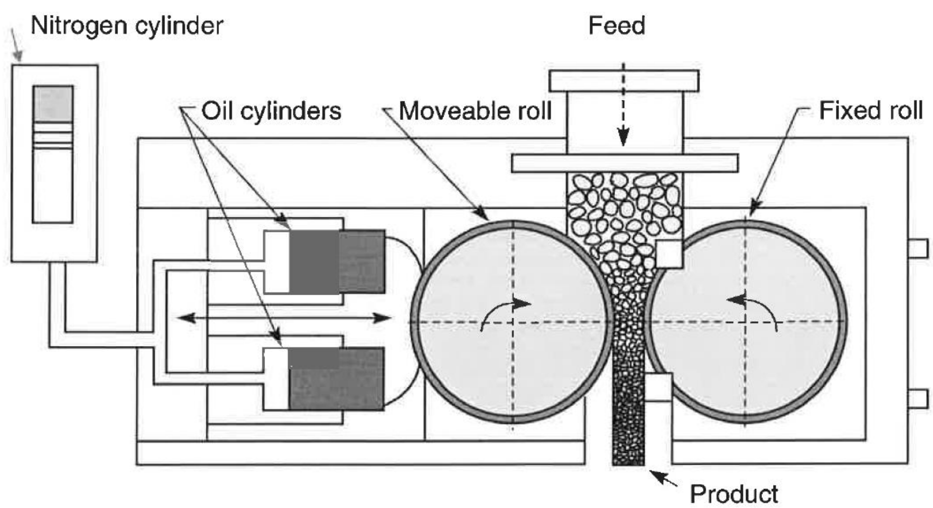

Figure 2-1: HPGR Design Components (Napier-Munn et al., 1996)

As illustrated in Figure 2-2, the HPGR has operational top feed sizes of 70 mm to 4 mm (Metso, 2015). HPGR can achieve a product size below 90 microns, which makes it well-suited to feed

Ball mill circuits. HPGR units are used in tertiary, quaternary, and pebble crushing applications in hard rock mining (Davaanyam, 2015).

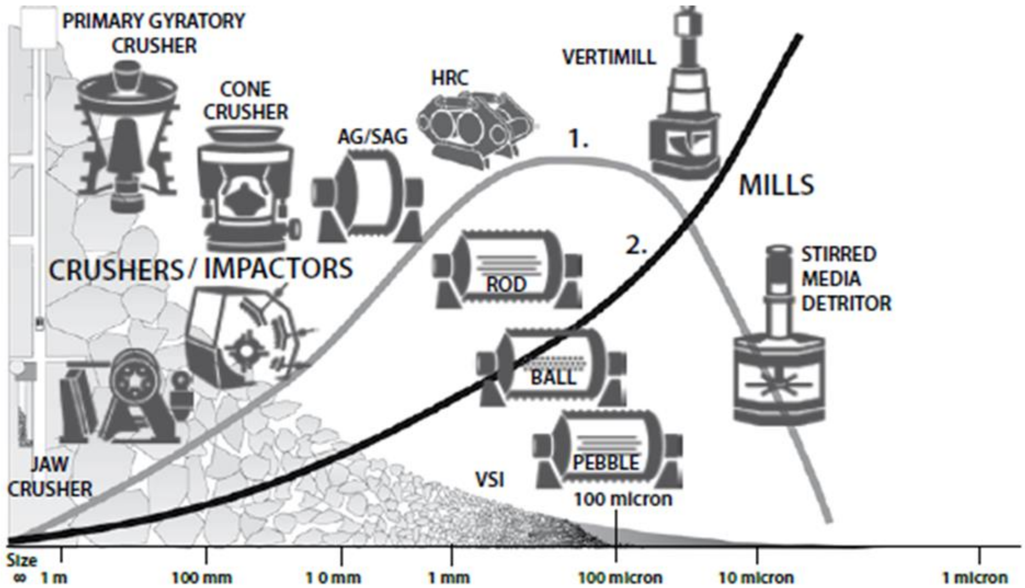

Figure 2-2: Feed Sizes for Various Comminution Equipment (Metso, 2015)

Circuit configuration plays a significant role in sizing and designing an HPGR circuit. To size HPGR, it is important to understand the circuit configuration that will be used, and HPGR performance varies depending on the circuit configuration.

In the hard rock mining industry, HPGRs are mostly operated in a closed-circuit configuration in conjunction with wet screening to break up product flake for additional screening (Davaanyam, 2015). HPGRs are commonly used as a replacement for SAG milling in SABC circuits. Common operations using this configuration include KGHM's Sierra Gorda Copper mine in Chile (Pincock et al., 2011) and Freeport-McMoRan's Cerro Verde mine in Peru (Banini, Villanueva, Hollow, & Mosher, 2011). The HPGR can be used as a pebble crusher to improve the throughput of the Ball mill circuit by reducing SAG mill product oversize.

2.2.1 Breakage Mechanics

Breakage is affected by particle heterogeneity, physical structure, and hardness. The five types of breakage include tensile, compression, impaction, shearing, and attrition (Figure 2-3).

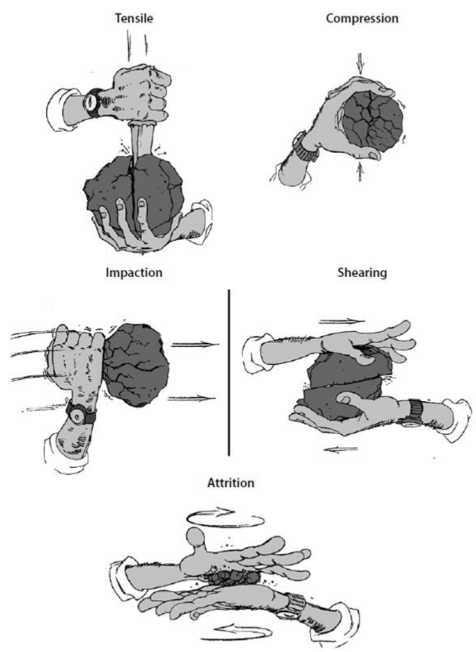

Figure 2-3: Types of Breakage (Metso 2015)

Breakage tends to occur along grain boundaries where imperfections exist within the material (Leißner et al., 2016; Wills and Atkinson, 1993). As the material is reduced in size, the number of imperfections reduce, resulting in higher energy requirements to reduce product size further (Kenneth, 1973). The HPGR is unique as it uses high-pressure inter-particle compression breakage for size reduction (F van der Meer, 2010). Inter-particle breakage reduces the friction heating loss associated with other forms of comminution (Fuerstenau et al., 1991), thereby, improving energy efficiency.

2.3 HPGR Operating Parameters

The HPGR's principle operating controls include specific pressing force and roll speed, can be influenced by multiple parameters including moisture, feed size, roll dimensions, and operating gap. The specifics of how these parameters effect operations are discussed in the sections below.

2.3.1 Specific Throughput Constant (ṁ or m-dot)

The specific throughput constant or ṁ is calculated by normalizing the HPGR's throughput by the roll dimension. The ṁ is considered the key sizing parameter for determining throughput and roll geometry (von Seebach & Knobloch, 1987). As shown in Equation 1, this parameter is calculated by dividing the machine's throughput by the geometry of the HPGR roll.

$$\dot{m} = \frac{\boldsymbol{M}}{\boldsymbol{D} * \boldsymbol{W} * \mu} \qquad \textbf{Equation 1}$$

Where,

$\dot{m}$ = specific through-put constant [ts/hm^3],

M = through-put [tonnes/h], D = roll diametre [m],

W = roll width [m], and

μ = roll speed [m/s].

To date, there are no alternative methods to determine the ṁ other than pilot and full-scale HPGR tests. From 177 pilot tests conducted at UBC, ṁ was found to vary from 170 to 280 ts/hm^3 (Davaanyam, 2015; M^{c}Clintock & Klein, 2016). Table 2-1 shows ṁ values from 177 pilot tests on 14 different types of ore conducted at the University of British Columbia (M^{c}Clintock & Klein, 2016).

Table 2-1: ṁ Values for Different Ores (McClintock & Klein, 2016)

Ore Type	Specific Throughput (M-dot; ts/hm^3)	Standard Deviation
Ag	234	2.8
Au	226	16.8
Cu-Au	215	16.5
Cu-Au-Ag	228	14.2
Cu-Mo	210	35.2
Dolomite	261	5.4
Granodiorite	187	14.9
Hematite	233	13.9
Kimberlite	172	37.0
Limestone	231	28.1
Ni	207	10.0
Pd	276	32.5
Taconite	269	8.6
Tungsten	242	14.4

Large differences are noted between full-scale and pilot HPGR. Numerous studies show full-scale HPGR ṁ are commonly higher than pilot testing indicates (Herman et al., 2015; Hart et al. 2011; Banani et al., 2011; Klymoswsky et al., 2002). For example, the ṁ was 30% higher at Freeport-McMoRan's Indonesia Grasberg mine than observed in pilot tests (Banini, Villanueva, Hollow, & Mosher, 2011). A similar conclusion was found at Boddington, where the ṁ was again 30% higher during operations compared to piloting (Hart, Parker, Rees, Manesh, & Mcgaffin, 2011). At Boddington, these investigations were carried out to examine strategies for reducing the HPGR effective capacity to increase the specific energy being applied to the material being processed (Banani et al., 2011; Nadolski, 2012). The discrepancy between pilot and full-scale HPGRs is theorized be an effect of a larger roll diametre results that improve the feed characteristics (Klymowsky, Knecht, & Burchardt, 2002). However, at the moment this relationship is not well understood, and more research is needed to fully ascertain how significant differences in roll geometry affect the $\dot{m}$. Nevertheless, the value is considered constant across small differences in HPGR geometries.

Davaanyam (2015) and Morley (2006) noted the following relationships for the $\dot{m}$:

- $\dot{m}$ increases with harder ore;
- $\dot{m}$ decreases with higher specific pressing force since the gap is also reduced which in turns restricts the feed;
- $\dot{m}$ increases with roll friction, as friction reduces roll slippage increasing the HPGR throughput;
- $\dot{m}$ decreases slightly but not significantly with reduced feed top-size;
- $\dot{m}$ increases as with lower feed bottom-sizes caused by the reduction in void space reducing the roll back pressure, which results in a wider gap.

2.3.2 Operating Gap

The operating gap is defined as the shortest distance between the fixed and floating rolls. The gap is a complex function that is dependent on throughput, moisture, roll speed, and the specific pressing force of the rolls (Nadolski, 2012). The gap ranges from 2-4 % of the roll diametre (van der Meer & Greendken, 2010) and will dynamically adjust to maintain throughput and the operating specific pressing force. HPGR units operate using a dynamic gap that adjusts to maintain a constant specific pressing force between the rolls. If the pressure is unable to be maintained the machine will be restricted to a minimum gap size to ensure the rolls do not touch and restrict material throughput.

2.3.3 Specific Pressing Force

The specific pressing force is commonly reported as N/mm^2 or kN/m^2. The specific pressing force is determined from the total force applied to the cross-sectional area of each roll, as stated in Equation 2.

$$\boldsymbol{F_{sp}} = \frac{\boldsymbol{F_{Total}}}{\boldsymbol{A_{C.S.}}} \qquad \textbf{Equation 2}$$

Where,

F_{sp} = pressing force [N],

F_{Total} = total force applied to each roll [N], and

$A_{C.S.}$ = cross sectional area of each roll [mm^2].

Specific pressing controls both product distribution and specific energy consumption. The specific pressing force often used to describe and compare HPGRs of different roll geometries (Schönert et al., 2002; Nadolski, 2012).

2.3.4 Moisture

The relationship between moisture and HPGR performance is not well understood. As illustrated in Figure 2-4, moisture effects are exacerbated at levels above 5%. At levels above 10%, the HPGR specific energy consumption increases significantly. It is believed that excessive moisture affects the material intake and results in an increase of roll slippage (Davaanyam, 2015). A better understanding is needed to understand how moisture contributes to HPGR performance. The literature on the mechanism of moisture on HPGR is limited. It is not clear how excessive moisture (in excess of 5%) contributes to excessive specific energy consumption (McClintock & Klein, 2016).

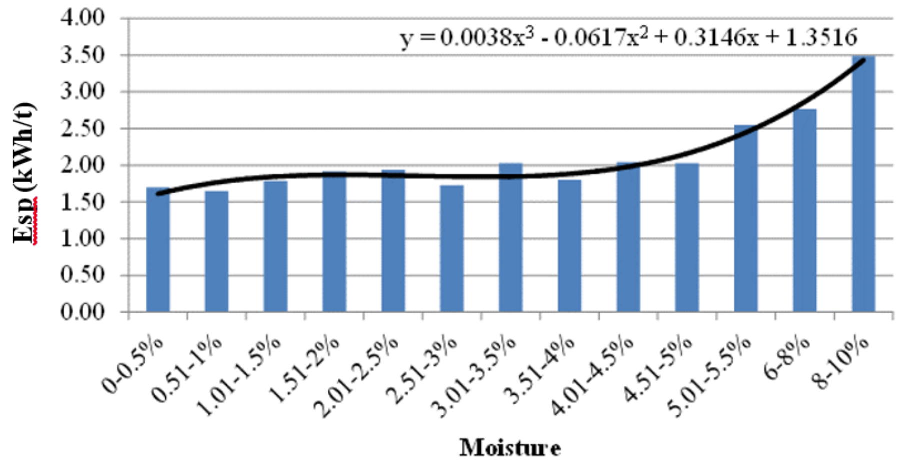

Figure 2-4: Effects of Moisture on Specific Energy (kWh/t)

Testing the effects of moisture on HPGR requires pilot HPGR testing at varying moisture levels at a constant roll speed and specific pressing force. Changes in moisture will affect the HPGR reduction ratio since moisture facilitates compression breakage by filling void space and allowing movement between particles during inter-particle breakage. As such, during moisture analysis, it is important to compare changes in specific energy consumption with improvements in reduction ratio breakage.

2.3.5 Specific Energy Consumption

The specific energy consumption is a function of the material, roll geometry and roll speed (F van der Meer, 2010). The net specific energy consumption is determined from the HPGR energy consumption subtracted by the HPGR's idle power and divided by the throughput for a given period (Daniel & Morrel, 2002). The term can be confusing as it is often used to describe the specific energy consumption both of HPGR operating in closed or open circuit. In an open circuit, the specific energy consumption will not reflect the reduction ratio performance of the HPGR.

2.3.6 Roll Speed

Roll speed has a considerable impact on $\dot{m}$, specific energy consumption, and gap size (van der Meer, 2010). By reducing roll speed, the specific energy consumption decreases while the $\dot{m}$ increases (Figure 2-5).

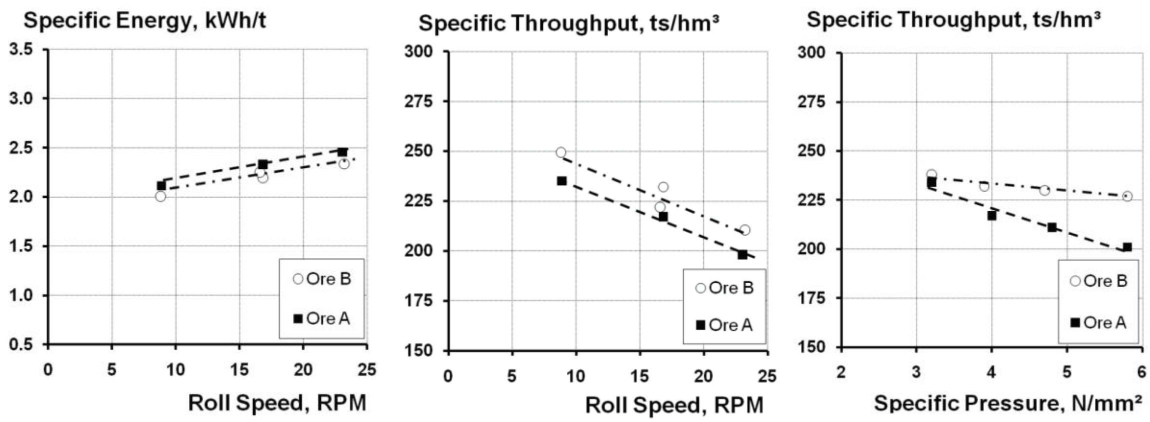

Figure 2-5: Effects of Rolls Speed and Specific Throughput Constant on Specific Energy (Van der Meer, 2010)

Van der Meer (2010) stated the following when comparing pilot testing HPGR to full-scale:

"If the calculated rotational roll speed of a production unit is higher than the equivalent speed of the tests on the pilot rolls, an adjustment has to be made to accommodate the effect of a narrower gap and thus a reduced specific throughput. This can be based on a relationship roll speed versus specific throughput as determined in testing (p. 1324)".

As van der Meer (2010) points out roll speed and improvements in the HPGR throughput will have an effect on the specific energy consumption of the HPGR. When comparing full-scale to pilot HPGR, it is important that test results are corrected for differences in rotational-roll speed to account for the differences in roll gap and throughput.

2.3.7 Compression and Nip Angles

Breakage occurs over a short rotational period occurring at the compression and nip angles. The compression and nip angles are important parameters for understanding the breakage and breakage mechanism of the HPGR. The compression and nip angles are dependent on the roll diametre, particle size, and interaction of the roll to the particle bed. An illustration of the pressure profile for an HPGR is shown in Figure 2.6. The compression angle is defined as the angle at which the pressure profile between the rolls occurs, resulting in the particle bed being stressed and is normally stated to be in the range of 7 to 12 degrees (Nadolski, 2012). Compression and the nip angles play an important role in the compression breakage of the HPGR as the pressure exerted during inter-particle breakage will occur during the compression and nip angles.

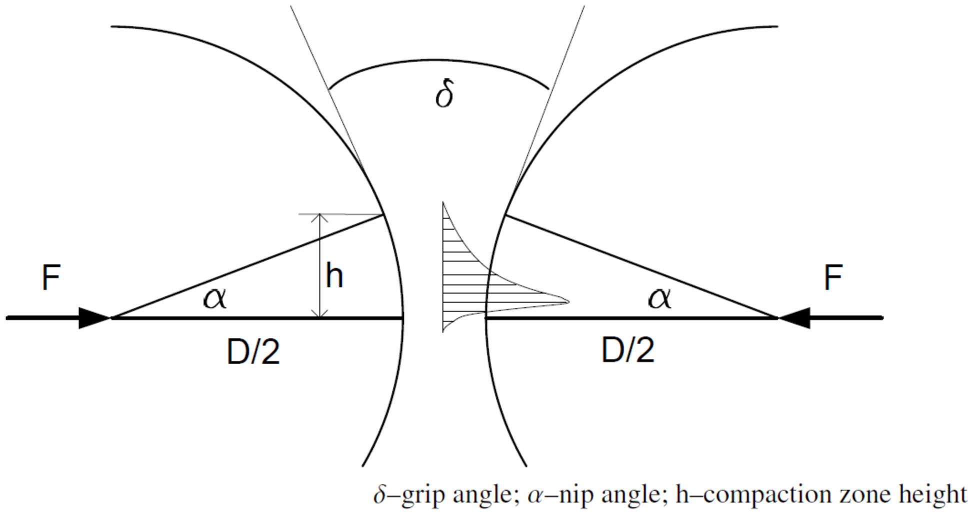

Figure 2-6: Illustration of the HPGR's Pressure Profile of the Particle Bed (FLS, 1990)

2.3.1 Edge Effect

The edge effect occurs because the pressure is not uniform across the roll surface. The material in the centre of the roll is laterally fixed in place by the outer material along the roll. The material passing along the edge of the roll does not have the same lateral pressure that the centre material has. Therefore, the edge of the roll has a lower pressure profile than the centre of the roll. The center material experiences higher inter-particle forces that result in higher comminution than at the edge of the roll. The edge effect becomes proportionally more pronounced as the roll width is decreased; hence, full-scale HPGR has less of an edge effect than pilot HPGR. Typically, strategies to deal with the edge effect include operating the HPGR in a closed circuit or recycling the edge product back to the HPGR. Cheek plates mounted to the edge of the HPGR are also used to reduce the edge effect by helping maintain the pressure at the edge of the rolls. Recently, Metso made improvements on the cheek plate design by replacing the cheek plates with a flange system mounted to one of the rolls. The flange acts as a lip that helps maintain the pressure along the edge (Figure 2-7) (Herman et al., 2015). As shown in Figure 2-8, the flanged tire pressure has a more uniform pressure profile than the traditional cheek plate design.

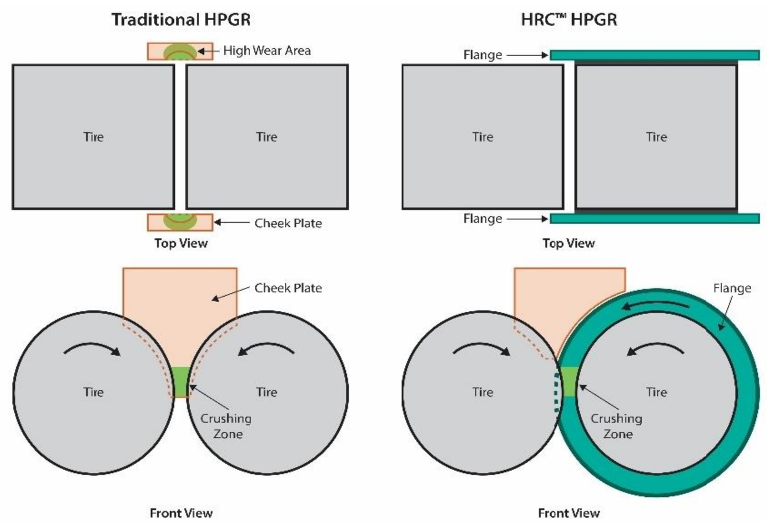

Figure 2-7: Side by Side Comparison of Cheek Plate and Flange Designs for HPGR (Herman et al., 2015)

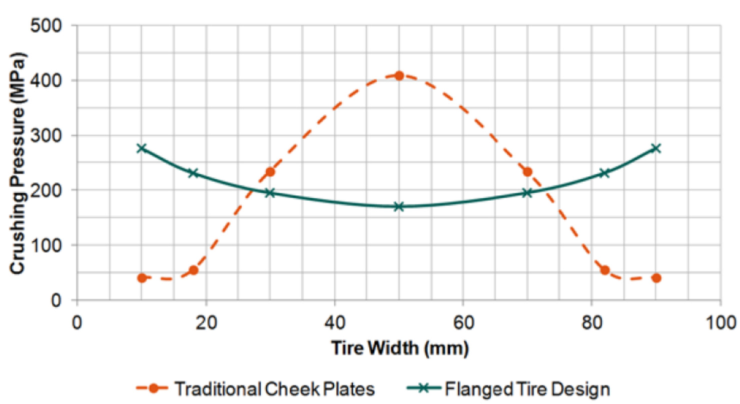

Figure 2-8: Pressure Profile for Check Plates and Flange Designs for the HPGR

2.4 HPGR Sizing

The current method of sizing the HPGR is challenging. Currently, the mining industry is reliant on HPGR piloting for designing HPGR circuits. A number of attempts have been made to standardize a bench scale test for HPGR amenability. This section covers the current methods for sizing the HPGR, including HPGR pilot testing, and alternative bench scale HPGR tests. To date, there is not an accepted bench-scale testing for an HPGR sizing.

2.4.1 HPGR Piloting

Pilot HPGR testing may include the following:

- Pressure testing: Three to four tests at different pressures;
- Speed testing: Two tests at different speeds;
- Moisture testing: Two tests at different moisture levels;
- Recycle or edge-recycle testing: lock cycle tests requiring a minimum of three passes;
- Wear testing of the liner.

Different levels of studies will have different test requirements. Currently, for scoping level to PEA level studies, a minimum of three pressure tests are required on at least one ore type. For higher level studies, further HPGR piloting is recommended. Generally, for PEA level studies 1 to 2 tonnes of material are needed. For additional studies, sample requirements can be as high as 10 tonnes per ore type (Davaanyam, 2015). Often additional drilling is required to generate a suitable metallurgical sample for HPGR piloting. Existing drill core may not be available as it may be limited in quantity, not be representable of the ore body, or be committed for alternative metallurgical programs. Therefore, the sample requirements for HPGR piloting represent the single most substantial barrier for HPGR pilot testing. For example, while pilot test-work could cost $20,000 CAD, the cost of acquiring the sample for piloting could exceed $100,000 CAD.

All-in costs of drilling currently can vary from just under $300 CAD to over $800 CAD per metre depending on core size, location, remoteness to the site, and drill-core recovery. Tables 2-2 and 2-3 illustrate the all-in costs for HPGR pilot testing. Costs were obtained from surveying various drilling programs conducted in 2017. All costs are presented in CAD, assume on 100% drill-core recovery, and a S.G. of 2.7.

Table 2-2: Drilling Core Cost (in CAD) per Metre

Location	Core Size	Cost/ m	Cost/Kg	Cost/ tonne
Northern Chile	PQ	$ 875.00	$ 59.31	$ 57,111
Port Hardy, Road Access	HTW	$ 300.00	$ 29.11	$ 28,032
Alaska - Helicopter Support	HQ	$ 418.00	$ 50.77	$ 48,885
Golden Triangle, BC	HQ	$ 352.94	$ 42.86	$ 41,276
Northern Canada - Helicopter	NQ	$ 325.00	$ 70.24	$ 67,642

Table 2-3: All-in Costs (in CAD) for the HPGR Piloting incl. Sample

HPGR Pilot Scoping Level Per Ore Type			
	Item	**Cost**	
Sample Requirement (HQ)	1 tonne	$CAD	41,276
Pilot testing	3-4 Pressure Test	$CAD	14,000
Total		**$CAD**	**55,276**
HPGR Pre-feasibility Per Ore Type			
		Cost	
Sample Requirement (HQ)	4 tonnes	$CAD	165,104
Pilot Testing	3-4 Pressure Test	$CAD	26,000
Moisture, Top Size, Speed, Wear, Recycle	10 Tests	$CAD	35,000
Total		**$CAD**	**226,104**

Based on Golden Triangle, BC; Based on ~ CA$ 353/m "all in" drilling cost.

2.5 Bench Scale Testing

There currently is not an industry accepted bench scale test for an HPGR design. Several manufacturers and universities have developed variations in an HPGR bench-scale testing. The following section is a summary of bench scale tests that either have been proposed or are currently offered to industry. All proposed tests to date have respective limitations when sizing HPGRs. Generally, limitations of bench scale tests for an HPGR design can be summarized by one of the following; 1) Unable to be independently reproduced independent laboratory 2) Different breakage mechanics than an HPGR, 3) Use a proprietary method to analyze results, that is difficult for independent engineering firms to replicate or analyze results.

2.5.1 SMC Testing – HPGR Index

The SMC test is part of the JK-drop weight test suite. The HPGR index ($M_{ih)}$ is determined by performing impact breakage testing on narrow size fractions. The M_{ih} uses SMC's extensive proprietary database and software to simulate closed and open HPGR circuits. It is not entirely clear how the M_{ih} is calibrated to a pilot HPGR (Nadolski, 2012). The analysis is performed by JK SimMet's proprietary software. The HPGR work index is determined from the SMC Equations 3 and 4:

$$\boldsymbol{S_h = K_s(x_1 * x_2)^{-0.2}}$$ **Equation 3**

Where,

S_h = coarse hardness parameter,

Ks = machine-specific constant (55 for conventional crushers, 35 for HPGRs),

x_1 = P_{80} of HPGR feed [microns], and

x_2 = P_{80} of HPGR product [microns].

$$W_i = S_h K_3 M_{ih} 4(x_2^{f(x_2)} - x_1^{f(x_1)})$$ **Equation 4**

Where,

K_3 = 1.0 for HPGR in a closed circuit, and 1.19 for an open circuit,

M_{ih} = HPGR ore index as determined by SMC testing.

The JK-drop weight test is an impressive and valuable tool for mill and flowsheet design. However, because it relies on impact breakage, it is unable to produce representative HPGR samples that can then be used by metallurgical downstream testing.

2.5.2 Piston Press Testing (UBC)

Davaanyam (2015) developed three Piston Press test methodologies using a Rock Mechanics MTS piston press machine at the University of British Columbia. The Piston Press test is capable of simulating HPGR performance. To date, the results are calibrated to over 177 HPGR pilot scale tests. The three methodologies developed for the test include the Database Calibrated, Direct Calibration, and Simulation methodologies. The test requires 5 to 10 kg of sample, depending on the selected methodology.

2.5.3 Database Calibrated Methodology

The Database Calibrated methodology uses multilinear regression models developed from UBC's database of pilot HPGR and Piston Press tests. The multi-linear regression equations, based on Davaanyam (2015), for the HPGR reduction ratio (RR50) and the specific pressing force (F_{sp}), are presented in Equations 5 and 6:

$$F_{sp}^{HPGR} = \frac{P_{piston} - (5.53 + 24.3w - 86.2\rho_{bulk} + 13.1F_{50}^{HPGR} - {}^{44.4F_{50}^{HPGR}}\!/\!{}_{F_{50}^{Piston}} + 2.98P_{1\,mm}^{Piston}}{53.3} \quad \textbf{Equation 5}$$

Where,

F_{sp}^{HPGR}= Specific pressing force for pilot HPGR N/mm^2,

w= moisture [%*100],

ρ_{bulk}= Compacted bulk density at 32 mm top-size [g/cc],

F_{50}^{HPGR} = Pilot HPGR feed size at 50% passing [mm], and

$P_{1\,mm}^{Piston}$= Piston product percent passing 1 mm [%*100].

$$\boldsymbol{RR_{50}^{HPGR} = 1.86 + 1.41RR_{50}^{Piston} + \frac{2.31F_{50}^{HPGR}}{F_{50}^{Piston}} - 0.41_{50}^{HPGR} - 1.02w} \quad \textbf{Equation 6}$$

Where,

RR_{50}^{HPGR}= Pilot HPGR reduction ratio at 50% passing [mm/mm],

RR_{50}^{Piston}= Piston reduction ratio at 50% passing [mm/mm], and

F_{50}^{Piston}= Piston feed size at 50% passing [mm].

The methodology applies Piston Press test results by developing calibrations for the specific pressing force and reduction ratio. The specific pressing force calibration involves calibrating the Piston Press test pressure to the HPGR specific pressing force by relating the specific energy consumption of the Piston Press test to the database. Calibrating the Piston Press test reduction ratios to the HPGR reduction ratio is done by relating the specific energy consumptions of the Piston Press test to the pilot HPGR database. The test is suitable for early-stage scoping level and PEA studies with an estimated accuracy of +/- 25% (Davaanam, 2015).

2.5.4 Direct Calibration Methodology

The Direct Calibration methodology involves conducting three to four pilot HPGR tests and four Piston Press tests at varying pressures. The test results of the pilot, HPGR and Piston Press test, are used to calibrate a regression model that predicts HPGR performance Davaanyam, 2015). Once the calibrated model is established on a single composite, the Piston Press test can be used for geo-metallurgical studies testing various rock types, lithologies, and alterations across a deposit. Figure 2-9 and Equations 7 to 10 illustrate the approach to calibrating the specific pressure of the Piston Press test to the specific pressing force of the HPGR. The same approach is used for calibrating the reduction ratios of the Piston Press test results to pilot HPGR results by relating the specific energy consumptions between the Piston Press test and the HPGR, respectively.

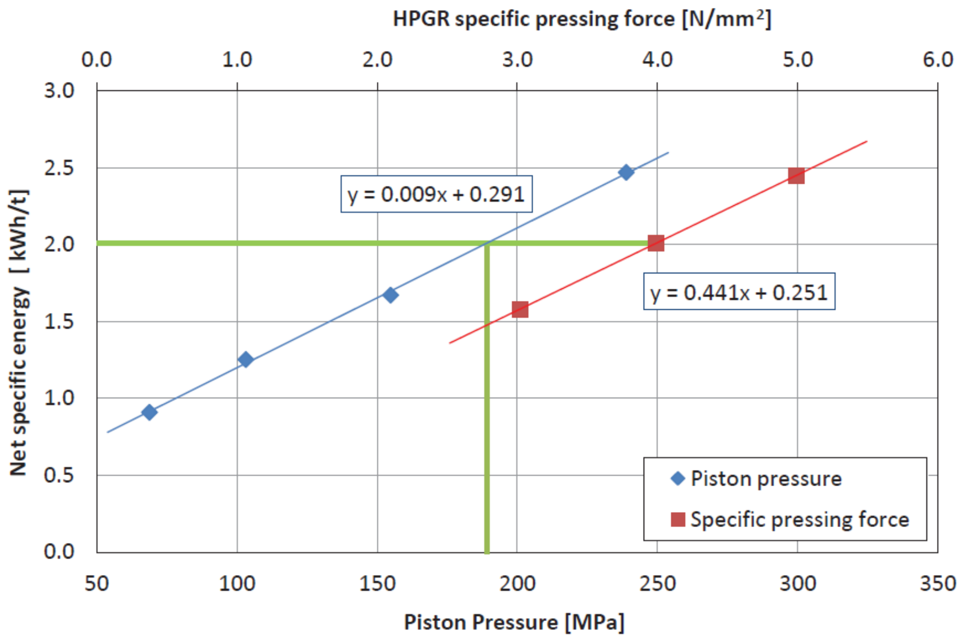

Figure 2-9 Illustration of Calibration of Piston Pressure to Pressing Force Using Direct Methodology (Davaanyam, 2015)

Approximately one tonne of sample is required for the pilot HPGR in order to establish a calibration model. The accuracy of the test is estimated to be in the range of +/- 10% and is suitable from PEA to production planning studies.

$$E_{sp}\left(\frac{kWh}{t}\right) = m_1 * P_{Piston}(Mpa) + b_1 = m_2 * F_{sp}(N/mm^2) + b_2 \quad \textbf{Equation 7}$$

$$E_{sp}\left(\frac{kWh}{t}\right) = m_2 * F_{sp}(N/mm^2) + b_2 \quad \textbf{Equation 8}$$

$$m_1 * P_{Piston}(Mpa) + b_1 = m_2 * F_{sp}(N/mm^2) + b_2 \quad \textbf{Equation 9}$$

$$P_{Piston} = \frac{m_1}{m_2} * F_{sp} + \frac{b_2 - b_1}{m_1} \quad \textbf{Equation 10}$$

2.5.5 Simulation Methodology

The Simulation methodology is similar to the JK Drop Weight test. This methodology involves conducting Piston Press tests on narrow size fractions. Piston Press test results are used to calibrate the t_{10} breakage index model. The model can be used to assess the effect of variations in ore type, feed size, and operating conditions such as transfer size. A minimum of five kg per ore type is required per sample. The accuracy will vary depending on whether the Database Calibrated or Direct Calibration methodology is used when calibrating the Piston Press test results to the HPGR.

2.5.6 Piston Work Index

As part of the research into the development of the Piston Press test, Davaanyam (2015) developed an operating index that relates the product size at 50% and 80% passing to the specific energy consumption. The Piston Work index is determined for each Piston Press test pressure. The Piston Work index for the sample is taken from the average of the test results for the respective samples. The following equations, 11 to 13, summarize the Piston Press test-work index as defined by Davaanyam (2015).

$$\boldsymbol{Wpi80_n = Esp / \left[10 * \left[\frac{1}{P80^{0.5}} - \frac{1}{F80^{0.5}}\right]\right]}$$ **Equation** 11

$$\boldsymbol{Wpi50_n = Esp / \left[10 * \left[\frac{1}{P50^{0.5}} - \frac{1}{F50^{0.5}}\right]\right]}$$ **Equation** 12

$$\boldsymbol{Wpi = \frac{\sum_i^n Wpi}{n}}$$ **Equation** 13

Where,

W_{pi} = Piston Work index [kWh/tonne],

E_{sp} = Specific energy consumption [kWh/tonne],

P_{50} and P_{80} = Product size at 80% or 50 % passing [mm], and

F_{50} and F_{80} [mm] = Feed product size at 80% or 50% passing [mm].

The Piston Work index can be used for geo-metallurgy studies to access HPGR amenability and variability of the deposit. More research and further development of the index is warranted in order to be able to use the index for sizing and design of HPGR circuits in a similar way as the Bond ball mill work index is used for sizing ball mills.

2.5.7 Comparison of Piston Press Test Database Calibrated Methodology and SMC Testing (Kumar et al., 2016)

In 2016, Kumar et al. published a paper at the 2016 IMPC proceedings that compared results from SMC testing to the Database Calibrated methodology. In the proceeding, Kumar et al. (2016) showed the Database Calibrated methodology produced better results than the SMC's HPGR index. The Database Calibrated methodology used for the Piston Press test calibration has an estimated accuracy of +/- 25% (Davaanyam, 2015). Kumar et al. (2016) compared the SMC and Piston Press test Database Calibrated methodology test results conducted for the same ore. Both sets of results were compared to the pilot HPGR testing that was carried out at UBC on a Köppern pilot HPGR with a roll diametre of 220 mm by a roll width of 750 mm. Results showed the Piston Press test specific energy consumption to be within 10% of the pilot HPGR. SMC testing showed results varying from ~32.9% to 5.71%. It should be noted that the SMC test and the Piston Press test reported results differently. The SMC predicts the specific energy consumption for a specific particle size. The Piston Press test predicts both the achievable product size and specific energy consumption for a given pressing force. Because of differences in how results are reported, a direct comparison between the SMC and Piston Press test was not made. Therefore, the error is contained in the specific energy consumption for the SMC test while the error of the Piston Press test is contained in both the specific energy consumption and the achieved product size. Nevertheless, the Piston Press test provided a more accurate prediction than the SMC test. Summary of test results for SMC and the Piston Press test Database Calibrated methodology are shown in Tables 2-4 and 2-5.

Table 2-4: SMC Testing versus Piston Press Test Database Calibrated Methodology- Specific Energy Comparison (Kumar et al. 2016)

Table 4 – Specific energy comparison

		Pilot scale	Piston press test		SMC test	
Test No.	Pressure (N/mm^2)	Specific energy (kWh/t)	Specific energy (kWh/t)	Error (%)	Specific energy (kWh/t)	Error (%)
1	3.02	1.58	1.66	5.06	2.10	32.91
2	3.99	2.01	2.13	5.97	2.40	19.40
3	4.99	2.45	2.62	6.94	2.59	5.71
Average				**5.99**		**19.34**
Standard deviation				**0.94**		**13.60**

Table 2-5: Comparison of the Piston Press Test and SMC HPGR Index to Pilot (Kumar et al. 2016)

Table 5 – Product size comparison

		Pilot scale		Piston press			
Test No.	Pressure (N/mm^2)	P_{80} (mm)	P_{50} (mm)	P_{80} (mm)	Error (%)	P_{50} (mm)	Error (%)
1	3.02	7.79	3.05	7.00	–10.14	2.62	–14.10
2	3.99	6.83	2.57	6.12	–10.40	2.31	–10.12
3	4.99	6.29	2.32	5.39	–14.31	2.03	–12.50
Average					**–11.61**		**–12.24**
Standard deviation					**2.34**		**2.00**

From the results, the Piston Press Database Calibrated methodology better-predicted pilot HPGR performance than the SMC test. These results are encouraging for the merits of the Piston Press test.

2.5.8 Bond Ball Mill Work Index Testing

The Bond Work index test is an industry-wide adopted bench scale test used to design Ball mill circuits developed by Bond (1961). It characterizes the energy requirements for Ball milling in terms of equation 14.

$$W = W_i * \left(\left(\frac{10}{\sqrt{P_{80}}} - \frac{10}{\sqrt{F_{80}}}\right)\right) \qquad \textbf{Equation 14}$$

Where,

W = Energy required to reduce from the feed to product size [kWh/tonne],

W_i = Bond mill work index [kWh/tonne],

F_{80} = Feed size at 80% passing [microns], and

P_{80} = Product size at 80% passing [microns].

The test requires 5 to 6 kg of sample passing 3.36 mm. The test uses a bench scale Ball mill with a diametre and length of 30.5 cm (Austin et al., 1984). The small sample size makes the Bond Work index economic for standard geo-metallurgy programs. The test determines the grindable size reduction from a specific energy input (Bond, 1965). The test is conducted as a lock cycle beginning with a feed sample of 700 mL with a standardized ball charge of ~ 20 kg (Table 2-6).

Ball diameter (cm)	No. of balls	Total weight (gm)
3.68	43	7880
2.97	67	7847
2.54	10	511
1.90	71	2143
1.55	94	1744
		20.125kg

Table 2-6: Ball Charge Requirement for 34.02 cm x 34.02 cm Ball Mill (Michaud, 2015)

After 100 revolutions the sample is removed and screened at a selected screen size. Screen undersize is removed and is replaced by fresh feed. A minimum of three cycles is performed. The test continues until a stable 250% recirculating load is achieved. During the test, the specific energy consumption is determined by the number of revolutions. The resulting Bond ball mill work index is determined from the test, according to Equation 15.

$$\boldsymbol{W_i = \frac{44.5}{P_1^{0.23} * Gpr^{0.82} * \left(\frac{10}{\sqrt{P_{80}}} - \frac{10}{\sqrt{F_{80}}}\right)}} \qquad \textbf{Equation 15}$$

Where,

P_1 = Closing screen size [microns],

Gpr = Average net mass of product for the last 3 cycles [g].

The Bond work index is well established and commonly used for characterizing ore. The Bond work index can be used to predict product size and specific energy requirements for different transfer sizes.

2.5.9 Bench-scale Roller Crusher

The concept of a bench scale roller crusher for sizing HPGR was developed at the Clausthal University of Technology (Fuerstenau et al.,1991). The unit is comprised of two counter-rotating 200 mm diametre rolls. Test results, including specific energy consumption and gap size, are scaled up using a population-based database. Since the database is proprietary, the scale-up factors used to scale the test results to pilot HPGR is proprietary. Since the edge effect becomes proportionally larger with decreasing roll width, it would be expected the edge effect would be more significant with the Bench Scale Roll crusher than pilot HPGR. From the literature, it is not clear how the edge effect is corrected. Figure 2-10 shows a side-by-side comparison of UBC's pilot HPGR versus the Bench-scale Roller Crusher.

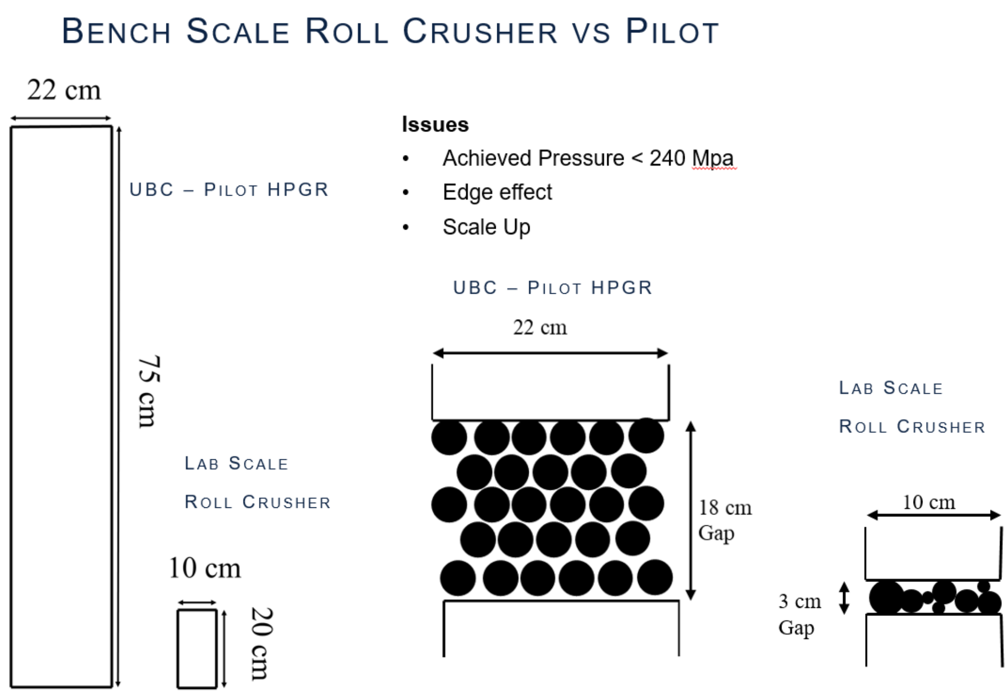

Figure 2-10: Roll Dimension Comparison of Pilot HPGR versus Bench-scale Roller Crusher

Since the breakage mechanics are different from the HPGR, a proprietary modelling approach is needed to analyze the results to simulate HPGR breakage. Another limitation of the test is it cannot produce sample for downstream metallurgical testing.

2.5.10 Static Pressure Test

The Static Pressure test (SPT) is a proprietary bench scale test to assess the HPGR. The SPT was developed to simulate a laboratory HPGR with diametres of 250 mm, and 710 mm (Bulled & Husain, 2008). The SPT is performed by using a hydraulic press to comminute crushed sample material in a piston press with a 100 mm diametre and 200 mm height. The piston press typical operates at a maximum pressure of 55 Mpa. An alternative smaller piston die can be used increase the piston press pressure to110 Mpa. Typically a 1.6 kg charge is required for the initial cycle (Bulled & Husain, 2008). Fines below a 6 mesh are screened and removed from the sample prior to the Static Pressure test. The fines are required to be screened, as the fines were found to reduce the achievable reduction breakage (Bulled & Husain, 2008). During testing the piston is loaded at a fixed rate of 3.4 mm/s. Following the first cycle of the Static Piston test, the piston product is screened at 6 mesh, and the fines are replaced with fresh sample feed. It is unclear if fines are removed from the fresh feed prior to adding the feed to the next cycle as testing procedures are not implicit in the literature. The SPT test records the force, comminution time and piston displacement. From this data, the specific energy consumption of the sample is determined by a force-displacement integration. The Static Piston test reports a Hydraulic Piston index (HPi) that is determined from the last three cycles during testing (Equation 16).

$$\boldsymbol{E = HP_i * 10 * \left[\frac{1}{P80^{0.5}} - \frac{1}{F80^{0.5}}\right]} \qquad \textbf{Equation 16}$$

Where,

E = Work index for SPC [kWh/t],

HP_i = Hydraulic Piston index [kWh/t].

The Static Piston test has three main deficiencies. First, sample preparation does not produce a representative sample for HPGR comminution. HPGR naturally has fines from upstream comminution, that affect the inter-particle breakage mechanics. Removing the fines affect comminution by reducing the number of point loadings on each particle (Figure 2-11). As can be expected, the SPT will have significantly higher reduction ratio breakage than HPGR at equivalent pressures. Second, the Static Piston test does not produce a representative HPGR product for downstream metallurgical testing. HPGR piloting would still need to produce material to evaluate the effects of the HPGR for on downstream metallurgical circuits, such as flotation or leaching. In addition, the calibration and analysis of the Static Piston test are proprietary. Proprietary testing and modelling, present challenges for the industry, as results cannot be verified nor analyzed by a third party engineering.

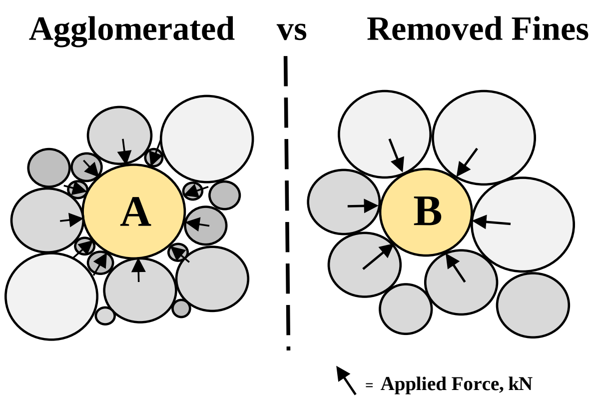

Figure 2-11: Effects of Fines on Comminution

2.6 Benefits of the HPGR

The HPGR has several benefits. Notably, energy savings as high as 30% to 50% (Casteel, 2005; Günter et al., 1996) have been recorded over traditional SAB circuits. Table 2-7 summarizes studies that confirm HPGR energy savings.

Table 2-7: Summary of Energy Savings for HPGR Projects (source Davaanyam, 2015)

Project	Units	SABC	HPGR	Energy Savings %	Reference
Boddington Gold	kWh/t	23.10	18.00	22.10	Parker et al. (2001)
Los Broncos Copper	kWh/t	16.21	13.02	19.70	Oestreicher and Spollen (2006)
Cerro Verde Copper	kWh/t	20.10	15.90	20.90	Vanderbeek et al. (2006)
Ruby Creek Moly	$/t	4.53	3.83	15.50	Auguelov et al. (2008)
Copper Gold project in Russia	$/t	0.78	0.53	32.10	Auguelov et al. (2008)
Courageous Lake Gold	$/t	3.59	2.47	31.20	Auguelov et al. (2008)
Morrison Copper/Gold/Moly	$/t	0.63	0.56	11.10	Auguelov et al. (2008)
Ajax Copper/Gold	$/t	0.60	0.47	21.70	Ghaffari et al. (2013)

Other benefits include micro-fracturing and increased fines. Esna-Ashari and Kellerwessel (1988), Patzelt (1995), and Baum (1997) all found improved liberation by HPGR. McNab (2006) noted that the HPGR could both improve liberation and improve leach kinetics for heap leaching by boosting extractions. In addition, the HPGR usually has shorter production ramp-up time and is less sensitive to ore changes than SAG and Ball mills. The HPGR also has higher reliability and availabilities that commonly exceed 95%. These improvements can be extremely beneficial, as maintenance shutdowns can be expensive when production is required to be shut down.

2.7 Disadvantages for High Pressure Grinding Rolls

Similar to all comminution technologies, the HPGR has disadvantages on select ore types and under specific conditions and circumstances. The HPGR has more complex and expensive bulk material handling than conventional SAG milling. In addition, the HPGR can be susceptible to excessive fines or material with excessive clays that can cause the HPGR rolls to jam. Moisture levels above 10% can cause excessive energy consumption. Finer product sizes can cause stabilization and percolation issues for heap leaching. However, adding cement to agglomerate ore before heap leaching can offset these issues. However, the additional cement consumption needs to be weighed against both the potential energy savings and potential increases in metal extraction for HPGR. Overall the HPGR offers significant operational benefits. Despite this, not all projects may warrant HPGR. Proper trade-off studies are always required when exploring the potential benefit HPGR could bring for a given project.

2.8 Demand for Lowering Power Costs

Currently, comminution circuits represent 30% to 40% of a mine’s energy costs (Davaanyam, 2015). This figure is likely to increase, as the industry trend of requiring finer grinding will continue over time. Global power costs have risen over the years and are likely to continue to increase faster than inflation. In 1970, the average power costs recommended for engineering estimates in North America was on average 1 cent per kWh (Weiss, 1973). In 2014, the Fraser Institute reported industrial power rates for 119 municipalities in Canada to be 8.92 cents per kWh. In the developed world, most of the best and most economical power resources have already been built. The next generation of power infrastructure will likely be more expensive. With any resource, the most economical and best sources are developed first. Recently permitting challenges have elevated project costs through delays or cancellations, such as the CA$36 billion LNG terminal (Financial Post, 2017) or the CA$8.8 billion BC Hydro Site C Dam. Site C’s initial cost of CA$7.9 billion in May 2011 rose as a result in part from delays (Garstin, Michaela, 2011). With increased challenges to permit and build new power facilities, energy supply will be challenged to meet demand. If lower-scale sized power projects are forced to be considered because of permitting challenges, power cost will likely escalate, as smaller projects do not have economies of scale. It is important that operations and projects look to increase energy efficiency.

Power is expected to become an increasingly important input cost for metal producers. For example, power costs and falling grades were the primary justifications for Freeport-McMoRan to install HPGR at its Morenci Mine in Arizona (Herman et al., 2015). In 2017, the U.S. Energy Information Administration (EIA) predicted global energy demand would increase by 48% by 2040. Figure 2-12 shows traditional low-cost energy productions like nuclear and hydro are expected to remain flat or fall. Nuclear power is expected to fall in the US as more nuclear power plants approach retirement (EIA, 2017). Projections, however, vary substantially according to the EIA, with increase estimates ranging from 5% to 20% from 2016 to 2040. Higher cost power such as oil and renewables will be required to meet future demand. Currently, electric car adoption is the most significant unknown factor for predicting energy demand.

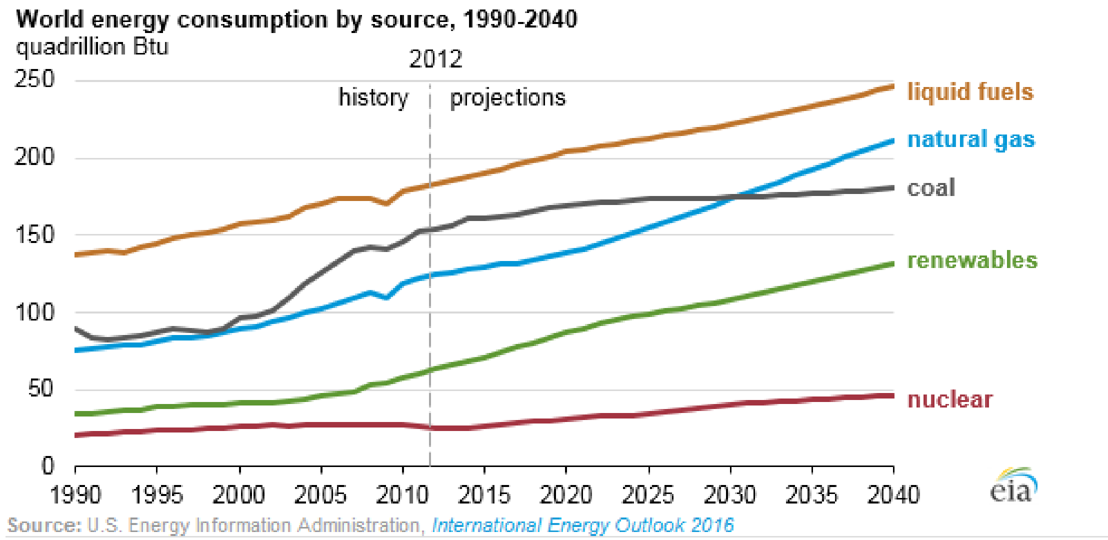

Figure 2-12: Future World Energy Consumption (source: EIA, 2017)

It is estimated that by 2025 hybrids, battery electric vehicles (BEV), and hydrogen fuel cells will represent 9% of all light vehicle sales (EIA, 2017). If the demand for electric cars continues to grow, the demand for electricity will continue to increase and restrict supply.

With the growing demand and supply of electric vehicles (Figure 2-13), additional demand will be placed on power. It is important that the mining industry continues to lower power consumption as resource grades are expected to continue to be exhausted with mineral depletion at current operations.

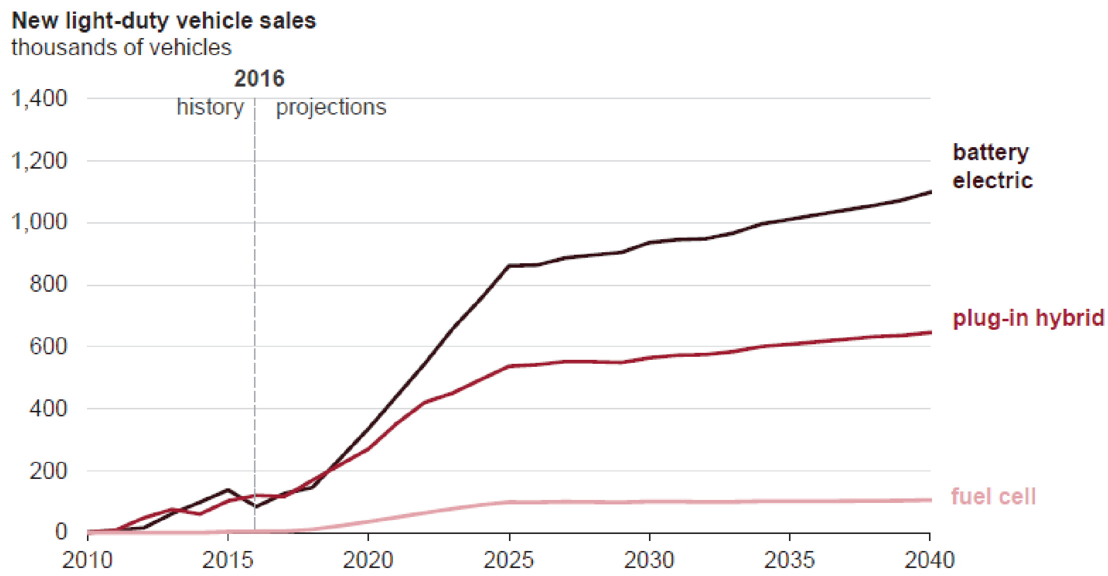

Figure 2-13: Light Vehicle Projections (source: DOE, 2017)

As demand for electricity continues to increase in the new age of battery storage and electric vehicles along with increased challenges to develop low-cost power, the mining industry will face greater pressure to lower specific energy consumption, and therefore are likely to examine the HPGR more aggressively.

2.9 Problems with the Adoption of High Pressure Grinding Rolls

Problems with HPGR adoption can be attributed to several factors. Earlier versions of the technology had excessive wear rates that deterred the industry from properly examining and adapting the technology for hard rock mining. Over time, the industry solved these issues by research and development of better tire (roll) liners. In-house testing began to characterize ore regarding wear rates, and engineers began to design flowsheets to minimize wear rates (Burchardt, Patzelt, Knecht, & R., 2011).

Above all, the significant issue preventing the adoption of HPGR comminution is the cost of pilot HPGR testing, specifically sample size. Often, additional metallurgical drill holes are required to provide the needed sample for HPGR piloting. The sample cost can often exceed the cost of an HPGR test work program. Most junior mining companies and the majority of early-stage projects have a limited supply of capital. Often companies have to decide between exploration drilling or alternative metallurgical programs that may have better risk-return profiles at the early project stages. Especially for PEA level studies, HPGR piloting may not be justified. As the project advances, the HPGR may require extensive re-evaluation and metallurgical testing of downstream processes, such as examining the effects on recoveries. Lastly, there may time or budgetary constraints that may deter from conducting the necessary studies and design for an HPGR.

2.10 Conclusion

Adoption of HPGR has been slow for hard rock mining. Initially, HPGR was adopted in the cement industry, which faced different challenges than hard rock mining. Cement plants have uniform feed material with lower abrasion, making variability, and piloting less important. Hard rock mining often deals with variable ore, which is harder and more abrasive. Although liner wear issues have largely been addressed, ore variability challenge still plays a significant role in HPGR adoption.

To date, HPGR pilot testing requires a significant amount of sample. For most projects, the HPGR is not feasible because either the sample is not available or capital restraints do not allow sample to be collected. Since later engineering designs are based on earlier evaluations, an

HPGR is at a disadvantage against alternative technologies. Re-evaluating the HPGR in the late stages of project development complicates engineering and elevates costs. Re-evaluating necessitates more engineering work to be done and redone. Evaluating HPGR sooner will help reduce later engineering costs and help understand the actual project economics early on.

Alternative bench scale tests for the HPGR amenability have been developed such as the JK Drop Weight test and its HPGR index, the bench-scale roller crusher, and the Static Pressure Test. However, these tests have not been able to replace the need for HPGR piloting. An industry-recognized test must have the same high-pressure breakage mechanism as the HPGR. To enable the industry to evaluate the HPGR properly, a bench scale test that is capable of accurately evaluating the HPGR early in the development stages is needed. A bench scale amenability test for the HPGR needs to be capable of indicating variability across an ore body, much the way the Bond Work index is used. The test requires small sample sizes and can provide a clear indication as to the amenability to the HPGR for an ore, for a client to know if the HPGR should be considered. Specifically, the test needs to provide an accurate prediction of the specific energy consumption and product distributions that could be in closed circuit HPGR simulation. Furthermore, the bench-scale test must be a standardized test that independent labs can set up, and provides reproducible results that are independently analyzed and verified.

Chapter 3: Structure of Research Methodology

This chapter has been written to present a general overview of the structure and organization of the methodology used for the research conducted in this thesis. The methodologies are discussed at length in each of the respective chapters. Methodologies developed for this research were selected to demonstrate and validate the Database Calibrated and Direct Calibration methodologies for industrial application. The validation of the methodologies was accomplished by formalizing the Piston Press test procedures, demonstrating the reproducibility of the Piston Press test.

To this end, the research was designed with consideration for the following objectives:

- Formalize standard operating procedures by evaluating the existing Piston Press test procedures;
- Demonstrate the Piston Press test methodologies are reproducible at independent metallurgical facilities;
- Validate the Piston Press est methodologies for a full-scale HPGR;
- Present a straightforward approach to interpret and analyze Piston Press test results.

To achieve the above objectives, a three-stage program was proposed as outlined in Figure 3-1. The program focused on formalizing the Piston Press test procedures, demonstrating the reproducibility of the test by an independent lab, and validating the methodologies on a full-scale HPGR.

- **Step 1:** Formalize a standard operating procedure for Piston Press testing that will assist in transferring the procedures commercially;
    - Understand the effects of moisture, dry versus wet splitting, and porosity on the Piston Press test;
- **Step 2:** Demonstrate repeatability by performing duplicate Piston Press testing at an independent commercial facility;
- **Step 3:** Validate Piston Press test methodologies against full-scale HPGR by comparing full-scale HPGR to both pilot HPGR and Piston Press testing using a straightforward analysis approach. Piston Press tests are calibrated to pilot and full-scale HPGR using both the Database Calibrated and Direct Calibration methodologies. Results are compared to full-scale HPGR operating data by using closed circuit simulation of an HPGR operating discharging to a 2 mm screen.

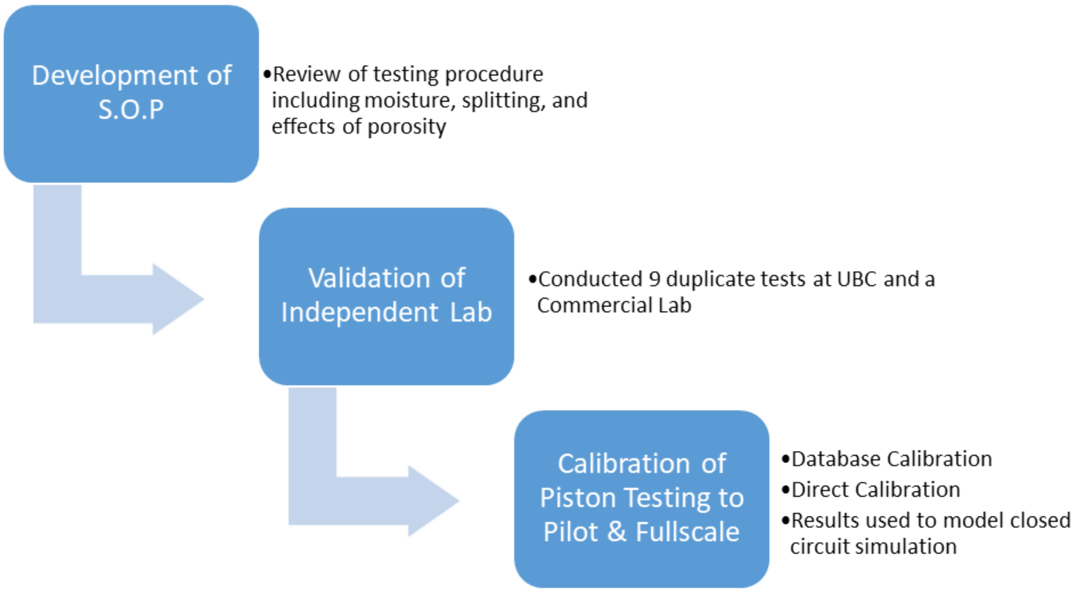

Figure 3-1: General Program Summary

3.1 Formalization of Standard Operating Procedures

For the Piston Press test to be adoptable by commercial metallurgical laboratories, a standard operating procedure is critical for facilitating and ensuring the Piston Press test is correctly transferred. Formalizing the test involved reviewing test procedures to identify possible variables that may influence results. These included both procedural and material property variables. The two procedural variables that warranted further examination were the effects of varying moisture and dry vs. wet splitting of the Piston Press test feed. In a separate program, the effects of material porosity were examined to determine the relationship of porosity to reduction breakage performance and specific energy consumption. The Piston Press test procedures of varying moisture levels and the practice of wet splitting for producing Piston Press test feed were evaluated using a single program that involved performing duplicate Piston Press tests. The duplicate Piston Press tests involved conducting test-work using both dry and wet splitting techniques at moisture levels of 5%, 3%, and 1.5 %. The effects of porosity (as represented by the degree of void space present in the material) were evaluated in a separate program that examined and compared ore variability for three different deposits. The three deposits were noted as Deposit A, B, and C. Deposit A has moderate levels of porosity, Deposit B has high levels of porosity, and Deposit C showed low levels of porosity. These results are discussed in Chapter 4.

3.2 Repeatability of the Piston Press Test

In collaboration with UBC, ALS Metallurgical in Perth, Australia, retrofitted two existing piston press machines previously used for UCS testing. The first stage of the program involved transferring basic Piston Press procedures and methodologies to ALS Metallurgy. Duplicate testing was conducted at UBC and ALS Metallurgy to compare Piston Press test results. The duplicate testing included Piston Press testing on the same composite sample splits for a composite of full-scale HPGR feed and a composite of 50% full-scale HPGR feed and 50% full-scale HPGR +2 mm recycle. From this program, six duplicate Piston Press tests were used for showing reproducibility between at ALS Metallurgy and UBC. Testing results from duplicate testing were compared by specific energy consumption, product size distribution, as well as using the Piston Work index as shown in Equation 13.

3.3 Full-Scale HPGR Validation

The sample for full-scale HPGR validation was collected at Tropicana Gold Mine's full-scale HPGR circuit along with the respective operating data for the day. The collected samples included, HPGR fresh feed and HPGR +2 mm recycle. A fresh/recycle composite was created representing 50% of the full-scale fresh feed and 50% full-scale HPGR + 2 mm recycle. Both the fresh/recycle composite and fresh feed composite were used for HPGR piloting and Piston Press testing. Piloting was conducted in Perth, Australia by ALS Metallurgy.

Piston Press test results were calibrated using the Database Calibrated methodology for the pilot HPGR and by the Direct Calibration methodology for both full-scale HPGR and pilot HPGR. The calibrations involved calibrating the Piston Press test pressure to the HPGR pressing force, as well as calibrating the Piston Press test reduction ratio for 50% passing (RR50) to full-scale and pilot HPGR.

Results from the respective calibrations and the respective normalized PSD distributions were used to develop the following closed-circuit simulations:

- Pilot HPGR to full-scale HPGR;
- Database Calibrated of Piston Press test result to pilot HPGR;
- Direct Calibration of Piston Press test results to pilot HPGR;
- Direct Calibration of Piston Press test results to full-scale HPGR.

3.4 Piston Press Test Procedures

All Piston Press tests conducted during this research used the same Piston Press test procedure as illustrated in Figure 3-2, which includes procedures for the Database Calibrated and Direct Calibration methodologies. The Database Calibrated and the Direct Calibration methodologies have different respective laboratory procedures.

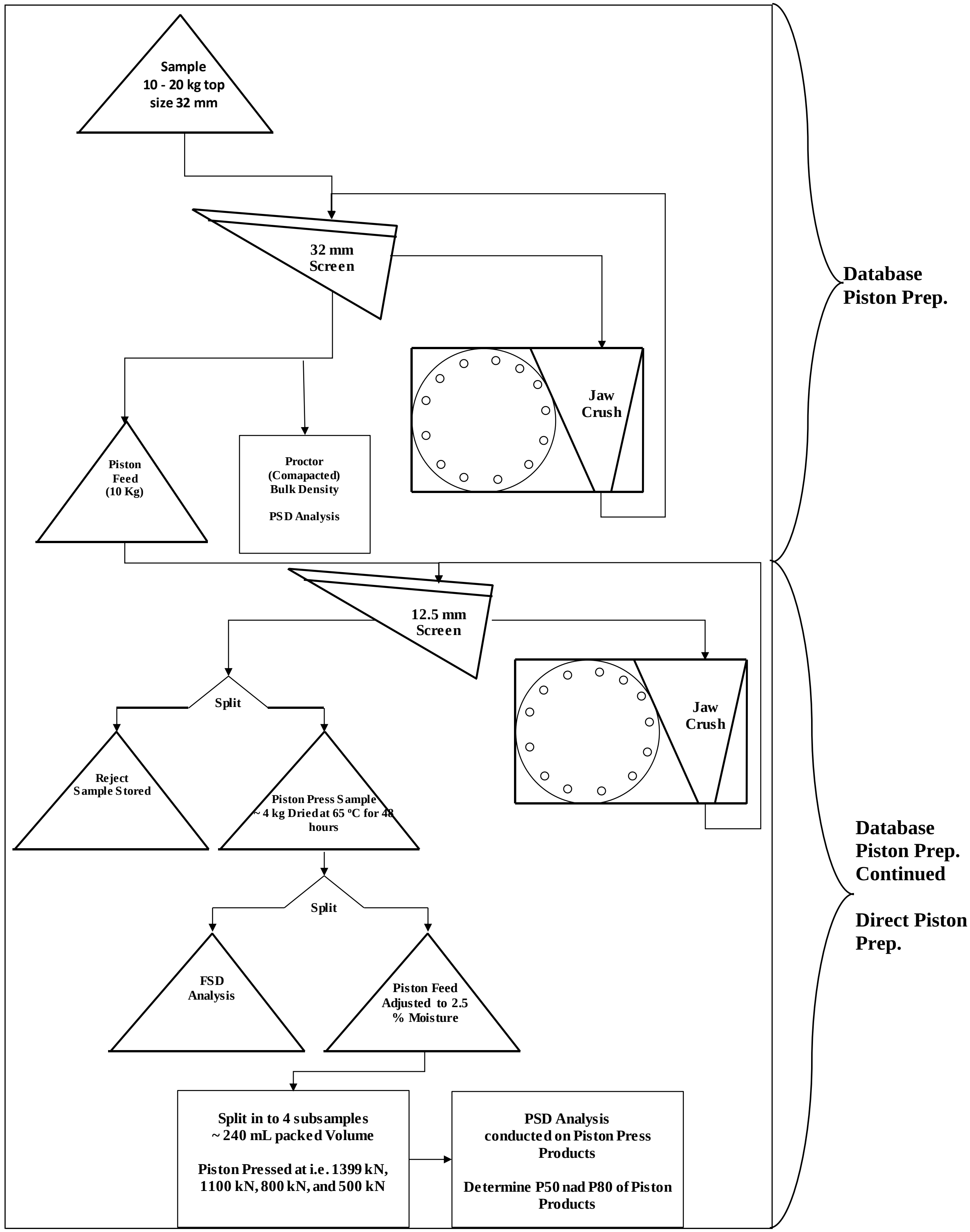

Figure 3-2: Piston Press Test Sample Preparation Procedure

The Piston Press test requires between 5 to 10 kg of material depending on the methodology used, deposit variability, and the level of study is being conducted. Depending on the study level and scope of the test, additional tests may be needed. For Direct Calibration methodology and more advanced studies, larger sample sizes may be required. The Piston Press test involves producing four separate Piston Press tests at different pressures on a single sample composite. In this thesis, pressures selected for the test were generally 1399 kN (240 Mpa), 1100 kN (186 Mpa), 800 kN (126 Mpa), and 500 kN (86 Mpa) kN. This range was selected in part because of the nature of the material, as well as to ensure a broad range of pressures to define better the energy breakage relationship of the material tested. All Piston Press test feed and product PSD analysis were conducted using wet screening. Wet screening breaks up flakes and has a higher screen efficiency than dry screening when fines are present. Energy and size reduction relationships were determined by comparing the specific energy consumption, measured by integrating the force-displacement curve, to the RR50 of the Piston Press test. The Piston Press test pressure was calibrated to the HPGR specific pressing force by determining the equivalent HPGR pressing force to deliver the same level of specific energy as the Piston Press test.

3.4.1 Database Calibrated Methodology

The Database Calibrated methodology requires additional sample preparation, measurement of the packed bulk density, and feed size passing 50% at a 32 mm top-size. All crushing during sample preparation was performed by reverse screening and is illustrated in Figure 3-2.

The two calibrations developed from testing are:

- Pressure to specific pressing force ($F_{sp)}$ related to specific energy consumption (E_{sp});
- Reduction ratio or RR50 (measured as the product size at 50% passing) to the E_{sp}.

From these calibrations, a model was built to determine the resulting RR_{50} and E_{sp} from an input for a given specific pressing force. This relationship was used to predict the PSD by using normalized PSD curves to simulate particle size at a given screen aperture.

3.4.2 Sample Preparation

The test uses 5 to 10 kg of crushed material per sample. Material is stage crushed in reverse closed-circuit at 12.5 mm passing. This practice produces fewer fines (Davaanyam, 2015). The following additional parameters are needed to perform the Database Calibrated methodology:

- Proctor (Compacted) Bulk density at 32 mm top size measured after performing reverse crushing at 32 mm.
- PSD analysis of 32 mm reverse crushed feed sizes at 50% and 80% passing.

Following crushing, homogenizing, and splitting, the material is dried at 60°C for a minimum of 24-48 hours before splitting. After the sample was dried, the sample was split into approximately 1 kg sizes for PSD analysis, 2 kg for Piston Press test feed, and reject. The split of the feed sample for the PSD is typically done dry with moisture being introduced later in the sample preparation. This practice is done to limit moisture loss that may arise during splitting. The moisture adjustment was made to the Piston Press test feed sample prior to splitting into 4 subsamples for Piston Press testing. Following the sample's moisture adjustment, the material was agglomerated and homogenized by repeated scooping and mixing. It is important that fines are agglomerated to the larger particles evenly, as doing so ensures a representative split. It also ensures that the sample remains homogenized during Piston Press testing, which will ensure consistent results. A photograph is shown in Figure 3-3 of the riffle splitter used for preparing the Piston Press test feed.

The Piston Press test feed is split into four subsamples based on a volume of 240 cc of sample. Prior to splitting, the sample material was loaded into a 2 L cylindrical fixed-volume container.

Figure 3-3: Photograph of Piston Press Test Splitter

The container was repeatedly tapped until the material was fully loaded. The compacted bulk density was measured and used to determine the required mass to fill 240 cc. All Piston Press test feeds were targeted to be within +/- 10 g of the determined target sample weight to fill the required volume. All samples were bagged to ensure minimal moisture was lost prior to testing. A strain measurement was taken prior to testing to determine the amount of strain during loading. These measurements were used to correct any displacement of the test during the analysis of the results. Piston Press testing was done at four different energy levels which were chosen based on the material. Typical max loading varied between 500 kN to 1399 kN. Higher loading can be done if the machine and setup are capable. Specific energy consumption during the test was measured by integrating the force-displacement curve. For this measurement, the strain caused by the loading of the die and spacers is accounted.

Piston Press test material was loaded into the die and tapped to ensure the material properly settled and filled the die. The sample weight was taken prior to Piston Press testing and after to verify the moisture levels as a quality check. After pressing the sample using a piston press machine, the samples were dried for 24 hours at 60^oC, prior to wet sieve analysis. Samples were then wet sieved to determine the PSD and P_{50} and P_{80}. From these results, the energy size reduction relationship was determined for the respective sample.

3.4.3 Importance of Agglomerating Piston Press Feed

Since high-pressure breakage occurs by inter-particle forces, fines play a key role in transferring energy through the sample by helping to increase the contact surface area between particles. Figure 3-4 to 3-6, visually demonstrate how the fines facilitate energy transfer through the particle bed by occupying voids which increases the number of contact points between larger particles. Furthermore, as evidence in Figure 3-5, lower moisture levels can lead to the fines of the piston bed stratifying during loading of material into the piston press die.

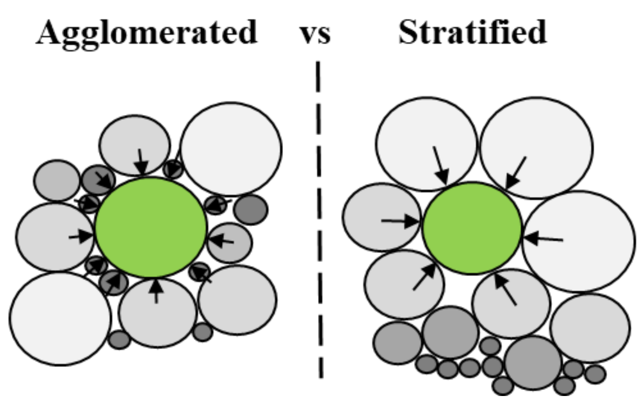

Figure 3-4: Comparison of Agglomerated and Stratified Particle Bed

A stratified bed will decrease the contact surface area between particles, which will then result in an increase in pressure at the contact points between particles.

Figure 3-5: Piston Test Loaded Before Testing at 3% and 1.5% Moisture, Respectively

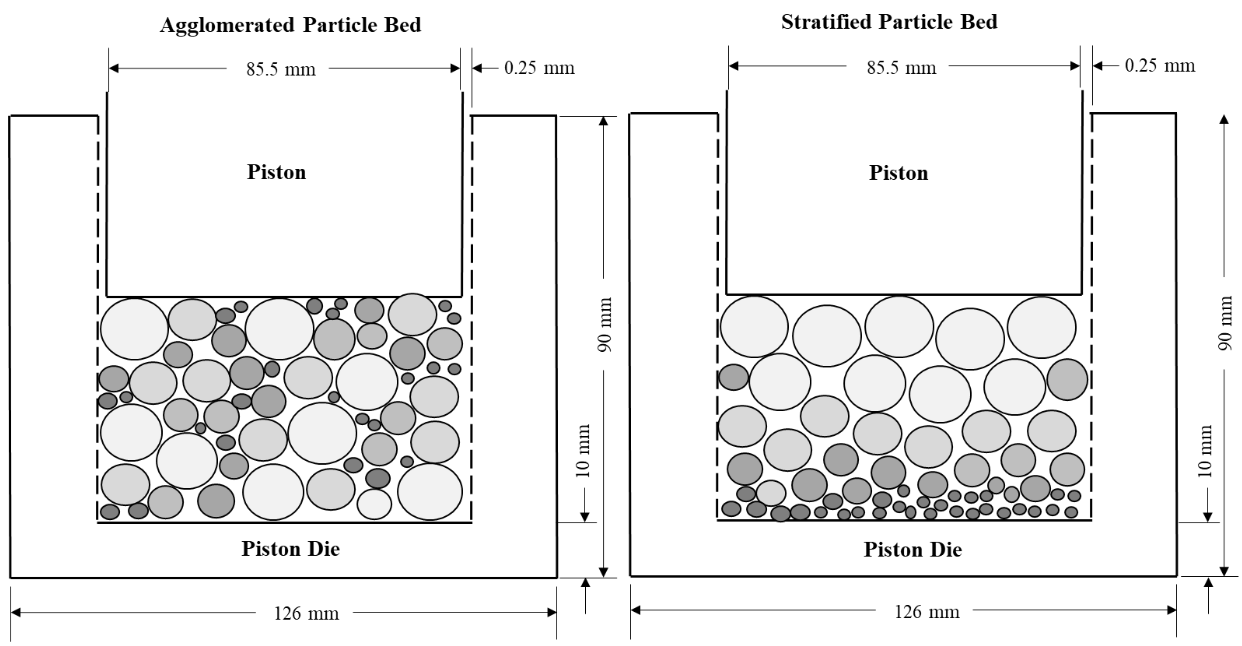

Figure 3-6: Agglomerated Particle Bed versus Partially Stratified Bed

After loading of the die, the die was tapped several times to ensure the material was properly settled and filled.

3.4.4 Strain-Displacement of Spacers

Depending on the setup configuration of the Piston Press test, the strain is measured at the maximum load. The strain is measured by conducting a Piston Press test while recording the piston displacement and force during loading of the bottom plate of the die. Strain measurement is required before testing. The strain measurement data is used to correct for strain displacement in the Piston Press test apparatus.

The strain of the die and spacers needs to be accounted for as it represents energy that is not transferred to the piston particle bed. As shown in Figure 3-7 not correcting for strain will result in the Piston Press test overestimating the amount of energy applied to the sample during the test.

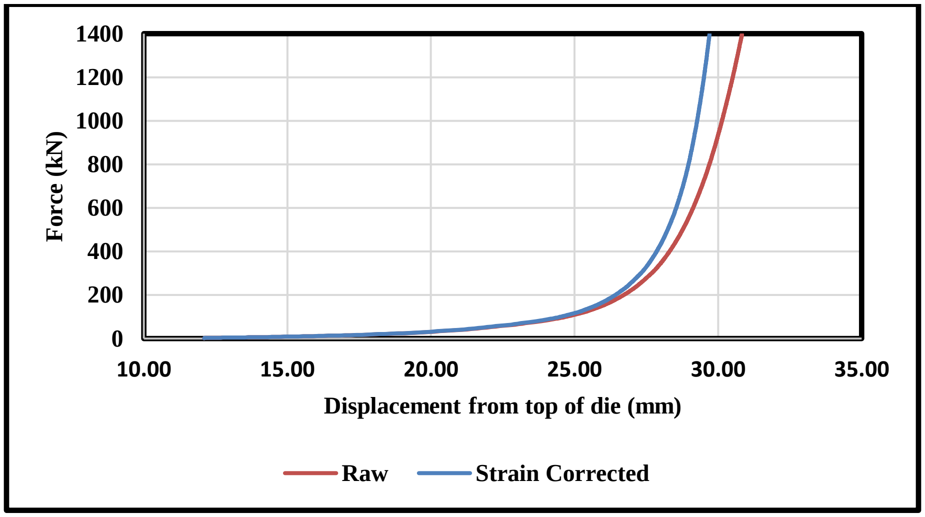

Figure 3-7 Effect of Strain on Piston Press Test

3.4.5 Piston Press Testing Specifications

It is important that the test setup matches UBCs', as varying setups may require additional validation and calibration when determining equivalent energy integration. The difficulties arising from alternative setups are discussed in Chapter 5. The following Piston Press specifications were used, and future tests should conform to them when possible:

1. Rock mechanics press capable of applying up to a minimum of 1399 kN of force;
2. Displacement instrument precision of 0.001 mm
3. Loading rate of 200 kN/min and 0.8 mm/s piston velocity or slower
4. 150 mm maximum stroke
5. Measurement interval of 0.25 s per reading

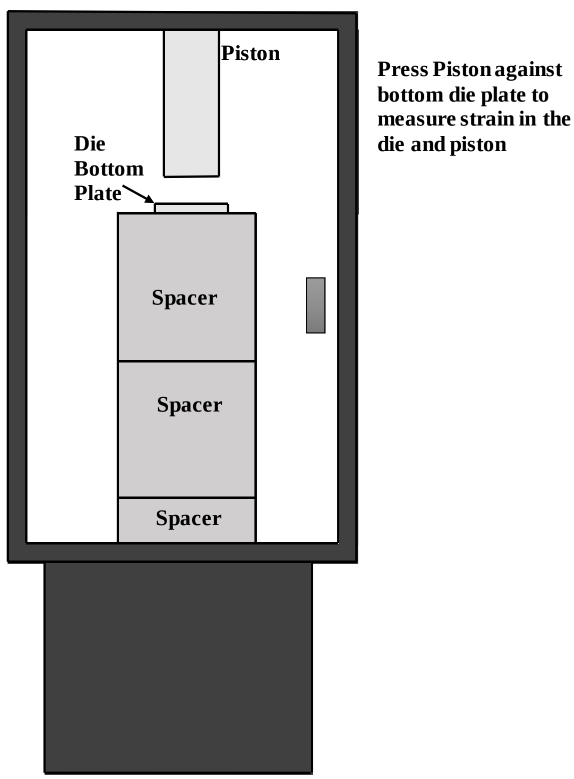

Figure 3-8: Illustration of Piston Press Setup at UBC during Strain Measurement

Chapter 4: Evaluation of Piston Press Procedures & Sample Properties

4.1 Summary

This chapter presents test-work carried out as part of the work conducted to formalize the Standard Operating Procedures of the Piston Press test. The test-work examined the effects of moisture, and wet versus dry splitting during the preparation of the Piston Press test feed. In addition, a separate program carried out investigated the influence of porosity on reduction breakage during Piston Press testing.

Moisture plays a significant role in HPGR comminution both in breakage and in energy consumption. It was necessary to understand the effects of moisture in the Piston Press test, specifically, if Piston Press tests performed at various moisture levels are comparable. Porosity was investigated since breakage tends to occur along planes of mineral weakness. The last variable was the practice of wet splitting during the Piston Press procedures. The practice of wet splitting was reviewed and validated to ensure wet splitting produced a representative sample.

Overall, porosity and moisture were found to be significant. Moisture showed improvements in energy efficiency breakage. Wet splitting was found to be important, as it was effective at agglomerating material prior to Piston Press testing. Wet splitting was also found to produce representative splits. Reduction breakage of Piston Press test samples proved to be well-correlated to sample material increases in porosity.

4.2 Methodology

Analysis of the significance of moisture and wet versus dry splitting was carried out in the same program. Porosity was determined from a separate program using material from three different copper porphyry deposits with significant differences in porosity. Porosity was determined by comparing relative densities determined by weight in air and in water to the true density as determined from pulverized using a pycnometer technique. Both programs used Piston Press testing procedures as carried out using the test procedures as outlined in Section 3.4. Piston Press testing included conducting Piston Press tests at four different energy levels, which used the following forces/pressures:

- 1399 kN (240 Mpa)
- 1100 kN (189 Mpa)
- 800 kN (Mpa)
- 500 kN (Mpa)

4.2.1 Moisture and Dry versus Wet Splitting

The methodology used to evaluate the effects of moisture and dry versus wet splitting is summarized in Figure 4.1. All test-work was conducted on a composite sample that represented 50% feed and 50% HPGR + 2mm recycle material that was obtained from a full-scale HPGR operation. Piston Press testing was performed on the composite at 5%, 3% and 1.5% levels of moisture. Each moisture level included testing a sample prepared by wet splitting and a duplicate sample prepared by dry sampling. The program included 16 piston tests per moisture levels at four energy levels each. Figure 4-1 shows a schematic of the program

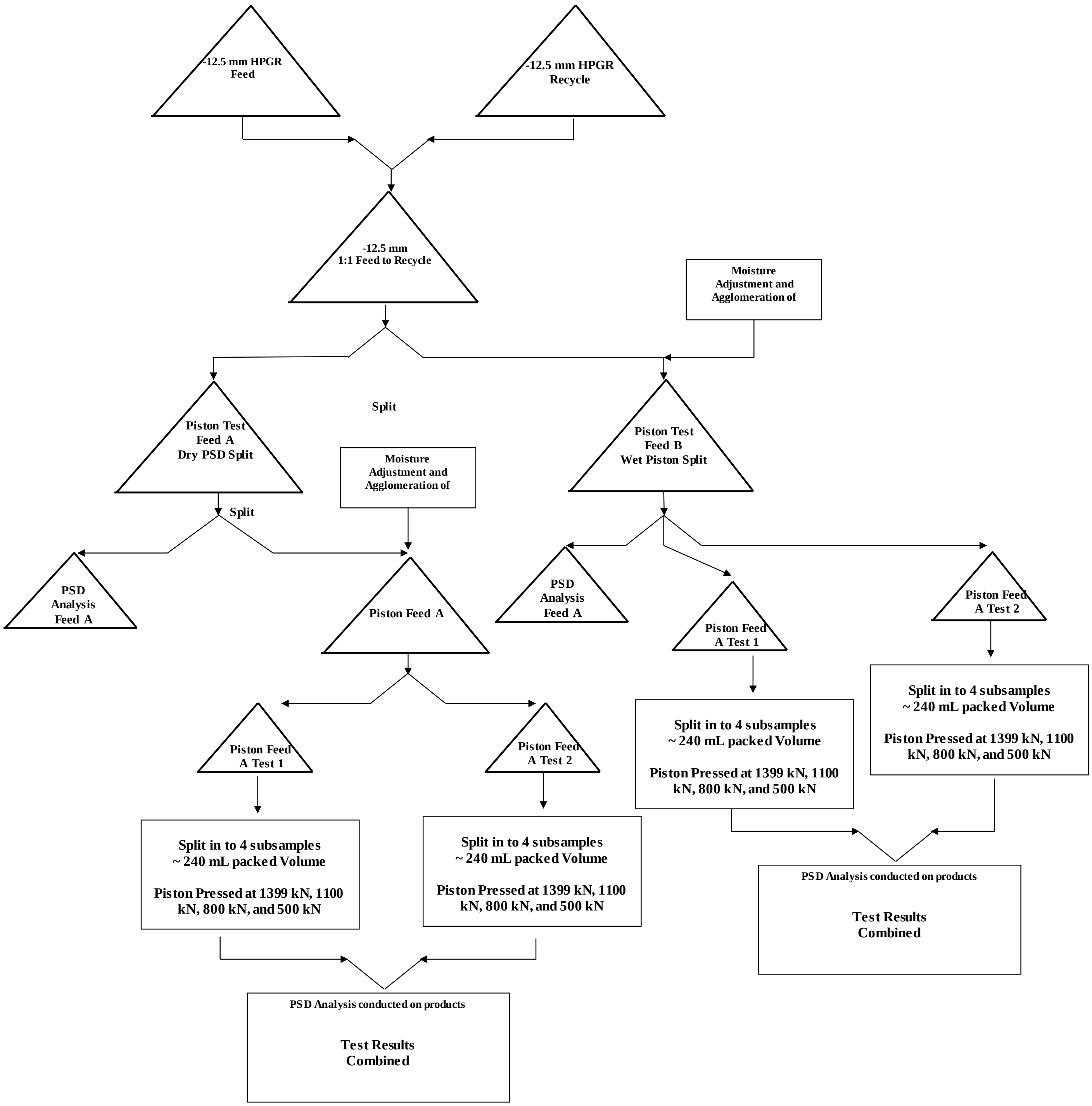

Figure 4-1: Methodology for Determining the Effects of Varying Levels of Moisture Piston Press Testing

Piston Press test preparation was done by ALS Metallurgy in Perth, Australia. The sample preparation included crushing the respective sample to 12.5 mm using reverse closed circuit. The sample was shipped to UBC where all sample was dried at 60^{o}C for 24 hours prior to sample preparation for Piston Press testing. Drying the sample was done to ensure the sample was completely dry prior to the moisture adjustment. In total, three composite samples comprising of 60 kg each were created for all three moisture levels. Following the creating of the composite samples for Piston Press testing the respective sample was split into two representative sub-samples that were further spilt using wet split and dry split, respectively. As shown in Figure 4.1, the wet split sample was corrected to the respective moisture level prior to splitting approximately 1 to 1.5 kg sample that was used to determine the Piston Press feed PSD. The remaining wet split sample was split into two duplicate Piston Press feed samples that were further split into four representative splits of ~240 cc sample for Piston Press testing. Results for the dry split and wet split at each moisture level were determined by a weighted average of the respective two duplicate Piston Press tests. Two Piston Press tests were conducted per type of split and moisture level to increase the sample size used during this research. Specific energy consumption and Piston Press feed and product PSDs were compared to understand the variations in the results.

4.2.2 Porosity

The program methodologies conducted for evaluating the effects of sample porosity during Piston Press testing summarized in Figure 4-2. The test-work carried out included Piston Press testing on three separate deposits, which each had different levels of porosity. Deposit B had the highest level of porosity, followed by Deposit A, and lastly, by Deposit C. Each sample tested during the program included Piston Press testing performed at 2.5% moisture at a maximum pressure of 240 Mpa. Test-work was conducted using the standard operating procedure outlined in Chapter 3. Porosities were determined by calculating the difference between true and relative densities in the samples for select samples of Deposit A and B. One sample of both Deposit A and Deposit B was selected for XRD analysis in order to determine the composition of the sample and verify the specific density of the material. Results of the XRD may be referred to in Appendix A.3.

Testing of Deposit A and B included 17 Piston Press tests. Piston Press testing included 8 and 9 Piston Press tests conducted on Deposit A and Deposit B, respectively. Results from Deposit A and B were compared to results from Deposit C. Deposit C, included a standard 31 sample Piston Press test program designed to examine HPGR amenability and variability.

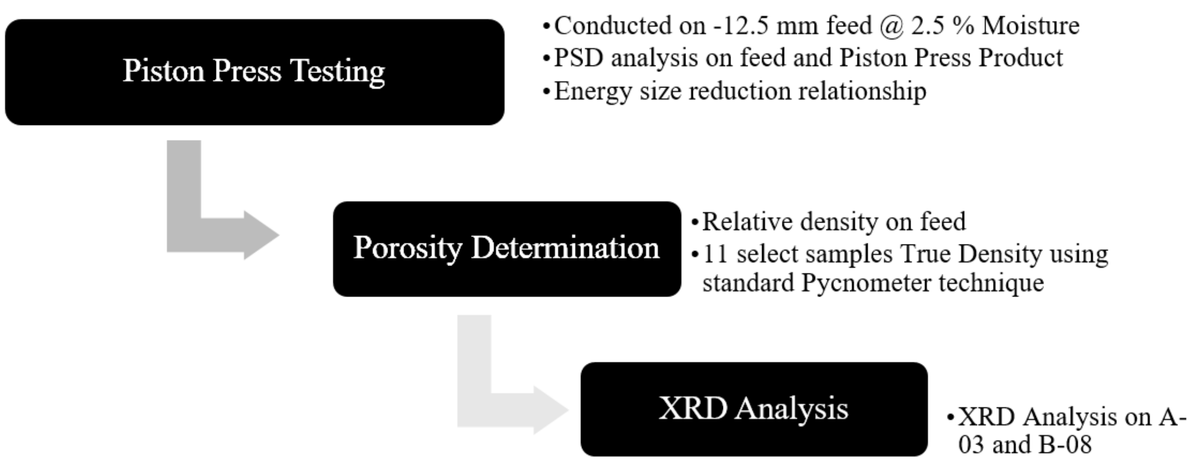

Figure 4-2: Overview of Test-work on Porosity

4.2.3 Determination of Porosity

Two methods were used to compare porosities and relative porosities between samples. The initial method included comparing the true material density of the pulverized sample to the relative density of water. The second method incorporated the measure bed density at maximum compression during Piston Press testing. The relative density was determined from the Piston Press test feed by weighing a minimum of 20 rocks both dry and in water.

The relative density and true density of samples were calculated as according to equation 17 and 18. The true density of a sample of approximately ~ 8 to 10 g was split from a 100 g pulverized split of the respective Piston Press test feed sample. The ~ 8 to 10 g was placed in the pycnometer with a known volume and filled with distilled water. Gas was removed from the pycnometer by boiling the samples and subsequently cooling weighing the pycnometer and sample at ambient temperature. A minimum of two true density measurements was performed for each sample to ensure consistent results. The true density was calculated according to Equation 17. The sample porosity was calculated according to equation 18. Porosity was determined by the percent of void space in the sample assuming that true S.G. density represented material with no void space.

$$\boldsymbol{\rho_R = \frac{W_{Air}}{W_{Air} - W_{H2O}} * \rho_{Water}}$$

Equation 17

Where,

ρ_R= Relative density to water, g/cc

W_{Air}= Weight measured dry, g

W_{H2O}= Weight measured in water, g

$\boldsymbol{\rho}_{Water}$ = Density of water, g/cc

$$\boldsymbol{\rho_s = \frac{M_s}{V_T-(M_T-M_s)*\rho_T}}$$ **Equation 18**

Where,

ρ_s = Density of solid, g/cc

M_s = Mass of solid, g

M_T Total mass of the pycnometer, water, and solid, g

V_T = Total volume of the pycometer, water, and solid, cc

ρ_T = Density of water at a known temperature, g/cc

$$\boldsymbol{Vv = 1 - \frac{\rho_R}{\rho_t}}$$ **Equation 19**

Where,

Vv = Volume of void space, %

ρ_t= True density, g/cc

A proxy density measurement was used to compare relative changes in porosity between samples of all three deposits using. The effect of porosity was compared for Deposit A, and Deposit B and Deposit C by using equation 19 to compare the Piston Press test final packed bed densities to the relative sample density to water for each respective sample.

This assumption was deemed acceptable since the density of the packed bed will approach the true density of the material at maximum compression.

$$\boldsymbol{\rho_p = P.B.D - \rho_R} \qquad \textbf{Equation 20}$$

Where,

ρ_p = Proxy density, g/cc

P.B.D = Packed bed density, g/cc

ρ_R = Relative density, g/cc

4.3 Duplicate Results of Testing of Dry and Wet Splitting

Overall, both dry and wet splitting the Piston Press test feed riffle yielded similar results in terms of specific energy input (consumption). Higher moisture samples of 5% and 3% for wet splitting and dry splitting yielded excellent matching PSDs. Minor differences were noted at lower moisture levels of 1.5%. However, overall Piston Press test-work conducted at higher moisture levels of 3% and 5% resulted in less variability of test results. A lack of agglomeration of the fines was noted at a 1.5% moisture level for Piston Press testing. At moisture of 1.5% sample did not appear to agglomerate as well as compared to 3% and 5% moisture levels. By visual inspection during Piston Press testing, slight stratification of the fines from larger particles was during loading of the piston die. When stratifications occurred, the large particles experience significantly higher point load on than when the fines are agglomerated. It is possible that the stratification of the bed varied depending on how the sample was loaded, which may have affected the packing characteristics of the sample during the Piston Press test.

The results indicate that moisture and agglomeration of fines are essential to improving reproducibility of the Piston Press test. Figures 4-3 to 4-5 show PSD feed sizes for the sample riffled at 5%, 3%, and 1.5% moisture compared to the duplicate sample riffled and split dry. All PSDs indicate that the wet splitting produced Piston Press test feed that is suitable for reproducible Piston Press test results.

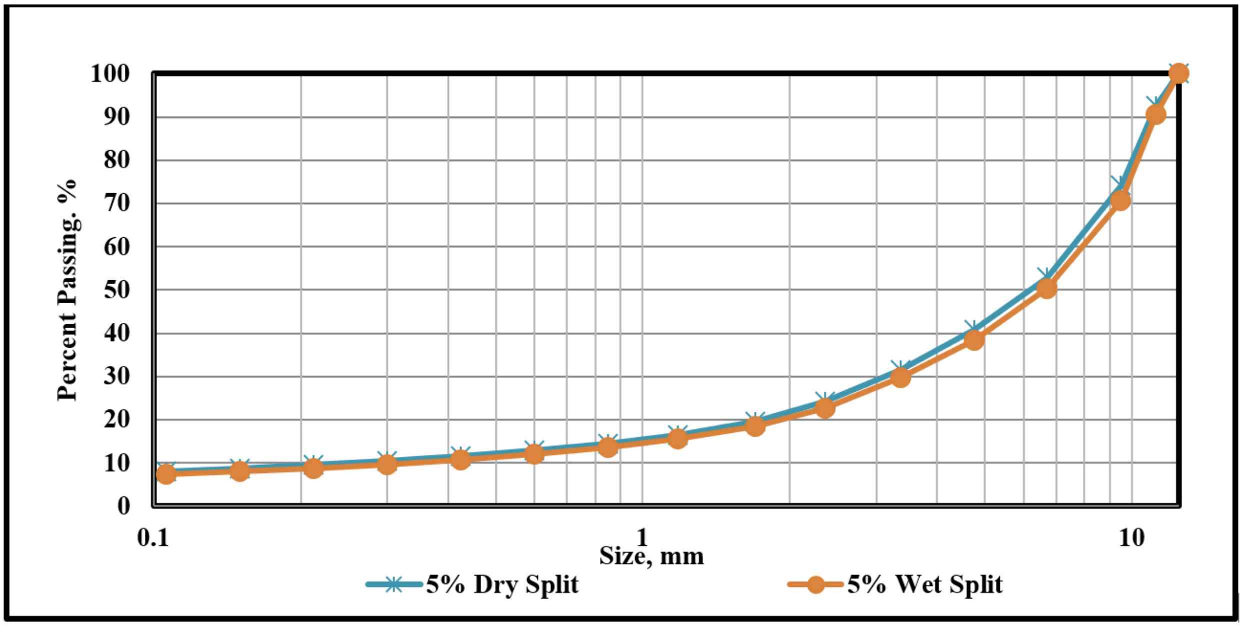

Figure 4-3: Comparison of the PSD of Wet (5% moisture) and Dry Splits

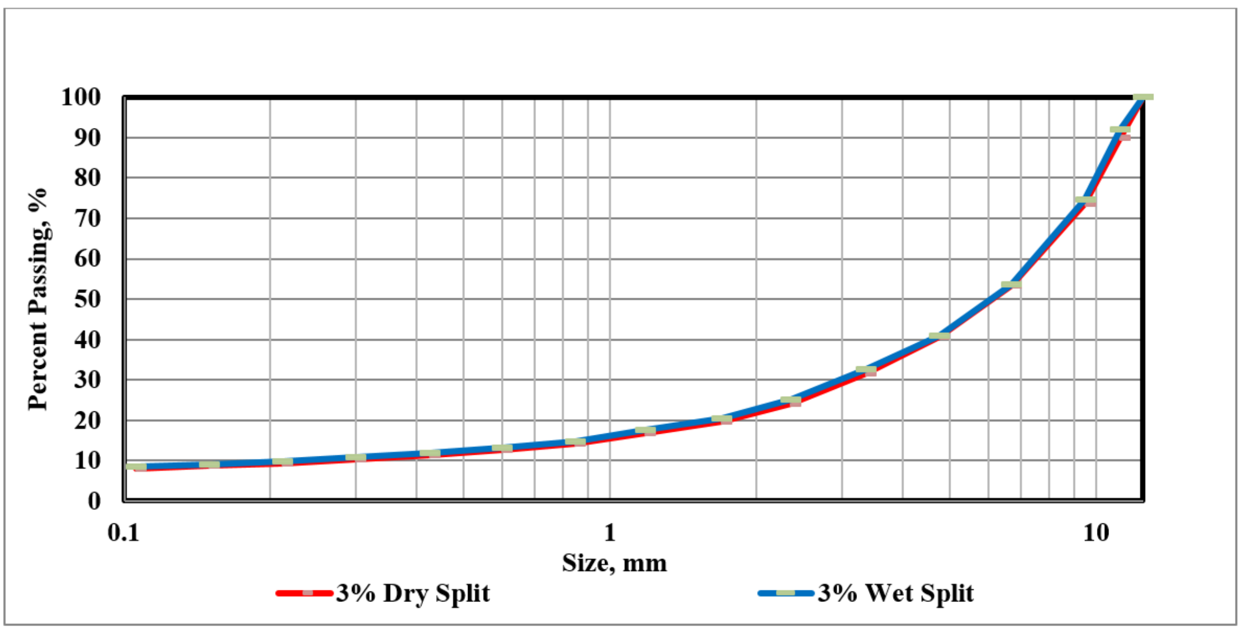

Figure 4-4: Comparison of the PSD of Wet (3% moisture) and Dry Splits

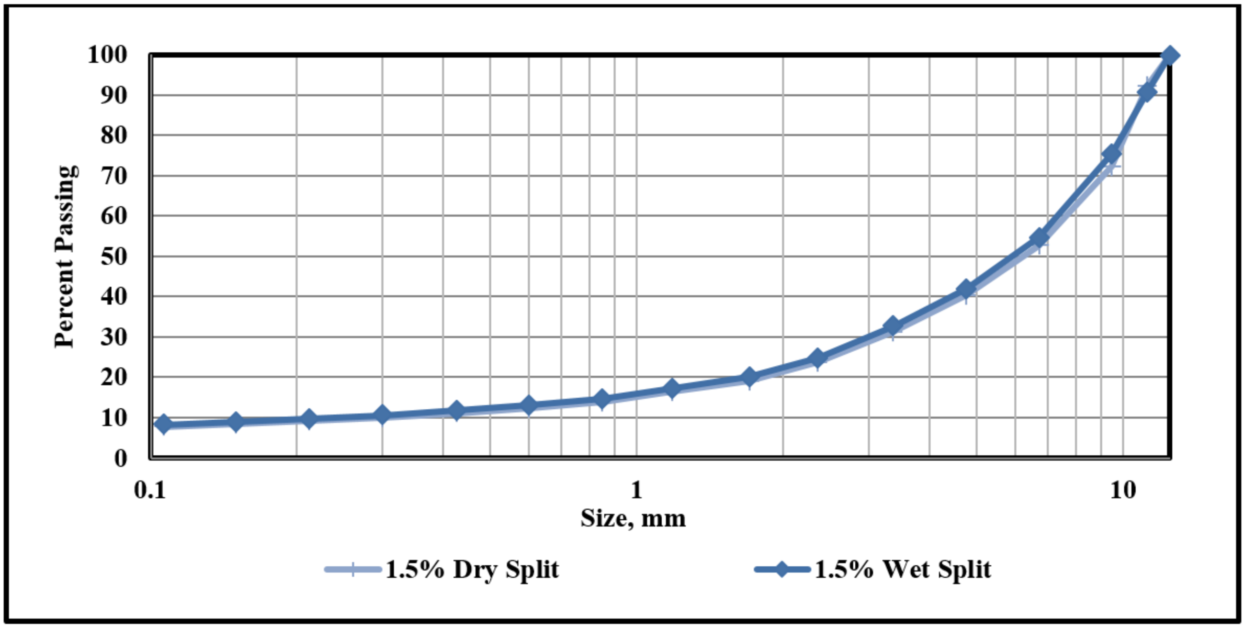

Figure 4-5: Comparison of the PSD of Wet (1.5% moisture) and Dry Splits

4.4 Effects of Moisture on the Piston Press Test

The results indicate that specific energy consumption remained consistent over varying energy levels and moisture. As shown in Figures 4-6 and 4-7, there was neither a clear trend nor a shift in the specific energy consumption over different moisture levels. However, breakage was found to improve consistency with increasing moisture levels. As evident in Figure 4-8 and 4-9, the energy reduction ratio curves shift upward with increased moisture. Increasing moisture levels improved energy transfer through the particle bed during Piston Press testing. The wet split duplicate test shown in Figure 4-9 showed a clear shift upward with increasing moisture than the dry split duplicate. This result is likely due to better agglomeration as the moisture is introduced earlier during the sample preparation. The improvement in breakage due to increasing moisture is likely a result of better packing, which facilitates inter-particle breakage during the test. This finding is similar to the HPGR results, which typically finds improvement in reduction ratio breakage with higher moisture levels.

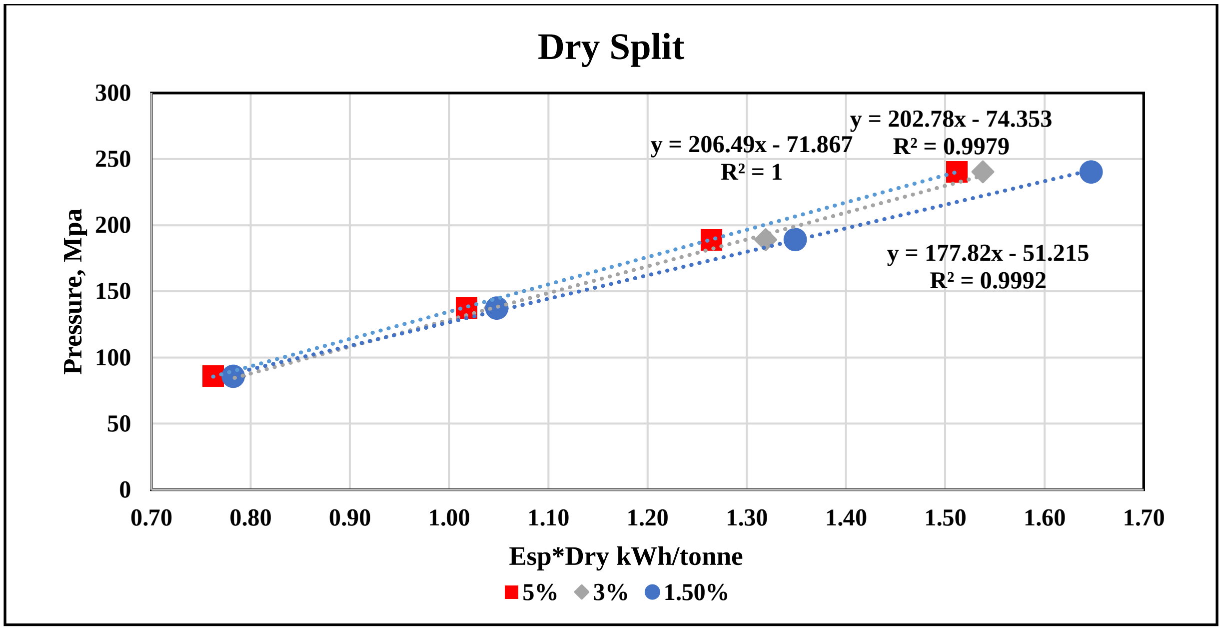

Figure 4-6: Specific Energy Consumption at Varying Moisture levels (Wet Split)

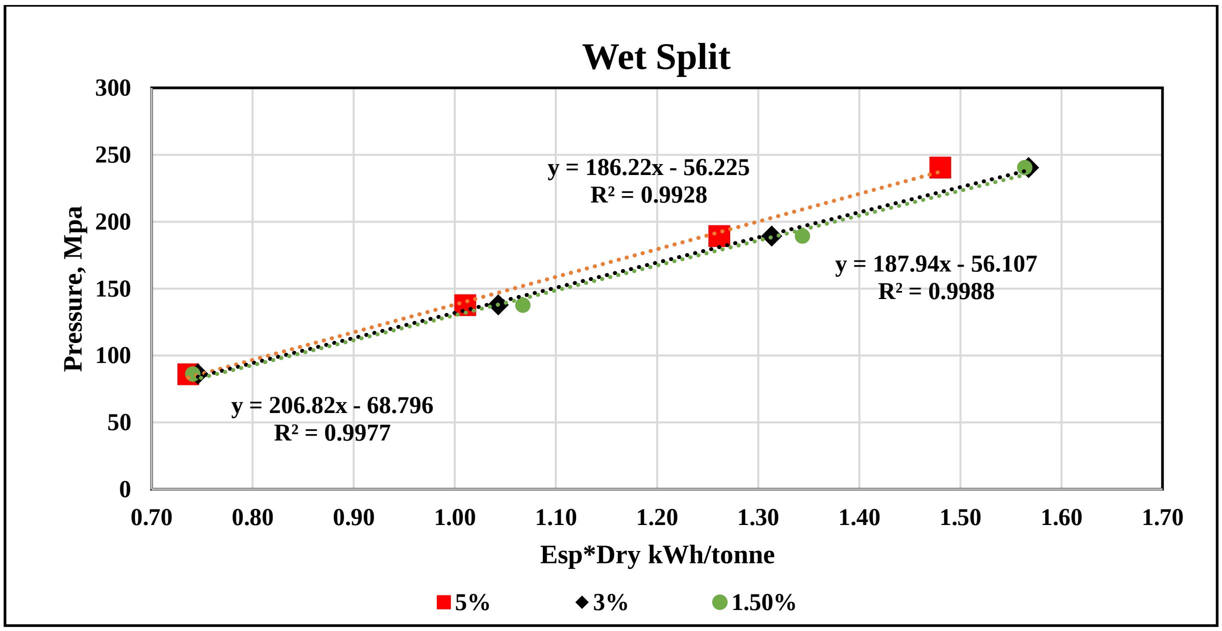

Figure 4-7: Specific Energy Consumption at Varying Moisture Levels (Wet Split)

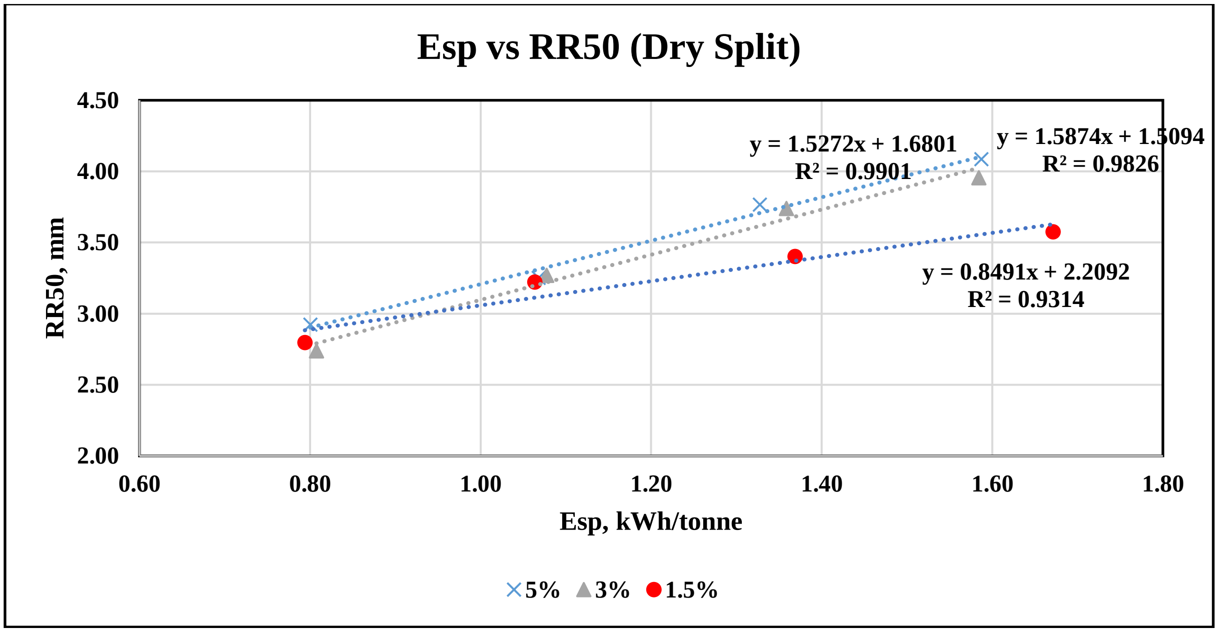

Figure 4-8: Reduction Ratio Performance on Dry Split Samples at Varying Moisture Levels

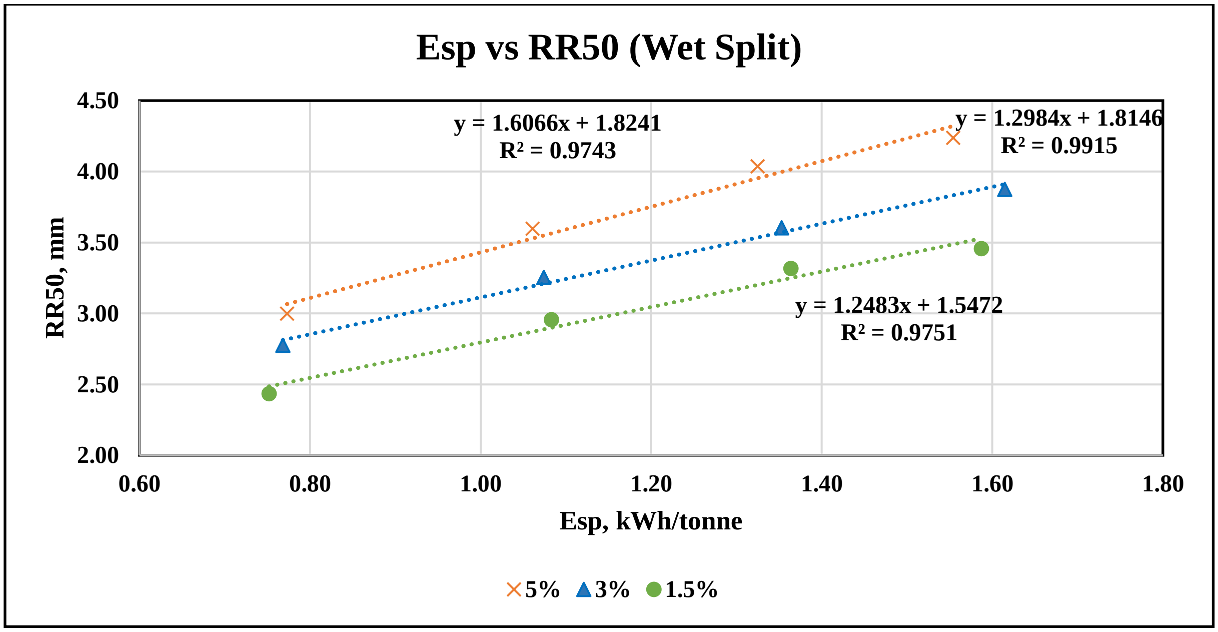

Figure 4-9: Reduction Ratio Performance on Dry Split Samples at Varying Moisture Levels

Test results as presented in Figures 4-6 and 4-7 found specific energy consumption on average decrease by 0.76% with an increase from 1.5% to 5% moisture. Both Piston Press duplicate tests showed the dry and wet splits had improved reduction breakage with increased moisture as shown in Figures 4-8 and 4-9. Results displayed in Table 4-1 showed the prepared wet split Piston Press tests had an improved reduction breakage (RR_{50}) of 14.3% from moisture increases from 1.5 % to 5%. Specific energy consumption fell by 5%. The duplicate dry split test showed similar results with the reduction ratio (RR50) increasing by 22.6 % while the specific energy consumption decreased by 2.1% over the same range of moisture.

Table 4-1: Summary of Effects of Moisture on Piston Press Testing

Wet Split		
	From 1.5% to 5% Moisture	
Pressure	**% increase in Esp**	**% Increase in RR50**
240 Mpa	-2.1%	22.6%
189 Mpa	-2.9%	21.7%
138 Mpa	-2.1%	21.7%
86 Mpa	2.8%	23.2%
Dry Split		
	From 1.5% to 5% Moisture	
Pressure	**% increase in Esp**	**% Increase in RR50**
240 Mpa	-5.0%	14.3%
189 Mpa	-3.0%	10.7%
138 Mpa	0.4%	0.9%
86 Mpa	0.8%	4.5%

Results from the Piston Press testing indicate that higher moistures from the range of 1.5% to 5% improved high-pressure compression breakage for the material tested. This finding may be a result of improved sample agglomeration with fine particles with improved packing characteristics. Increasing fines dispersed within the bed may have helped facilitate energy transfer evenly throughout, resulting in higher efficiency. This finding is consistent with the common belief that the loss of energy efficiency of the HPGR at higher moisture is principally related to the loss of material throughput caused by roll slippage. In other words, excessive moisture can reduce the coefficient of friction between the material and the roll, leading to increased roll slippage. If this finding is correct, increasing friction along the roll of the HPGR may help improve material intake for levels of moisture above 5% when roll slippage begins to increase. The majority of the research on liners has been performed to reduce roll wear and not to improve material throughput. Therefore, the finding that an increase of moisture from 1.5% to 5% improved breakage in high-pressure comminution is worth considering in future research. The research carried on was done on two different composites. However, more research is needed to see if a similar effect is possible on different ore types.

4.5 Correlation of Porosity to Piston Press Testing

Data from three different deposits were examined to determine if porosity was significant to the Piston Press test. Samples represented varying lithologies, alterations and rock types across each deposit. During Piston Press testing, tests conducted on Deposit A and Deposit B noted exceptional reduction ratio performance. It was also noted that during testing, the density of the compacted bed at maximum compression in some cases exceeded the S.G. of the sample. As such, S.G. was re-measured using a pycnometer technique that was verified using XRD analysis to determine mineralogical composition for two of the samples. The XRD results were used to determine the composition of the select samples in order to verify the S.G. of the material. The Piston Press test results demonstrate that porosity significantly affects the reduction ratio breakage.

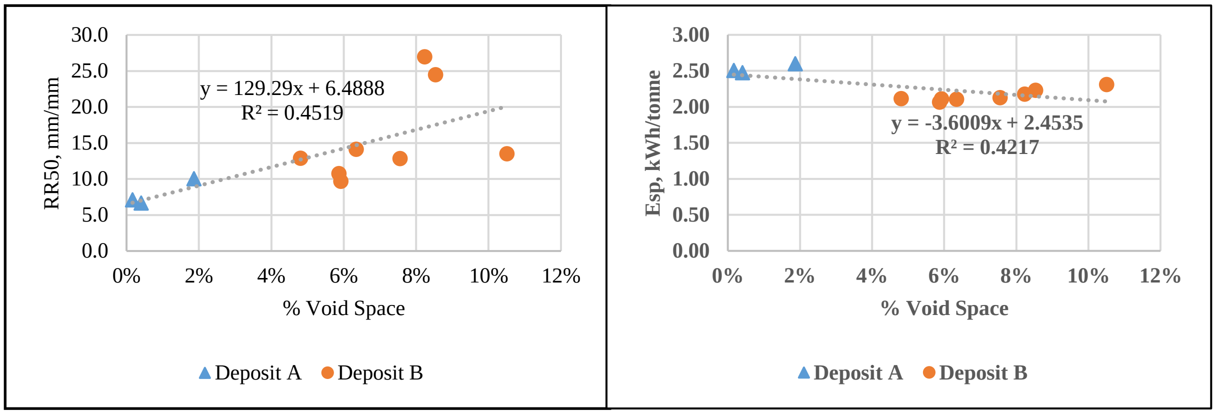

Figure 4-10: Effect of Porosity on Piston Press Testing

Figure 4-10 shows the relationship between the percent void space of Piston Press test sample to the reduction ratio breakage and specific energy consumption for Deposit A and Deposit B. As can be seen the porosity appears to an exhibit a relationship to the breakage performance.

Figure 4-10 shows the Piston Press test achieved higher reduction ratios on samples with higher levels of porosity. However, the specific energy consumption showed smaller changes to increased porosity than the reduction ratio.

Table 4-2: Statistical Significance of Porosity on Deposit A and B

	RR50	Esp
T-Test	2.23	2.23
P-Value	4.27E-05	1.05E-10
T-Value	6.89	27.19

For Piston Press tests on samples of which porosity was measured Both the T-test and P values (Table 4-2) indicate that porosity's effect on breakage performance is statistically significant for Deposits A and B. The statistical significance was further validated using equation 19 when examining Deposit A and B.

Figure 4-11 shows the correlation of porosity to reduction ratio performance using both equations 18 and 19, respectively. As is evident, the equation 19 (proxy density) showed similar shape when comparing to the relationship found between the porosity and reduction ratio performance of Deposit A and Deposit B.

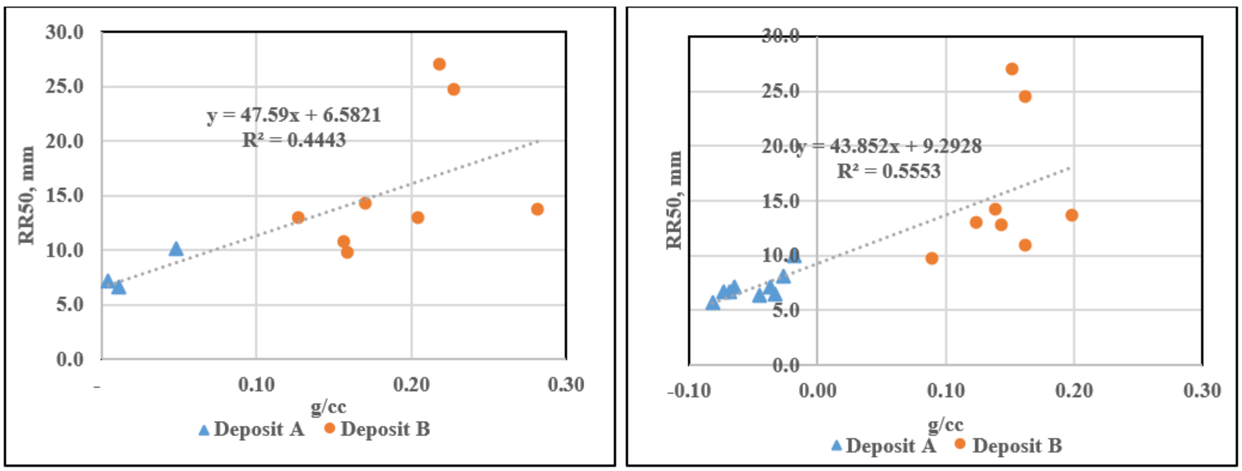

Figure 4-11 Comparison of Using True Density versus P.B.D (Density Proxy) to Determine the Effects of Porosity

When including Deposit C using equation 19, the proxy density showed the reduction ratio breakage being well correlated to porosity for all three deposits. As is shown in Figure 4-12, Deposit C, which had the lowest Piston Press test variability and porosity, showed the lowest levels of reduction ratio breakage. Table 4-3, further confirms the statistical significance of porosity to reduction ratio performance.

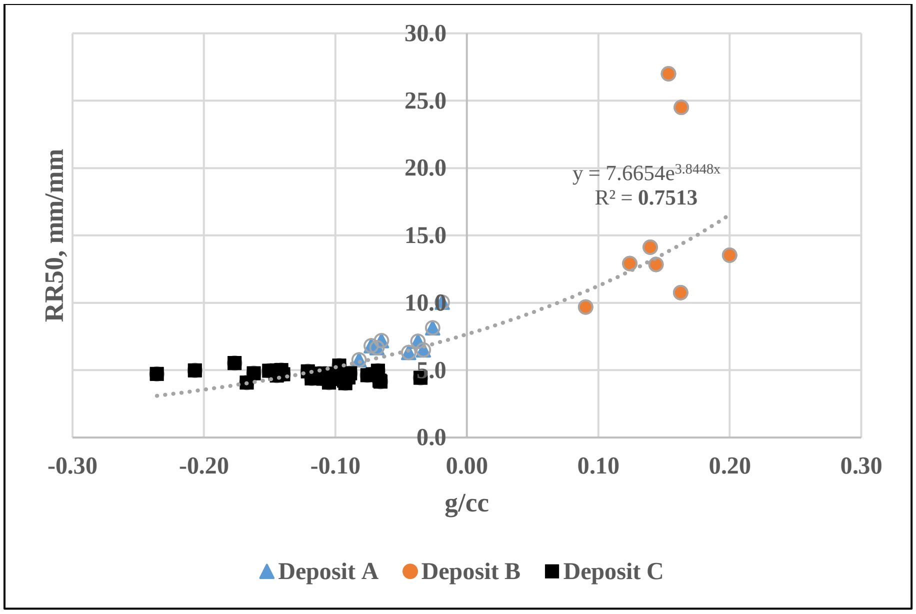

Figure 4-12: Correlation of the Proxy Density to RR50 Breakage for Deposits A, B, and C

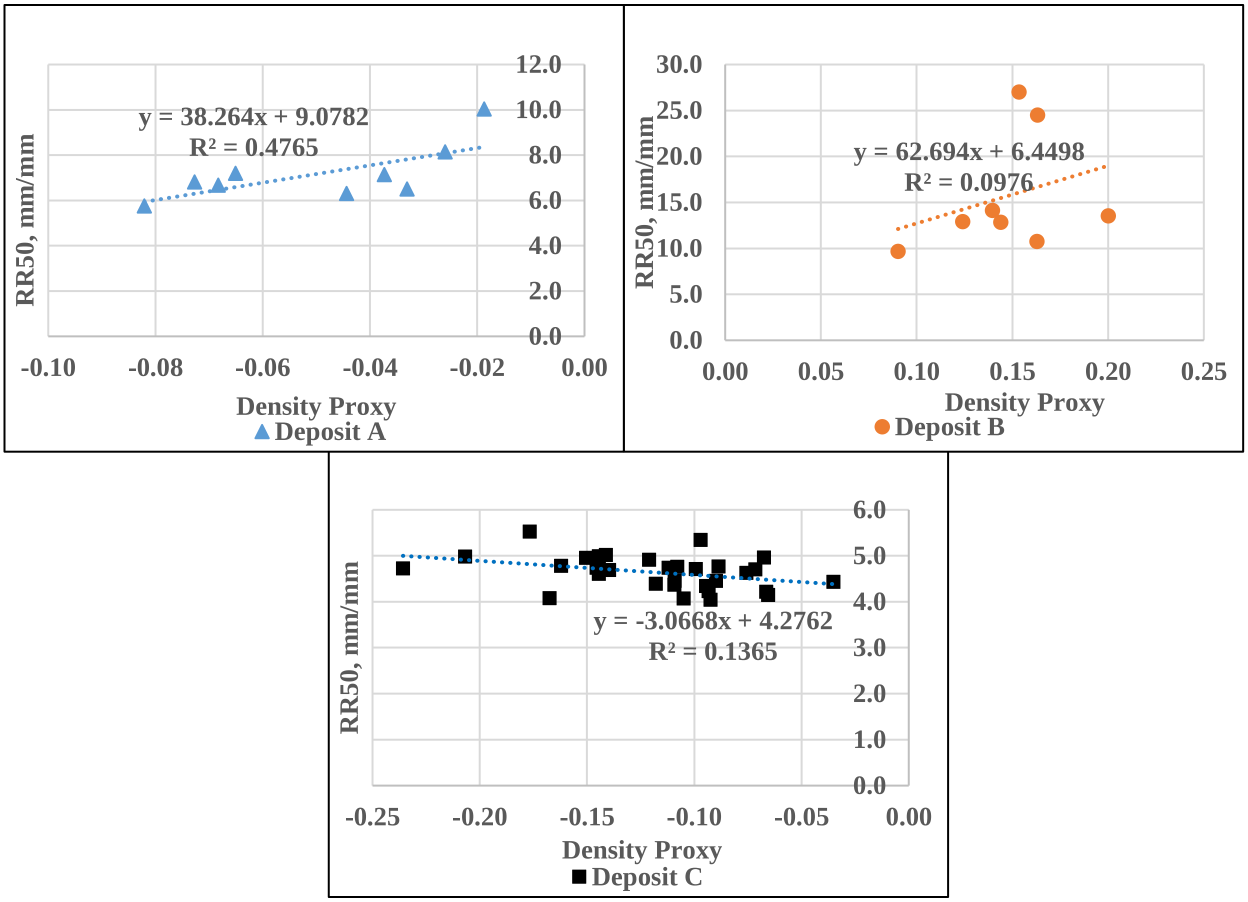

Figure 4-13: Correlation of Density Proxy to RR50 Breakage for Deposits A, B, and C

Table 4-3: Statistical Correlation between Porosity and the Density Proxy for Deposits A, B & C

	Porosity Proxy (A to C)		Porosity Proxy (A& B)		Porosity Proxy C	
T-Test	2.01	2.01	2.12	2.12	2.04	2.04
P-Value	1.18E-13	3.44E-47	1.18E-06	3.22E-15	1.07E-34	2.56E-35
T-Value	10.31	63.42	7.54	28.82	69.43	72.85

The correlation between the Piston Press test and porosity was further exploring the relationship with respect to the Piston Work Index (W_{pi}) (equation 13). An exponential relationship was found between the Proxy Density and the W_{pi}, as shown in Figure 4.14. In total, 48 paired data sets were used to determine if the significance of the correlation with regards to deposits tests. As evident in Table 4-4, both the $W_{pi}50$ and $W_{pi}80$ appear statistically significant for all deposits.

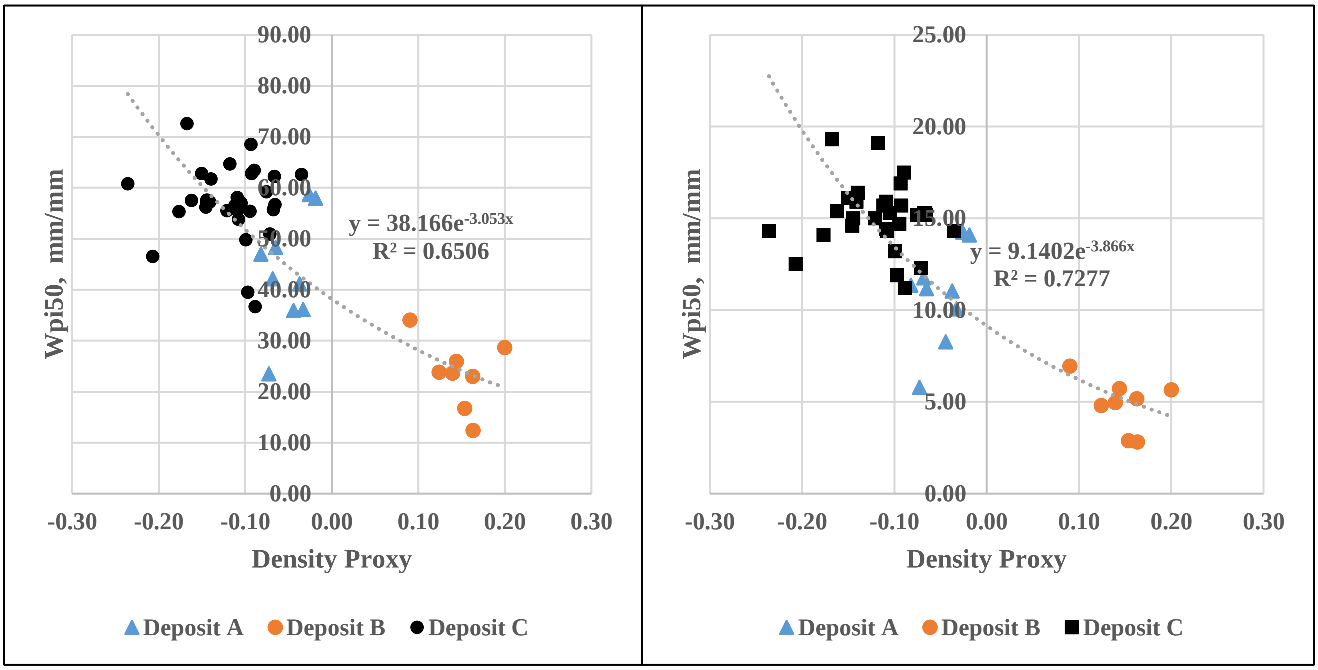

Figure 4-14: The Correlation of Porosity to the Piston Press Work Index ($W_{pi}50$ and $W_{pi}80$)

Table 4-4: Statistical Significance between the Piston Work Index to the Porosity Proxy

	Porosity Proxy (A to C)		Porosity Proxy (A& B)		Porosity Proxy C	
	Wpi50	Wpi80	Wpi50	Wpi80	Wpi50	Wpi80
T-Test	2.01	2.01	2.12	2.12	2.04	2.04
P-Value	1.17E-24	5.78E-27	1.97E-07	2.06E-08	1.01E-29	9.42E-29
T-Value	2.01	22.69	8.65	10.21	47.24	43.80

4.5.1 Discussion

All three deposits had varying levels of porosity. Porosity was well correlated to reduction ratio breakage. In some instances, the relationship of porosity to the reduction ratio breakage was dramatic with reduction ratios ranging from ~5 to 15 or higher for sample with higher levels of porosity. In addition, the porosity as indicated by the Density Proxy method is statistically significant for the three deposits analyzed. More study will be needed to confirm if porosity is significant over varying deposits and deposit types. However, if porosity is found to be significant in future test programs on varying ore types, porosity may help understand ore variability in regards to HPGR amenability.

The effect of porosity on reduction ratio is likely a consequence of fatigue crack propagation. As illustrated in Figure 4-13, the outer surface of the void space experiences a higher pressure difference between the external and internal forces at the surface of the void. This increased loading at the surface of the void acts as a catalyst for fractures to form and propagate. The new fractures that form become new weakness plans that are driven by a high differential between the internal and external forces along the surface of the crack. This pressure difference acts as a catalyst for the fracture to continue to propagate.

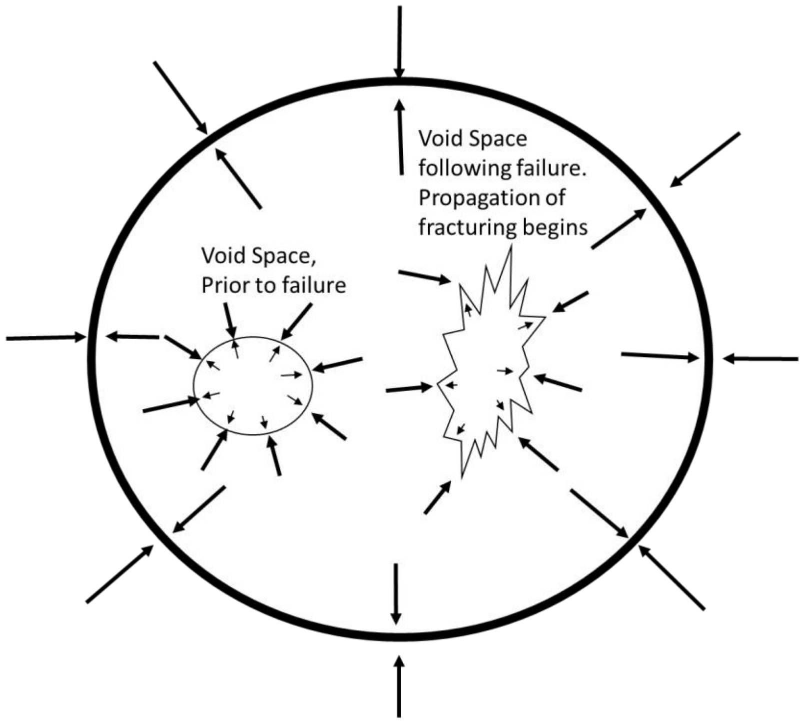

Figure 4-15: Effect of Porosity on Comminution

Clusters of the voids likely act as propagation networks which, increases the number of fracture planes that occur. Fatigue crack propagation is likely the mechanism for which the reduction ratio breakage improves with increases of porosity. To date, little literature or research has been conducted to evaluate the impact of porosity on the HPGR performance. It is not currently a property that is measured and used for sizing by vendors and manufacturers.

The proxy density (equation 19) could easily be incorporated into the current operating procedures for the Piston Press test. If further testing demonstrates porosity to be significant across additional deposits and ore types, it is recommended to incorporate the proxy density in the Database Calibrated methodology. Historically, porosity has not been a variable that was considered nor measured in past test-work at UBC, and therefore, cannot be easily incorporated into the current Database Calibrated methodology. Further testing across additional deposits and rock types are needed to establish if a similar correlation exists in general between reduction ratio breakage and porosity.

Chapter 5: Reproducibility of Piston Press Testing

The reproducibility of the Piston Press test was evaluated by conducting duplicate tests at UBC and an independent metallurgical lab, ALS Metallurgy. Careful consideration was needed to ensure the Piston Press test produced a reproducible product, as well as matching specific energy consumption. A specific approach for integrating the force-displacement data in order to calibrate the specific energy consumption measurement to the Piston Press test facility at UBC. This approach could be applied to modify existing piston press equipment and facilities to allow Piston Press tests at other metallurgical labs to be conducted. This chapter covers the specific program methodology, laboratory facilities, and results carried as part of this test-work.

The duplicate Piston Press tests showed reproducible results. Both labs produced a similar product from the same Piston Press test material. However, reproducing the specific energy consumption proved to be more difficult as both the frequency of measurements and precision differed between the labs. Ultimately, it was found that the Piston Press test results from ALS Metallurgy required a correction that averaged the data by a set number of data points in order to have a similar measurement frequency of Piston Press tests conducted at UBC tests. This correction was needed in order to compare the specific energy consumption of test results from both labs. After incorporating the recommended approach for comparing the results from the two labs, the duplicate testing showed that both Piston Press test lab facilities produced equivalent test results for determining the energy size reduction relationship of a same given material.

5.1 Methodology

The program involved performing Piston Press testing at ALS Metallurgy on duplicate samples of two known feed samples. The testing was carried out on material collected from the Tropicana Gold mine full-scale HPGR operation including both the HPGR feed and HPGR + 2 mm recycle material. An overview of the methodology used in evaluating the reproducibility of the Piston Press test is presented in Figure 5-1. ALS Metallurgy crushed the homogenized feed and recycle material to -12.5 mm and split the samples into batches of approximately 10 kg sub-samples. Roughly, 100 kg of full-scale HPGR feed and 100 kg of full-scale HPGR +2 mm recycle was sent to UBC. The respective Piston Press test feeds were prepared by the respective lab in accordance with the Piston Press testing procedures presented in Chapter 3. PSD Piston Press feeds produced at UBC and ALS were matching, which was necessary to ensure uniform testing conditions.

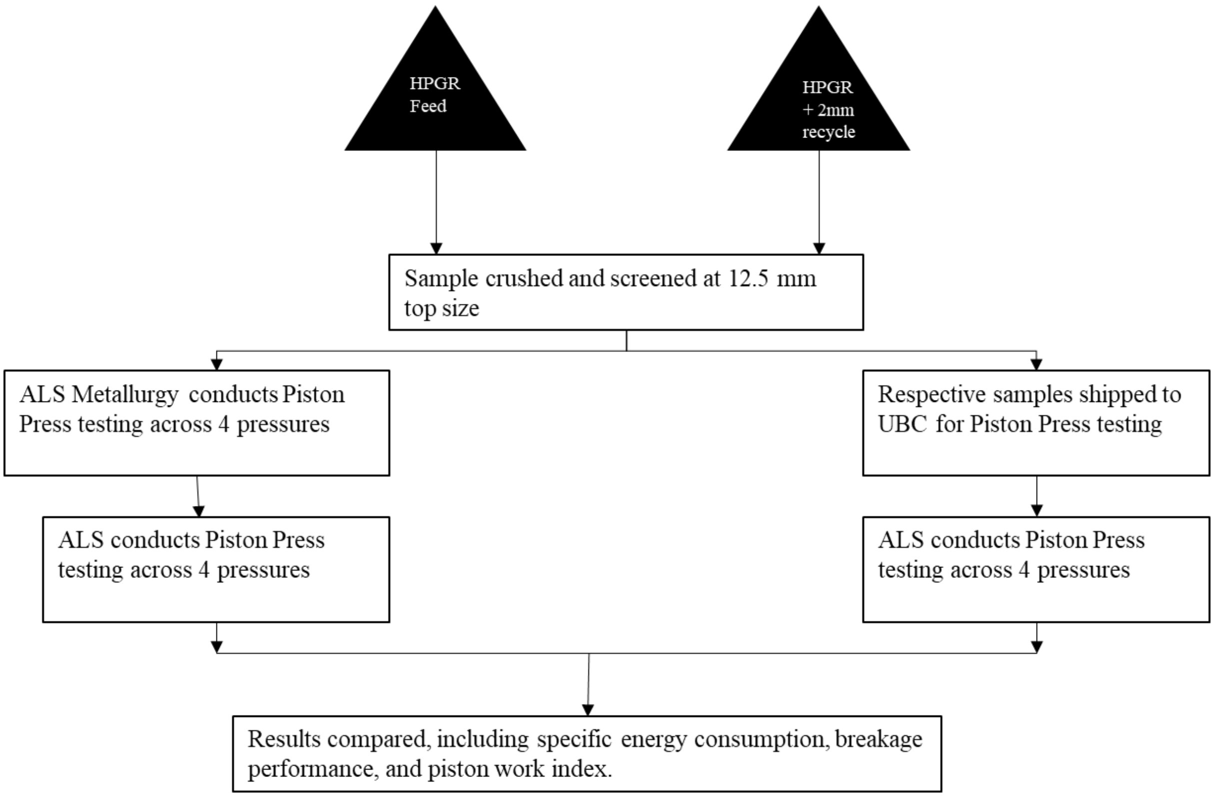

Figure 5-1: Methodology for Evaluating the Reproducibility of the Piston Press Test

In total duplicate testing was compared between the two labs on four Piston Press tests which included performing a minimum of 16 piston presses and 16 different Piston Press test products at each facility. Results from both labs were compared for the respective specific energy consumption, feed size, and PSD analysis of each sample tested. The comparisons properly evaluate the energy reduction ratio relationship of the respective samples. Results were compared using the Piston Work index, which as an operator's work index can be used to compare HPGR amenability of various samples. The Piston Work index is determined from the average of the Piston Press test results, typically 4 to 8 tests. The Piston Work index is determined according to equation 13 (Refer to Section 2.5).

$$\boldsymbol{Wpi80_n} = \boldsymbol{Esp} / \left[\mathbf{10} * \left[\frac{\mathbf{1}}{\boldsymbol{P80^{0.5}}} - \frac{\mathbf{1}}{\boldsymbol{F80^{0.5}}}\right]\right] \quad \textbf{Equation 11}$$

$$\boldsymbol{Wpi50_n} = \boldsymbol{Esp} / \left[\mathbf{10} * \left[\frac{\mathbf{1}}{\boldsymbol{P50^{0.5}}} - \frac{\mathbf{1}}{\boldsymbol{F50^{0.5}}}\right]\right] \quad \textbf{Equation 12}$$

$$\boldsymbol{Wpi(50,80)} = \frac{\sum_i^n \boldsymbol{Wpi(50,80)}}{\boldsymbol{n}} \quad \textbf{Equation 13}$$

Where,

$W_{pi(50/80)}$ = Piston Work index (50% or 80%) [kWh/tonne],

Esp = Specific energy consumption [kWh/tonne],

P_{80} and P_{50} = Product size at 80% or 50 % passing [mm], and

F_{50} and F_{80} [mm] = Feed product size at 80% or 50% passing [mm].

5.2 Laboratory Setup

The Piston Press (UCS) rock mechanics facility at ALS Metallurgy in Perth, WA was modified to mirror the setup developed at UBC. This process included a minimum capable applied force of 1400 kN equating to a pressure in the piston of 240 Mpa. A separate displacement sensor was installed that was capable of measuring at a precision of 0.001 mm at a frequency of approximately 22 displacement and force measurements per second.

5.3 Machine Specifications

The following is a technical comparison between the two labs. The principle differences that caused issues were the measurement intervals and precision differences.

5.3.1 UBC Specifications

- Max loading 1399 kN
- Loading rate 200 kN/min
- Measurement interval 0.25 s/interval
- Precision of displacement reading 0.1 x 10^{-9} mm
- Die DxH = 86 mm, 60 m

5.3.2 ALS Specifications

- Max loading > 1400 kN
- Loading rate 180 kN/min
- Measurement interval ~0.045 s (~ 22 reading /s)
- Die DxH = 86 mm, 60 mm
- Precision of displacement reading of 0.01 mm

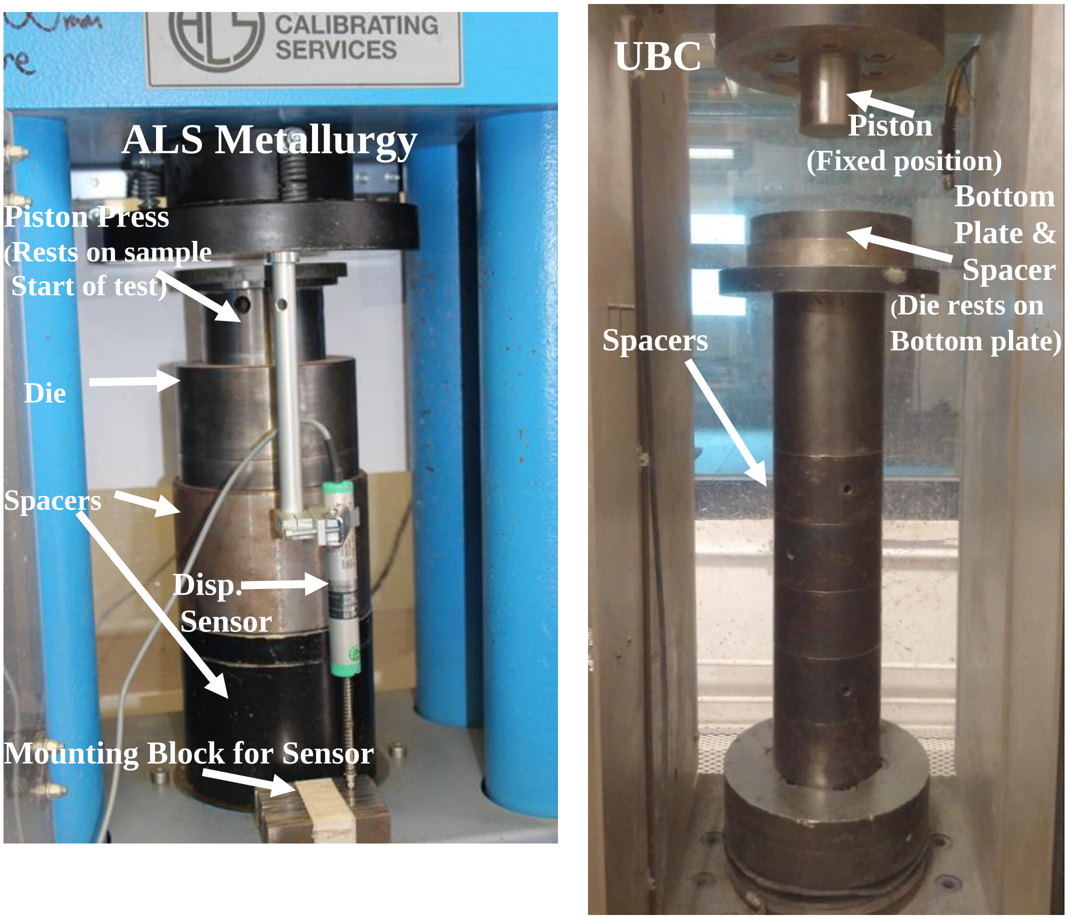

Figure 5-2: Piston Press Test Setups for Reproducibility

The ALS Metallurgy's Piston Press test setup differed from UBC. As shown in Figure 5.1, the main differences included the displacement instrument precision and frequency of measurements. The load rate varied as well, but the difference in load rate was deemed to be negligible. The difference in frequency and precision between Piston Press tests conducted at the two labs created challenges when comparing the respective Piston Press tests for specific energy consumptions of the duplicate tests.

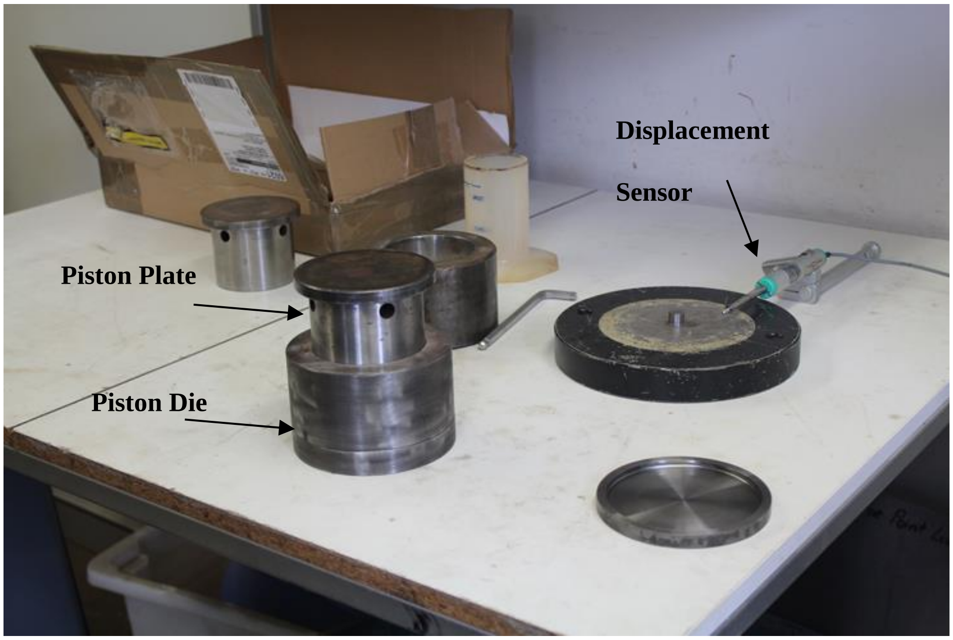

Figure 5-3: Piston and Die at ALS Metallurgy

As shown in Figure 5-2, the ALS Metallurgy Piston Press test setup used a sensor that measures net displacement during the test. The sensor is vertically mounted between the piston of the machine the base of the piston press. This type of design allows for a shorter set up time. However, it does not allow for measurements of the final material at maximum compression, because the vertical location is not known for the piston relative to the die. Therefore, at the end of the Piston Press test, the vertical location of the piston inside the die under loading is unknown.

5.4 Duplicate Testing

Duplicate testing was carried out at ALS Metallurgy and UBC to demonstrate reproducibility. Duplicate testing occurred in two phases. The initial phase included Piston Press test feed samples that were prepared at UBC. These samples were crushed to 12.5 mm passing and homogenized. A subsample of 5 to 6 kg was split and sent to ALS Metallurgy. A series of validation tests were carried out at ALS Metallurgy to ensure the Piston Press tests were carried out in accordance to UBC standard operating procedures and evaluate the ALS Metallurgy Piston Press testing facility.

Both UBC and ALS Metallurgy carried out Piston Press testing at the same pressures. Wet sieve analysis was conducted on all Piston Press test feed and Piston. Results showed matching feed and product size distributions. However, the specific energy consumption differed. The difference could be explained by the difference in the measurement intervals or frequency. As indicated in Table 5-1, the ALS Metallurgy setup took ~5.5 readings for every reading UBC took. The difference in the frequency of measurement affected the force-displacement integration by noise in the displacement curve. The higher frequency of measurement led to a consistent overestimation of the specific energy consumption when the test data was integrated. By adjusting the data to a similar frequency this issue relating to noise was resolved. Table 5-1 illustrates the difference in the frequency of measurements between UBC and ALS Metallurgy piston press machines.

Table 5-1: Force & Displacement Measurement Frequency UBC to ALS

Force, kN	Data Points per Test		
	UBC	ALS Metallurgy	UBC:ALS
1400	1676	9307	5.55
1100	1318	7307	5.54
800	958	5305	5.54
500	600	3315	5.53
	1668	9299	5.57

5.5 Specific Energy Determination

The specific energy integration of the force-displacement curve is performed using a trapezoidal function (as shown in Figure 5-3).

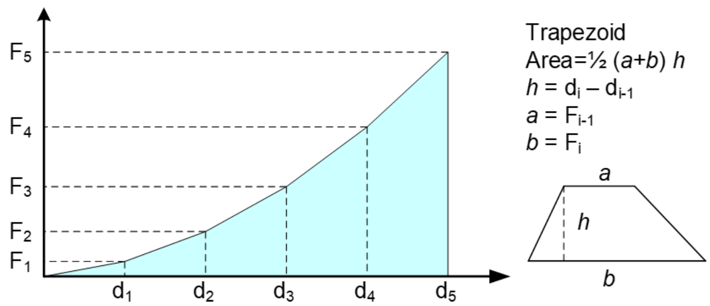

Figure 5-4: Trapezoid Method of Integration *Source Davaanyam, 2015

As the measurement frequency increases, more area will be integrated as the function approaches a better fit of the curve using the trapezoid method for integration. In addition, higher frequency of the displacement instrument measurement increases the likeliness of capturing the Piston Press tests' natural vibrations and noise. Table 5-2 is an example of a raw data reading from ALS Metallurgy. As can be seen in Table 5-2 the displacement measurement does not constantly increase with force, as the displacement vibrates between higher and lower changes of displacements as the piston die is loaded.

Table 5-2: Example of Noise during Strain Measurement

Force kN		Displacement mm	
82.136		0.172	
82.184	0.06%	0.162	-6.17%
82.372	0.23%	0.16	-1.25%
82.701	0.40%	0.173	7.51%
82.889	0.23%	0.173	0.00%
82.936	0.06%	0.161	-7.45%
83.172	0.28%	0.16	-0.63%

As Figure 5-5 demonstrates, the displacement reading at certain times captures a displacement reading lower than the previous reading which may have at a higher loaded force. During integration, this noise of the displacement curve caused a re-integration of the area, resulting in an overestimation of specific energy consumption. As Figure 5-5 demonstrates, the additional area under the curve from the displacement point D3 to D2 was being re-integrated. This effect is amplified with the frequency and at higher forces during the Piston Press test.

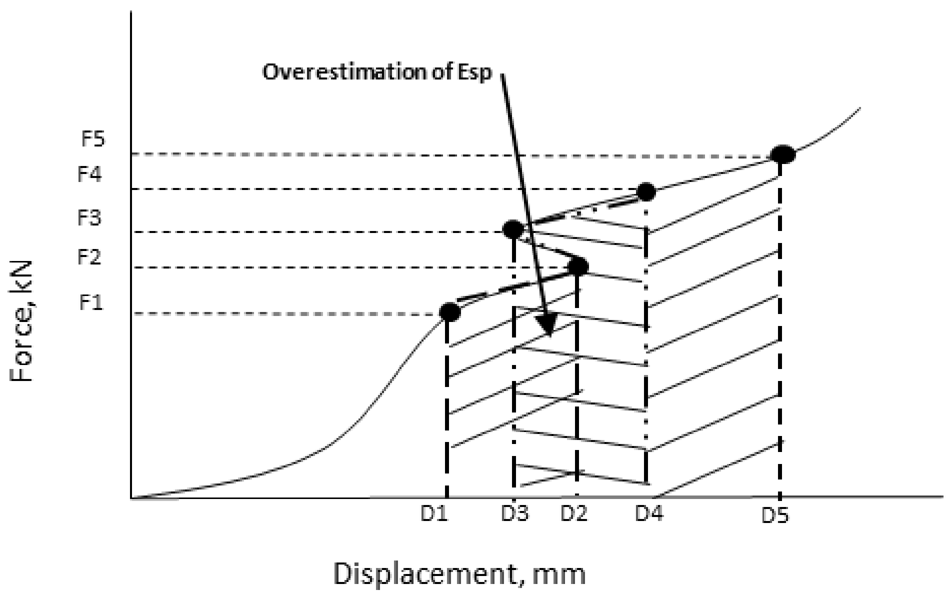

Figure 5-5: Illustration of Issue of Displacement Noise in Force-Displacement Curve

This issue was resolved by altering the algorithm used for calculating the specific energy input. The new algorithm (referred to as the non-negative displacement algorithm for the purpose of this research) is illustrated in Figure 5-6. The non-negative displacement algorithm will default to use the last highest displacement measurement when a lower displacement measurement is recorded at a higher force. Using the non-negative displacement algorithm was necessary to develop an approach that could be applied to compare the Piston Press test results from UBC and ALS Metallurgy.

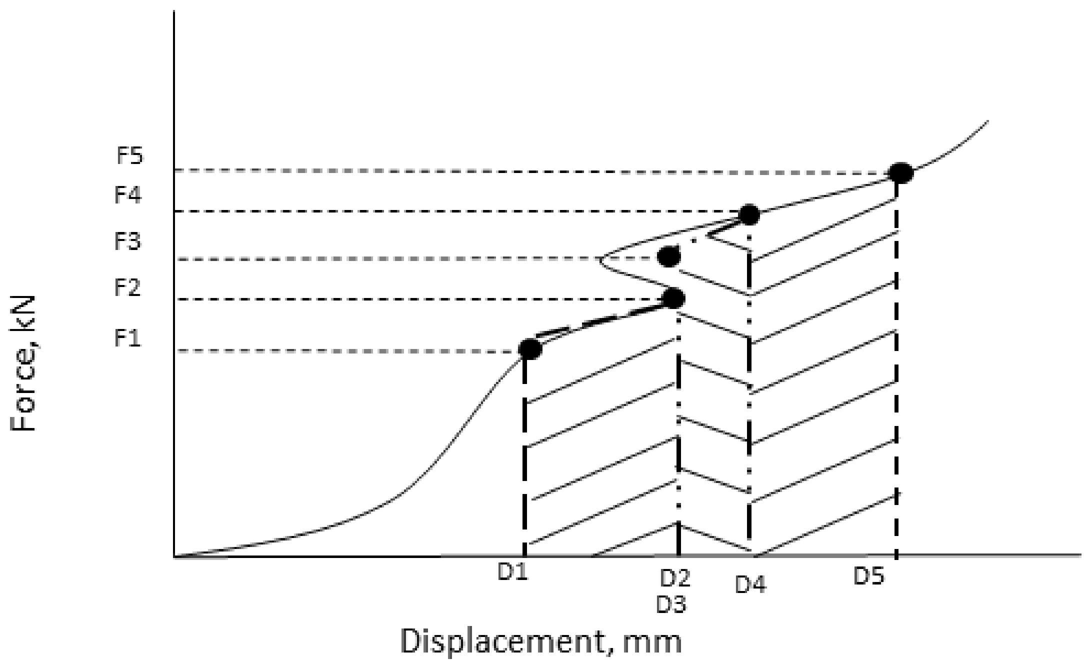

Figure 5-6 Illustration of New Algorithm for Integration of Force-Displacement Curve

To further reduce the effect of varying measurement frequency of the Piston Press test results, the raw data from the ALS Metallurgy Piston Press tests were averaged. The raw data from the ALS Metallurgy Piston Press tests were averaged to approximate a similar frequency to the UBC Piston Press test. The frequency was adjusted by determining the specific energy consumption from the raw data produced during the ALS Metallurgy Piston Press tests by 5 and 6 data points (referred to as averaging (5.5)). The average between the two values was then used as the reported specific energy consumption of the respective Piston Press test for ALS Metallurgy. This approach, as evident in Figure 5-7, adjusted the frequency and reduced the noise in the ALS

Metallurgy Piston Press tests. An additional benefit to averaging the raw data for ALS Metallurgy was that it effectively increased the precision of the displacement sensor which was significantly lower than UBC.

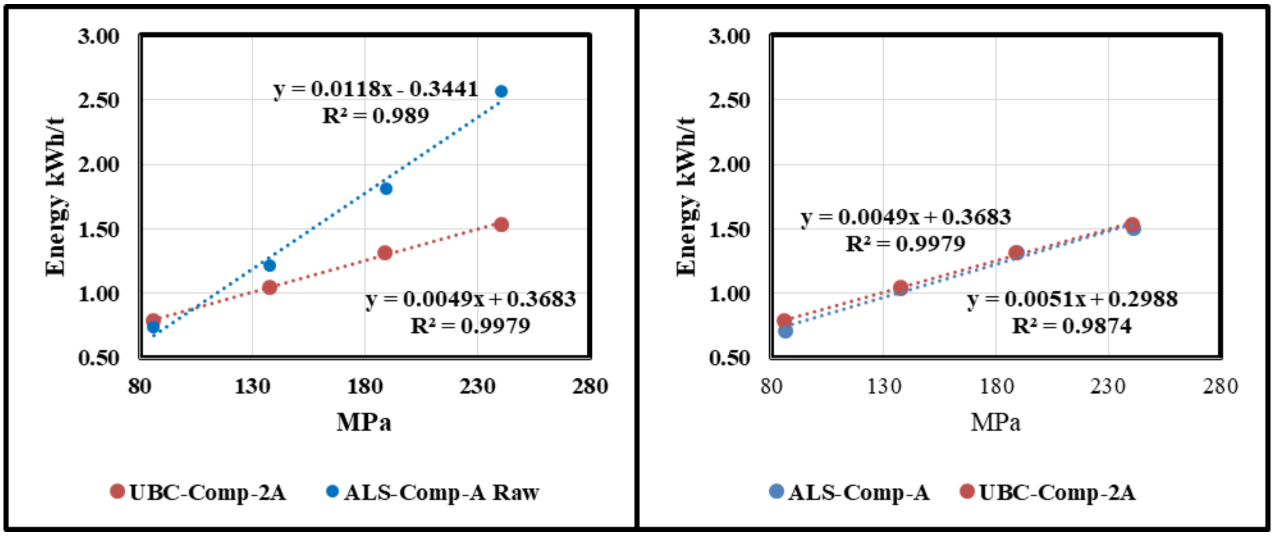

Figure 5-7: Before and After Correction to ALS Specific Energy Correction

Figures 5-8 to 5-11 demonstrates the effect the frequency of the displacement measurement is when comparing the ALS Metallurgy Piston Press test results to UBC. Figures 5-8 to 5-11, include data for four UBC and ALS Metallurgy duplicate Piston Press tests that were conducted at pressures of ~240 Mpa. The figures show that averaging the ALS Metallurgical test data by 5 to 6 points resulted in the specific energy consumptions of the duplicate tests approach similar values. As is evident in Figures 5-8 to 5-11, maintaining the frequency of measurement is important when comparing Piston Press test on varying piston press machines. The frequency of the measurement as well as the precision of the displacement instrument needs to be accounted.

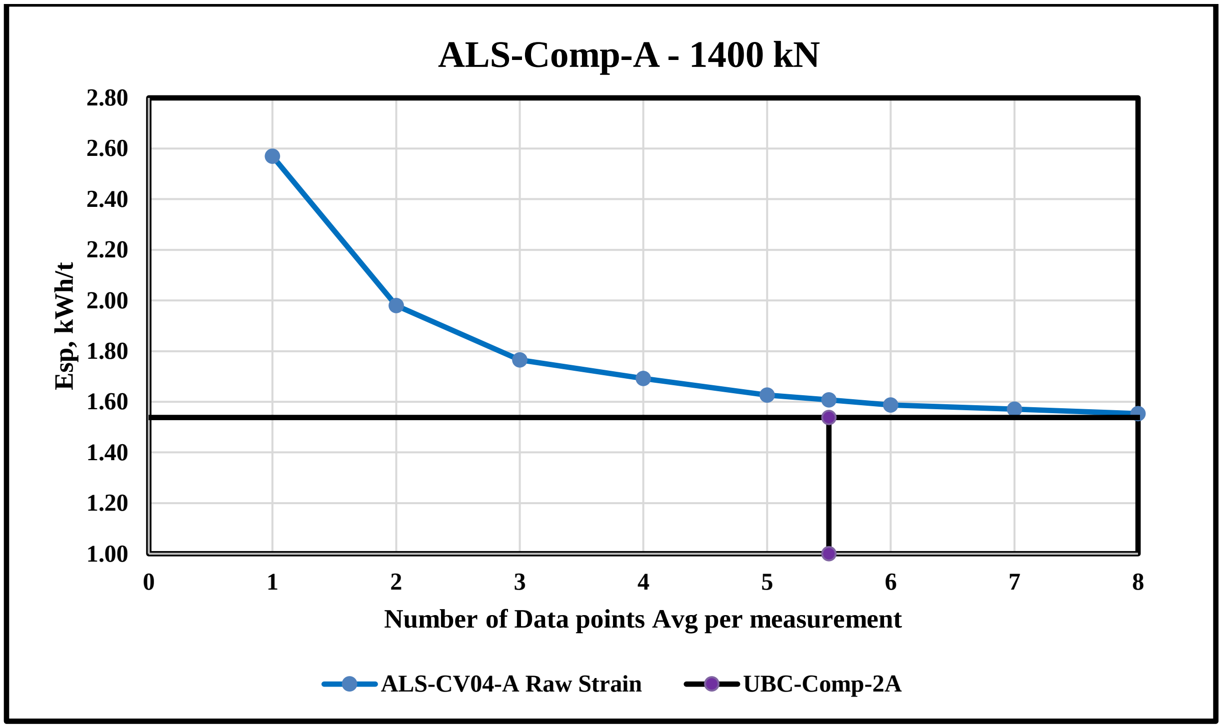

Figure 5-8: Effect of Frequency on Specific Energy Integration ALS-Comp-A @ 1400 kN

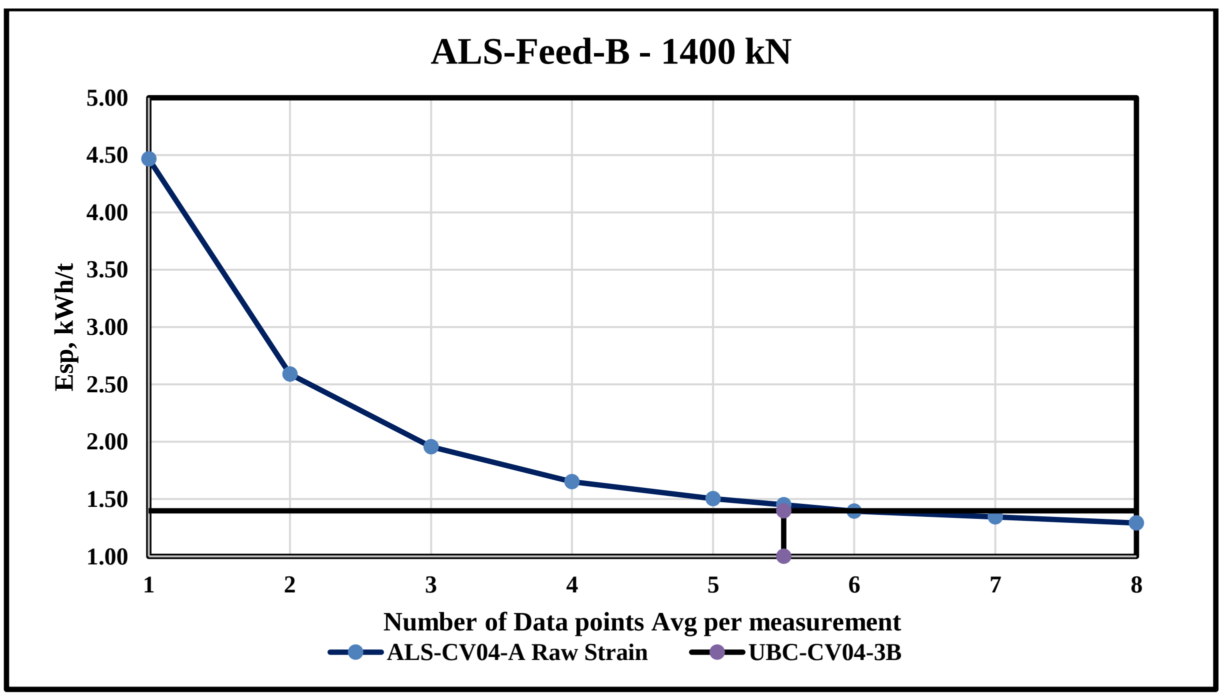

Figure 5-9: Effect of Frequency on Specific Energy Integration ALS-Feed-B @ 1400 kN

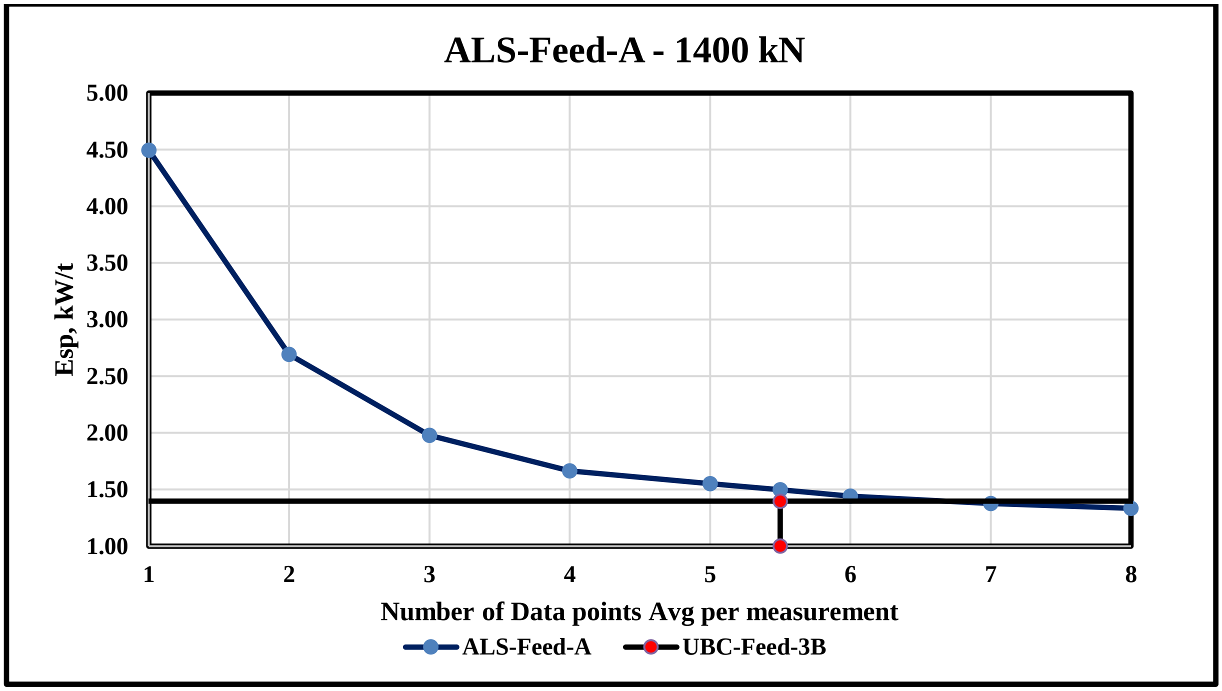

Figure 5-10: Effect of Frequency on Specific Energy Integration ALS-Feed-A @ 1400 kN

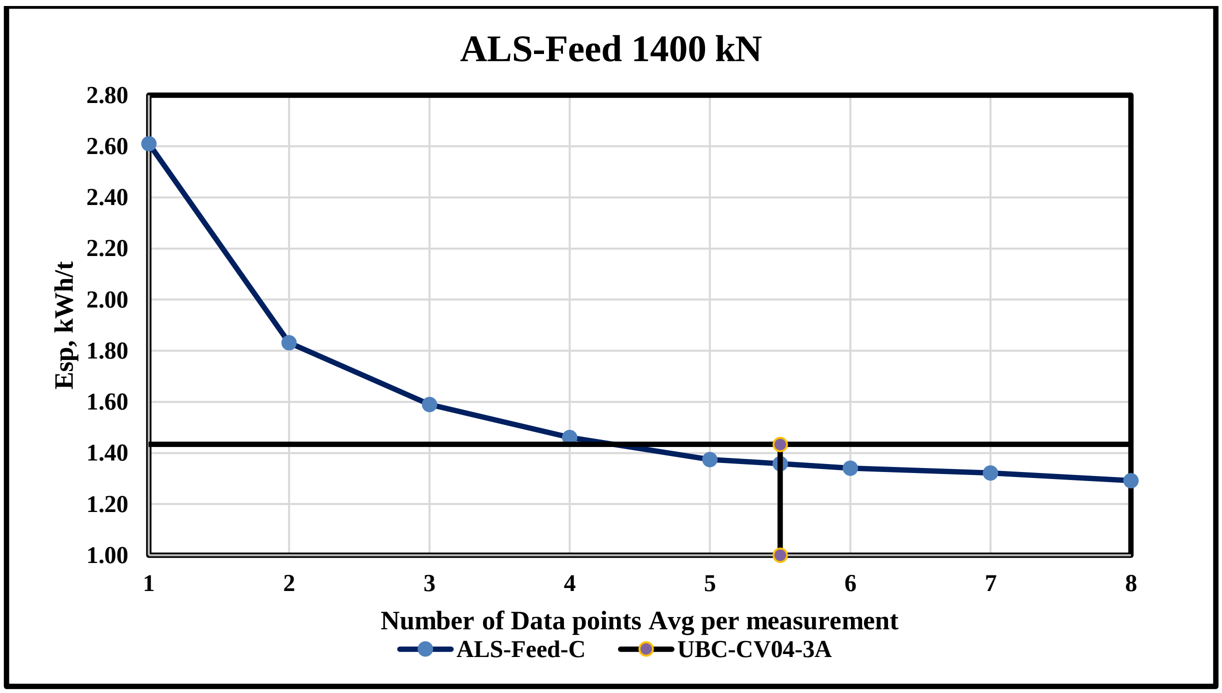

Figure 5-11: Effect of Frequency on Specific Energy Integration ALS-Feed-C @ 1400 kN

The final comparison of specific energy consumption between UBC and ALS Metallurgy Piston Press test results were similar. The specific energy consumptions were compared for the 16 piston presses that were performed during the program.

Comparison of the corrected specific energy consumption of the Piston Press test results for ALS Metallurgy and UBC the Piston Press test for each pressure are reported in Table 5-3 and 5-4. The test results showed Piston Press testing between UBC and ALS Metallurgy had a standard error of +/- 0.057 kWh/tonne and a correlation of variance of 5.4%. In comparison, 20 duplicate Piston Press tests conducted just at UBC an error of 0.034 kWh/tonne with a correlated variance of 2.9.

Table 5-3: Specific Energy Consumption Variability Duplicate Testing for ALS Metallurgy

ALS		UBC		
Sample	Esp kWh/tonne	Sample	Esp kWh/tonne	ABS Error kWh/tonne
ALS-Feed-A-P1	1.50	UBC-Feed-3B-P1	1.40	0.10
ALS-Feed-A-P2	1.18	UBC-Feed-3B-P2	1.14	0.04
ALS-Feed-A-P3	0.95	UBC-Feed-3B-P3	0.91	0.04
ALS-Feed-A-P4	0.76	UBC-Feed-3B-P4	0.64	0.12
ALS-Feed-B-P1	1.45	UBC-Feed-3B-P1	1.40	0.05
ALS-Feed-B-P2	1.08	UBC-Feed-3B-P2	1.14	0.07
ALS-Feed-B-P3	0.94	UBC-Feed-3B-P3	0.91	0.03
ALS-Feed-B-P4	0.71	UBC-Feed-3B-P4	0.64	0.07
ALS-Feed-C-P1	1.36	UBC-Feed-3A-P1	1.40	0.04
ALS-Feed-C-P2	1.18	UBC-Feed-3A-P2	1.14	0.03
ALS-Feed-C-P3	0.80	UBC-Feed-3A-P3	0.91	0.11
ALS-Feed-C-P4	0.57	UBC-Feed-3A-P4	0.64	0.06
ALS-Feed-A	1.61	UBC-Feed-2-P1	1.55	0.05
ALS-Feed-A	1.34	UBC-Feed-2-P2	1.32	0.03
ALS-Feed-A	1.04	UBC-Feed-2-P3	1.04	0.00
ALS-Feed-A	0.71	UBC-Feed-2-P4	0.76	0.05
Mean	1.07		1.06	0.06
C.V.				5.4%

Table 5-4: Specific Energy Consumption Variability of Duplicate Testing at UBC

Sample	Esp kWh/tonne	Sample	Esp kWh/tonne	ABS Error kWh/tonne
UBC-Comp-1A-P1	1.45	UBC-Comp-1A2-P1	1.58	0.13
UBC-Comp-1A-P2	1.27	UBC-Comp-1A2-P2	1.26	0.02
UBC-Comp-1A-P3	1.01	UBC-Comp-1A2-P3	1.02	0.01
UBC-Comp-1A-P4	0.75	UBC-Comp-1A2-P4	0.77	0.02
UBC-Comp-1B1-P1	1.48	UBC-Comp-1B2-P1	1.48	0.00
UBC-Comp-1B1-P2	1.23	UBC-Comp-1B2-P2	1.30	0.07
UBC-Comp-1B1-P3	0.97	UBC-Comp-1B2-P3	1.05	0.07
UBC-Comp-1B1-P4	0.71	UBC-Comp-1B2-P4	0.77	0.06
UBC-Comp-2A1P1	1.55	UBC-Comp-2A2-P1	1.53	0.02
UBC-Comp-2A1P2	1.33	UBC-Comp-2A2-P2	1.31	0.01
UBC-Comp-2A1P3	1.06	UBC-Comp-2A2-P3	1.04	0.02
UBC-Comp-2A1P4	0.78	UBC-Comp-2A2-P4	0.79	0.00
UBC-Comp-2B1-P1	1.57	UBC-Comp-2B2-P1	1.57	0.00
UBC-Comp-2B1-P2	1.33	UBC-Comp-2B2-P2	1.29	0.04
UBC-Comp-2B1-P3	1.04	UBC-Comp-2B2-P3	1.05	0.01
UBC-Comp-2B1-P4	0.75	UBC-Comp-2B2-P4	0.75	0.00
UBC-Comp-3A1-P1	1.62	UBC-Comp-3B2-P1	1.58	0.03
UBC-Comp-3A1-P2	1.30	UBC-Comp-3B2-P2	1.38	0.07
UBC-Comp-3A1-P3	1.04	UBC-Comp-3B2-P3	1.07	0.03
UBC-Comp-3A1-P4	0.80	UBC-Comp-3B2-P4	0.75	0.05
Mean	1.15		1.17	0.03
C.V.				2.9%

The residual plot (Figure 5-12) of the specific energy consumption of the error is non-biased and appears randomly dispersed. The residual plot suggests that the approaches used to correct the ALS Metallurgy Piston Press data produced a good and non-biased result when determining the specific energy consumption.

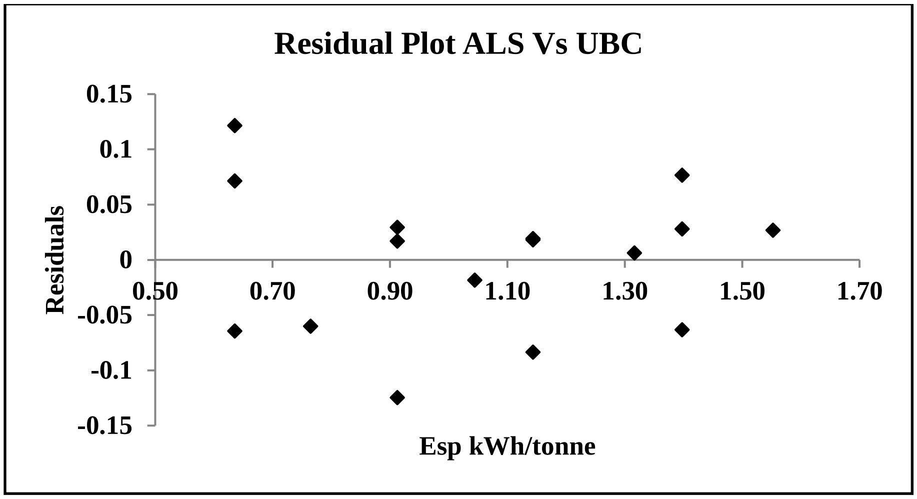

Figure 5-12: Residual Plot of the Standard Error of Duplicate Testing

Despite the variability, being higher between UBC and ALS Metallurgy the variability between the two labs is considered acceptable. With additional experience performing the Piston Press test, the level of variability between the two labs is expected to improve.

5.6 Reproducibility of Piston Product

Particle size distributions of Piston Press test feed between duplicate test-work carried out at ALS Metallurgy and UBC strongly produced consistent results. Both the P_{80} and P_{50} between all Piston Press test feeds, and products were similar. This was an expected result as careful consideration was done to ensure that both labs prepared Piston Press test feed similarly. It was important that the feed PSD matched to ensure Piston Press testing performed at each lab was being conducted on the representative material. Figures 5-13 and 5-14 and Tables 5-5 and 5-6 summarize the PSD for the Piston Press test feeds between both labs for the full-scale HPGR fresh/recycle composite and HPGR feed, respectively.

Table 5-5: Particle Size Analysis on Fresh/Recycle Full-scale HPGR Composite of Duplicate Testing

Sample	Feed (mm) ALS-Comp-A	UBC-Comp-2A	UBC-Comp-2B
P50	5.68	6.17	6.14
P80	9.92	10.16	10.02

Table 5-6: Particle Size Analysis of the HPGR Feed of Duplicate Testing

Product	Feed (mm) ALS-Feed-A	ALS-Feed-B	ALS-Feed-C	UBC-Feed-3A/B
P50	5.17	5.17	4.99	4.90
P80	9.94	9.94	9.99	9.94

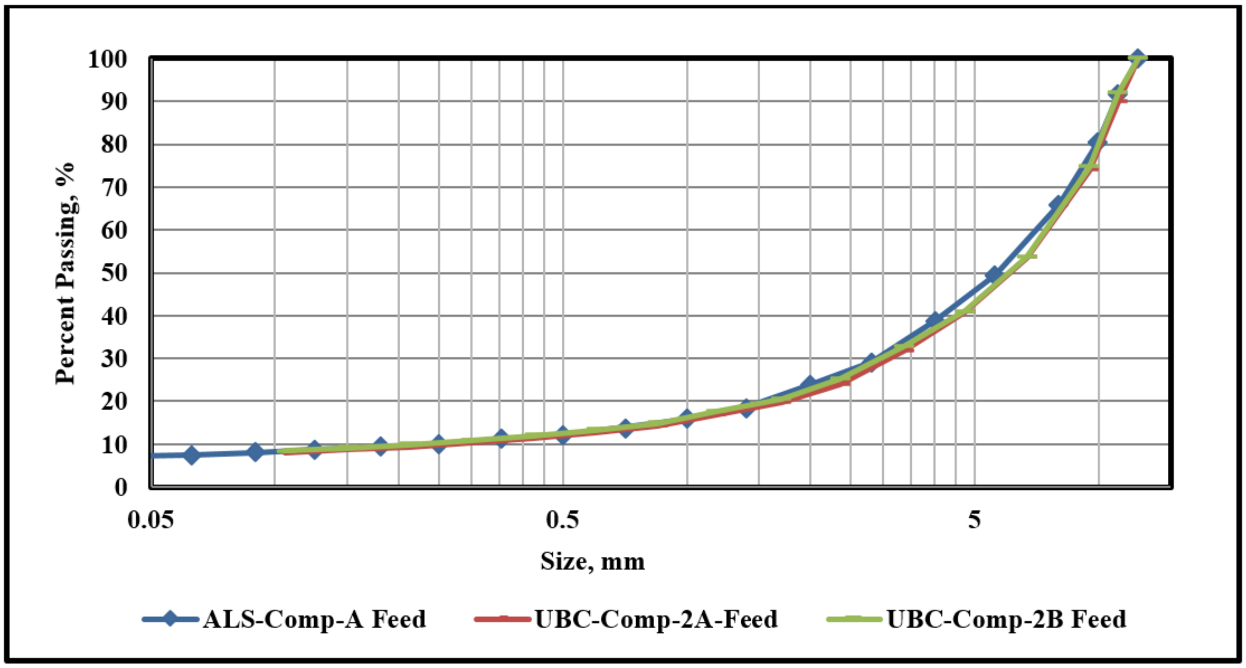

Figure 5-13: Piston Press Test Feed for Fresh/Recycle Full-scale HPGR Composite Piston Press Feed at UBC and ALS Metallurgy

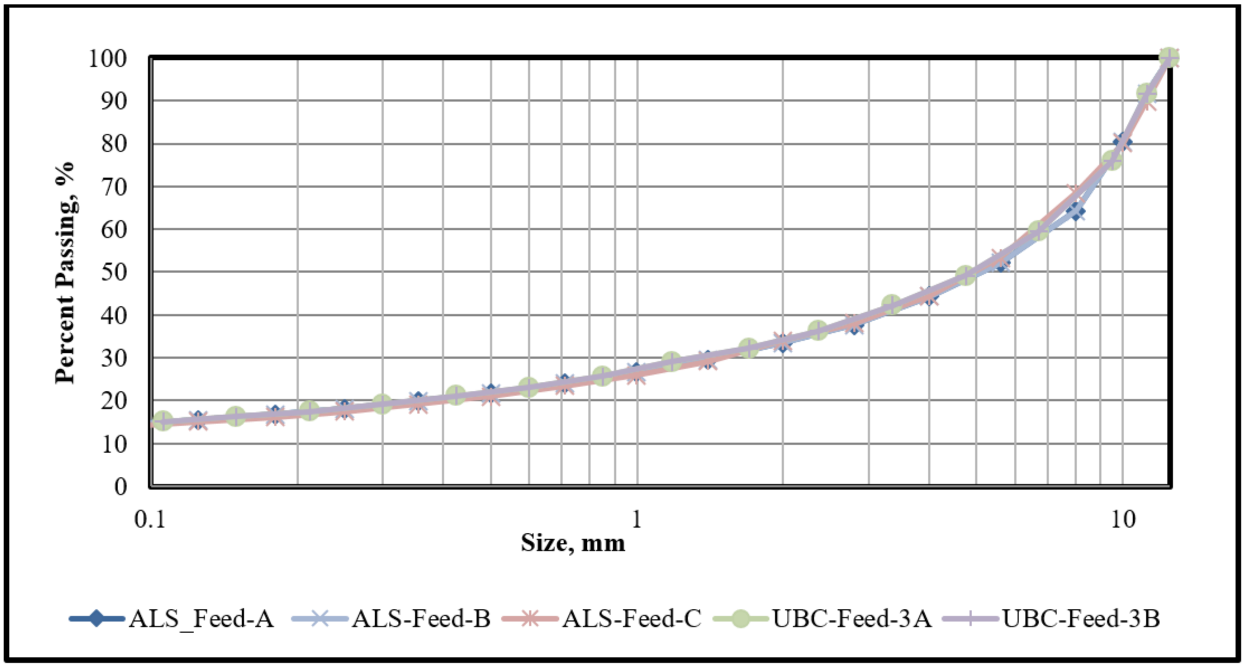

Figure 5-14: Piston Press Test feed for Fresh/Recycle Full-scale HPGR Composite Testing at UBC and ALS Metallurgy

5.6.1 Piston Product Particle Size Distribution of Duplicate Testing

Figures 5-15 to 5-22 show the Piston Press test product PSD values for the full-scale HPGR fresh/recycle composite and full-scale HPGR feed for both UBC and ALS Metallurgy. Producing an identical Piston Press test product is a key result of the program, and is a key finding supporting that the Piston Press test is reproducible independently. These results show that the Piston Press test product can be produced on different piston press machine press configuration. This finding is significant as is demonstrates the Piston Press test is consistent at producing the equivalent product. Producing equivalent PSD for the two products is impressive result as the Piston Press feed had sample sizes in the range of 300 to 450 g sample sizes. It also indicates that the Piston Press test has a flexible test which can be performed on retrofitted setups. Being able to produce uniform high-pressure product enables metallurgical sample to be produced cost-effectively for downstream metallurgical studies without requiring more costly HPGR piloting.

Table 5-7: Particle Size Analysis for Products of Duplicate Tests

	1400 kN Product (mm)			1100 kN Product (mm)		
Sample	ALS-Comp-A	UBC-Comp-2A	UBC-Comp-2B	ALS-Comp-A	UBC-Comp-2A	UBC-Comp-2B
P50	1.55	1.56	1.59	1.62	1.65	1.71
P80	5.44	5.78	5.27	5.61	5.56	5.67
	800 kN Product (mm)			500 kN Product (mm)		
	ALS-Comp-A	UBC-Comp-2A	UBC-Comp-2B	ALS-Comp-A	UBC-Comp-2A	UBC-Comp-2B
P50	1.82	1.89	1.89	2.11	2.25	2.21
P80	6.30	6.11	6.00	6.52	6.95	6.56

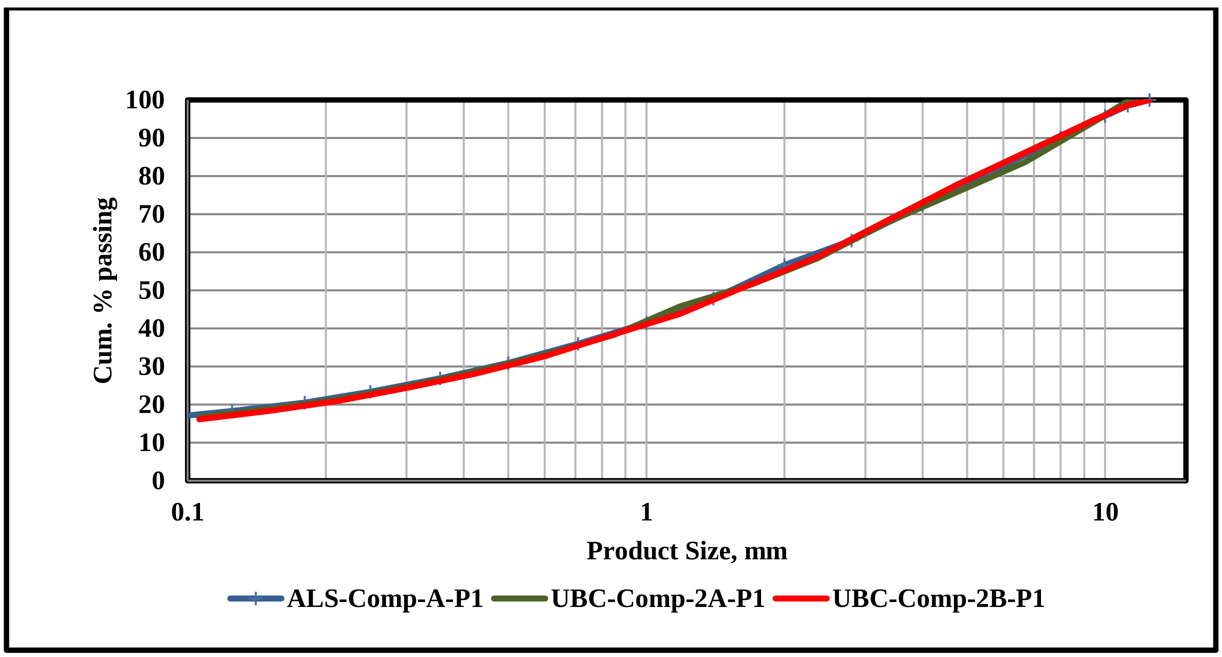

Figure 5-15: 1400 kN Duplicate Piston Press Test Product on Fresh/Recycle Full-scale HPGR Composite

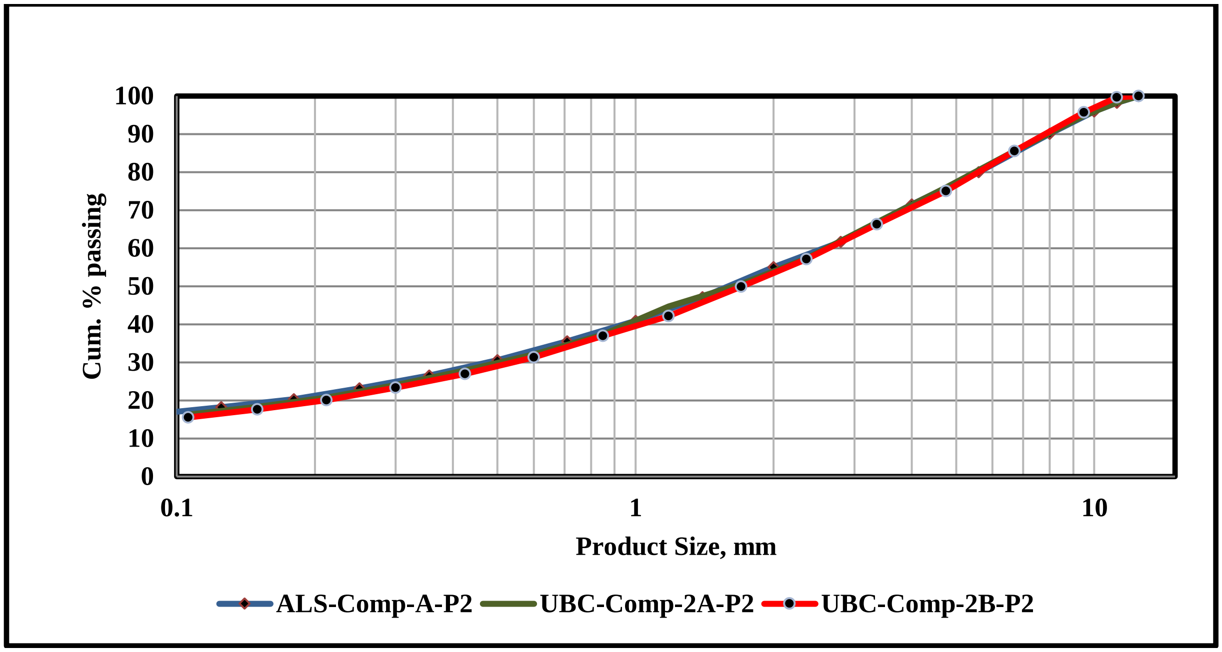

Figure 5-16: 1100 kN Duplicate Piston Press Test Product on Fresh/Recycle Full-scale HPGR Composite

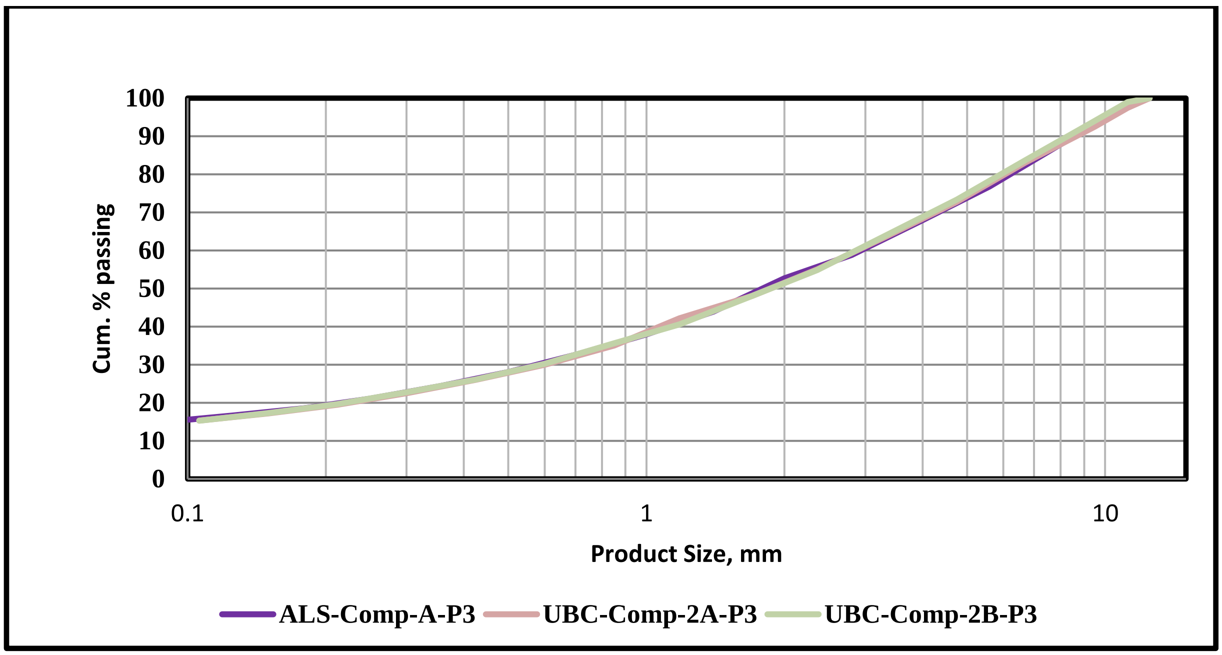

Figure 5-17: 800 kN Duplicate Piston Press Test Product on Fresh/Recycle Full-scale HPGR Composite

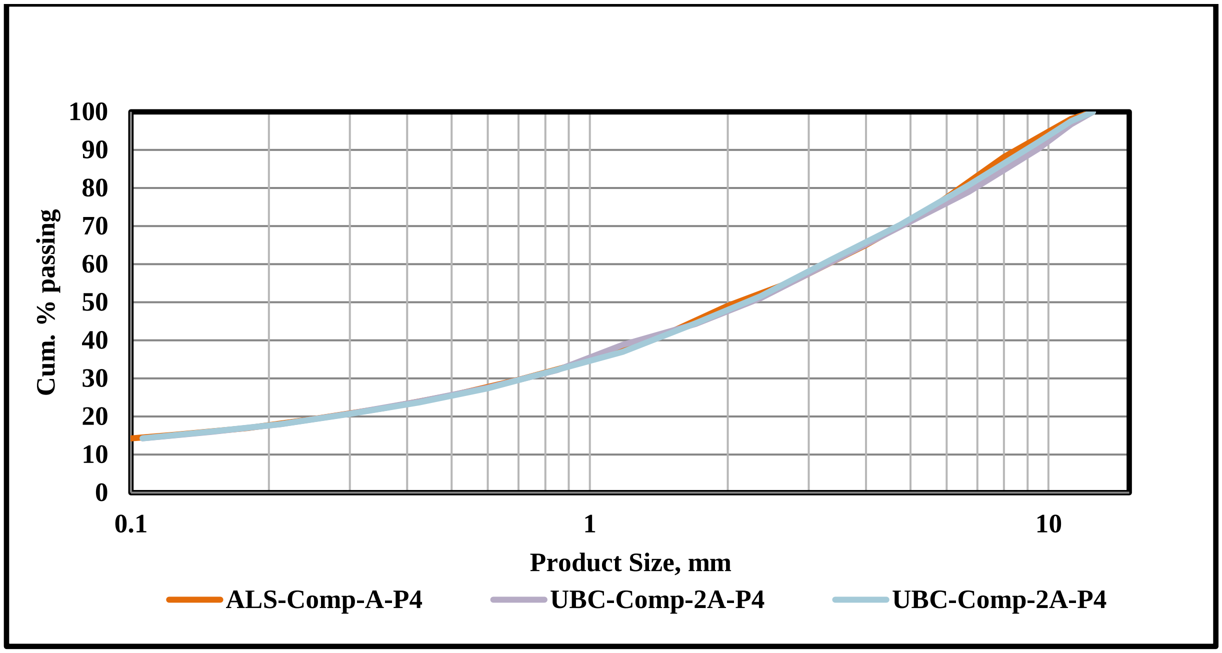

Figure 5-18: 500 kN Duplicate Piston Press Test Product on Fresh/Recycle Full-scale HPGR Composite

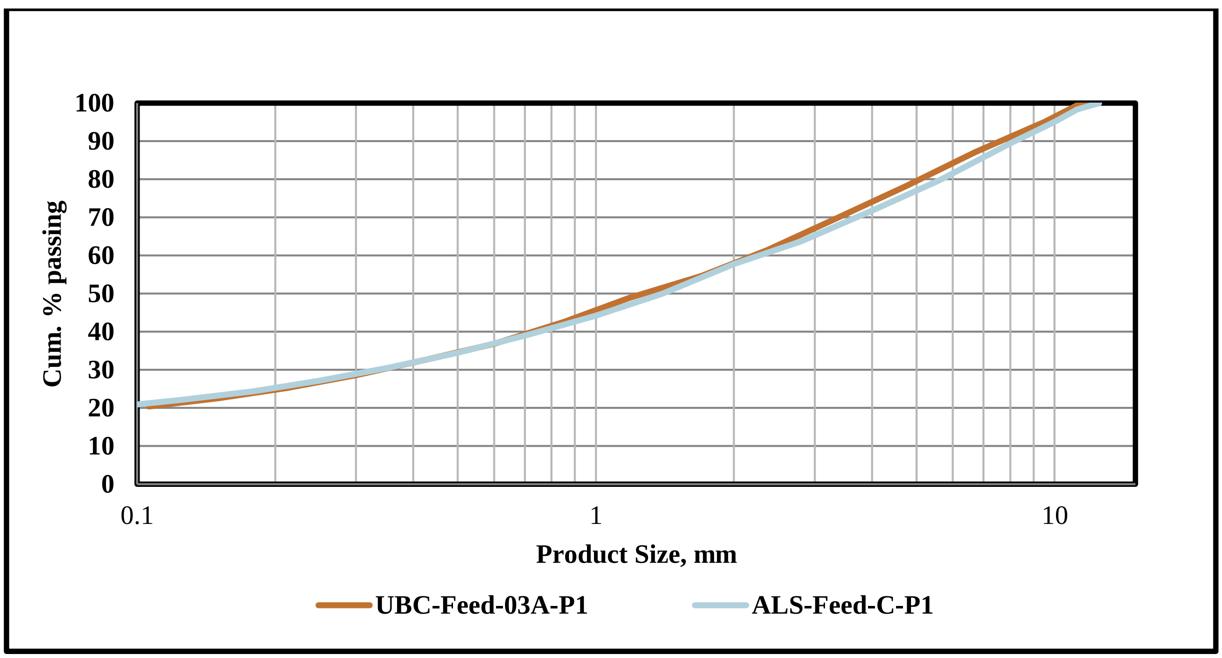

Figure 5-19: 1400 kN Duplicate Piston Press Test Product for the HPGR Feed

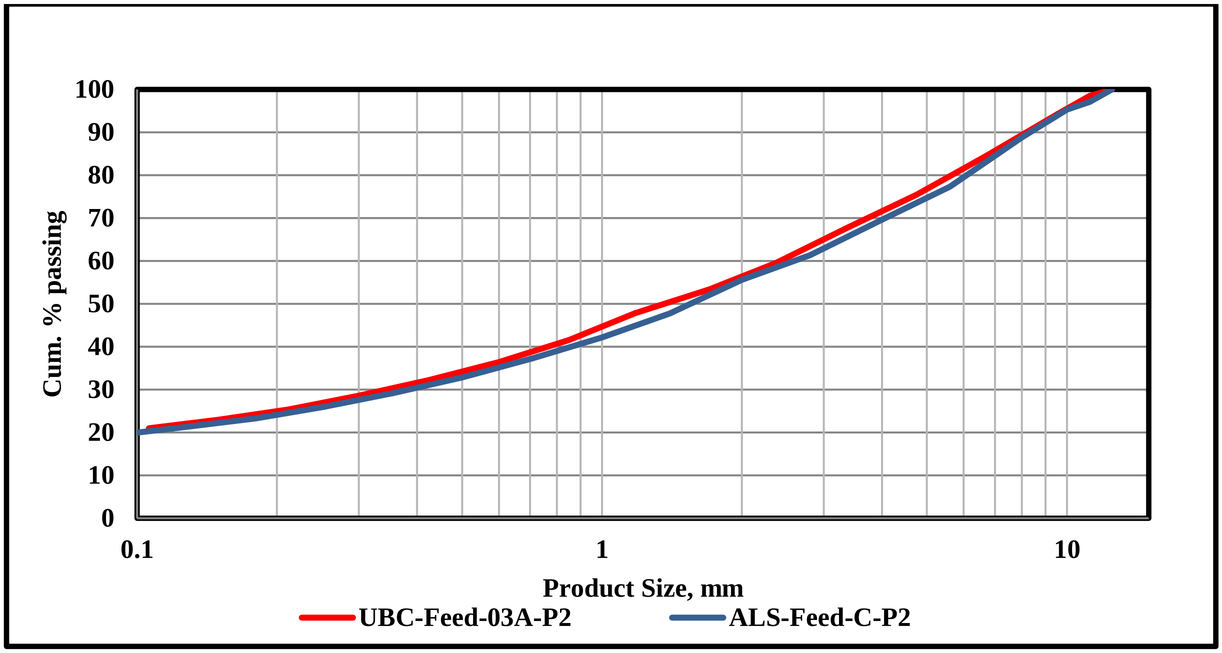

Figure 5-20: 1100 kN Duplicate Piston Press Test Product for the HPGR Feed

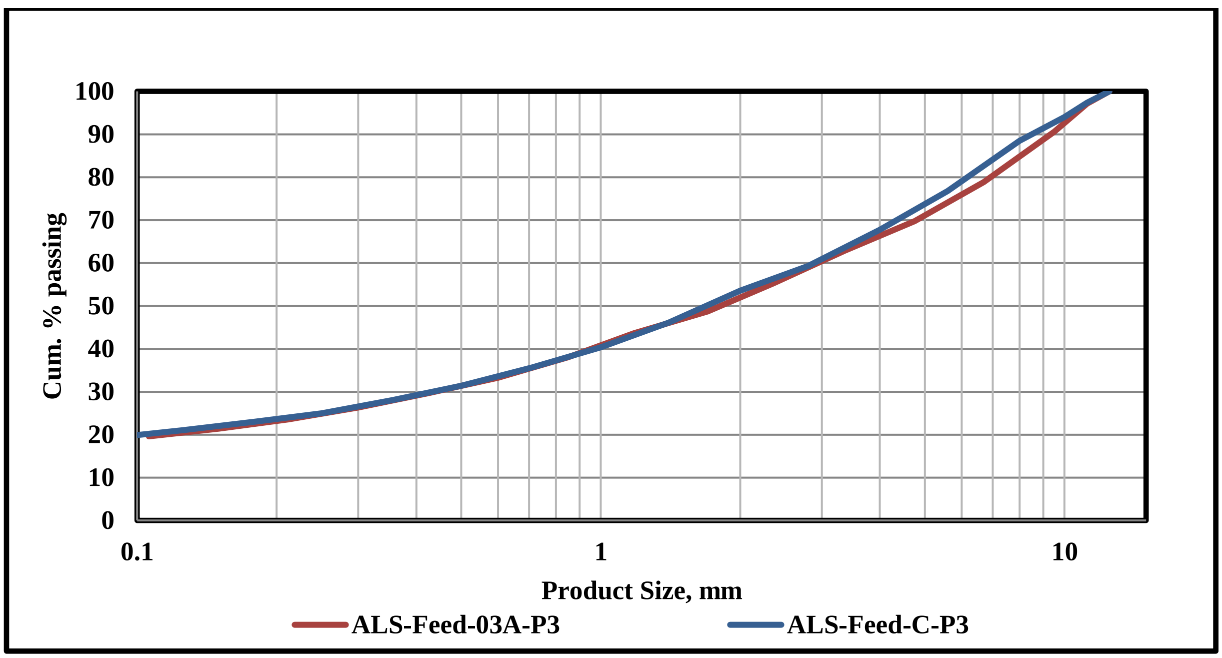

Figure 5-21: 800 kN Duplicate Piston Press Test Product for the HPGR Feed

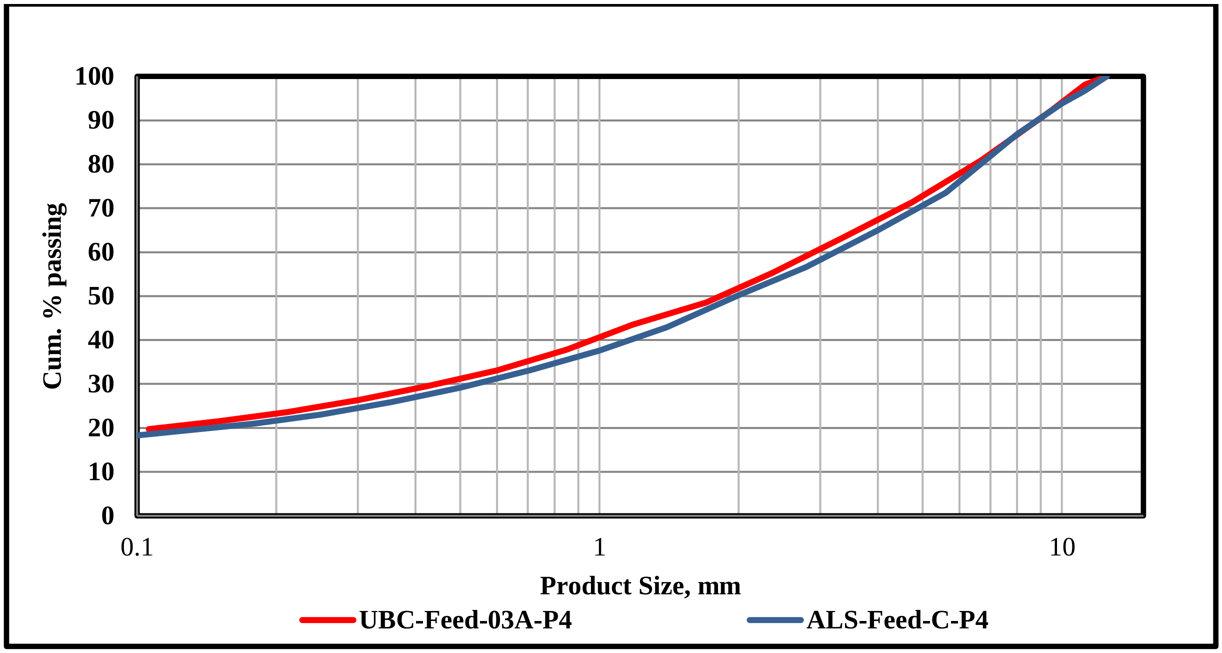

Figure 5-22: 500 kN Duplicate Piston Press Test Product for the HPGR Feed

5.7 Piston Work Index (W_{pi})

Higher Piston Work indices are noted at higher Piston Press test pressures. As a result, when comparing the Piston Work index, it may be important to ensure that tests are conducted at the same pressure. As is evident in Table 5-8, both UBC and ALS Metallurgy produced similar W_{pi} values for the samples tested. This finding further validates and demonstrates that the Piston Press test is reproducible, provided careful analysis is performed when determining the test's specific energy consumption. Results showed UBC and ALS had similar Piston Work indexes overall. The correlation of variability for full-scale HPGR fresh/recycle composite tests was 1.0% for $W_{pi}50$ and 5.8% for $W_{pi}80$. Variability for the HPGR feed showed a correlation of variance of 3.9% for $W_{pi}50$ and 2.2% for $W_{pi}80$. The Piston Press index results indicate that the test is reproducible with low variability.

Table 5-8: Piston Work Index of Duplicate Piston Press Testing

Sample	Moisture	Wpi50 kWh/t	Wpi80 kWh/t
Fresh/Recycle Composite			
UBC-Comp2A1	3.0%	10.94	43.13
UBC-Comp2A2	3.0%	10.62	37.56
UBC-Comp2B1	3.0%	10.74	37.16
UBC-Comp2B2	3.0%	10.86	37.29
ALS-CompA	2.5%	10.85	39.27
Mean		**10.80**	**38.88**
STD		**0.11**	**2.26**
C.V		**1.0%**	**5.8%**
HPGR Feed			
UBC-Feed-03A	2.5%	8.88	35.39
UBC-Feed-03B	5.0%	9.51	34.51
ALS-Feed-A	5.0%	9.90	36.35
ALS-Feed-B	5.0%	9.18	34.17
ALS-Feed-C	5.0%	9.08	35.43
Mean		**9.31**	**35.17**
STD		**0.36**	**0.77**
C.V.		**3.9%**	**2.2%**

5.8 Discussion of Reproducibility of the Piston Press Test

The program was able to demonstrate the Piston Press test is reproducible. Representative Piston Press test product was able to be reproduced between UBC and ALS Metallurgy. Reproducible product was produced despite both labs having varying Piston Press test installations.

As evident in Figures 5-15 to 5-25, the product PSDs were remarkably similar. In addition, the Piston Work index showed similar values for samples tested by UBC and ALS Metallurgy. Special consideration had to be made when determining the specific energy consumption during testing of the respective sample. Differences in the frequency of measurements affected the force-displacement integration when determining the specific energy consumption. The difference in frequencies of the measurements was resolved by averaging the displacement and force data to ensure Piston Press test data between ALS Metallurgy and UBC was integrated over similar frequency. Improvements can be made with regards to improving reproducibility. The correlation of variance was higher when comparing duplicate testing between ALS Metallurgy and UBC than for comparing duplicate testing at just UBC. The correlation of variance was found to be 5.4% compared to 2.9%. Moving towards a modelling approach to compare may help further improve reproducibility in the future.

Similar challenges will be expected for future alternative installations in at other independent labs if existing piston press machines operate at different specifications than UBC. It is imperative that any future Piston Press test facility installation similar or the same design specifications as UBC Piston Press facility, particularly in terms of measurement frequency and instrument precision. Ensuring future installations are built with similar specifications is especially important for the Database Calibrated methodology.

Chapter 6: Validation of Full-Scale HPGR

The program intended to determine if the Piston Press Database Calibrated and Direct Calibration methodologies can be validated against a full-scale HPGR operation. The Database Calibrated and Direct Calibration methodologies were developed and validated in 2015 (Davaanyam, 2015; Davaanyam et al., 2015) against a pilot HPGR. However, the Piston Press test methodologies had not been validated against a full-scale HPGR operation. The pilot HPGR used to develop the Piston Press test methodologies was a pilot HPGR, located at the Coal Mineral Processing (CMP) lab at UBC.

The program included collecting 5 tonnes of sample (in total) from full-scale HPGR feed and +2 mm recycle from Tropicana Gold Mine's full-scale HPGR circuit, located in Western Australia. Operational data for the full-scale HPGR was captured for a 24-hour period that included operating periods before and following sampling. Later stage test-work included HPGR piloting and Piston Press testing. In conjunction with the Database Calibrated and Direct Calibration methodologies, closed circuit simulations were created using the Piston Press test, and pilot HPGR results and compared to the full-scale HPGR.

The result of the closed circuit simulations demonstrates that the Piston Press test Database Calibrated and Direct Calibrations modelled well against full-scale HPGR, predicting the specific energy consumption closer than pilot HPGR indicated.

6.1 Program Methodology

The program methodology was carried out in six steps as shown in Figure 6-1. Approximately 5 tonnes of total sample was collected from the full-scale HPGR circuit, including both full-scale fresh feed and full-scale + 2 mm recycle. Data for a 24-hour operating period was collected on the day of sampling which included both periods before and following sampling. Piloting HPGR testing was carried out by ALS Metallurgy on the full-scale HPGR feed and full-scale HPGR fresh/recycle composite (50% full-scale HPGR feed and 50% full-scale HPGR + 2 mm recycle). HPGR piloting was done at specific pressing forces of 2 N/mm^2, 3 N/mm^2, and 4 N/mm^2.

In conjunction with pilot HPGR testing, Piston Press testing was carried by UBC and ALS Metallurgy on -12.5 mm crushed fresh feed and the feed/recycle composite.
Following Piston Press testing, and HPGR piloting, Piston Press test results were calibrated to the full-scale HPGR and pilot HPGR. The Database Calibrated and Direct Calibration methodologies are discussed in Section 6.2.

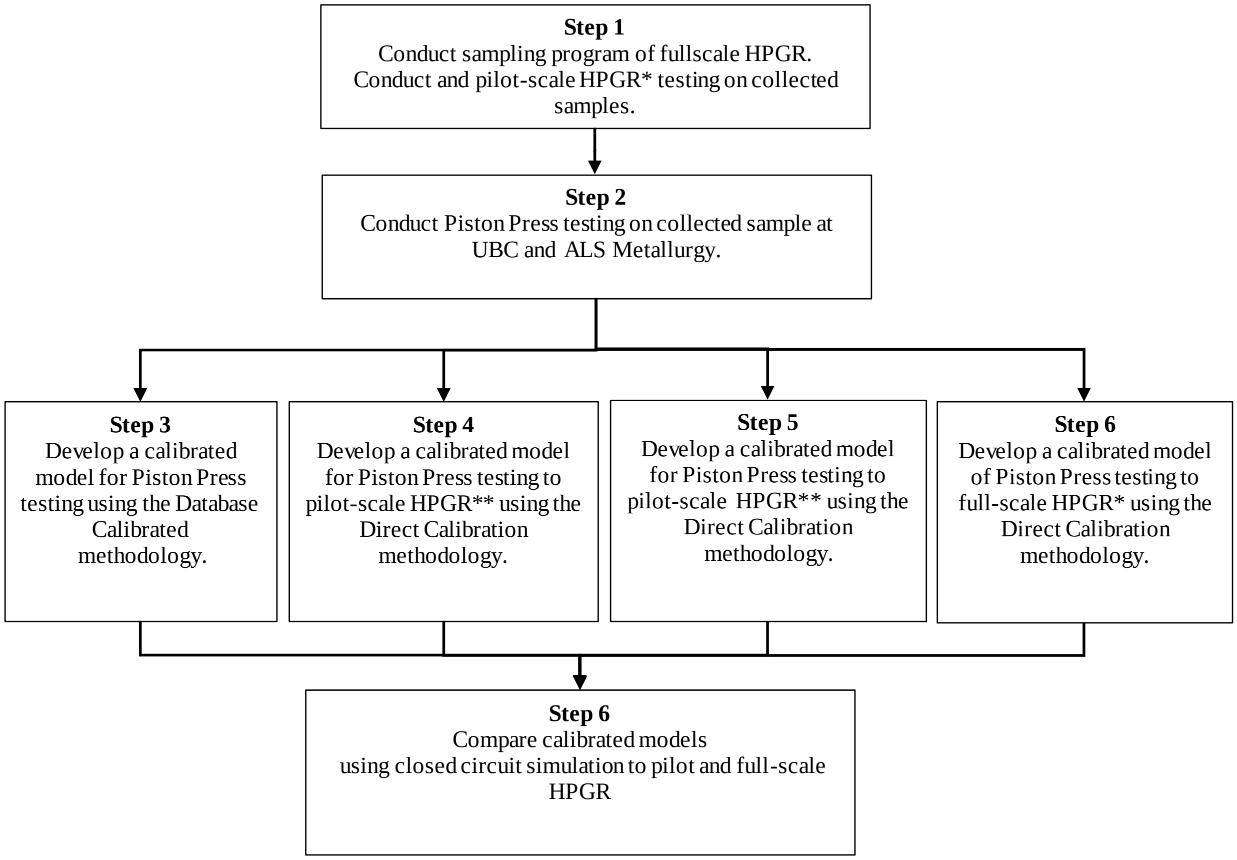

*The full-scale HPGR was sample at the Tropicana Gold Mine, located in WA, Australia
**The Pilot scale HPGR testing was performed by ALS Metallurgy, in Perth, WA, Australia

Figure 6-1: Methodology of Full-Scale Validation

6.1.1 Sampling and Test-work

Test-work carried out included the collection of full-scale HPGR feed sample, full-scale HPGR operational data, pilot HPGR, and Piston Press testing. Specifically, the program included the following:

- Collection of feed and recycle samples:
    - ~3 tonnes of HPGR feed;
    - ~2 tonnes of HPGR +2 mm recycle;
    - Collection of full-scale operational data for 24 hours.

- Pilot HPGR test-work:
  - HPGR feed @ 4 N/mm^2, 3 N/mm^2, and 2 N/mm^2;
  - HPGR fresh/recycle composite (50% feed, 50% + 2 mm Recycle) @ 4 N/mm^2, 3 N/mm^2, and 2 N/mm^2.
- Piston Press testing:
  - HPGR feed @ 240 Mpa, 190 Mpa, 140 Mpa, and 86 Mpa;
  - HPGR composite (50% feed, 50% + 2 mm Recycle) @ 240 Mpa, 190 Mpa, 140 Mpa, and 86 Mpa.

The following is a summary of the Piston Press test calibration methodologies used, as well as the closed circuit simulations developed in this research:

Calibrated and Calibration Models

- Pilot HPGR using Database Calibrated and Direct Calibration methodologies;
- Full-scale HPGR using the Direct Calibration methodology.

Closed Circuit Simulation

- Pilot HPGR and full-scale HPGR;
- Pilot HPGR to Database Calibrated and Direct Calibration;
- Full-scale HPGR to Direct Calibration to full-scale.

6.2 Piston Press Calibrations

The Piston Press test requires two specific calibrations for each calibration methodology. These calibrations are the calibration for the Piston Press test's pressure to the equivalent HPGR's or pilot HPGR's specific pressing force, and, the Piston Press test's reduction ratio to the HPGR's or pilot HPGR's reduction ratio. The specific energy consumption relates both these calibrations. The Database Calibrated methodology uses two multi-linear regression models developed from a database of historical Piston Press test and the HPGR pilot test results conducted at UBC. The Direct Calibration methodology uses two linear regression models established from the respective pilot or the HPGR calibration test.

6.2.1 Database Calibrated Methodology

The Database Calibrated methodology is shown by equations 5 and 6. Both of these equations were presented in Section 2.5 as part of the literature review. Both equations are multi-linear regression models that were established from 177 pilot HPGR test results in conjunction with the respective Piston Press tests (Davanyam, 2015). The Database Calibrated methodology currently has an established accuracy of +/- 25% (Davaanyam, 2015; Davaanyam et al., 2015). The five current parameters for the Database Calibrated methodology are the pilot HPGR's percent moisture of the total feed, proctor bulk density at 32 mm top size, F50 for the pilot HPGR being simulated, and the F_{50} and P_{80} of the respective Piston Press test. The values for the five parameters are stated in Table 6-3. A moisture level of 2.6% was used to simulation match the operational data gathered from the full-scale HPGR. The bulk density was determined by during HPGR piloting at ALS Metallurgy.

$$F_{sp}^{HPGR} = \frac{P_{piston} - (5.53 + 24.3w - 86.2\rho_{bulk} + 13.1F_{50}^{HPGR} - {}^{44.4F_{50}^{HPGR}}\!\big/\!{}_{F_{50}^{Piston}} + 2.98P_{1\,mm}^{Piston}}{53.3} \qquad \textbf{Equation 5}$$

$$RR_{50}^{HPGR} = 1.86 + 1.41RR_{50}^{Piston} + \frac{2.31F_{50}^{HPGR}}{F_{50}^{Piston}} - 0.41_{50}^{HPGR} - 1.02w \qquad \textbf{Equation 6}$$

Table 6-1 Parameters for Database Calibrated Methodology

	Moisture (%)	Proctor bulk density (g/cc)	F_{50} HPGR (mm/mm)	F_{50} piston (mm/mm)	RR_{50} piston (mm/mm)
Pilot HPGR feed	2.60	1.99	11.9	See Appendix B.1. Determined from respective Piston Press test	See Appendix B.1. Determined from respective Piston Press test
Pilot HPGR composite	2.60	1.96	8.9	See Appendix B.1. Determined from respective Piston Press test	See Appendix B.1. Determined from respective Piston Press test

6.2.2 Direct Calibration Methodology

The Direct Calibration methodology uses two linear regression models that are established from a pilot HPGR 3 pressure test in conjunction with Piston Press tests on a calibration sample. The Direct Calibration methodology is shown in equations 23 and 24. These equations are derived from equations 7 to 10 presented in Section 2.5. A visual illustration of the Direct Calibration methodology is shown in Figures 6-2 and 6-3. The Direct Calibration methodology involves determining a correction function for both the y-intercept and slope to equate the Piston Press test results to the respective HPGR test.

$$Fsp = \frac{m_{Piston} * P_{Piston} + (B_{piston} + B_{HPGR})}{m_{HPGR}} \qquad \textbf{Equation 21}$$

$$RR50_{HPGR} = \frac{m_{Piston} * RR50_{piston} + (B_{piston} + B_{HPGR})}{m_{HPGR}} \qquad \textbf{Equation 22}$$

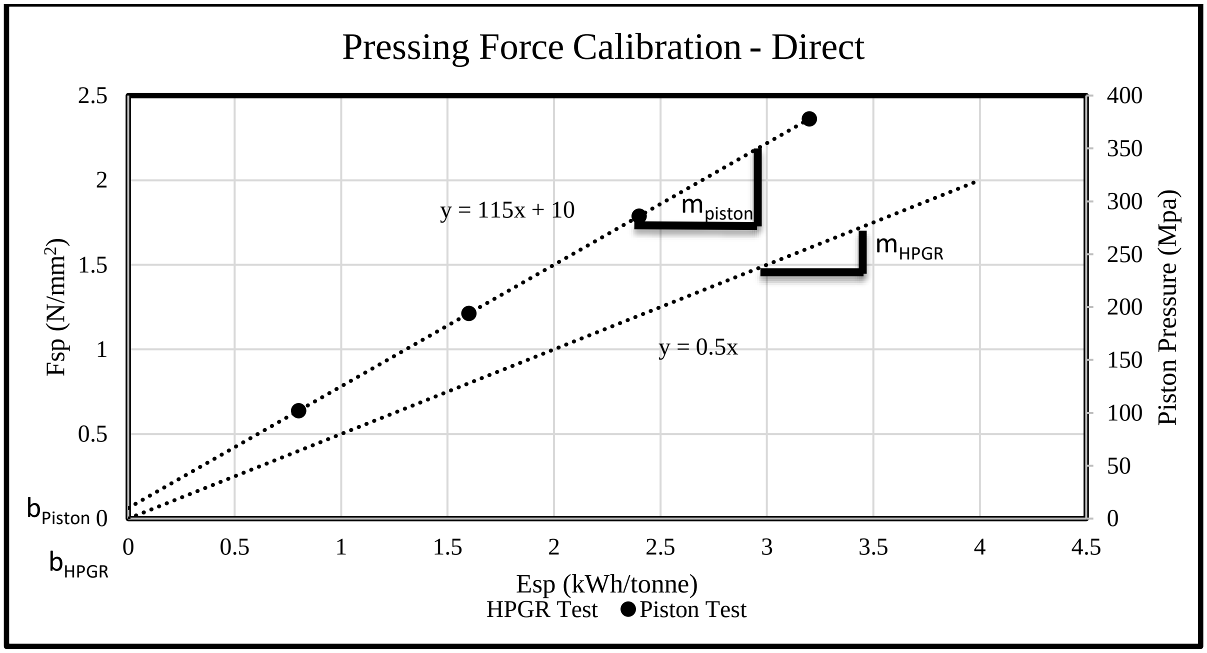

Figure 6-2: Direct Calibration of Pressure Piston Press to the HPGR Pressing Force

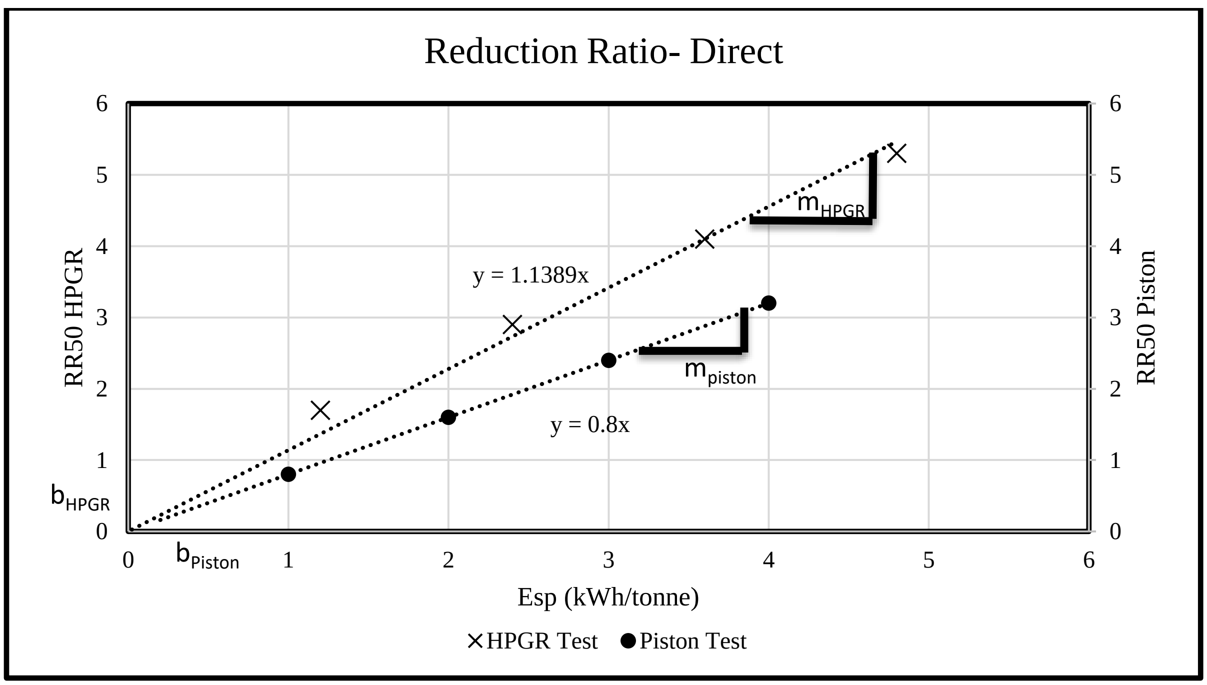

Figure 6-3 Direct Calibration of Piston Reduction Ratio to the HPGR Reduction Ratio

6.2.3 Closed-Circuit Simulation

Closed-simulations were created using the Database Calibrated and the Direct Calibration methodologies, to compare the Piston Press testing results to full-scale HPGR. All the closed circuit simulations were created using Microsoft Excel software with iterative calculations enabled. Closed circuit simulations were required to account for differences in product size when examining and comparing the differences in the specific energy consumption of the calibrated Piston Press test results, pilot HPGR, and full-scale HPGR. The closed-circuit simulations modelled the specific energy consumption for producing a passing 2 mm particle size. The specific energy consumptions were predicted for pilot HPGR and full-scale HPGR using calibrated Piston Press test results to predict the specific energy consumption and respective recycle load. This methodology assumed the specific energy applied to HPGR feed would be similar for the recycle material. In other words, the recirculating load would not significantly affect the specific energy consumption by per tonne of total feed. This assumption was deemed appropriate as pilot HPGR testing found the full-scale HPGR feed and composite material to have similar specific energy consumption in an open circuit configuration (Figure 6-4). Therefore, this finding suggests the feed size distribution between the full-scale HPGR feed and composite had a marginal effect on the specific energy consumption in the open circuit configuration.

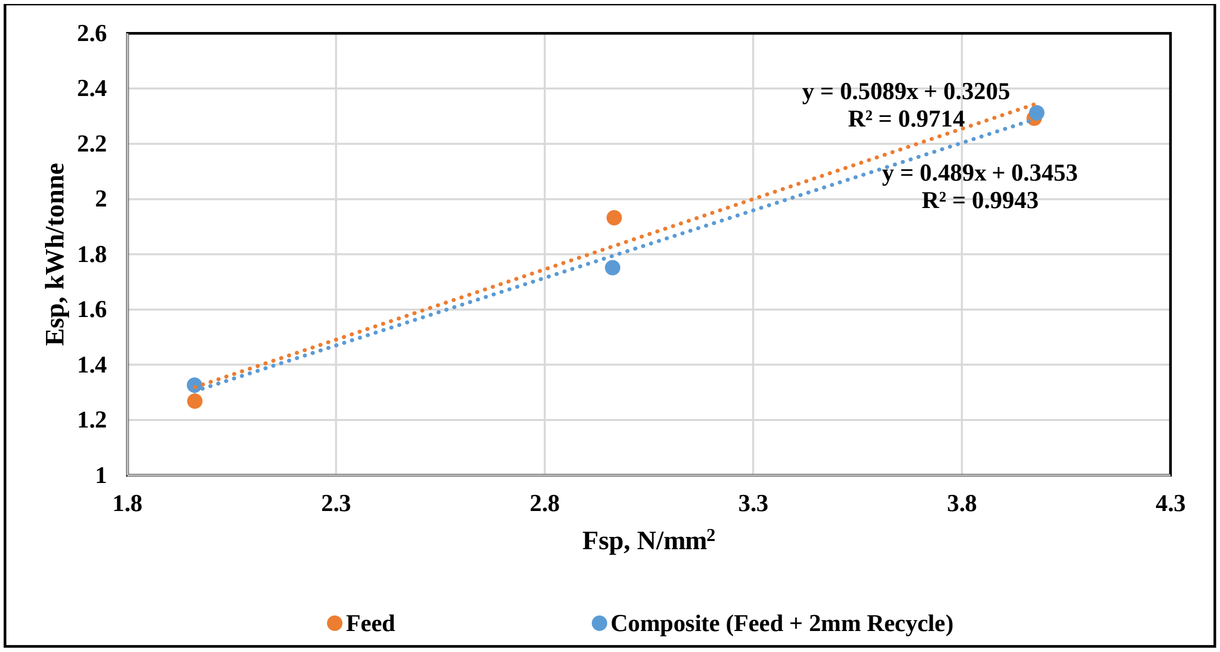

Figure 6-4: Pilot HPGR Open Circuit Specific Energy Consumption

The calculated percent passing 2 mm needed to determine the recycle load for calibrated Piston Press test results was determined from the respective normalized PSD for a given median feed size (F50) value. The median (F50) feed sizes were determined from values reported during pilot HPGR testing for the composite and fresh feed, respectively. All closed circuit simulations were modelled for a specific pressing force of 3 N/mm^2 which targeted the full-scale HPGR design and operating parameters.

A schematic of the closed circuit analysis is shown in Figure 6-5. The top size for the HPGR feed was not adjusted when comparing pilot HPGR results to full-scale HPGR. This decision was made as it is not standard industry practice to adjust pilot HPGR data for top size when sizing full-scale HPGR when designing full-scale HPGR from pilot HPGR testing. The top sizes for pilot HPGR and full-scale HPGR were 32 mm and 38 mm, respectively. In practice, this difference in top size would be expected to have some effect on HPGR performance. The closed-circuit simulations were based on an assumed 92% screen efficiency, selected to match the full-scale HPGR screen efficiency. In addition, all closed-circuit simulation using the Direct Calibration methodology used a calibration that was established from one of the Piston Press sample test results and not an average of multiple samples. In other words, the same calibration was used to calibrate the remaining Piston Press test results. This practice was selected to ensure calibration was established from a different Piston Press test result respective Piston Press test result. Had the calibration been established by multiple duplicate tests the calibrated results likely been better.

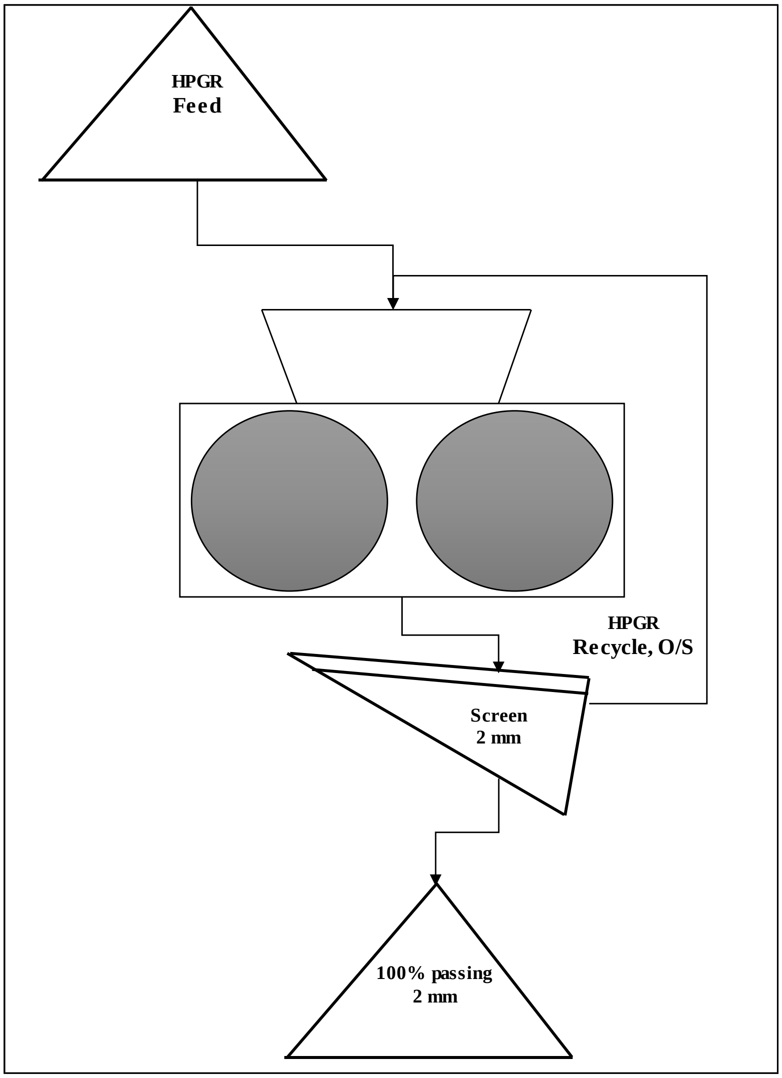

Figure 6-5: Schematic of Closed-Circuit Model Approach

6.3 Tropicana Gold Mine

Tropicana Gold Mine is located in Western Australia, approximately 330 km east-northeast of Kalgoorlie. The mine was commissioned in 2013 in a 70:30 joint venture partnership between AngloGold Ashanti Australia Ltd. and Independence Group NL. In 2017, Tropicana produced 332,000 oz, of gold. Current gold production for 2018 is forecasted between 478,000 to 492,000 oz (Tropicana JV, 2018). Operating throughput at Tropicana was 930 t/h in 2017, up from 780 t/h in 2015. A 20% improvement in throughput was achieved in 2016, which was largely attributed to improvements in material handling, and optimization of the transfer sizes between the HPGR and Ball mill circuits (Ballantyne et al., 2016).

A simplified flowsheet of Tropicana is presented in Figure 6-6. Run of mine (ROM) material is crushed via a gyratory crusher, with crushed material reporting to a primary stockpile. The primary stockpiled material is reclaimed via two apron feeders which feed the secondary cone crushing circuit. The secondary cone crushers operate in reverse closed circuit with the screen undersize feeding to the HPGR circuit (Figure 6-7). The HPGR is a Köppern, 2 m by 1.85 m unit that operates using two 2,200 kW variable speed motors. A portion of the HPGR discharge is diverted to an HPGR fines emergency stockpile that is reclaimed by a front-end loader during periods the crushing circuit is shut down (Ballantyne et al., 2016). HPGR discharge is de-agglomerated and screened by wet screening via two double deck banana wet screens. The oversize is recycled back to the HPGR hopper while the undersize HPGR product reports to a reverse-closed circuit Ball mill. A P80 of 75 microns reports to the Carbon in Leach (CIL) circuit.

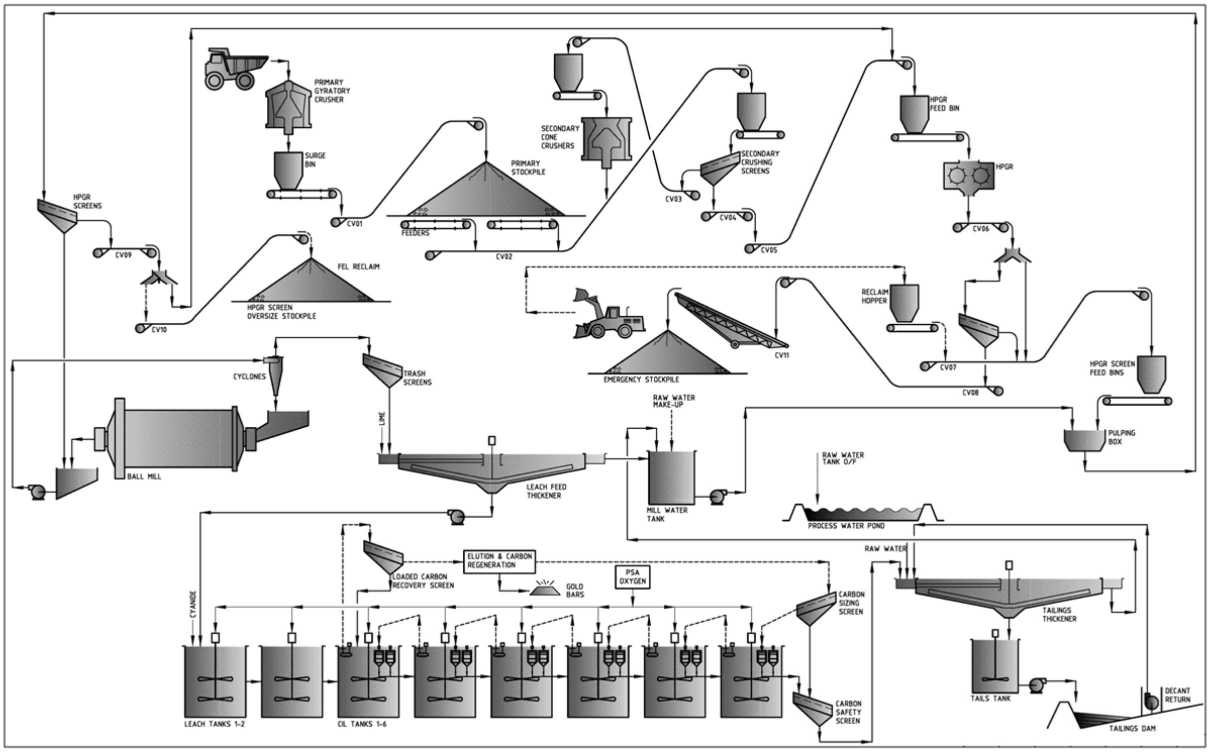

Figure 6-6: Process Flowsheet at Tropicana JV (Gardula et al., 2015)

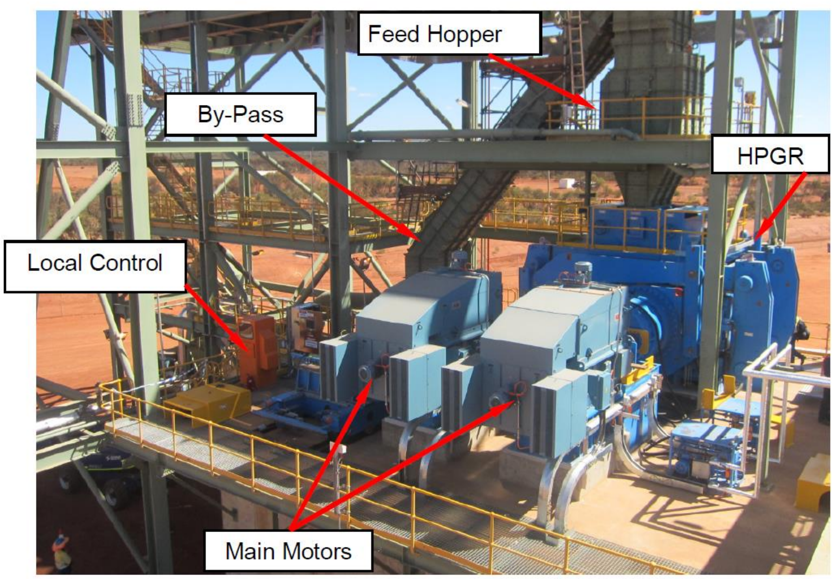

Figure 6-7: The HPGR at Tropicana JV (Gardula et al., 2015)

6.4 Full-scale HPGR Operational Data

Full-scale HPGR feed and full-scale HPGR + 2 mm recycle were sampled by belt cut. Operational data was taken before and after sampling on the same day for a 24-hour period. The operational data was analyzed at varying quartiles to determine the relationship between specific pressing force and specific energy consumption. Results are presented in Table 6-1. Values presented in Table 6-1 are reported based on total tonnes of feed (including the recycle load) to the full-scale HPGR. The operating throughputs are summarized in Figure 6-8. The 2nd quartile was taken to as the mean operating point. The 2nd quartile showed full-scale HPGR to have a specific energy consumption of 1.17 kWh/tonne of total feed (including recycle) at a specific pressing force of 3 N/mm^2, with an $\dot{m}$ of 339 ts/hm^3 at a recycle load of 103%. The specific energy consumption ranged from 1.14 to 1.24 kWh/tonne of total feed over a specific pressing force range of 2.6 N/mm^2 to 3.4 N/mm^2.

Table 6-2: Summary of Full-Scale HPGR Operating Data

Item	Summary of Results 1st Quartile	2nd Quartile	3rd Quartile	4th Quartile	Units [s]
HPGR Bearing Drive Side Roller Gap	42.4	**43.0**	43.8	54.6	[mm]
HPGR Bearing Non-Drive Side Roller Gap	52.3	**54.2**	55.9	61.1	[mm]
Actual Specific Pressing Force (Average)	3.0	**3.0**	3.0	3.4	[N/mm2]
Idle Power Draw	75.0	75.0	75.0	75.0	[kW]
Total Specific Energy Consumption	1.17	**1.20**	1.22	1.27	[kWh/total t*]
Net Specific Energy Consumption	1.14	**1.17**	1.19	1.24	[kWh/total t*]
Fresh Feed Weightometer (Natural moisture)	1082	**1176.3**	1278.9	1566.0	[t/h]
Recycle Weightometer (Wet)	1541	**1648.9**	1711.5	1881.5	[t/h]
Total Feed Weightometer (Wet)	2561	**2602.8**	2646.3	2910.8	[t/h]
% Recycle (at 92% screen efficiency)	45	**49.2**	53.6	78.7	%
Specific Throughput Constant m-dot	333	339	344	377	[ts/hm^3]

*Fresh feed + Recycle feed

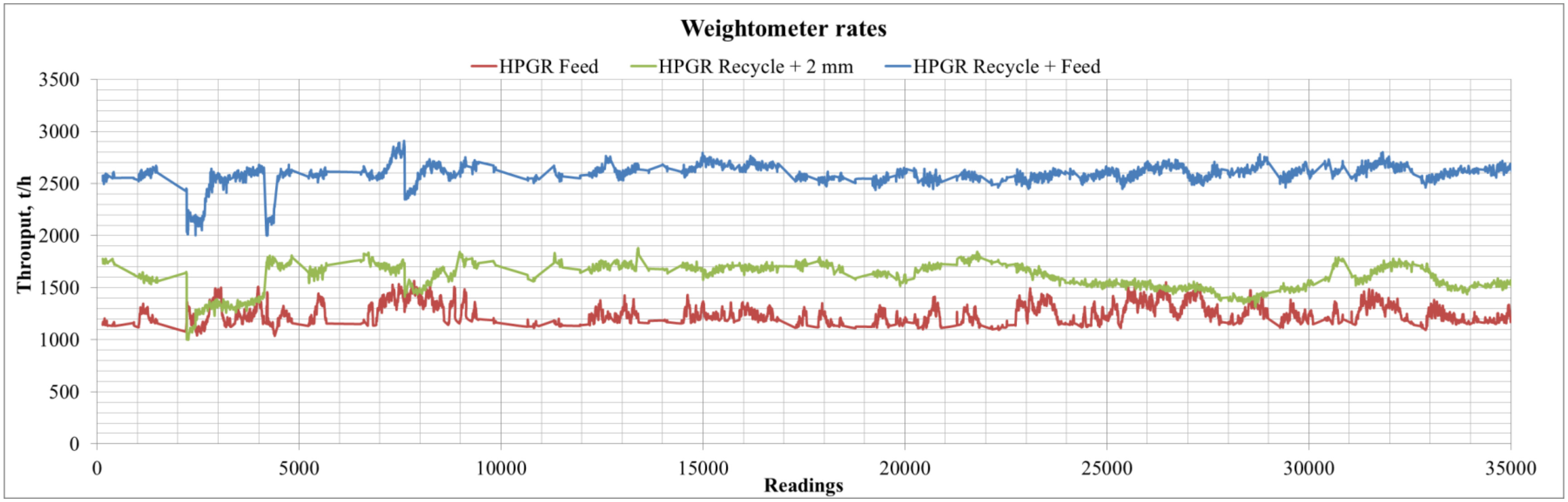

Figure 6-8: Summary of Full-Scale HPGR Throughput

6.5 Pilot Test Results

Pilot HPGR test-work was carried out on the full-scale HPGR feed and composite sample (50% full-scale HPGR fresh feed and 50% full-scale HPGR + 2 mm recycle) at specific pressing forces at 2 N/mm^2, 3 N/mm^2, and 4 N/mm^2. This range was selected to provide a broad range to better understand the relationship between specific pressing force, specific energy consumption, and reduction ratio breakage. Pilot HPGR test-work was carried out at natural moisture levels of moisture of ~0.7% and 1.55% for the full-scale HPGR feed and full-scale HPGR recycle, respectively. Pilot HPGR edge effect ranged from ~16% to 20% over the test work. The product PSD of the pilot HPGR was adjusted to reflect a 90% centre and 10% edge product. Results for the pilot HPGR testing on the composite are summarized in Table 6.2. The full-scale HPGR feed and the composite showed similar specific energy consumption. As expected, a higher reduction ratio was achieved on the full-scale HPGR feed sample than the full-scale HPGR composite.

Results presented in Table 6.2 include operational and reduction performance of the fresh/recycle composite sample. The full test results may be referred to in Appendix C. The pilot HPGR had an approximately 36% lower $\dot{m}$ than the full-scale HPGR. The higher $\dot{m}$ is likely a result of improved intake characteristics and roll geometry, the full-scale HPGR between the pilot HPGR and full-scale HPGR. The roll gap increases with the $\dot{m}$, which allows more material to enter in between the rolls. As a result, the specific energy applied to the particle bed is distributed across more tonnes, resulting in a higher throughput with a lower net specific energy.

Table 6-3: Summary of Pilot HPGR testing on Fresh/Recycle Composite Sample

Roller Diametre (**D**)	[m]	1.000	**Feed + (+ 2 mm Recycle)**		
Roller Width (**W**)	[m]	0.250			
Description	**Test Number:**		**Comp 1**	**Comp 2**	**Comp 3**
Specific pressing Force	$\mathbf{F_{SP}}$	**[N/mm²]**	4.0	3.0	2.0
Average Actual Speed:	$\mathbf{w_{AV}}$	[m/s]	0.75	0.75	0.75
Actual Roller gap (average)	$\mathbf{X_{gAV}}$	**[mm]**	22.35	21.98	24.59
Actual Specific pressure (average)	$\mathbf{F_{SPAV}}$	**[N/mm²]**	3.98	2.96	1.96
Net Specific Energy Consumption	$\mathbf{E_{SP\ net}}$	**[kWh/t]**	2.31	1.75	1.33
Specific Throughput Constant	**m dot**	**[ts/hm³]**	**222.1**	**217.5**	**214.7**

6.6 Pressing Force Calibration using Database Calibrated Methodology

As illustrated in Figure 6-9, the full-scale HPGR showed ~ 33% lower specific energy consumption than the pilot HPGR composite (50% full-scale HPGR feed to 50% +2 mm recycle). An HPGR operating in closed-circuit with a 2 mm screen was simulated. This closed simulation modelling approach was used in this research to account for differences in HPGR + 2mm recycle load as determined from the specific test result.

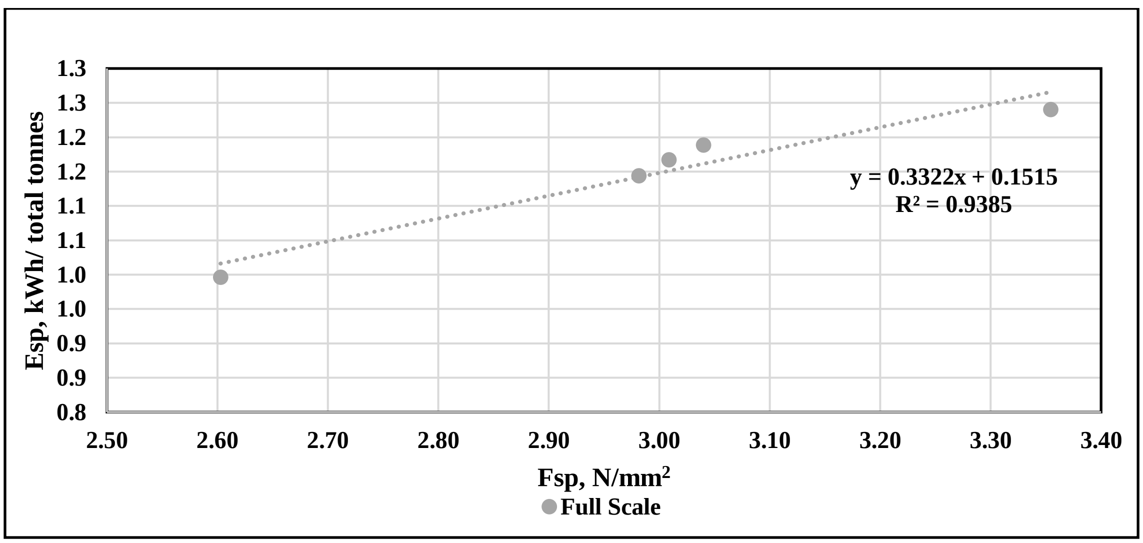

Figure 6-9: Comparison of Specific Pressing Force to Specific Energy Consumption of Full-Scale HPGR Fresh/Recycle Composite Testing

The specific energy consumption for the HPGR is linearly related to the specific throughput constant and roll speed (Van der Feer, 2010). At 3 N/mm^2, the pilot HPGR had a 36% lower $\dot{m}$ of 217.5 ts/hm^2 compared to the full-scale HPGR of 339 ts/hm^2. However, the relationship between the specific energy consumption and the reduction ratio breakage was similar. The Database Calibrated methodology showed a closer calibration for the Piston Press test results for the composite to the full-scale HPGR than the HPGR pilot. The full-scale HPGR showed approximately 34% lower specific energy consumption than the pilot HPGR showed. In contrast, the Database Calibrated methodology showed specific energy consumption to be 3.5% higher than the full-scale for the composite sample.

The finding that the Database Calibrated methodology produced a closer specific energy consumption to the full-scale HPGR than the pilot HPGR (at a 3 N/mm^2 specific pressing force) was not expected. The expectation was that the Database Calibrated methodology would reflect a relationship between the specific energy consumption to specific pressing force that approximated the pilot HPGR. It is typical to find a significant difference in specific energy consumption to the specific pressing force between the pilot and full-scale HPGRs (Hart et al. 2011; Herman et al. 2015).

It should be noted that the Database Calibrated methodology is a multi-linear regression model derived from the pilot HPGR installed at UBC. The pilot HPGR installed at UBC differs in roll geometry and design than the pilot HPGR at ALS Metallurgy. The ALS Metallurgy has a 33% larger diametre pilot HPGR at UBC. At an equivalent roll speed of 0.75 m/s, the pilot HPGR at UBC retains material in the compaction zone for approximately 33% less time than the ALS

Metallurgy pilot HPGR because of the different roll geometries. The different roll geometry may explain why the pilot HPGR showed higher specific energy consumption when processing the composite than both full-scale and the Database Calibrated methodology, however, more study is needed to compare various HPGRs with differing roll geometries.

6.7 Calibration of Piston Press Reduction Ratio

As evidenced in Figures 6-10 and 6-11, calibration of the reduction ratio was similar for both the Database Calibrated methodology and pilot HPGR testing results. More test variation was noted in the Database Calibrated methodology for the full-scale HPGR feed than the full-scale HPGR composite. The Database Calibrated methodology predicted a reduction ratio (Figure 6-10 and 6-11) within the published error to the Pilot HPGR tests of +/- 25% (Davaanyam, 2015; Davaanyam et al., 2015). This finding is positive as supports the reported error of the Database Calibrated methodology. The relationship between the specific energy consumption to the reduction breakage was similar for the Database Calibrated methodology and the pilot HPGR test results. This finding supports the conclusion that the UBC pilot HPGR transfers different amounts of specific energy to the particle bed at a given specific pressing force than ALS Metallurgy pilot. Further study is warranted between the ALS Metallurgy and UBC HPGRs' to understand differences in operational performance.

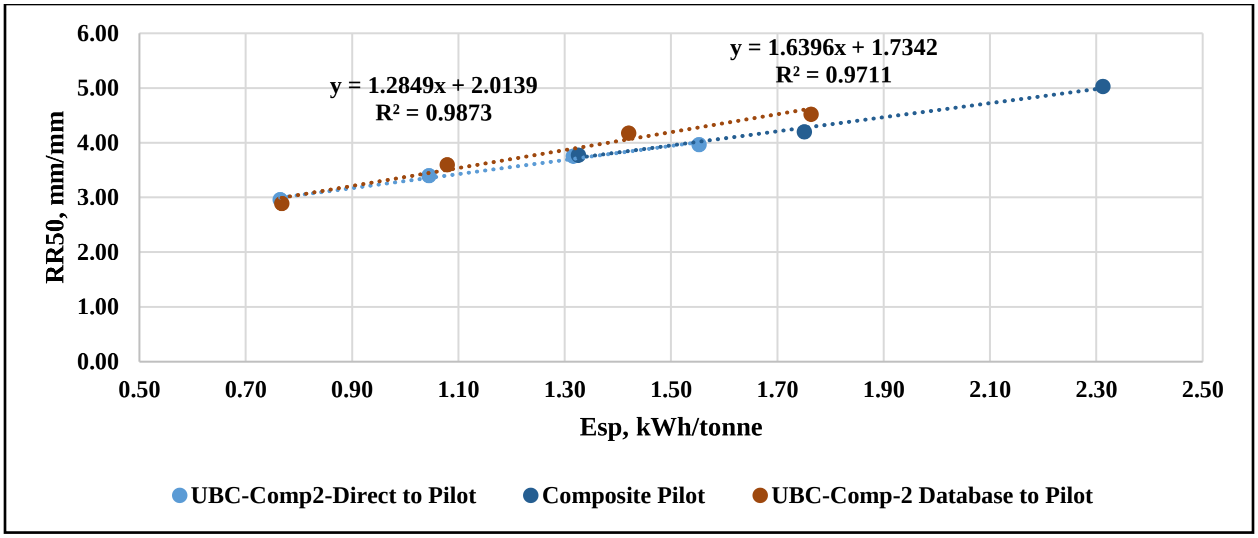

Figure 6-10: Full-scale HPGR Fresh/Recycle Composite Energy Size Reduction Ratio

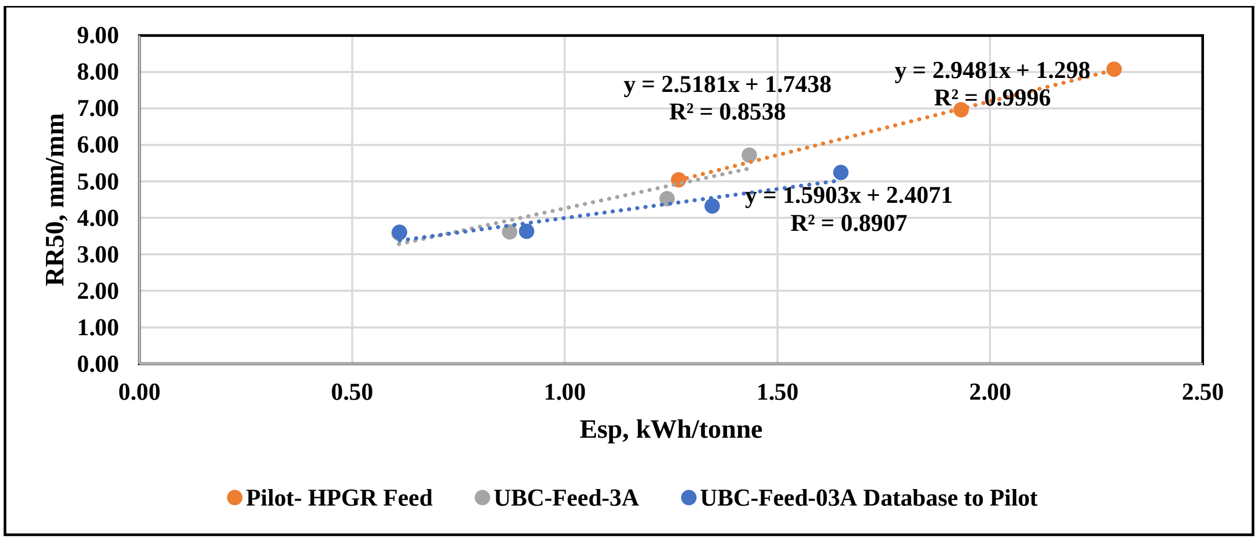

Figure 6-11: Full-scale HPGR Feed Energy Size Reduction Ratio

The roll geometries vary between the UBC pilot HPGR and ALS Metallurgy pilot HPGR. The UBC pilot HPGR has a 33% smaller diameter than the ALS Metallurgy pilot HPGR. In addition, the UBC pilot HPGR has a smooth Hexadur© liner (trademark of Köppern), as opposed to the ALS Metallurgy's studded roll surface. It is documented in the literature that studded rolls tend to have higher levels of friction along the roll surface than smooth liners (Lim, 1999). It is unclear how much of an effect the difference in the liner at roll diametre would have on pilot HPGR performance. More research needs to be done on the relationship between roll geometry, and roll surface, and specific energy. A better understanding of the relationship of roll geometry would help facilitate proper comparisons of the HPGR operating results across different manufacturers and designs. It would also help understand the differences in predicted energy consumption between full-scale HPGR and pilot HPGR.

6.8 Comparison of Pilot and Full-scale HPGR

The full-scale HPGR was found to be significantly more efficient than the HPGR pilot. The full-scale HPGR had a higher reduction ratio and lower specific energy consumption than the pilot HPGR. A comparison of the pilot HPGR and full-scale HPGR are presented in Table 6-4. The recycle load for the pilot HPGR was determined from the PSD analysis on the pilot HPGR product performed on the full-scale HPGR composite at a specific pressing force of 3 N/mm2. The recycle load for full-scale HPGR was determined from the operational data at a 92% screen efficiency. On a tonne per fresh feed basis, the full-scale HPGR had a 35% lower specific energy consumption than pilot HPGR test results indicated at a specific pressing force of 3 N/mm^2. Multiple operations have reported similar findings of full-scale HPGR achieving better energy efficiency than the pilot HPGR (Herman et al., 2015; Hart et al., 2015; Banini, 2011). Freeport-McMoRan’s Morenci found its HPGR (operation to be 20% more energy efficient than its pilot plant HPGR on a total tonne basis (Herman et al., 2015).

Table 6-4 Comparison of Pilot HPGR to Full-Scale HPGR

	Esp kWh/tonne @ 3 N/mm2	Esp kWh/tonne-Fresh @ 3 N/mm2	Recycle Load, % @ 3 N/mm2
Pilot HPGR - Feed	1.85	3.83	107%
Pilot HPGR - Composite	1.81	3.97	119%
Full-scale HPGR	1.17	2.30	103%

6.9 Database Calibrated Closed Circuit Simulation

The Database Calibrated closed circuit simulation predicted specific energy consumption to be 25% and 29% lower than pilot HPGR testing indicated for the full-scale HPGR feed and composite, respectively. This result is higher than the 25% requirement for PEA studies (Davaanyam, 2015). The full-scale HPGR had 18% and 20% lower specific energy consumption than the Database Calibrated closed circuit simulation for the full-scale HPGR feed and composite samples, which is within the accuracy requirement for PEA study. Results of the Database Calibrated closed circuit simulation are presented in Table 6-5. The closed-circuit simulation for the pilot HPGR composite predicted an average specific energy consumption of 3.97 kWh/tonne of fresh feed with a recirculating load of 119%. In comparison the Database Calibrated closed circuit simulation on the composite (using a 92% screen efficiency) predicted an average specific energy consumption of 2.83 kWh/tonne fresh feed for the full-scale HPGR composite and 2.87 kWh/tonne of fresh feed for the full-scale HPGR feed; with recirculating loads of 135% and 133%, respectively. These values compared well with full-scale HPGR operational data, which showed a specific energy consumption of 2.30 kWh/tonne with a 103% recycle load.

Table 6-5: Database Calibrated Closed Circuit Simulation

Sample	Esp (kWh/tonne) @ 3 N/mm^2	Esp (kWh/tonne-Fresh) @ 3 N/mm^2	Recycle Load, % @ 3 N/mm^2
Composite (1:1 Feed to Recycle)			
Composite Test A	1.19	2.78	134%
Composite Test B	1.19	2.84	138%
Composite (Avg)	1.19	2.81	134%
HPGR Feed			
Feed (ALS)	1.18	2.62	121%
Feed Test A	1.22	3.00	140%
Feed Test B	1.22	2.99	144%

6.10 Direct Closed Circuit Simulation on Pilot HPGR

The Direct Calibration closed circuit simulation modelled well against the pilot HPGR closed-circuit simulation. As evident in Table 6-6, all samples had specific energy consumption within 15% of pilot HPGR. The Direct Calibration closed circuit simulation for the full-scale HPGR composite sample predicted a specific energy consumption 6% higher specific energy than the pilot HPGR of at 4.21 to 3.97 kWh/tonne of fresh feed, respectively. In addition, test-work carried out on the composite showed low variability in terms of specific energy consumption energy.

Table 6-6: Direct Closed Circuit Simulation on Pilot HPGR

Sample	Esp kWh/tonne @ 3 N/mm2	Esp kWh/tonne-Fresh @ 3 N/mm^2	Recycle Load, % @ 3 N/mm^2	Difference to Pilot %
Composite (1:1 Feed to Recycle)				
Composite Test A	1.79	4.25	118%	7%
Composite Test B	1.83	4.42	122%	10%
Composite (Avg)	1.81	4.33	120%	8%
Composite Test (ALS)	1.75	3.97	127%	0%
Mean	**1.79**	**4.21**	**122%**	**6%**
Pilot-Composite	1.81	3.97	119%	
HPGR Feed				
Feed Test (ALS)	1.75	3.37	93%	-13%
Feed Test A	1.85	3.90	111%	2%
Feed Test B	1.80	3.87	115%	1%
Mean	**1.80**	**3.71**	**106%**	**-3%**
Pilot-Feed	1.85	3.83	107%	

6.11 Direct Calibration on Full-Scale

The Direct Calibration methodology to full-scale HPGR used the relationship between the specific energy consumption to specific pressing force established from the full-scale operational data and the relationship between the reduction ratio and specific energy consumption established from pilot HPGR testing. Results of the Direct Calibration closed circuit simulation is presented in Table 6-7. The closed-circuit simulation of the full-scale HPGR ranged from 2.07 to 2.56 kWh/tonne fresh feed over the 1st to 3rd quartile of operating data. The closed-circuit simulation found predicted recycle loads to be higher for the Direct Calibration closed circuit simulation of the Piston Press test results for the full-scale HPGR fresh feed and fresh/recycle composite samples. This result was expected as the Direct Calibration methodology used the pilot HPGR results to calibrate the reduction ratio, which is typically lower for pilot HPGR than full-scale HPGR.

Table 6-7: Direct Scale Closed Circuit Simulation on Full-scale HPGR

Sample	Esp kWh/tonne @ 3 N/mm^2	Esp kWh/ Fresh tonne @ 3 N/mm2	Recycle Load, % @ 3 N/mm2	Difference of Full-scale To Direct
Composite (Avg)	1.15	2.76	140%	20%
Feed Test A	1.15	2.73	137%	18%
Feed Test B	1.12	2.66	138%	15%
Pilot HPGR (Composite)	1.81	3.97	119%	73%
Full-scale	**1.17**	**2.30**	**103%**	
Full-scale (1st Quartile)	1.14	2.07	122%	-10%
Full-scale (3rd Quartile)	1.19	2.56	87%	11%

6.12 Discussion

The Piston Press test Database Calibrated and Direct Calibration results were compared to full-scale HPGR and pilot HPGR using closed circuit simulations. The full-scale HPGR feed and composite samples showed similar predictions using both the Database Calibrated and Direct Calibration closed circuit simulation. A summary of the closed circuit simulation is presented in Table 6-8. The Direct Calibration to full-scale closed circuit simulation better predicted the relationship between specific pressing force and specific energy consumption than the pilot HPGR testing. The Direct Calibration closed circuit simulation of full-scale HPGR showed a 20% higher specific energy consumption than full-scale HPGR for the composite sample. Significant differences in the relationship between specific energy consumption and pressing force were found between HPGR piloting and full-scale HPGR. This result is supported by the literature, which indicates it is common for the HPGR production units to have increased throughput, improved reduction ratio performance, and lower specific energy consumption compared to pilot HPGR (Herman et al., 2015; Banini et al., 2011). Pilot HPGR test results showed a 36% lower $\dot{m}$ than full-scale HPGR. This significant difference indicates that the full-scale HPGR had superior material intake characteristics. The HPGR operating gap increases with the $\dot{m}$. This result in more tonnage through the HPGR, which will cause the specific energy, applied to the material to be dispersed over more tonnes. The difference in $\dot{m}$ makes a comparison of the pilot HPGR and full-scale HPGR difficult as these units are operating at different operating points. Even accounting for this, the full-scale HPGR showed improved reduction ratio performance that ultimately led to a much lower specific energy consumption than the piloting predicted.

Table 6-8: Summary of Closed-Circuit Simulation for Full-scale Composite Sample

Closed Circuit Simulation	Methodology	Esp kWh/tonne-Fresh @ 3 N/mm^2	Recycle Load, % @ 3 N/mm^2	% Difference to Full-scale HPGR
Pilot HPGR	N/A	3.97	119%	73%
Full-scale HPGR	N/A	2.30	103%	N/A
Direct to HPGR	Direct to Full-scale	2.76	140%	20%
Database to Pilot HPGR	Database to Pilot	2.81	134%	22%

The Database Calibrated methodology specific energy consumption compared closely to full-scale HPGR. The closed-circuit analysis using the Database Calibrated methodology predicted specific energy consumption 22% higher than the full-scale HPGR. The energy reduction relationship was similar both for the pilot HPGR and the Database Calibrated methodology. It is currently difficult to fully explain why the relationship between the specific pressing force and specific energy consumption differed so much between the Database Calibrated methodology and the ALS Metallurgy pilot HPGR. This result seems to suggest that the UBC pilot HPGR may exhibit a different relationship between specific pressing force and specific energy consumption. Since comminution occurs within a relatively small area in the HPGR as defined as the compaction zone at high pressures, it is difficult to study how the energy transfer occurs. The literature review did not find any studies that conducted comparisons between different pilot HPGR machines. It, therefore, is difficult to conclude the exact cause of reason for this result. A proper comparison would need to be conducted comparing the HPGR performances between the UBC and ALS Metallurgy pilot HPGR to understand differences in the pilot HPGR machines.

As was noted (section 6.6) roll dimensions vary between the pilot HPGR at ALS Metallurgy and the pilot HPGR at UBC that was used to develop the database for the Database Calibrated methodology. In hindsight, roll speed for pilot HPGR testing should have been selected to approximate a similar residence time in the compaction zone as the full-scale when performing the pilot HPGR testing. Adjustments in the roll speed may have ensured that similar energy transfer was achieved during pilot HPGR testing as full-scale HPGR. However, the degree of this effect is not clear and further testing would be needed.

The Piston Press test Database Calibrated and Direct Calibration methodologies had similar predicted specific energy consumption to full-scale HPGR. The methodologies used to simulate full-scale HPGR can easily be applied to other operations. The Database Calibrated and Direct Calibration methodologies have significant potential for predicting HPGR performance that may be used for geo-metallurgy studies and production planning. The Piston Press test methodologies can assist in predicting and understanding variations in production caused by changes in lithology and alterations. Currently, this type of production forecast cannot be determined without extensive piloting, which is not practical.

Chapter 7: Conclusions & Recommendations

Currently, the industry does not recognize a standard bench-scale laboratory test for sizing nor modelling the HPGR for hard rock mining. As a result, metallurgical studies are prohibitively expensive and uneconomical for early-stage projects, such as scoping level and PEA studies. The purpose of this research was to validate the Piston Press test, specifically the Database Calibrated, and Direct Calibration methodologies as an industry standard bench-scale amenability test for the HPGR. A research methodology was structured to demonstrate the Piston Press test as a suitable bench-scale test for HPGR amenability by meeting the following criteria:

- The Piston Press test uses the same breakage mechanism as the HPGR (established, Davaanyam, 2015);
- The Piston Press test is reproducible by independent metallurgical laboratories;
- The Piston Press test results can be applied to full-scale HPGR in a non-proprietary manner.

Specifically, the research formalized the Piston Press test procedures by examining the effects of moisture, dry versus wet splitting (agglomeration), and porosity. The research demonstrated the Piston Press test as being independently reproducible. Lastly, the research program validated the Piston Press test Database Calibrated and Direct Calibration methodologies for modelling full-scale HPGR using a non-proprietary approach to simulate a closed circuit HPGR.

7.1 Evaluation of Piston Press Test Procedures

The research in Chapter 4 found moisture improved reduction ratio breakage during Piston Press testing. On the contrary, changes in specific energy consumption were found to be relatively negligible to increases of moisture from the range of 1.5% to 5%. These findings indicate that elevated moisture from 1.5% to 5% improved energy transfer within the particle-bed during high-pressure compression breakage. The findings on the effects of moisture conform to the concept that the loss of energy efficiency in the HPGR is primarily related to roll slippage and not inter-particle breakage. At Piston Press testing at 240 Mpa, an average increase of moisture from 1.5% moisture to 5% moisture (wet split) resulted in a 22.6% higher reduction ratio with an average decrease in specific energy consumption of 2.1%.

In addition, it was found that a proper level of moisture is necessary for the Piston Press test to ensure proper agglomeration of the fines. Lack of agglomeration of the fines led to stratification of the particle-bed during loading the piston die for Piston Press testing. Stratification will affect the inter-particle bed and breakage mechanics. In other words, moisture is necessary to ensure reproducible and accurate results during the Piston Press test.

Porosity was found to correlate to Piston Press test results for the three deposits tested. Samples with high levels of porosity had significantly higher reduction ratio breakage than samples with low porosity. The relationship between porosity and reduction ratio is likely driven by fatigue crack propagation that occurs at void spaces. As the surface walls of the voids begin to fail, fracturing introduces additional planes of weakness which cause new fractures to begin and propagate along. Comparing the maximum packed bed density to the S.G., as determined by the relative density method, helped identify high porosity ores. These findings warrant further study on the effects of porosity on the Piston Press test, specifically, evaluating the effects of porosity on various lithology, alteration, and ore deposits. Further research is warranted to understand if the correlation between porosity and reduction ratio breakage extends to other deposits.

7.2 Reproducibility of the Piston Press Test

Test-work carried out in Chapter 5 included duplicate test-work conducted at UBC and ALS Metallurgy. The test-work demonstrated the Piston Press test is independently reproducible. The Piston Press test is capable of being adapted to alternate piston press machine configurations. The most significant challenge during duplicate testing was ensuring the analysis for the specific energy consumption accounted for different frequencies in the measurement data from the two metallurgical labs. A method was developed that averaged the ALS Metallurgy's force and displacement readings to replicate a similar frequency as UBC's piston press machine. The higher frequency of the displacement and force readings at ALS Metallurgy caused noise in the Piston Press raw data. This noise initially led to an overestimating of the specific energy consumption. The overestimation of specific energy was rectified by modifying the integration algorithm of the force-displacement curve by disregarding negative fluctuations of the displacement during loading.

Both the specific energy consumption and product size distribution matched well between the duplicate tests carried out between UBC and ALS Metallurgy. Duplicate results from testing by UBC and ALS Metallurgy showed a correlation of variability for the Piston Work index of 1.0% and 5.8% for the product size passing 50%, and 80%, respectively for the HPGR feed. The composite sample showed a correlation of variance of 3.9% and 2.2% for the product size passing 50%, and 80%, respectively.

7.3 Validation of Full-scale HPGR

Results from Chapter 6 demonstrated that both the Database Calibrated and Direct Calibration methodologies are suitable for simulating full-scale HPGR. The Direct Calibration closed circuit simulation was capable of modelling full-scale HPGR within 20%, which was significantly better than pilot HPGR testing. Had the reduction ratio of the Piston Press tests been directly calibrated to full-scale HPGR rather than to pilot HPGR, the accuracy of the closed circuit simulation likely would have been better.

The Database Calibrated closed circuit simulation was found to be 22% higher than full-scale HPGR and ~26 % lower than HPGR piloting. It is unclear as to the exact explanation why the Database Calibrated closed circuit simulation modelled closer to the full-scale than ALS Metallurgy's pilot HPGR testing. The cause of this result may be due to a difference in roll geometry. The Database Calibrated methodology was developed using a database built from HPGR pilot test-work conducted at UBC's (750 mm diametre), which has a smaller roll diametre than the pilot HPGR at ALS Metallurgy (1000 mm diametre). From the test-work carried out, it is unclear what effect changes in roll geometry would have on testing. The Database Calibrated methodology cannot be used as a direct comparison of the UBC pilot HPGR to the ALS Metallurgy's pilot HPGR. It was noted that the pilot HPGR for ALS Metallurgy and the full-scale HPGR had a different residence time regarding the compaction and nip angle zones based on the roll geometry and roll speed. Differences in roll geometry may have enabled more energy to be input into the HPGR feed during comminution during pilot HPGR. However, more study is required to investigate this result fully.

This thesis successfully demonstrates the reproducibility of Piston Press test methodologies by retrofitting an independent lab that demonstrated the Piston Press test to be transferable and reproducible. This comparison, combined with validating the methodologies against full-scale HPGR, shows the results analysis is straightforward, and non-proprietary for independent engineering consultants to conduct.

7.4 Recommendations

Based on the research conducted, the following improvements to current standard operating procedures are recommended for future testing both at UBC and future installations:

7.4.1 Improvements in the Current Piston Press Test Procedures

- Explore the effects of porosity on indicating HPGR amenability, and determine if similar results are found across other deposit types. The proxy density method can be easily integrated into current test procedures at UBC. Currently, there is limited research available on the effects of porosity on the HPGR performance. Assuming similar correlations are found across ore types, porosity may be useful information when understanding HPGR amenability and geo-metallurgy variability. Improved understanding of the effects of porosity on HPGR may assist in the detail engineering and design stage of development or for mill production forecasting.

- The density proxy, if significant across additional ore bodies should be included in the UBC's HPGR database, as the density proxy might help improve the accuracy of the Database Calibrated methodology.
- Incorporate the Piston Press test moisture into the Database Calibrated methodology. Because moisture was found to improve breakage during Piston Press testing, moisture should be added as an input to the Database Calibrated methodology. Currently, the database for HPGR pilot tests at UBC includes testing at various levels of moisture. The current average moisture in the UBC pilot HPGR database of past test-work is ~2.5%. It is recommended future Piston Press testing be standardized to moisture levels between 2.5% to 3 %.

7.4.2 Reproducibility of the Piston Press Test

- Ensure future Piston Press test installations at independent metallurgical laboratories closely match UBC's Piston Press test specifications. Standerizing furture installations will facilitate the specific energy consumption calibration to UBC's piston press machine.
- UBC should conduct ongoing reproducibility and duplicate testing at any independent installations of the Piston Press test.
- The non-negative displacement algorithm should be used for future testing programs.

7.4.3 Piston Press test Full-Scale Calibration

More research is needed to understand the effects of roll geometry on the HPGR performance, specifically concerning varying designs of HPGR pilot machines. Therefore, it is recommended to carry out a duplicate three pressure pilot HPGR test program at both UBC and ALS Metallurgy, in order to compare the specific energy consumptions of the two machines.

Bibliography

Altun, O., Benzer, H., & Aydogan, N. (February 2011). Comparison of Open and Closed Circuit HPGR Application on Dry Circuit Performance. *Minerals Engineering*, 267-275.

Amelunxen, P. (2012, December 6). The Implication of Ore Hardness variability on Comminution Circuit Energy Efficiency (and Some Other Thoughts). *Aminpro Chile*.

Austin, L. G., Klimpel, R. R., & Luckie, P. T. (1984). Process Engineering Size Reduction. New York, N.Y.: Society of Mining Engineers of the AIME.

Bamber, A., Klein, B., Nadolski, S., & Drozdiak, J. (2009). *The Development of an Appropriate Small-Scale Test Suite and Associated Procedure for the Selection and Sizing of High Pressure Grinding Roller Presses (HPGR) for Hard Rock Ores.* Vancouver, British Columbia, Canada: NSERC Proposal.

Banini, G., Villanueva, A., Hollow, J., & Mosher, J. (2011). Evaluation of Sale Up Effect on High Pressure Grinding Roll (HPGR) Implementation at P.T. Freeport Indonesia. *SAG Conference.* Vancouver: SAG Conference.

Bond, F. C. (1961). Crushing and Grinding Calculations, Part I-III. *British Chemical Engineering*, 6: 378-385, 543-548.

Bulled, D., & Husain, K. (2008). The Development of a Small-Scale Test to Determine Work Index for High Pressure Grinding Rolls. (pp. Technical Paper 2008-49). SGS Mineral Services.

Burchardt, E., Patzelt, N., Knecht, J., & R., K. (2011). HPGR's in Minerals: What do Existing Operations Tell Us for the Future? *SAG Conference.* Vancouver.

Casteel, K. (2005). High-Pressure Grinding--Playing a Wider Role. *Mining and Quarry World , (3)(09)*, 12-7.

Daniel, M., & Morrel, S. (2002). *HPGR Verification and Scale-up. Master of Engineering Science.* University of Queensland.

Davaanyam, Z. (2015). *Piston Test Procedures for Predicting Energy-Size Reduction of High Pressure Grinding Rolls.* Vancouver, British Columbia, Canada: University of British Columbia.

Davaanyam, Z., Klein, B., & Nadolski, S. (2015). Using Piston Press Tests for Determining Optimal Energy Input for an HPGR Operation. *Presented at SAG Conference 2015.* Vancouver.

Eckel, E., & Martin, T. (1905). *Edison: His Life and Inventions.* New York: Harper and Brothers Publishers.

Ennis, S., & Hertel, M. (2012). *Soledad Mountain Project Technical Report.* Prepared for Golden Queen Mining. AMEC. Retrieved from Retrieved from www.sedar.com

Esna-Ashari, M., & Kellerwessel, H. (1988). Roller Press Comminution Improves Heap Leach Recovery. *Randol Perth International Gold Conference*, (pp. pp 50-53). Perth.

FLSmidth. (1990). *General Theory of Material Pressures and Capacities of Roller Press.* Internal Report.

Fuerstenau, D., Shukla, A., & Kapur, P. (1991). Energy Consumption and Product Size Distribution in Choke-fed, High-compression Roll Mills. *International Journal of Mineral Processing, 32,* 59-79.

Hart, S., Parker, B., Rees, T., Manesh, A., & Mcgaffin, I. (2011). Commissioning and Ramp up of the HPGR Circuit at Newmont Boddington Gold. *SAG Conference.* Vancouver: SAG Conference.

Herman, V. S., Harbold, K. A., Mular, M. A., & Biggs, L. J. (2015). Building the World's Largest HPGR-the HRC3000 at the Morenci Metcalf Concentrator. *SAG Conference.* Vancouver: SAG Conference.

Johanson, J. (1965). A Rolling Theory for Granular Solids. *Journal of Applied Mechanics Series*(E 32(4)), 842.

Kenneth, H. (1973). Mineral Processing. (G. Cummins, Ed.) *SME Mining Engineering Handbook*, 27-37-38.

Klymowsky, R. P., Knecht, J., & Burchardt, E. (2002). Selection and Sizing of High Pressure Grinding Rolls. *Mineral Processing Plant* (pp. pp. 636-668). Control Proceedings.

Kumar, A., F., W., Klein, B., & Davaanyam, Z. (2016). Comparison of Model Based Energy Estimation for an HPGR Application. *International Mineral Processing Congress.* Quebec City: Canadian Institute of Mining, Metallurgy, and Petroleum.

Kurtz, B., & Barduhn, A. (1960). Compacting granular solids. *Chemical Engineering Progress*, 56(1).

Leißner, T., Hoang, D., T., H., Bachmann, K., Gutzmer, J., Schubert, H., & Peuker, U. (2016). A Mineral Liberation Study of Grain Boundary Fracture Based on Measurements of the Surface Exposure After Milling. *International Journal of Mineral Processing*, 3-13.

Lim, W. I. (1999). Some Benefits of using Studed Surfaces in High Pressure Grinding Rolls. *Minerals Engineering*, 187-203.

Lynch A.J., C. R. (2009). *The History of Grinding.* Littleton, Colorado, U.S.A: Society for Mining, Metallurgy, and Exploration.

McClintock, M. a. (2016). Piston Press Calibration and Database for HPGR Sizing. *International Mineral Processing Congress* (p. Paper 745). Quebec City: International Mineral Processing Congress.

McNab, B. (2006). Exploring HPGR Technology for Heap Leaching of Fresh Rock Gold Ores. *IRR Crushing & Grinding Conference.* Townsville, Qld.

Metso. (2015). *Basics in Minerals Processing* (Vol. Edition 10). Helsinki, Finland: Metso. Retrieved from www.metso.com

Morell, S. (November 2004). HPGR Model Verification and Scale-up. *Minerals Engineering*.

Morley C., a. D. (2010). HPGR- FAQ. *The Journal of the Southern African Institute of Mining and Metallurgy, September*, 157-168.

Morley, C. (2006). High Pressure Grinding Rolls- A Technology Review. In S. In Kawatra (Ed.), *Advances in Comminution.* Society for Mining, Metallurgy, and Exploration.

Morrell, S. (n.d.). *Predicting SAG/AG Mill and HPGR Specific Energy Requirements Using the SMC Rock Characterisation Test.* SMCC Pty Ltd.

Nadolski, S. (2012). *Development of a Laboratory Scale Procedure for Predicting Throughput of High Pressure Grinding Rolls.* Vancouver, British Columbia, Canada: University of British Columbia.

Patzelt, N. K. (1995). Advances in POLYCOM High-Pressure Roll Grinding of Refractory Gold Ores. *Randol Gold Forum*, (pp. pp 107-123). Perth.

Pincock, Allen & Holt Consultants. (2011). *Technical Report for the Sierra Gorda Project.* Prepared for Quadra FNX Mining Ltd.

Pownell, J. &. (2013, June). Putting HPGR Technology Through its Paces. *Mining Magazine*, 74-76.

Rashidi, S., Rajamani, R., & Fuerstenau, D. (2016). A Review of the Modeling of High Pressure Grinding Rolls. *Kona Powder and Particle*, 125-140.

Research Association of the British Paint. (1953). Colour and Varnish Manufacturers. Corn and Paint.

Schönert, k. (1988). A First survey of Grinding with High-Compression Roller Mills . *International Journal of Mineral Processing 22*, 401-402.

SMC. (n.d.). Using the SMC Test to Predict Comminution Circuit Performance. Retrieved November 2017, from www.smctesting.com: http://www.smctesting.com/documents/Using_the_SMC_Test.pdf

Tropicana JV. (2018, July 17). *Tropicana Joint Venture*. Retrieved from http://www.tropicanajv.com.au: http://www.tropicanajv.com.au/irm/content/operations.aspx?RID=407

van der Meer, F. (2010, September). High Pressure Grinding Rolls Scale-up and Experiences. (pp. 1319-1331). Brisbane: International Mineral Processing Congress.

van der Meer, F., & Greendken, A. (2010). Flowsheet Considerations for Optimal use of Hogh Pressure Grinding Rolls. *Minerals Engineering, 23(9)*, 663-669.

von Seebach, M., & Knobloch, O. R. (1987). High Pressure Grinding Rolls in Industrial Application. Denver, Colorado: Society of Mining Engineers.

W., B., Patzelt, N., & Knecht, J. (1997). Metallurgical Benefits of High Pressure Roll Grinding for Gold and Copper Recovery. (pp. pp 111-116). Denver: Society of Mining, Metallurgy, and Exploration.

Weiss. (1973). Selection of Mill Site. In I. Given (Ed.), *SME Mining Engineering Handbook* (pp. 28-29). New York: Society of Mining Engineers of the American Institute of Mining, Metallurgical, and Petroleum Engineers, Inc.

Wills, B., & Atkinson, K. (1993). Some Observations on Fracture and Liberation of Mineral Assemblies. *Miner. Eng. 6*, 697-706.

Appendices

Appendix A Piston Press Test Data

A.1 Detailed Research Outline

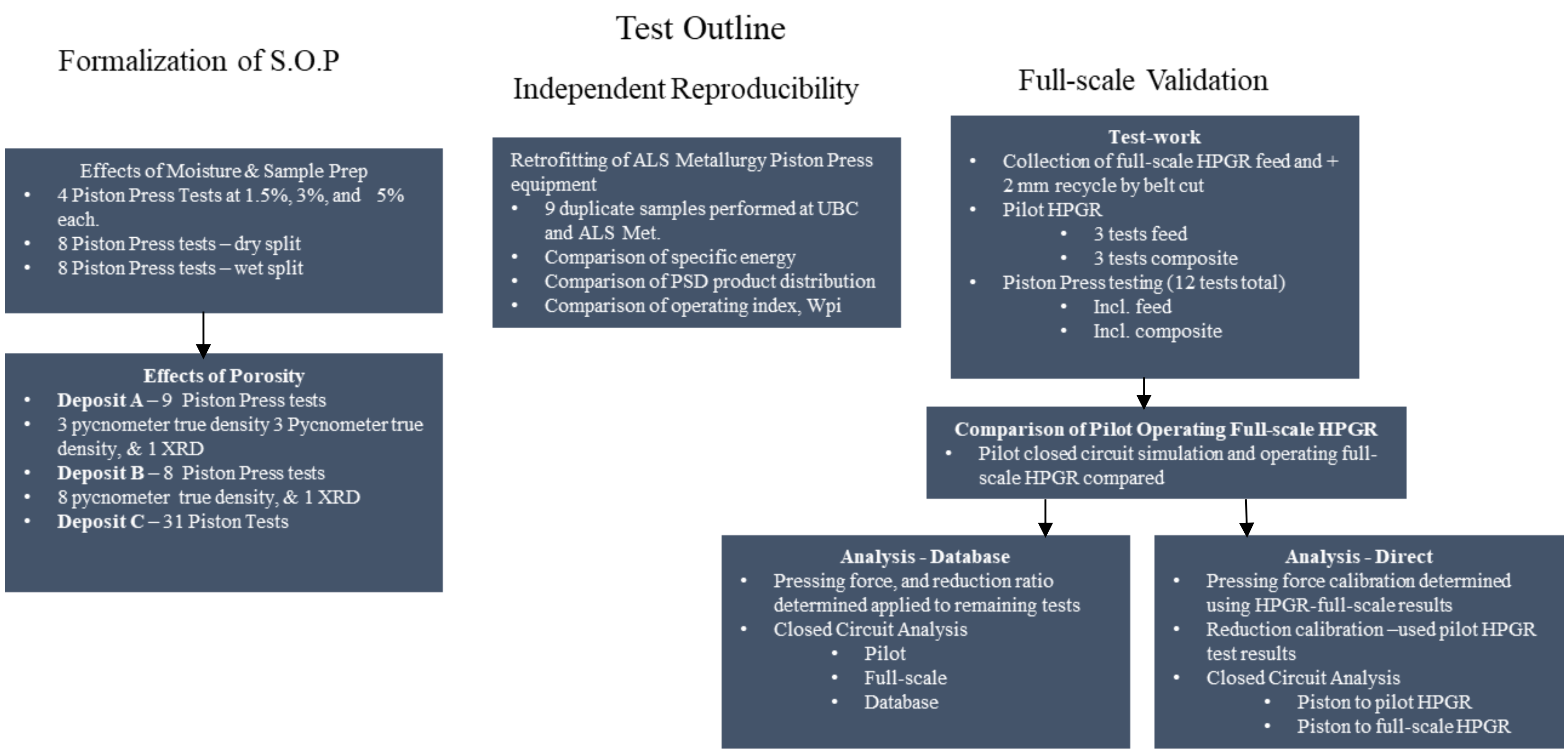

A.2 Piston Press Test Data

Piston Press Test Data Summary												
	UBC-Comp1A1				UBC-Comp1A2				UBC-Comp1A			
Test	UBC-Comp-1A-1-P1	UBC-Comp-1A-1-P2	UBC-Comp-1A-1-P3	UBC-Comp-1A-1-P4	UBC-Comp-1A-2-P1	UBC-Comp-1A-2-P2	UBC-Comp-1A-2-P3	UBC-Comp-1A-2-P4	UBC-Comp-1A-P1	UBC-Comp-1A-P2	UBC-Comp-1A-P3	UBC-Comp-1A-P4
Force kN	1397.45	1098.58	798.96	499.47	1396.66	1098.78	799.34	499.05	1397.06	1098.68	799.15	499.26
Pressure Mpa	240.58	189.12	137.54	85.98	240.44	189.16	137.61	85.91	240.51	189.14	137.58	85.95
Energy kWh/t - Direct	1.45	1.27	1.01	0.75	1.58	1.26	1.02	0.77	1.51	1.26	1.02	0.76
Energy kWh/t - Database	1.61	1.35	1.04	0.75	1.75	1.37	1.04	0.77	1.68	1.36	1.04	0.76
Moisture, %	5.0	5.0	5.0	5.0	5.0	5.0	5.0	5.0	5.0	5.0	5.0	5.0
Thickness mm	30.31	30.31	30.58	31.21	30.32	30.15	30.90	31.79	30.32	30.23	30.74	31.50
Density g/cc	2.83	2.76	2.70	2.61	2.79	2.76	2.69	2.61	2.81	2.76	2.70	2.61
Mass g												
	UBC-Comp1B1				UBC-Comp1B2				UBC-Comp1B			
Test	UBC-Comp-1B-1-P1	UBC-Comp-1B-1-P2	UBC-Comp-1B-1-P3	UBC-Comp-1B-1-P4	UBC-Comp-1B-2-P1	UBC-Comp-1B-2-P2	UBC-Comp-1B-2-P3	UBC-Comp-1B-2-P4	UBC-Comp-1B-P1	UBC-Comp-1B-P2	UBC-Comp-1B-P3	UBC-Comp-1B-P4
Force kN	1396.90	1099.21	799.41	498.89	1395.51	1098.85	799.10	499.55	1396.21	1099.03	799.25	499.22
Pressure Mpa	240.48	189.23	137.62	85.88	240.24	189.17	137.57	86.00	240.36	189.20	137.59	85.94
Energy kWh/t - Direct	1.48	1.23	0.97	0.71	1.48	1.30	1.05	0.77	1.48	1.26	1.01	0.74
Energy kWh/t - Database	1.70	1.30	1.00	0.71	1.65	1.40	1.07	0.77	1.68	1.35	1.04	0.74
Moisture, %	5.0	5.0	5.0	5.0	5.0	5.0	5.0	5.0	5.0	5.0	5.0	5.0
Thickness mm	30.08	31.01	30.53	31.80	29.82	30.63	30.63	31.57	29.95	30.82	30.58	31.69
Density g/cc	2.82	2.76	2.71	2.61	2.83	2.73	2.70	2.60	2.82	2.75	2.70	2.61
Mass g												
	UBC-Comp2A1				UBC-Comp2A2				UBC-Comp2A			
Test	UBC-Comp-2A-1-P1	UBC-Comp-2A-1-P2	UBC-Comp-2A-1-P3	UBC-Comp-2A-1-P4	UBC-Comp-2A-2-P1	UBC-Comp-2A-2-P2	UBC-Comp-2A-2-P3	UBC-Comp-2A-2-P4	UBC-Comp-2A-P1	UBC-Comp-2A-P2	UBC-Comp-2A-P3	UBC-Comp-2A-P4
Force kN	1397.12	1097.29	799.52	498.95	1397.05	1098.36	798.99	499.25	1397.08	1097.83	799.25	499.10
Pressure Mpa	240.52	188.90	137.64	85.89	240.51	189.09	137.55	85.95	240.51	188.99	137.59	85.92
Energy kWh/t - Direct	1.55	1.33	1.06	0.78	1.53	1.31	1.04	0.79	1.54	1.32	1.05	0.78
Energy kWh/t - Database	1.77	1.42	1.09	0.78	1.72	1.43	1.07	0.79	1.74	1.42	1.08	0.79
Moisture, %	3.0	3.0	3.0	3.0	3.0	3.0	3.0	3.0	3.0	3.0	3.0	3.0
Thickness mm	27.69	28.31	28.53	29.05	27.86	28.39	28.76	29.86	27.77	28.35	28.64	29.46
Density g/cc	2.80	2.73	2.67	2.60	2.80	2.73	2.70	2.60	2.80	2.73	2.68	2.60
Mass g												
	UBC-Comp2B1				UBC-Comp2B2				UBC-Comp2B			
Test	UBC-Comp-2B-1-P1	UBC-Comp-2B-1-P2	UBC-Comp-2B-1-P3	UBC-Comp-2B-1-P4	UBC-Comp-2B-2-P1	UBC-Comp-2B-2-P2	UBC-Comp-2B-2-P3	UBC-Comp-2B-2-P4	UBC-Comp-2B-P1	UBC-Comp-2B-P2	UBC-Comp-2B-P3	UBC-Comp-2B-P4
Force kN	1396.76	1098.54	799.50	499.33	1396.66	1098.22	799.54	499.61	1396.71	1098.39	799.52	499.47
Pressure Mpa	240.46	189.12	137.64	85.96	240.44	189.06	137.64	86.01	240.45	189.09	137.64	85.99
Energy kWh/t - Direct	1.57	1.33	1.04	0.75	1.57	1.29	1.05	0.75	1.57	1.31	1.04	0.75
Energy kWh/t - Database	1.75	1.45	1.07	0.75	1.82	1.38	1.08	0.75	1.78	1.42	1.08	0.75
Moisture, %	3.0	3.0	3.0	3.0	3.0	3.0	3.0	3.0	3.0	3.0	3.0	3.0
Thickness mm	27.86	28.49	28.46	29.14	27.69	28.03	29.05	29.29	27.78	28.26	28.76	29.21
Density g/cc	2.79	2.74	2.69	2.60	2.81	2.74	2.67	2.61	2.80	2.74	2.68	2.61
Mass g												
	UBC-Comp3A1				UBC-Comp3A2				UBC-Comp3A			
Test	UBC-Comp-3A-1-P1	UBC-Comp-3A-1-P2	UBC-Comp-3A-1-P3	UBC-Comp-3A-1-P4	UBC-Comp-3A-2-P1	UBC-Comp-3A-2-P2	UBC-Comp-3A-2-P3	UBC-Comp-3A-2-P4	UBC-Comp-B-P1	UBC-Comp-B-P2	UBC-Comp-B-P3	UBC-Comp-B-P4
Force kN	1396.62	1099.15	799.38	499.72	1397.02	1098.88	798.85	499.06	1396.82	1099.02	799.12	499.39
Pressure Mpa	240.43	189.22	137.62	86.03	240.50	189.17	137.52	85.91	240.47	189.20	137.57	85.97
Energy kWh/t - Direct	1.62	1.30	1.04	0.80	1.67	1.39	1.05	0.76	1.65	1.35	1.05	0.78
Energy kWh/t - Database	1.81	1.38	1.06	0.80	1.82	1.48	1.09	0.76	1.82	1.43	1.08	0.78
Moisture, %	1.5	1.5	1.5	1.5	1.5	1.5	1.5	1.5	1.5	1.5	1.5	1.5
Thickness mm	30.41	30.48	31.53	32.51	30.53	31.46	31.11	32.06	30.47	30.98	31.32	32.29
Density g/cc	2.71	2.69	2.64	2.54	2.70	2.65	2.62	2.52	2.71	2.67	2.63	2.53
Mass g												
	UBC-Comp3B1				UBC-Comp3B2				UBC-Comp3B			
Test	UBC-Comp-3B-1-P1	UBC-Comp-3B-1-P2	UBC-Comp-3B-1-P3	UBC-Comp-3B-1-P4	UBC-Comp-3B-2-P1	UBC-Comp-3B-2-P2	UBC-Comp-3B-2-P3	UBC-Comp-3B-2-P4	UBC-Comp-B-P1	UBC-Comp-B-P2	UBC-Comp-B-P3	UBC-Comp-B-P4
Force kN	1396.88	1098.86	799.31	499.56	1396.80	1098.92	799.22	499.38	1396.84	1098.89	799.26	499.47
Pressure Mpa	240.48	189.17	137.60	86.00	240.46	189.18	137.59	85.97	240.47	189.18	137.59	85.99
Energy kWh/t - Direct	1.54	1.31	1.06	0.73	1.58	1.38	1.07	0.75	1.56	1.34	1.07	0.74
Energy kWh/t - Database	1.74	1.38	1.08	0.73	1.78	1.46	1.09	0.75	1.76	1.42	1.09	0.74
Moisture, %	1.5	1.5	1.5	1.5	1.5	1.5	1.5	1.5	1.5	1.5	1.5	1.5
Thickness mm	30.46	31.08	30.87	32.31	31.11	31.21	31.08	32.13	30.79	31.15	30.98	32.22
Density g/cc	2.73	2.66	2.60	2.53	2.71	2.67	2.62	2.51	2.72	2.67	2.61	2.52
Mass g												

Piston Press Test Data Summary Continued								
	ALS-FEED-A				ALS-FEED-B			
Test	P1	P2	P3	P4	P1	P2	P3	P4
Force kN	1400.05	1099.44	899.75	699.47	1399.72	1099.38	899.66	699.74
Pressure Mpa	241.02	189.27	154.89	120.42	240.96	189.26	154.88	120.46
Energy kWh/t (Avg (5.5))	1.50	1.18	0.95	0.76	1.45	1.08	0.94	0.71
Moisture, %	5.0	5.0	5.0	5.0	5.0	5.0	5.0	5.0
Thickness mm	26.20	26.03	26.17	26.01	25.77	26.01	26.48	28.54
Density g/cc (w/ Rebound)	2.70	2.66	2.63	2.65	2.67	2.66	2.61	2.44
Mass g	410.80	402.10	400.40	399.90	400.10	402.10	400.70	405.20
	ALS-Comp-A				ALS-FEED-C			
Test	P1	P2	P3	P4	P1	P2	P3	P4
Force kN	1399.61	1099.96	799.74	500.12	1399.710429	1099.599	799.8294	499.6668
Pressure Mpa	240.95	189.36	137.68	86.10	240.96	189.30	137.69	86.02
Energy kWh/t (Avg (5.5))	1.61	1.34	1.04	0.71	1.36	1.18	0.80	0.57
Moisture, %	2.5	2.5	2.5	2.5	2.5	2.5	2.5	2.5
Thickness mm	28.55	28.92	29.09	29.66	28.87	29.13	29.26	29.67
Density g/cc (w/ Rebound)	2.59	2.57	2.50	2.48	2.59	2.62	2.55	2.52
Mass g	430.00	431.40	422.70	427.60	434.80	442.80	432.80	433.70
	UBC-Feed-03A				UBC-Feed-03B			
Test	P1	P2	P3	P4	P1	P2	P3	P4
Force kN	1396.53	1099.07	799.64	499.14	1396.44	1099.07	798.85	499.64
Pressure Mpa	240.42	189.18	137.66	85.93	240.40	189.21	137.52	86.01
Energy kWh/t - Direct	1.434	1.241	0.870	0.610	1.40	1.14	0.91	0.64
Energy kWh/t - Database	1.649	1.347	0.910	0.612	1.646	1.288	0.956	0.642
Moisture, %	2.5	2.5	2.5	2.5	5.0	5.0	5.0	5.0
Thickness mm	27.68	27.96	28.85	29.47	25.14	25.79	25.81	26.59
Density g/cc	2.81	2.77	2.68	2.61	2.89	2.83	2.76	2.69
Mass g								

Piston Press Test Summary - Reduction Performance

		UBC-Comp-1A-1-P1	**UBC-Comp-1A-1-P2**	**UBC-Comp-1A-1-P3**	**UBC-Comp-1A-1-P4**		**UBC-Comp-1A-2-P1**	**UBC-Comp-1A-2-P2**	**UBC-Comp-1A-2-P3**	**UBC-Comp-1A-2-P4**		**UBC-Comp-1A-P1**	**UBC-Comp-1A-P2**	**UBC-Comp-1A-P3**	**UBC-Comp-1A-P4**
F50, mm	6.24	1.54	1.63	1.95	2.13	6.24	1.52	1.69	1.89	2.14	6.24	1.53	1.66	1.92	2.14
F80, mm	10.04	6.01	6.09	6.72	6.56	10.04	5.57	5.84	6.17	6.66	10.04	5.78	5.97	6.43	6.61
RR50		4.06	3.83	3.20	2.93		4.11	3.70	3.30	2.92		4.09	3.77	3.25	2.92
RR80		1.67	1.65	1.50	1.53		1.80	1.72	1.63	1.51		1.74	1.68	1.56	1.52
		UBC-Comp-1B-1-P1	**UBC-Comp-1B-1-P2**	**UBC-Comp-1B-1-P3**	**UBC-Comp-1B-1-P4**		**UBC-Comp-1B-2-P1**	**UBC-Comp-1B-2-P2**	**UBC-Comp-1B-2-P3**	**UBC-Comp-1B-2-P4**		**UBC-Comp-1B-P1**	**UBC-Comp-1B-P2**	**UBC-Comp-1B-P3**	**UBC-Comp-1B-P4**
F50, mm	6.64	1.66	1.64	1.85	2.24	6.64	1.46	1.66	1.84	2.19	6.64	1.57	1.65	1.85	2.22
F80, mm	10.29	6.41	5.62	6.28	6.91	10.29	5.20	5.77	6.04	6.82	10.29	5.78	5.69	6.16	6.86
RR50		3.99	4.06	3.59	2.96		4.56	4.00	3.61	3.04		4.24	4.04	3.60	3.00
RR80		1.60	1.83	1.64	1.49		1.98	1.78	1.70	1.51		1.78	1.81	1.67	1.50
		UBC-Comp-2A-1-P1	**UBC-Comp-2A-1-P2**	**UBC-Comp-2A-1-P3**	**UBC-Comp-2A-1-P4**		**UBC-Comp-2A-2-P1**	**UBC-Comp-2A-2-P2**	**UBC-Comp-2A-2-P3**	**UBC-Comp-2A-2-P4**		**UBC-Comp-2A-P1**	**UBC-Comp-2A-P2**	**UBC-Comp-2A-P3**	**UBC-Comp-2A-P4**
F50, mm	6.17	1.62	1.64	1.86	2.33	6.17	1.50	1.66	1.91	2.18	6.17	1.56	1.65	1.89	2.25
F80, mm	10.16	6.11	5.55	5.93	7.41	10.16	5.44	5.57	6.29	6.53	10.16	5.78	5.56	6.11	6.95
RR50		3.81	3.76	3.32	2.65		4.10	3.72	3.22	2.82		3.96	3.74	3.27	2.74
RR80		1.66	1.83	1.71	1.37		1.87	1.82	1.62	1.56		1.76	1.83	1.66	1.46
		UBC-Comp-2B-1-P1	**UBC-Comp-2B-1-P2**	**UBC-Comp-2B-1-P3**	**UBC-Comp-2B-1-P4**		**UBC-Comp-2B-2-P1**	**UBC-Comp-2B-2-P2**	**UBC-Comp-2B-2-P3**	**UBC-Comp-2B-2-P4**		**UBC-Comp-2B-P1**	**UBC-Comp-2B-P2**	**UBC-Comp-2B-P3**	**UBC-Comp-2B-P4**
F50, mm	6.14	1.60	1.76	1.78	2.19	6.14	1.58	1.66	2.00	2.24	6.14	1.59	1.71	1.89	2.21
F80, mm	10.02	5.26	5.84	5.73	6.59	10.02	5.27	5.48	6.28	6.53	10.02	5.27	5.67	6.00	6.56
RR50		3.85	3.49	3.46	2.81		3.90	3.69	3.07	2.74		3.87	3.60	3.25	2.77
RR80		1.90	1.72	1.75	1.52		1.90	1.83	1.60	1.54		1.90	1.77	1.67	1.53
		UBC-Comp-3A-1-P1	**UBC-Comp-3A-1-P2**	**UBC-Comp-3A-1-P3**	**UBC-Comp-3A-1-P4**		**UBC-Comp-3A-2-P1**	**UBC-Comp-3A-2-P2**	**UBC-Comp-3A-2-P3**	**UBC-Comp-3A-2-P4**		**UBC-Comp-3A-P1**	**UBC-Comp-3A-P2**	**UBC-Comp-3A-P3**	**UBC-Comp-3A-P4**
F50, mm	6.28	1.75	1.82	1.92	2.11	6.28	1.77	1.87	1.99	2.40	6.28	1.76	1.85	1.95	2.25
F80, mm	10.16	5.83	6.15	6.16	6.26	10.16	5.67	6.40	6.42	6.90	10.16	5.75	6.26	6.29	6.57
RR50		3.59	3.45	3.28	2.99		3.56	3.36	3.16	2.61		3.58	3.40	3.22	2.80
RR80		1.74	1.65	1.65	1.62		1.79	1.59	1.58	1.47		1.77	1.62	1.62	1.55
		UBC-Comp-3B-1-P1	**UBC-Comp-3B-1-P2**	**UBC-Comp-3B-1-P3**	**UBC-Comp-3B-1-P4**		**UBC-Comp-3B-2-P1**	**UBC-Comp-3B-2-P2**	**UBC-Comp-3B-2-P3**	**UBC-Comp-3B-2-P4**		**UBC-Comp-3B-P1**	**UBC-Comp-3B-P2**	**UBC-Comp-3B-P3**	**UBC-Comp-3B-P4**
F50, mm	6.00	1.75	1.78	2.09	2.39	6.00	1.72	1.83	1.97	2.54	6.00	1.73	1.81	2.03	2.46
F80, mm	10.01	6.19	5.68	6.42	6.93	10.01	5.93	5.93	5.87	7.22	10.01	6.06	5.81	6.12	7.08
RR50		3.43	3.37	2.87	2.51		3.48	3.27	3.05	2.36		3.46	3.32	2.96	2.43
RR80		1.62	1.76	1.56	1.44		1.69	1.69	1.71	1.39		1.65	1.72	1.64	1.41

Piston Press Test Summary - Reduction Performance Continued															
		ALS-Feed-A-P1	ALS-Feed-A-P2	ALS-Feed-A-P3	ALS-Feed-A-P4		ALS-Feed-B-P1	ALS-Feed-B-P2	ALS-Feed-B-P3	ALS-Feed-B-P4		ALS-Feed--C-P1	ALS-Feed--C-P2	ALS-Feed--C-P3	ALS-Feed--C-P4
F50, mm	5.17	1.53	1.54	1.68	1.74	5.17	1.44	1.54	1.66	1.71	4.99	1.40	1.57	1.72	1.98
F80, mm	9.94	5.47	6.09	6.11	5.91	9.94	5.58	5.70	6.11	6.14	9.99	5.69	6.16	6.26	6.77
RR50		3.39	3.37	3.07	2.97		3.59	3.35	3.11	3.02		3.57	3.18	2.91	2.52
RR80		1.82	1.63	1.63	1.68		1.78	1.74	1.63	1.62		1.76	1.62	1.60	1.48
		ALS-Comp-A-P1	ALS-Comp-A-P2	ALS-Comp-A-P3	ALS-Comp-A-P4		UBC-Feed-3A-P1	UBC-Feed-3A-P2	UBC-Feed-3A-P3	UBC-Feed-3A-P4		UBC-Feed-3B-P1	UBC-Feed-3B-P2	UBC-Feed-3B-P3	UBC-Feed-3B-P4
F50, mm	5.68	1.55	1.62	1.82	2.11	4.90	1.28	1.54	1.83	1.84	4.90	1.47	1.46	1.72	1.89
F80, mm	9.92	5.44	5.61	6.30	6.52	9.94	5.13	5.99	6.98	6.51	9.94	5.53	5.81	6.33	6.25
RR50		3.67	3.51	3.13	2.69		3.83	3.18	2.68	2.66		3.34	3.35	2.85	2.59
RR80		1.82	1.77	1.58	1.52		1.94	1.66	1.42	1.53		1.80	1.71	1.57	1.59

A.3 Porosity Test Data

Sample	True Density (g/cc) (Picometer)	Relative Density (ALS) (g/cc)	Final Packed Density during Piston Teting @ 240 Mpa (g/cc)	RR50 , mm/mm	Esp, kW/h	Porosity,g/cc	Porosity Proxy
A-01	2.57	2.57	2.53	7.13	2.51	0.00	-0.04
A-02	2.56	2.51	2.49	10.04	2.60	0.05	-0.02
A-03	2.62	2.61	2.54	6.67	2.48	0.01	-0.07
A-04	N/A	2.55	2.52	6.50	2.74	N/A	-0.03
A-05	N/A	2.54	2.47	6.82	2.63	N/A	-0.07
A-06	N/A	2.57	2.53	6.31	2.41	N/A	-0.04
A-07	N/A	2.58	2.55	8.14	2.05	N/A	-0.03
A-08	N/A	2.57	2.48	5.76	2.68	N/A	-0.08
A-09	N/A	2.57	2.50	7.20	2.61	N/A	-0.07
B-01	2.68	2.40	2.60	13.54	2.31	0.28	0.20
B-02	2.68	2.53	2.69	10.75	2.07	0.16	0.16
B-03	2.70	2.53	2.67	14.13	2.11	0.17	0.14
B-04	2.67	2.45	2.60	26.99	2.18	0.22	0.15
B-05	2.69	2.53	2.62	9.68	2.11	0.16	0.09
B-06	2.66	2.54	2.66	12.91	2.12	0.13	0.12
B-07	2.72	2.52	2.66	12.85	2.13	0.21	0.14
B-08	2.68	2.45	2.61	24.51	2.23	0.23	0.16
C-01	N/A	2.68	2.59	4.23	2.36	N/A	-0.09
C-02	N/A	2.67	2.44	4.72	2.21	N/A	-0.24
C-03	N/A	2.67	2.46	4.98	2.22	N/A	-0.21
C-04	N/A	2.65	2.54	4.45	2.42	N/A	-0.11
C-05	N/A	2.73	2.64	4.76	2.07	N/A	-0.09
C-06	N/A	2.71	2.62	4.34	2.20	N/A	-0.09
C-07	N/A	2.68	2.57	4.75	2.38	N/A	-0.11
C-08	N/A	2.72	2.62	4.04	2.16	N/A	-0.09
C-09	N/A	2.68	2.57	4.07	2.51	N/A	-0.10
C-10	N/A	2.71	2.64	4.15	2.74	N/A	-0.07
C-11	N/A	2.70	2.59	4.37	2.63	N/A	-0.11
C-12	N/A	2.65	2.55	4.71	2.41	N/A	-0.10
C-13	N/A	2.69	2.62	4.70	2.05	N/A	-0.07
C-14	N/A	2.67	2.56	4.74	2.60	N/A	-0.11
C-15	N/A	2.65	2.58	4.96	2.68	N/A	-0.07
C-16	N/A	2.68	2.61	4.22	2.61	N/A	-0.07
C-17	N/A	2.66	2.49	4.08	2.66	N/A	-0.17
C-18	N/A	2.68	2.58	5.34	2.21	N/A	-0.10
C-19	N/A	2.67	2.52	4.74	2.34	N/A	-0.15
C-20	N/A	2.67	2.55	4.91	2.36	N/A	-0.12
C-21	N/A	2.67	2.52	4.95	2.49	N/A	-0.15
C-22	N/A	2.67	2.51	4.78	2.47	N/A	-0.16
C-23	N/A	2.67	2.53	4.69	2.44	N/A	-0.14
C-24	N/A	2.66	2.52	4.60	2.41	N/A	-0.14
C-25	N/A	2.66	2.52	4.99	2.41	N/A	-0.14
C-26	N/A	2.68	2.50	5.52	2.46	N/A	-0.18
C-27	N/A	2.71	2.63	4.63	2.25	N/A	-0.08
C-28	N/A	2.72	2.60	4.39	2.64	N/A	-0.12
C-29	N/A	2.76	2.67	4.45	2.43	N/A	-0.09
C-30	N/A	2.75	2.71	4.43	2.11	N/A	-0.04
C-31	N/A	2.66	2.52	5.02	2.50	N/A	-0.14

Mineral	Ideal Formula	B-08 (%)	A-09 (%)	S.G. Mineral (g/cc)		
				*Min	*Max	*Avg
Alunite	$K_2Al_6(SO_4)_4(OH)_{12}$	0.8		2.60	2.90	2.75
Biotite	$K(Mg,Fe^{2+})_3AlSi_3O_{10}(OH)_2$		1.4	2.70	2.90	2.83
Calcite	$CaCO_3$		1.7	2.71	2.71	2.71
Chalcopyrite	$CuFeS_2$		0.9	4.10	4.30	4.19
Clinochlore	$(Mg,Fe^{2+})_5Al(Si_3Al)O_{10}(OH)_8$		3.5	2.55	2.75	2.65
Diaspore	$AlO(OH)$	2.4		3.30	3.50	3.38
Goethite	α-$Fe^{3+}O(OH)$	2.4		3.30	4.30	4.27
Hematite	α-Fe_2O_3	2.6		5.30	5.30	5.30
Illite/ Muscovite 2M	$K_{0.65}Al_{2.0}Al_{0.65}Si_{3.35}O_{10}(OH)_2$ /$KAl_2AlSi_3O_{10}(OH)_2$	12.8	2.9	2.77	2.88	2.83
Kaolinite	$Al_2Si_2O_5(OH)_4$	13.3		2.60	2.60	2.60
K-feldspar	$KAlSi_3O_8$	6.8	17.3	2.56	2.56	2.56
Plagioclase	$NaAlSi_3O_8 – CaAl_2Si_2O_8$		47.6	2.61	2.76	2.69
Pyrite	FeS_2		0.5	5.00	5.02	5.01
Pyrophyllite	$Al_2Si_4O_{10}(OH)_2$	8.1		2.80	2.90	2.84
Quartz	SiO_2	49.8	24.3	2.60	2.65	2.65
Rutile	TiO_2	0.8		4.25	4.25	4.25
Schorl	$NaFe_3^{2+}Al_6(BO_3)_3Si_6O_{18}(OH)_4$	0.3		3.10	3.20	3.15
Total		**100**	**100**			

A.4 Piston Press Test PSD

FSD & PSD																
Sample		UBC-Comp1A-			UBC-Comp-1A-P1			UBC-Comp-1A-P2			UBC-Comp-1A-P3			UBC-Comp-1A-2-P4		
Force																
Moisture		2.5	%			5	%		5	%		5	%		5	%
Force		N/A	kN			1397.06	kN		1098.68	kN		799.15	kN		499.05	kN
Pressure		N/A	MPa			240.51	MPa		189.14	MPa		137.58	MPa		85.91	MPa
Energy		N/A	kWh/t			1.51	kWh/t		1.26	kWh/t		1.02	kWh/t		0.77	kWh/t
Thickness		N/A	mm			30.32	mm		30.23	mm		30.74	mm		31.79	mm
Density		N/A	g/cc			2.81	g/cc		2.76	g/cc		2.70	g/cc		2.61	g/cc
Sieve #	Size (mm)	Weight (g)	Cum. % passing	Size (mm)	Weight (g)	Cum. % passing	Normalized	Weight (g)	Cum. % passing	Normalized	Weight (g)	Cum. % passing	Normalized	Weight (g)	Cum. % passing	Normalized
1/2 inch	12.5	0.00	100.00	12.5	0.00	100.00	8.178	0	100.00	7.540	0	100.00	6.507	0.00	100.00	5.851
7/16 inch	11.2	210.80	92.59	11.2	12.10	98.68	7.328	16.3	98.20	6.755	6.7	99.26	5.830	13.10	98.57	5.243
3/8 inch	9.5	525.00	74.13	9.5	36.30	94.73	6.215	50.1	92.67	5.730	56.3	93.07	4.945	60.00	92.01	4.447
1/4 inch	6.7	605.40	52.84	6.7	96.70	84.20	4.383	80.4	83.79	4.041	106.3	81.38	3.488	105.80	80.45	3.136
4 Mesh	4.75	345.40	40.69	4.75	81.30	75.35	3.108	91.2	73.71	2.865	90.4	71.44	2.473	93.10	70.28	2.224
6 Mesh	3.36	264.20	31.40	3.36	64.70	68.30	2.198	63.9	66.66	2.027	76.6	63.02	1.749	78.10	61.75	1.573
8 Mesh	2.36	203.60	24.24	2.36	79.10	59.69	1.544	78.6	57.97	1.423	75.5	54.72	1.229	84.80	52.49	1.105
10 Mesh	1.7	133.40	19.55	1.7	68.50	52.23	1.112	67.2	50.55	1.025	64.5	47.62	0.885	67.10	45.15	0.796
14 Mesh	1.18	86.20	16.52	1.18	62.00	45.48	0.772	61.8	43.73	0.712	59.5	41.08	0.614	59.00	38.71	0.552
20 Mesh	0.85	60.40	14.40	0.85	57.90	39.17	0.556	56.2	37.52	0.513	54.1	35.13	0.442	51.10	33.13	0.398
28 Mesh	0.6	45.60	12.79	0.6	49.40	33.79	0.393	48	32.22	0.362	44.9	30.20	0.312	42.80	28.45	0.281
35 Mesh	0.425	34.40	11.58	0.425	40.40	29.39	0.278	38.8	27.93	0.256	36.1	26.23	0.221	33.90	24.75	0.199
48 Mesh	0.3	32.80	10.43	0.3	38.20	25.23	0.196	36.2	23.93	0.181	33.8	22.51	0.156	31.10	21.35	0.140
65 Mesh	0.212	25.00	9.55	0.212	28.50	22.13	0.139	27	20.95	0.128	24.5	19.82	0.110	29.10	18.17	0.099
100 Mesh	0.15	24.20	8.70	0.15	26.20	19.27	0.098	24.6	18.24	0.090	23.2	17.26	0.078	20.90	15.89	0.070
150 Mesh	0.106	19.60	8.01	0.106	20.80	17.01	0.069	19.8	16.05	0.064	18.2	15.26	0.055	16.60	14.07	0.050
	Pan	227.80		Pan	156.20			145.3			138.8			128.80		
	Total wt.	2843.80	F50		918.3	P50		905.4	P50		909.4	p50		915.3	p50	
	Initial wt.		6.24			1.53			1.66			1.92			2.14	
	Delta		F80			P80			P80			p80			p80	
	Delta %		10.04			5.78			5.97			6.43			6.61	
	Reduction Ratio					4.09			3.77			3.25			2.92	
	PP 1 mm		**13.522**													

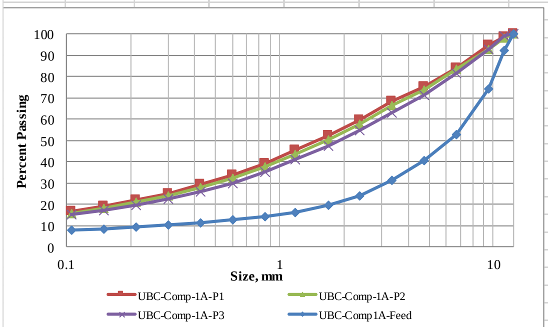

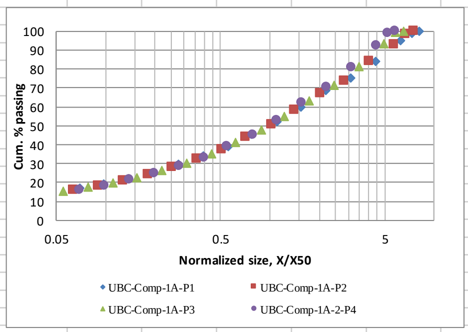

							FSD & PSD									
Sample		UBC-Comp1B-			UBC-Comp-1B-P1			UBC-Comp-1B-P2			UBC-Comp-1B-P3			UBC-Comp-1B-P4		
Force																
Moisture		5	%			5	%		5	%		5	%		5.0	%
Force		N/A	kN			1396.2	kN		1099.03	kN		799	kN		499.2	kN
Pressure		N/A	MPa			240.4	MPa		189.20	MPa		138	MPa		85.9	MPa
Energy		N/A	kWh/t			1.5	kWh/t		1.26	kWh/t		1.01	kWh/t		0.7	kWh/t
Thickness		N/A	mm			29.9	mm		30.82	mm		31	mm		31.7	mm
Density		N/A	g/cc			2.8	g/cc		2.75	g/cc		3	g/cc		2.6	g/cc
Sieve #	Size (mm)	Weight (g)	Cum. % passing	Size (mm)	Weight (g)	Cum. % passing	Normalized	Weight (g)	Cum. % passing	Normalized	Weight (g)	Cum. % passing	Normalized	Weight (g)	Cum. % passing	Normalized
1/2 inch	12.5	0.00	100.00	12.5	0.00	100.00	7.972	0	100.00	7.594	0	100.00	6.766	0.00	100.00	5.642
7/16 inch	11.2	131.00	90.65	11.2	18.50	97.96	7.143	7.8	99.15	6.804	18.4	97.96	6.063	26.80	97.06	5.055
3/8 inch	9.5	278.80	70.74	9.5	33.90	94.21	6.059	30.6	95.83	5.771	43.4	93.16	5.142	56.40	90.86	4.288
1/4 inch	6.7	285.50	50.35	6.7	89.70	84.31	4.273	95.6	85.45	4.070	94.5	82.69	3.627	104.90	79.34	3.024
4 Mesh	4.75	169.40	38.25	4.75	82.70	75.18	3.029	97.2	74.89	2.886	88.3	72.92	2.571	92.40	69.19	2.144
6 Mesh	3.36	118.50	29.79	3.36	71.30	67.31	2.143	77	66.53	2.041	82.7	63.76	1.819	79.10	60.50	1.516
8 Mesh	2.36	99.60	22.68	2.36	75.50	58.97	1.505	80.5	57.79	1.434	76.3	55.31	1.277	81.40	51.55	1.065
10 Mesh	1.7	61.00	18.32	1.7	66.60	51.62	1.084	65.7	50.66	1.033	61.8	48.47	0.920	64.70	44.45	0.767
14 Mesh	1.18	39.10	15.53	1.18	57.70	45.25	0.753	58.4	44.32	0.717	55.7	42.31	0.639	55.50	38.35	0.533
20 Mesh	0.85	28.60	13.49	0.85	62.40	38.36	0.542	63.3	37.44	0.516	59.9	35.67	0.460	56.70	32.12	0.384
28 Mesh	0.6	21.90	11.93	0.6	48.50	33.00	0.383	48.6	32.16	0.364	45.1	30.68	0.325	42.00	27.51	0.271
35 Mesh	0.425	16.50	10.75	0.425	39.00	28.70	0.271	39.1	27.92	0.258	35.9	26.71	0.230	33.10	23.87	0.192
48 Mesh	0.3	15.50	9.64	0.3	35.70	24.75	0.191	36	24.01	0.182	33.2	23.03	0.162	29.80	20.60	0.135
65 Mesh	0.212	12.00	8.78	0.212	29.10	21.54	0.135	28.8	20.88	0.129	25.9	20.16	0.115	23.60	18.01	0.096
100 Mesh	0.15	11.40	7.97	0.15	24.30	18.86	0.096	24	18.28	0.091	21.6	17.77	0.081	19.70	15.84	0.068
150 Mesh	0.106	8.80	7.34	0.106	20.10	16.64	0.068	19.8	16.13	0.064	18	15.78	0.057	16.20	14.06	0.048
	Pan	102.8		Pan	150.70			148.5			142.5			128.00		
	Total wt.	1400.40	F50		905.7	P50		920.9	P50		903.2	p50		910.3	p50	
	Initial wt.		6.64			1.57			1.65			1.85			2.22	
	Delta		F80			P80			P80			p80			p80	
	Delta %		10.29			5.78			5.69			6.16			6.86	
	Reduction Ratio					4.24			4.04			3.60			3.00	
	PP 1 mm		**12.636**													

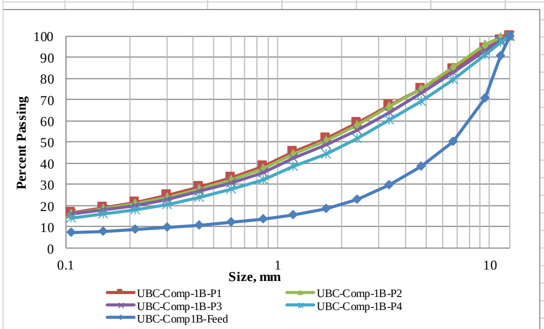

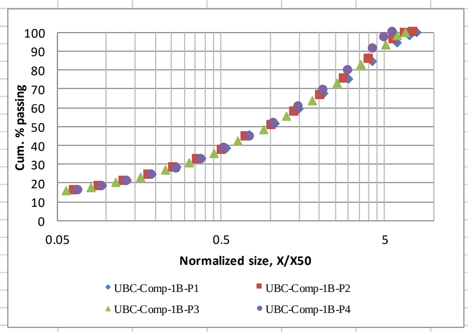

FSD & PSD

Sample		UBC-Comp2A-			UBC-Comp-2A-P1			UBC-Comp-2A-P2			UBC-Comp-2A-P3			UBC-Comp-2A-P4		
Force																
Moisture		3	%			3.00	%		3	%		3.00	%		3.00	%
Force		N/A	kN			1397.08	kN		1097.83	kN		799.25	kN		499.10	kN
Pressure		N/A	MPa			240.51	MPa		188.99	MPa		137.59	MPa		85.92	MPa
Energy		N/A	kWh/t			1.54	kWh/t		1.32	kWh/t		1.05	kWh/t		0.78	kWh/t
Thickness		N/A	mm			27.77	mm		28.35	mm		28.64	mm		29.46	mm
Density		N/A	g/cc			2.80	g/cc		2.73	g/cc		2.68	g/cc		2.60	g/cc
Sieve #	Size (mm)	Weight (g)	Cum. % passing	Size (mm)	Weight (g)	Cum. % passing	Normalized	Weight (g)	Cum. % passing	Normalized	Weight (g)	Cum. % passing	Normalized	Weight (g)	Cum. % passing	Normalized
1/2 inch	12.5		100.00	12.5	0.00	100.00	8.019	0	100.00	7.581	0	100.00	6.627	0.00	100.00	5.551
7/16 inch	11.2	127.80	89.89	11.2	2.30	99.73	7.185	14	98.34	6.793	21.3	97.48	5.938	27.80	96.73	4.974
3/8 inch	9.5	204.20	73.74	9.5	45.30	94.34	6.095	29.1	94.90	5.762	42.1	92.50	5.037	55.20	90.22	4.219
1/4 inch	6.7	256.10	53.48	6.7	89.50	83.69	4.298	78.7	85.58	4.063	79.3	83.12	3.552	95.20	79.01	2.976
4 Mesh	4.75	160.60	40.78	4.75	66.00	75.84	3.047	81	75.99	2.881	87.2	72.81	2.518	77.90	69.84	2.109
6 Mesh	3.36	114.60	31.72	3.36	66.60	67.92	2.156	77.8	66.79	2.038	75.7	63.85	1.781	79.50	60.48	1.492
8 Mesh	2.36	97.10	24.04	2.36	80.00	58.40	1.514	80.3	57.28	1.431	74.6	55.03	1.251	79.50	51.11	1.048
10 Mesh	1.7	55.20	19.67	1.7	57.10	51.61	1.091	56.6	50.58	1.031	59.2	48.02	0.901	57.60	44.33	0.755
14 Mesh	1.18	35.10	16.89	1.18	49.70	45.69	0.757	49.8	44.69	0.716	49.5	42.17	0.626	46.70	38.83	0.524
20 Mesh	0.85	34.30	14.18	0.85	61.90	38.33	0.545	62.1	37.33	0.516	60.5	35.01	0.451	56.30	32.20	0.377
28 Mesh	0.6	20.50	12.56	0.6	44.90	32.99	0.385	44.6	32.05	0.364	42.3	30.01	0.318	39.20	27.58	0.266
35 Mesh	0.425	15.40	11.34	0.425	36.30	28.67	0.273	35.4	27.86	0.258	33.4	26.06	0.225	30.70	23.97	0.189
48 Mesh	0.3	13.80	10.25	0.3	33.20	24.72	0.192	32.5	24.02	0.182	30.2	22.49	0.159	27.50	20.73	0.133
65 Mesh	0.212	11.90	9.31	0.212	28.30	21.35	0.136	27.5	20.76	0.129	25.3	19.49	0.112	22.90	18.03	0.094
100 Mesh	0.15	8.30	8.65	0.15	21.10	18.84	0.096	20.6	18.32	0.091	19.1	17.23	0.080	17.40	15.98	0.067
150 Mesh	0.106	8.40	7.99	0.106	17.80	16.73	0.068	17.3	16.28	0.064	16.2	15.32	0.056	14.60	14.26	0.047
	Pan	101.0		Pan	140.60			137.5			129.5			121.10		
	Total wt.	1264.30	F50		840.6	P50		844.8	P50		845.4	p50		849.1	p50	
	Initial wt.		6.17			1.56			1.65			1.89			2.25	
	Delta		F80			P80			P80			p80			p80	
	Delta %		10.16			5.78			5.56			6.11			6.95	
	Reduction Ratio					3.96			3.74			3.27			2.74	
	PP 1 mm		**13.297**													

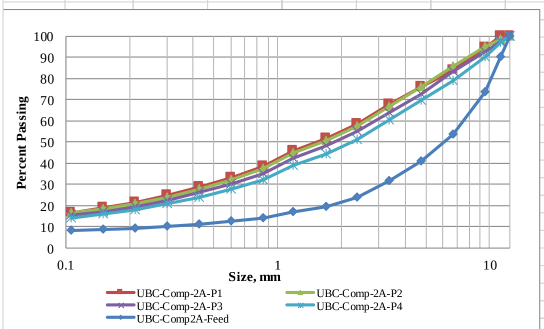

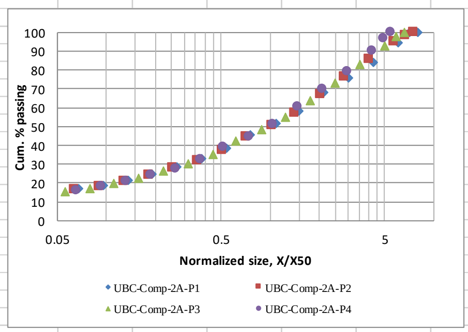

FSD & PSD																
Sample		UBC-Comp2B-			UBC-Comp-2B-P1			UBC-Comp-2B-P2			UBC-Comp-2B-P3			UBC-Comp-2B-P4		
Force																
Moisture		5	%			3.00	%		3	%		3.00	%		3.00	%
Force		N/A	kN			1396.71	kN		1098.39	kN		799.52	kN		499.47	kN
Pressure		N/A	MPa			240.45	MPa		189.09	MPa		137.64	MPa		85.99	MPa
Energy		N/A	kWh/t			1.57	kWh/t		1.31	kWh/t		1.04	kWh/t		0.75	kWh/t
Thickness		N/A	mm			27.78	mm		28.26	mm		28.76	mm		29.21	mm
Density		N/A	g/cc			2.80	g/cc		2.74	g/cc		2.68	g/cc		2.61	g/cc
Sieve #	Size (mm)	Weight (g)	Cum. % passing	Size (mm)	Weight (g)	Cum. % passing	Normalized	Weight (g)	Cum. % passing	Normalized	Weight (g)	Cum. % passing	Normalized	Weight (g)	Cum. % passing	Normalized
1/2 inch	12.5		100.00	12.5	0.00	100.00	7.880	0	100.00	7.330	0	100.00	6.618	0.00	100.00	5.644
7/16 inch	11.2	105.90	92.08	11.2	11.00	98.69	7.061	2.6	99.69	6.567	8.3	99.02	5.930	20.70	97.56	5.057
3/8 inch	9.5	233.10	74.65	9.5	32.00	94.88	5.989	33.2	95.75	5.570	42.2	94.01	5.030	46.80	92.03	4.289
1/4 inch	6.7	281.80	53.59	6.7	73.00	86.18	4.224	86.2	85.51	3.929	87.3	83.66	3.547	95.30	80.78	3.025
4 Mesh	4.75	168.20	41.01	4.75	70.70	77.76	2.994	88	75.07	2.785	86.6	73.39	2.515	88.60	70.32	2.145
6 Mesh	3.36	111.20	32.70	3.36	78.70	68.38	2.118	73.6	66.33	1.970	77.4	64.22	1.779	77.30	61.19	1.517
8 Mesh	2.36	100.10	25.21	2.36	80.30	58.82	1.488	77.1	57.17	1.384	78.7	54.88	1.250	81.50	51.56	1.066
10 Mesh	1.7	64.40	20.40	1.7	59.30	51.75	1.072	60.9	49.94	0.997	57.7	48.04	0.900	60.20	44.46	0.768
14 Mesh	1.18	38.20	17.54	1.18	67.20	43.75	0.744	65.5	42.16	0.692	63.2	40.55	0.625	63.10	37.01	0.533
20 Mesh	0.85	36.20	14.83	0.85	44.40	38.46	0.536	44	36.94	0.498	41.8	35.59	0.450	39.90	32.29	0.384
28 Mesh	0.6	21.80	13.20	0.6	48.60	32.67	0.378	47.1	31.35	0.352	44.8	30.28	0.318	41.20	27.43	0.271
35 Mesh	0.425	16.40	11.98	0.425	38.20	28.12	0.268	36.9	26.97	0.249	34.9	26.14	0.225	31.50	23.71	0.192
48 Mesh	0.3	15.20	10.84	0.3	31.70	24.34	0.189	30.4	23.36	0.176	28.7	22.74	0.159	25.70	20.68	0.135
65 Mesh	0.212	13.00	9.87	0.212	28.50	20.94	0.134	27.3	20.11	0.124	25.8	19.68	0.112	22.40	18.03	0.096
100 Mesh	0.15	10.20	9.11	0.15	22.10	18.31	0.095	21	17.62	0.088	20.1	17.30	0.079	17.00	16.02	0.068
150 Mesh	0.106	9.10	8.43	0.106	18.30	16.13	0.067	17.5	15.54	0.062	16.9	15.30	0.056	14.80	14.28	0.048
	Pan	112.7		Pan	135.40			130.9			129			120.90		
	Total wt.	1337.50	F50		839.4	P50		842.2	P50		843.4	p50		846.9	p50	
	Initial wt.		6.14			1.59			1.71			1.89			2.21	
	Delta		F80			P80			P80			p80			p80	
	Delta %		10.02			5.27			5.67			6.00			6.56	
	Reduction Ratio					3.87			3.60			3.25			2.77	
	PP 1 mm		**13.945**													

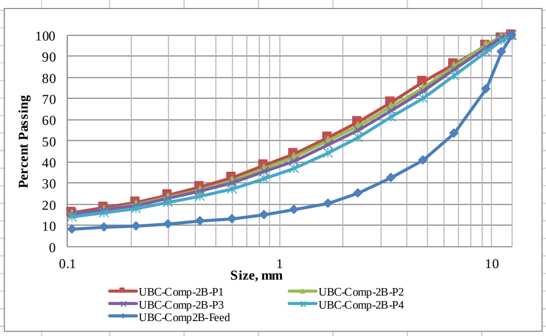

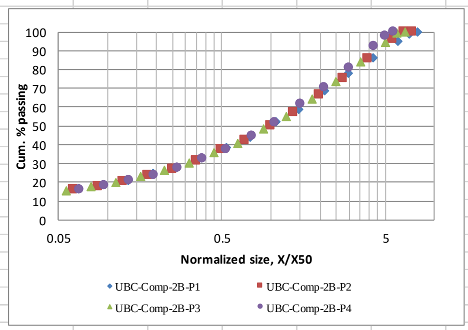

							FSD & PSD									
Sample		UBC-Comp3A-			UBC-Comp-3A-P1			UBC-Comp-3A-P2			UBC-Comp-3A-P3			UBC-Comp-3A-P4		
Force																
Moisture		1.5	%			1.50	%		1.5	%		1.50	%		1.50	%
Force		N/A	kN			1396.82	kN		1099.02	kN		799.12	kN		499.39	kN
Pressure		N/A	MPa			240.47	MPa		189.20	MPa		137.57	MPa		85.97	MPa
Energy		N/A	kWh/t			1.65	kWh/t		1.35	kWh/t		1.05	kWh/t		0.78	kWh/t
Thickness		N/A	mm			30.47	mm		30.98	mm		31.32	mm		32.29	mm
Density		N/A	g/cc			2.71	g/cc		2.67	g/cc		2.63	g/cc		2.53	g/cc
Sieve #	Size (mm)	Weight (g)	Cum. % passing	Size (mm)	Weight (g)	Cum. % passing	Normalized	Weight (g)	Cum. % passing	Normalized	Weight (g)	Cum. % passing	Normalized	Weight (g)	Cum. % passing	Normalized
1/2 inch	12.5		100.00	12.5	0.00	100.00	7.112	0	100.00	6.766	0	100.00	6.408	0.00	100.00	5.565
7/16 inch	11.2	107.60	92.21	11.2	10.80	98.81	6.373	21.5	97.66	6.063	17.2	98.13	5.741	34.50	96.21	4.986
3/8 inch	9.5	275.00	72.29	9.5	40.90	94.31	5.405	55.8	91.57	5.143	51.1	92.57	4.870	56.70	89.99	4.229
1/4 inch	6.7	271.40	52.64	6.7	86.70	84.76	3.812	88.3	81.95	3.627	96.8	82.03	3.435	84.40	80.72	2.983
4 Mesh	4.75	170.80	40.27	4.75	88.90	74.97	2.703	79.8	73.24	2.571	88.7	72.38	2.435	96.40	70.14	2.115
6 Mesh	3.36	125.70	31.17	3.36	78.90	66.28	1.912	77.1	64.84	1.819	80.3	63.65	1.722	83.50	60.98	1.496
8 Mesh	2.36	101.20	23.84	2.36	88.10	56.57	1.343	85.3	55.54	1.278	82.8	54.64	1.210	88.20	51.30	1.051
10 Mesh	1.7	64.20	19.19	1.7	65.40	49.37	0.967	65.4	48.41	0.920	68.7	47.16	0.871	68.40	43.79	0.757
14 Mesh	1.18	36.80	16.53	1.18	54.10	43.41	0.671	53.2	42.61	0.639	52.8	41.41	0.605	51.20	38.17	0.525
20 Mesh	0.85	34.90	14.00	0.85	65.40	36.21	0.484	64	35.63	0.460	62.6	34.60	0.436	58.60	31.73	0.378
28 Mesh	0.6	22.90	12.34	0.6	51.20	30.57	0.341	49.3	30.26	0.325	48.5	29.33	0.308	43.40	26.97	0.267
35 Mesh	0.425	16.40	11.15	0.425	38.20	26.37	0.242	37.7	26.14	0.230	36.4	25.36	0.218	32.40	23.41	0.189
48 Mesh	0.3	15.40	10.04	0.3	35.50	22.46	0.171	35.2	22.31	0.162	33.5	21.72	0.154	29.60	20.16	0.134
65 Mesh	0.212	12.60	9.12	0.212	28.10	19.36	0.121	28	19.25	0.115	26.7	18.81	0.109	23.50	17.59	0.094
100 Mesh	0.15	10.30	8.38	0.15	21.60	16.98	0.085	21.5	16.91	0.081	20.9	16.54	0.077	18.40	15.57	0.067
150 Mesh	0.106	8.30	7.78	0.106	17.00	15.11	0.060	16.9	15.07	0.057	16.2	14.78	0.054	14.40	13.98	0.047
	Pan	107.4		Pan	137.20			138.2			135.8			127.40		
	Total wt.	1380.90	F50		908.0	P50		917.2	P50		919	p50		911.0	p50	
	Initial wt.		6.28			1.76			1.85			1.95			2.25	
	Delta		F80			P80			P80			p80			p80	
	Delta %		10.16			5.75			6.26			6.29			6.57	
	Reduction Ratio					3.58			3.40			3.22			2.80	
	PP 1 mm		**13.094**													

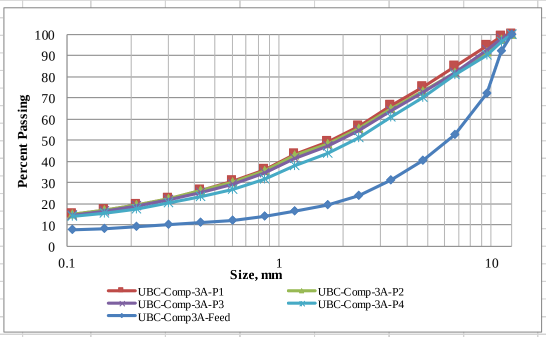

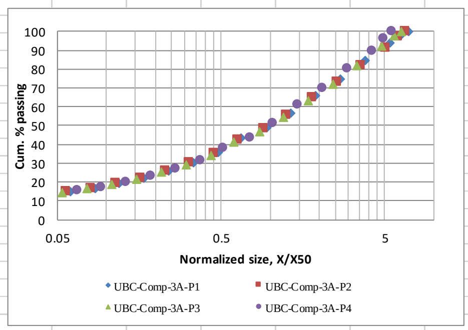

FSD & PSD

Sample		UBC-Comp3B-			UBC-Comp-3B-P1			UBC-Comp-3B-P2			UBC-Comp-3B-P3			UBC-Comp-3B-P4		
Force																
Moisture		1.5	%			1.50	%		1.5	%		1.50	%		1.50	%
Force		N/A	kN			1396.84	kN		1098.89	kN		799.26	kN		499.47	kN
Pressure		N/A	MPa			240.47	MPa		189.18	MPa		137.59	MPa		85.99	MPa
Energy		N/A	kWh/t			1.56	kWh/t		1.34	kWh/t		1.07	kWh/t		0.74	kWh/t
Thickness		N/A	mm			30.79	mm		31.15	mm		30.98	mm		32.22	mm
Density		N/A	g/cc			2.72	g/cc		2.67	g/cc		2.61	g/cc		2.52	g/cc
Sieve #	Size (mm)	Weight (g)	Cum. % passing	Size (mm)	Weight (g)	Cum. % passing	Normalized	Weight (g)	Cum. % passing	Normalized	Weight (g)	Cum. % passing	Normalized	Weight (g)	Cum. % passing	Normalized
1/2 inch	12.5		100.00	12.5	0.00	100.00	7.205	0	100.00	6.915	0	100.00	6.161	0.00	100.00	5.073
7/16 inch	11.2	124.80	90.60	11.2	8.50	99.08	6.456	7.5	99.19	6.196	8.6	99.05	5.520	19.40	97.88	4.545
3/8 inch	9.5	201.30	75.45	9.5	59.90	92.60	5.476	37.9	95.08	5.255	48.1	93.73	4.682	66.20	90.65	3.855
1/4 inch	6.7	277.00	54.60	6.7	89.80	82.89	3.862	100.2	84.24	3.706	95.9	83.14	3.302	113.00	78.30	2.719
4 Mesh	4.75	169.30	41.85	4.75	81.20	74.11	2.738	85.6	74.97	2.628	95	72.64	2.341	98.80	67.51	1.928
6 Mesh	3.36	121.90	32.67	3.36	78.30	65.64	1.937	86.7	65.58	1.859	85.3	63.22	1.656	85.40	58.18	1.364
8 Mesh	2.36	103.30	24.90	2.36	82.00	56.77	1.360	86.8	56.19	1.305	86.4	53.67	1.163	83.60	49.05	0.958
10 Mesh	1.7	63.70	20.10	1.7	66.10	49.62	0.980	68.3	48.79	0.940	66.2	46.35	0.838	68.00	41.62	0.690
14 Mesh	1.18	37.30	17.29	1.18	56.40	43.52	0.680	55.3	42.81	0.653	53.5	40.44	0.582	50.70	36.08	0.479
20 Mesh	0.85	34.20	14.72	0.85	66.20	36.36	0.490	65.4	35.73	0.470	61.7	33.62	0.419	56.50	29.91	0.345
28 Mesh	0.6	22.60	13.02	0.6	51.90	30.75	0.346	49.9	30.32	0.332	46.4	28.50	0.296	42.10	25.31	0.243
35 Mesh	0.425	16.60	11.77	0.425	38.70	26.56	0.245	37.9	26.22	0.235	34.8	24.65	0.209	31.10	21.91	0.172
48 Mesh	0.3	15.30	10.62	0.3	35.90	22.68	0.173	34.4	22.50	0.166	31.6	21.16	0.148	27.70	18.89	0.122
65 Mesh	0.212	12.70	9.66	0.212	28.90	19.55	0.122	27.5	19.52	0.117	25.3	18.36	0.104	22.30	16.45	0.086
100 Mesh	0.15	10.20	8.89	0.15	22.50	17.12	0.086	21.3	17.21	0.083	20	16.15	0.074	17.10	14.58	0.061
150 Mesh	0.106	8.20	8.27	0.106	17.50	15.23	0.061	16.8	15.39	0.059	15.4	14.45	0.052	13.50	13.11	0.043
	Pan	109.9		Pan	140.80			142.2			130.8			120.00		
	Total wt.	1328.30	F50		924.6	P50		923.7	P50		905	p50		915.4	p50	
	Initial wt.		6.00			1.73			1.81			2.03			2.46	
	Delta		F80			P80			P80			p80			p80	
	Delta %		10.01			6.06			5.81			6.12			7.08	
	Reduction Ratio					3.46			3.32			2.96			2.43	
	PP 1 mm		**13.790**													

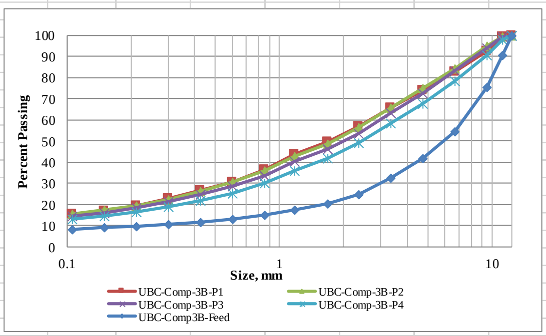

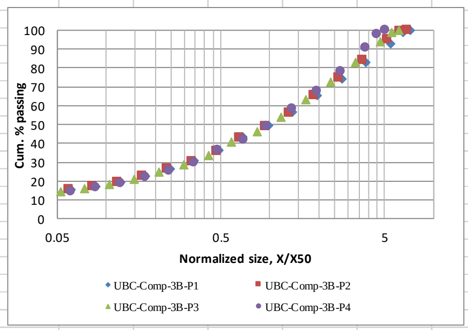

FSD & PSD

Sample		ALS-Feed-A Feed			ALS-Feed-A- P1			ALS-Feed-A- P2			ALS-Feed-A- P3			ALS-Feed-A- P4		
Force																
Moisture		5	%			5.00	%		5.00	%		5.00	%		5.00	%
Force		N/A	kN			1400.05	kN		1099.44	kN		899.75	kN		699.47	kN
Pressure		N/A	MPa			241.02	MPa		189.27	MPa		154.89	MPa		120.42	MPa
Energy		N/A	kWh/t			1.50	kWh/t		1.18	kWh/t		0.95	kWh/t		0.76	kWh/t
Thickness		N/A	mm			26.20	mm		26.03	mm		26.17	mm		26.01	mm
Density		N/A	g/cc			2.70	g/cc		2.66	g/cc		2.63	g/cc		2.65	g/cc
Sieve #	Size (mm)	Weight (g)	Cum. % passing	Size (mm)	Weight (g)	Cum. % passing	Normalized	Weight (g)	Cum. % passing	Normalized	Weight (g)	Cum. % passing	Normalized	Weight (g)	Cum. % passing	Normalized
1/2 inch	12.5	0	100.00	12.5	0	100.00	8.188	0	100.00	8.138	0	100.00	7.435	0	100.00	7.184
7/16 inch	11.2	83.6	91.64	11.2	6.7	98.27	7.336	4.8	98.75	7.291	6.9	98.19	6.661	7.3	98.07	6.436
	10	111.3	80.51	10	5.7	96.80	6.550	11.4	95.78	6.510	12	95.04	5.948	11.4	95.06	5.747
	8	162.3	64.28	8	24.3	90.52	5.240	33.9	86.95	5.208	29.5	87.31	4.758	26.1	88.16	4.597
	5.6	121.7	52.11	5.6	37.8	80.76	3.668	33.6	78.20	3.646	35.4	78.02	3.331	35.5	78.78	3.218
	4	78.4	44.27	4	36	71.46	2.620	28.8	70.70	2.604	35	68.84	2.379	36.3	69.19	2.299
	2.8	65.8	37.69	2.8	33.4	62.84	1.834	32.8	62.15	1.823	30.8	60.77	1.665	34.4	60.11	1.609
	2	42.5	33.44	2	26.9	55.89	1.310	25	55.64	1.302	25.7	54.03	1.190	26.9	53.00	1.149
	1.4	38.2	29.62	1.4	28.9	48.42	0.917	28	48.35	0.911	28.9	46.45	0.833	26.2	46.08	0.805
	1	30.9	26.53	1	22	42.74	0.655	21.6	42.72	0.651	22	40.68	0.595	20.9	40.55	0.575
	0.71	24.6	24.07	0.71	19	37.84	0.465	19	37.77	0.462	19.2	35.64	0.422	17.8	35.85	0.408
	0.5	23.5	21.72	0.5	19.2	32.88	0.328	19	32.82	0.326	17.7	31.00	0.297	17.7	31.18	0.287
	0.355	18.6	19.86	0.355	13.8	29.31	0.233	13.2	29.38	0.231	12.8	27.64	0.211	12.9	27.77	0.204
	0.25	17.5	18.11	0.25	11.8	26.27	0.164	12.5	26.13	0.163	12.3	24.42	0.149	10.9	24.89	0.144
	0.18	12.9	16.82	0.18	10.4	23.58	0.118	10.3	23.44	0.117	9.6	21.90	0.107	8.9	22.54	0.103
	0.125	13.2	15.50	0.125	8.6	21.36	0.082	8.5	21.23	0.081	7.8	19.85	0.074	7.7	20.50	0.072
	0.09	9.8	14.52	0.09	7	19.55	0.059	7	19.41	0.059	6.5	18.15	0.054	5.7	19.00	0.052
	0.063	9.2	13.60	0.063	7.7	17.56	0.041	7.6	17.43	0.041	7.2	16.26	0.037	5.4	17.57	0.036
	0.045	8.2	12.78	0.045	3.8	16.58	0.029	3.9	16.41	0.029	3.1	15.45	0.027	3	16.78	0.026
	Pan	127.8	0.00	Pan	64.2	0.00		63	0.00		58.9	0.00		63.5	0.00	
	Total wt.	1000.00	F50		387.2	P50		383.9	P50		381.3	p50		378.5	p50	
	Initial wt.		5.17			1.53			1.54			1.68			1.74	
	Delta		F80			P80			P80			p80			p80	
	Delta %		9.94			5.47			6.09			6.11			5.91	
	Reduction Ratio					3.39			3.37			3.07			2.97	
	PP 1 mm		**24.070**													

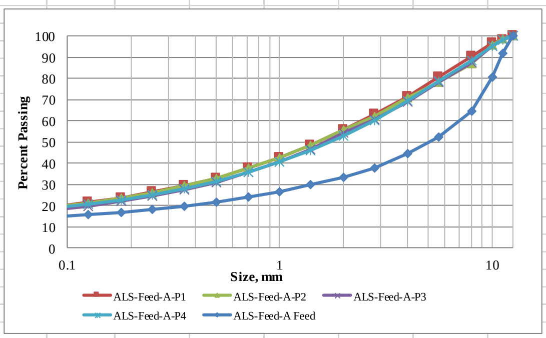

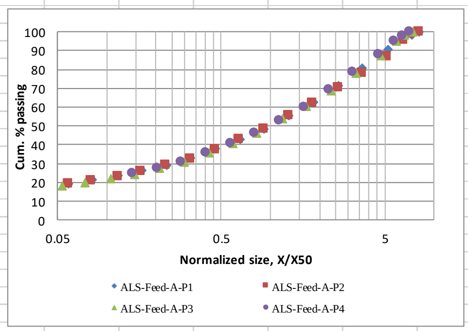

FSD & PSD

Sample		ALS-Feed-B Feed			ALS-Feed-B-P1			ALS-Feed-B-P2			ALS-Feed-B-P3			ALS-Feed-B-P4		
Force																
Moisture		5	%			5.00	%		5.00	%		5.00	%		5.00	%
Force		N/A	kN			1399.72	kN		1099.38	kN		899.66	kN		699.74	kN
Pressure		N/A	MPa			240.96	MPa		189.26	MPa		154.88	MPa		120.46	MPa
Energy		N/A	kWh/t			1.45	kWh/t		1.08	kWh/t		0.94	kWh/t		0.71	kWh/t
Thickness		N/A	mm			25.77	mm		26.01	mm		26.48	mm		28.54	mm
Density		N/A	g/cc			2.67	g/cc		2.66	g/cc		2.61	g/cc		2.44	g/cc
Sieve #	**Size (mm)**	**Weight (g)**	**Cum. % passing**	**Size (mm)**	**Weight (g)**	**Cum. % passing**	**Normalized**	**Weight (g)**	**Cum. % passing**	**Normalized**	**Weight (g)**	**Cum. % passing**	**Normalized**	**Weight (g)**	**Cum. % passing**	**Normalized**
1/2 inch	12.5	0	100.00	12.5	0	100.00	8.692	0	100.00	8.096	0	100.00	7.515	0	100.00	7.308
7/16 inch	11.2	83.6	91.64	11.2	5	98.68	7.788	7.9	97.93	7.254	16.7	95.61	6.734	8.2	97.87	6.548
	10	111.3	80.51	10	9.9	96.06	6.954	6.1	96.32	6.477	13.8	91.97	6.012	15.4	93.86	5.846
	8	162.3	64.28	8	22.3	90.17	5.563	25.2	89.71	5.181	20.1	86.68	4.810	22.6	87.97	4.677
	5.6	121.7	52.11	5.6	38.1	80.11	3.894	38.6	79.57	3.627	32.2	78.21	3.367	39.6	77.66	3.274
	4	78.4	44.27	4	30.9	71.94	2.782	33.4	70.81	2.591	34.5	69.13	2.405	33	69.07	2.339
	2.8	65.8	37.69	2.8	32.2	63.43	1.947	31.6	62.51	1.814	33.5	60.32	1.683	31	61.00	1.637
	2	42.5	33.44	2	25	56.83	1.391	26.9	55.45	1.295	25	53.74	1.202	28.4	53.61	1.169
	1.4	38.2	29.62	1.4	27.6	49.54	0.974	27.3	48.28	0.907	25.3	47.08	0.842	28.7	46.13	0.818
	1	30.9	26.53	1	21.9	43.75	0.695	21.9	42.53	0.648	21.3	41.47	0.601	21.4	40.56	0.585
	0.71	24.6	24.07	0.71	18	39.00	0.494	18.6	37.65	0.460	18.5	36.61	0.427	18.2	35.82	0.415
	0.5	23.5	21.72	0.5	18.7	34.06	0.348	17.4	33.08	0.324	17.1	32.11	0.301	17.3	31.32	0.292
	0.355	18.6	19.86	0.355	13.3	30.54	0.247	12.9	29.69	0.230	12.6	28.79	0.213	12.8	27.99	0.208
	0.25	17.5	18.11	0.25	12.7	27.19	0.174	12	26.54	0.162	11.6	25.74	0.150	12	24.86	0.146
	0.18	12.9	16.82	0.18	10	24.54	0.125	9.5	24.05	0.117	9.2	23.32	0.108	9.5	22.39	0.105
	0.125	13.2	15.50	0.125	8.5	22.30	0.087	7.9	21.97	0.081	7.6	21.32	0.075	8.3	20.23	0.073
	0.09	9.8	14.52	0.09	6.5	20.58	0.063	6.2	20.35	0.058	5.8	19.79	0.054	6.8	18.46	0.053
	0.063	9.2	13.60	0.063	6	19.00	0.044	6	18.77	0.041	5.7	18.29	0.038	6.5	16.77	0.037
	0.045	8.2	12.78	0.045	3	18.20	0.031	3.2	17.93	0.029	2.9	17.53	0.027	3.3	15.91	0.026
	Pan	127.8	0.00	Pan	68.9	0.00		68.3	0.00		66.6	0.00		61.1	0.00	
	Total wt.	1000.00	F50		378.5	P50		380.9	P50		380	p50		384.1	p50	
	Initial wt.		5.17			1.44			1.54			1.66			1.71	
	Delta		F80			P80			P80			p80			p80	
	Delta %		9.94			5.58			5.70			6.11			6.14	
	Reduction Ratio					3.59			3.35			3.11			3.02	
	PP 1 mm		**24.070**													

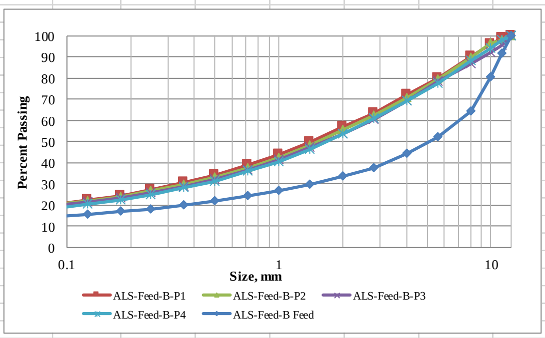

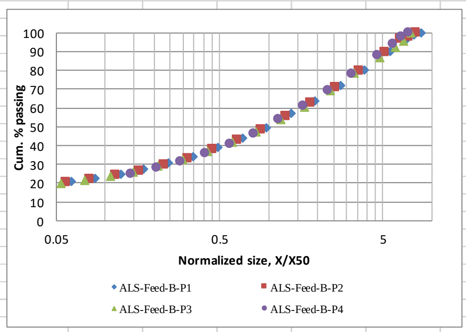

FSD & PSD

Sample		ALS-Feed-C Feed			ALS-Feed-C-P1			ALS-Feed-C-P2			ALS-Feed-C-P3			ALS-Feed-C-P4		
Force																
Moisture		5	%			2.50	%		2.50	%		2.50	%		2.50	%
Force		N/A	kN			1400.10	kN		1099.53	kN		799.91	kN		499.88	kN
Pressure		N/A	MPa			241.03	MPa		189.29	MPa		137.71	MPa		86.06	MPa
Energy		N/A	kWh/t			1.36	kWh/t		1.18	kWh/t		0.80	kWh/t		0.57	kWh/t
Thickness		N/A	mm			28.87	mm		29.13	mm		29.26	mm		29.67	mm
Density		N/A	g/cc			2.59	g/cc		2.62	g/cc		2.55	g/cc		2.52	g/cc
Sieve #	**Size (mm)**	**Weight (g)**	**Cum. % passing**	**Size (mm)**	**Weight (g)**	**Cum. % passing**	**Normalized**	**Weight (g)**	**Cum. % passing**	**Normalized**	**Weight (g)**	**Cum. % passing**	**Normalized**	**Weight (g)**	**Cum. % passing**	**Normalized**
	12.5	0	100.00	12.5	0	100.00	8.934	0	100.00	7.953	0	100.00	7.283	0	100.00	6.299
	11.2	49.6	89.80	11.2	7	98.35	8.005	12.4	97.13	7.126	11.2	97.34	6.526	13.8	96.73	5.644
	10	47.4	80.05	10	14	95.05	7.147	8	95.28	6.363	14.2	93.97	5.827	12.4	93.79	5.039
	8	56.5	68.44	8	23.7	89.46	5.718	28.1	88.79	5.090	23.1	88.49	4.661	29.3	86.85	4.032
	5.6	73.2	53.38	5.6	41.6	79.65	4.002	49.6	77.32	3.563	49.4	76.77	3.263	56.3	73.51	2.822
	4	43.5	44.44	4	33.4	71.78	2.859	33.4	69.60	2.545	38.1	67.73	2.331	35.9	65.00	2.016
	2.8	31.2	38.02	2.8	34.3	63.69	2.001	35.8	61.33	1.782	35.4	59.34	1.631	35.5	56.59	1.411
	2	19.5	34.01	2	25.3	57.72	1.429	24.8	55.59	1.273	24.5	53.52	1.165	27	50.19	1.008
	1.4	23.7	29.14	1.4	32.7	50.01	1.001	33.9	47.76	0.891	31.4	46.07	0.816	30.7	42.91	0.706
	1	15.4	25.97	1	24.5	44.23	0.715	24.1	42.19	0.636	24	40.38	0.583	22.4	37.61	0.504
	0.71	12.6	23.38	0.71	21.3	39.21	0.507	20.9	37.36	0.452	20	35.63	0.414	18.6	33.20	0.358
	0.5	12	20.91	0.5	20.1	34.47	0.357	19.5	32.85	0.318	17.8	31.41	0.291	17.1	29.15	0.252
	0.355	8.9	19.08	0.355	16.5	30.58	0.254	15.9	29.17	0.226	14.1	28.07	0.207	13.7	25.90	0.179
	0.25	7.9	17.46	0.25	14.6	27.14	0.179	14	25.94	0.159	13.2	24.93	0.146	12	23.06	0.126
	0.18	6.3	16.16	0.18	11.8	24.36	0.129	11.5	23.28	0.115	8.1	23.01	0.105	8.6	21.02	0.091
	0.125	5.5	15.03	0.125	9.4	22.14	0.089	9.1	21.17	0.080	8.3	21.04	0.073	7.2	19.31	0.063
	0.09	4.6	14.09	0.09	7.7	20.33	0.064	7.7	19.39	0.057	6.9	19.41	0.052	6.4	17.80	0.045
	0.063	4.2	13.22	0.063	6.9	18.70	0.045	7	17.78	0.040	6.1	17.96	0.037	5.8	16.42	0.032
	0.045	3.6	12.48	0.045	5.5	17.40	0.032	5.6	16.48	0.029	4.7	16.84	0.026	4.7	15.31	0.023
	Pan	60.7	0.00	Pan	73.8	0.00		71.3	0.00		71	0.00		64.6	0.00	
	Total wt.	486.30	F50		424.1	P50		432.6	P50		421.5	p50		422.0	p50	
	Initial wt.		4.99			1.40			1.57			1.72			1.98	
	Delta		F80			P80			P80			p80			p80	
	Delta %		9.99			5.69			6.16			6.26			6.77	
	Reduction Ratio					3.57			3.18			2.91			2.52	
	PP 1 mm		**23.381**													

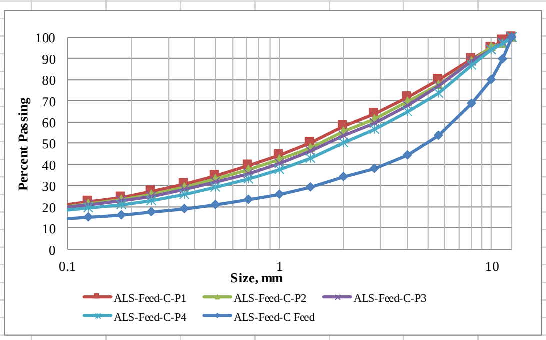

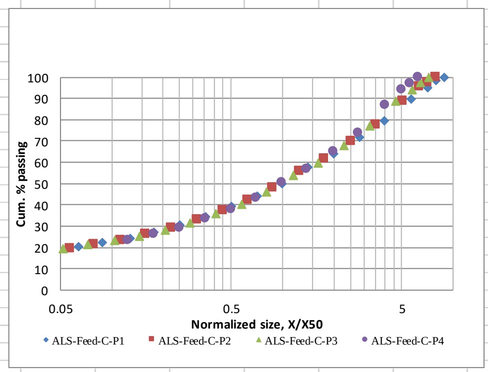

FSD & PSD

Sample		ALS-Comp-A- Feed			ALS-Comp-A-P1			ALS-Comp-A-P2			ALS-Comp-A-P3			ALS-Comp-A-P4		
Force																
Moisture		2.5	%			2.50	%		2.50	%		2.50	%		2.50	%
Force		N/A	kN			1399.61	kN		1099.96	kN		799.74	kN		500.12	kN
Pressure		N/A	MPa			240.95	MPa		189.36	MPa		137.68	MPa		86.10	MPa
Energy		N/A	kWh/t			1.61	kWh/t		1.34	kWh/t		1.04	kWh/t		0.71	kWh/t
Thickness		N/A	mm			28.55	mm		28.92	mm		29.09	mm		29.66	mm
Density		N/A	g/cc			2.59	g/cc		2.57	g/cc		2.50	g/cc		2.48	g/cc
Sieve #	**Size (mm)**	**Weight (g)**	**Cum. % passing**	**Size (mm)**	**Weight (g)**	**Cum. % passing**	**Normalized**	**Weight (g)**	**Cum. % passing**	**Normalized**	**Weight (g)**	**Cum. % passing**	**Normalized**	**Weight (g)**	**Cum. % passing**	**Normalized**
	12.5	0	100.00	12.5	0	100.00	8.075	0	100.00	7.724	0	100.00	6.883	0	100.00	5.919
	11.2	40	91.77	11.2	6.5	98.45	7.235	7.3	98.27	6.921	7.8	98.11	6.167	7.8	98.13	5.303
	10	54.5	80.56	10	11.3	95.76	6.460	9.8	95.94	6.179	14	94.71	5.506	13.8	94.82	4.735
	8	71	65.95	8	23.4	90.20	5.168	24.8	90.05	4.944	28.3	87.85	4.405	27.8	88.16	3.788
	5.6	80.2	49.44	5.6	39.3	80.85	3.618	42.4	79.97	3.460	45.7	76.77	3.083	55.1	74.95	2.652
	4	51.8	38.79	4	35.9	72.31	2.584	35.5	71.54	2.472	36.2	67.99	2.202	41.2	65.08	1.894
	2.8	47.3	29.05	2.8	38.6	63.12	1.809	41.4	61.70	1.730	37.7	58.85	1.542	38.9	55.75	1.326
	2	25.6	23.79	2	27.2	56.65	1.292	28	55.05	1.236	25.5	52.67	1.101	27.9	49.07	0.947
	1.4	25.1	18.62	1.4	37.1	47.82	0.904	33.4	47.11	0.865	35.9	43.96	0.771	35.7	40.51	0.663
	1	13.2	15.91	1	26.8	41.45	0.646	26.2	40.89	0.618	24.7	37.97	0.551	24.1	34.73	0.474
	0.71	9.7	13.91	0.71	23	35.97	0.459	22.6	35.52	0.439	21.4	32.78	0.391	20.3	29.87	0.336
	0.5	8.3	12.20	0.5	21.3	30.91	0.323	20.9	30.55	0.309	19.5	28.06	0.275	18	25.55	0.237
	0.355	5.6	11.05	0.355	17	26.86	0.229	16.7	26.59	0.219	15.4	24.32	0.195	14.1	22.17	0.168
	0.25	4.7	10.08	0.25	14.7	23.36	0.162	14.4	23.16	0.154	13.3	21.10	0.138	12	19.30	0.118
	0.18	3.6	9.34	0.18	12.1	20.49	0.116	11.9	20.34	0.111	10.5	18.55	0.099	9.6	16.99	0.085
	0.125	3.3	8.66	0.125	9	18.34	0.081	9	18.20	0.077	8	16.61	0.069	7.4	15.22	0.059
	0.09	2.8	8.09	0.09	7.4	16.58	0.058	7.2	16.49	0.056	6.4	15.06	0.050	5.9	13.81	0.043
	0.063	2.4	7.59	0.063	6.4	15.06	0.041	6.3	14.99	0.039	5.7	13.68	0.035	5.1	12.58	0.030
	0.045	1.9	7.20	0.045	4.8	13.92	0.029	5	13.80	0.028	4.4	12.61	0.025	4	11.63	0.021
	Pan	35	0.00	Pan	58.5	0.00		58.1	0.00		52	0.00		48.5	0.00	
	Total wt.	486.00	F50		420.3	P50		420.9	P50		412.4	p50		417.2	p50	
	Initial wt.		5.68			1.55			1.62			1.82			2.11	
	Delta		F80			P80			P80			p80			p80	
	Delta %		9.92			5.44			5.61			6.30			6.52	
	Reduction Ratio					3.67			3.51			3.13			2.69	
	PP 1 mm		**13.909**													

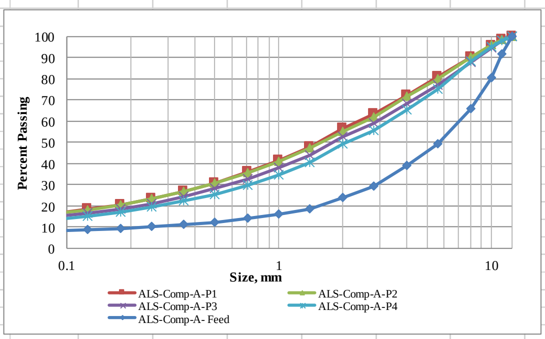

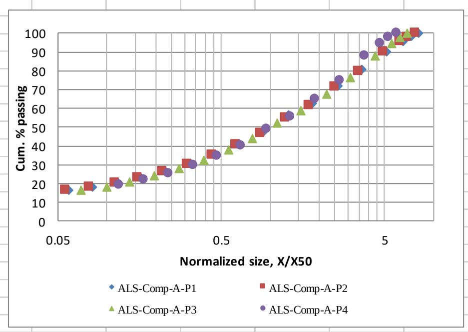

FSD & PSD																
Sample		UBC-Feed-3A-Feed			UBC-Feed-3A-P1			UBC-Feed-3A-P2-B			UBC-Feed-3A-P3			UBC-Feed-3A-P4		
Force																
Moisture		5%	%			2.50	%		2.5	%		2.50	%		2.50	%
Force		N/A	kN			1396.53	kN		1099.07	kN		799.64	kN		499.14	kN
Pressure		N/A	MPa			240.42	MPa		189.18	MPa		137.66	MPa		85.93	MPa
Energy		N/A	kWh/t			1.43	kWh/t		1.24	kWh/t		0.87	kWh/t		0.61	kWh/t
Thickness		N/A	mm			27.68	mm		27.96	mm		28.85	mm		29.47	mm
Density		N/A	g/cc			2.81	g/cc		2.77	g/cc		2.68	g/cc		2.61	g/cc
Sieve #	Size (mm)	Weight (g)	Cum. % passing	Size (mm)	Weight (g)	Cum. % passing	Normalized	Weight (g)	Cum. % passing	Normalized	Weight (g)	Cum. % passing	Normalized	Weight (g)	Cum. % passing	Normalized
1/2 inch	12.5	0.00	100.00	12.5		100.00	9.755		100.00	9.039		100.00	6.828		100.00	6.780
7/16 inch	11.2	108.80	91.54	11.2	2.20	99.48	8.740	6.4	98.48	8.099	12.1	97.16	6.117	7.90	98.15	6.075
3/8 inch	9.5	200.60	75.93	9.5	18.50	95.07	7.414	18.4	94.11	6.870	28.1	90.57	5.189	24.90	92.30	5.153
1/4 inch	6.7	212.00	59.44	6.7	33.50	87.09	5.229	40.6	84.45	4.845	50	78.83	3.660	48.50	80.92	3.634
4 Mesh	4.75	131.80	49.19	4.75	36.90	78.30	3.707	37.9	75.45	3.435	38.7	69.75	2.594	40.70	71.37	2.577
6 Mesh	3.36	90.20	42.17	3.36	35.30	69.89	2.622	32.7	67.67	2.430	29.4	62.85	1.835	34.40	63.30	1.823
8 Mesh	2.36	76.50	36.22	2.36	35.70	61.39	1.842	34.6	59.45	1.707	32.3	55.27	1.289	34.40	55.23	1.280
10 Mesh	1.7	52.60	32.13	1.7	28.40	54.62	1.327	25.6	53.36	1.229	28	48.70	0.929	28.50	48.55	0.922
14 Mesh	1.18	40.10	29.01	1.18	24.10	48.88	0.921	23.2	47.85	0.853	21.6	43.63	0.645	21.60	43.48	0.640
20 Mesh	0.85	43.60	25.62	0.85	26.60	42.54	0.663	26.4	41.57	0.615	23.7	38.07	0.464	24.20	37.80	0.461
28 Mesh	0.6	32.90	23.06	0.6	23.90	36.85	0.468	21.8	36.39	0.434	20.6	33.23	0.328	20.20	33.06	0.325
35 Mesh	0.425	26.00	21.04	0.425	17.80	32.61	0.332	17.5	32.23	0.307	15.3	29.64	0.232	15.10	29.52	0.231
48 Mesh	0.3	25.10	19.09	0.3	16.90	28.59	0.234	15.3	28.60	0.217	14.1	26.33	0.164	13.60	26.33	0.163
65 Mesh	0.212	20.90	17.46	0.212	14.10	25.23	0.165	13.4	25.41	0.153	11.9	23.54	0.116	11.60	23.60	0.115
100 Mesh	0.15	16.00	16.22	0.15	11.20	22.56	0.117	10.2	22.99	0.108	9.3	21.36	0.082	9.00	21.49	0.081
150 Mesh	0.106	14.80	15.07	0.106	9.10	20.39	0.083	8.4	20.99	0.077	7.5	19.60	0.058	7.50	19.73	0.057
	Pan	193.7		Pan	85.60			88.3			83.5			84.10		
	Total wt.	1285.60	F50		419.8	P50		420.7	P50		426.1	p50		426.2	p50	
	Initial wt.		4.90			1.28			1.38			1.83			1.84	
	Delta		F80			P80			P80			p80			p80	
	Delta %		9.94			5.13			5.74			6.98			6.51	
	Reduction Ratio					3.83			3.55			2.68			2.66	
	PP 1 mm		**24.226**													

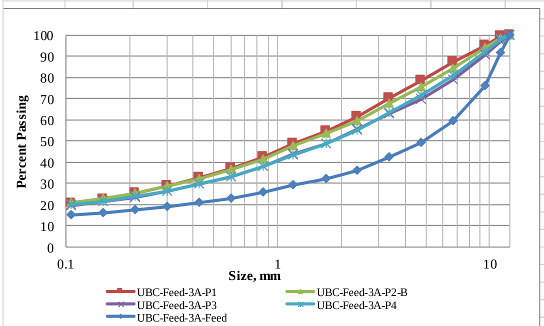

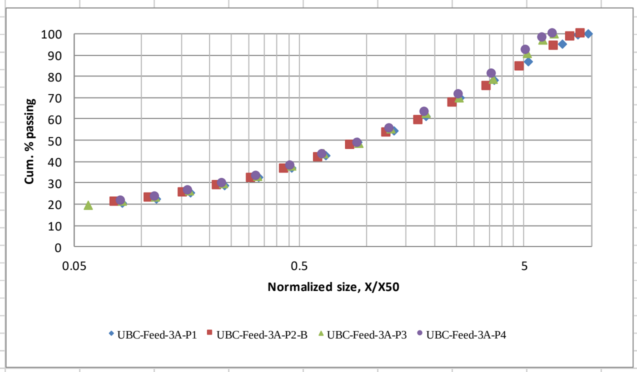

FSD & PSD																
Sample		**UBC-Feed-3B-Feed**			**UBC-Feed-3B-P1**			**UBC-Feed-3B-P2**			**UBC-Feed-3B-P3**			**UBC-Feed-3B-P4**		
Force																
Moisture		5%	%			5.00	%		5	%		5.00	%		5.00	%
Force		N/A	kN			1396.44	kN		1099.07	kN		798.85	kN		499.64	kN
Pressure		N/A	MPa			240.40	MPa		189.21	MPa		137.52	MPa		86.01	MPa
Energy		N/A	kWh/t			1.40	kWh/t		1.14	kWh/t		0.91	kWh/t		0.64	kWh/t
Thickness		N/A	mm			25.14	mm		25.79	mm		25.81	mm		26.59	mm
Density		N/A	g/cc			2.89	g/cc		2.83	g/cc		2.76	g/cc		2.69	g/cc
Sieve #	**Size (mm)**	**Weight (g)**	**Cum. % passing**	**Size (mm)**	**Weight (g)**	**Cum. % passing**	**Normalized**	**Weight (g)**	**Cum. % passing**	**Normalized**	**Weight (g)**	**Cum. % passing**	**Normalized**	**Weight (g)**	**Cum. % passing**	**Normalized**
1/2 inch	12.5	0.00	100.00	12.5		100.00	8.515		100.00	8.547		100.00	7.257		100.00	6.612
7/16 inch	11.2	108.80	91.54	11.2	1.90	99.50	7.629	10.9	97.17	7.658	4.3	98.87	6.502	7.80	97.98	5.925
3/8 inch	9.5	200.60	75.93	9.5	19.00	94.51	6.471	19	92.23	6.496	23.4	92.74	5.515	27.00	90.99	5.025
1/4 inch	6.7	212.00	59.44	6.7	34.50	85.45	4.564	30.7	84.25	4.581	42.2	81.67	3.890	33.40	82.34	3.544
4 Mesh	4.75	131.80	49.19	4.75	34.70	76.34	3.236	36	74.90	3.248	33.1	72.99	2.758	38.80	72.29	2.513
6 Mesh	3.36	90.20	42.17	3.36	33.20	67.62	2.289	30.2	67.05	2.297	31.8	64.65	1.951	34.00	63.49	1.777
8 Mesh	2.36	76.50	36.22	2.36	32.00	59.22	1.608	29.7	59.33	1.614	31.7	56.33	1.370	33.60	54.79	1.248
10 Mesh	1.7	52.60	32.13	1.7	26.00	52.39	1.158	26.4	52.47	1.162	25	49.78	0.987	26.00	48.06	0.899
14 Mesh	1.18	40.10	29.01	1.18	20.40	47.03	0.804	20.8	47.06	0.807	19.9	44.56	0.685	19.40	43.03	0.624
20 Mesh	0.85	43.60	25.62	0.85	23.90	40.76	0.579	23.1	41.06	0.581	21.9	38.81	0.493	21.30	37.52	0.450
28 Mesh	0.6	32.90	23.06	0.6	20.10	35.48	0.409	20.2	35.81	0.410	19.4	33.73	0.348	18.50	32.73	0.317
35 Mesh	0.425	26.00	21.04	0.425	15.10	31.51	0.290	15	31.91	0.291	14	30.06	0.247	13.90	29.13	0.225
48 Mesh	0.3	25.10	19.09	0.3	13.90	27.86	0.204	14	28.27	0.205	13.1	26.62	0.174	12.50	25.89	0.159
65 Mesh	0.212	20.90	17.46	0.212	11.90	24.74	0.144	11.7	25.23	0.145	10.9	23.76	0.123	10.60	23.15	0.112
100 Mesh	0.15	16.00	16.22	0.15	9.20	22.32	0.102	9.2	22.84	0.103	8.4	21.56	0.087	8.30	21.00	0.079
150 Mesh	0.106	14.80	15.07	0.106	7.70	20.30	0.072	7.6	20.87	0.072	7	19.72	0.062	6.80	19.24	0.056
	Pan	193.7		Pan	77.30			80.3			75.2			74.30		
	Total wt.	1285.60	F50		380.8	P50		384.8	P50		381.3	p50		386.2	p50	
	Initial wt.		4.90			1.47			1.46			1.72			1.89	
	Delta		F80			P80			P80			p80			p80	
	Delta %		9.94			5.53			5.81			6.33			6.25	
	Reduction Ratio					3.34			3.35			2.85			2.59	
	PP 1 mm		**24.226**													

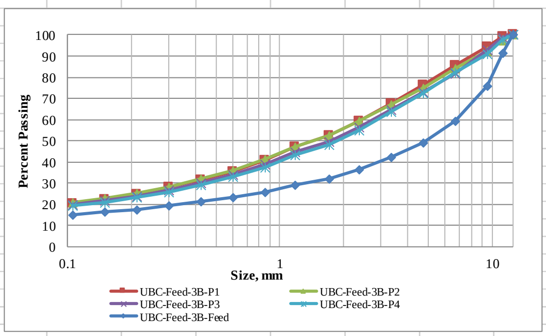

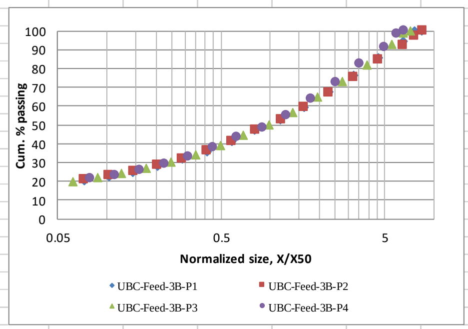

Appendix B Database Calibrated Piston Press Test Parameters

B.1 Database Piston Press Parameters

Database-Calibrated Parameters																		
	Piston Pressure Mpa				Calc Fsp N/mm2				Energy Input, kWh/tonne									
Sample	P1	P2	P3	P4	P1	P2	P3	P4	P1	P2	P3	P4	HPGR Moisture %	pbulk g/cc	F50 Piston, mm	F50 HPGR, mm	Percent Passing (Piston) 1mm, %
UBC-Comp1A1	241	189	138	86	4.64	3.67	2.71	1.74	1.61	1.35	1.04	0.75	2.6	1.96	6.2	8.9	13.5
UBC-Comp1A2	240	189	138	86	4.6	3.7	2.7	1.7	1.75	1.37	1.04	0.77	2.6	1.96	6.2	8.9	13.5
UBC-Comp1A	241	189	138	86	4.6	3.7	2.7	1.7	1.68	1.36	1.04	0.76	2.6	1.96	6.2	8.9	13.5
UBC-Comp1B1	240	189	138	86	4.6	3.7	2.7	1.7	1.70	1.30	1.00	0.71	2.6	1.96	6.6	8.9	12.6
UBC-Comp1B2	240	189	138	86	4.6	3.7	2.7	1.7	1.65	1.40	1.07	0.77	2.6	1.96	6.6	8.9	12.6
UBC-Comp1B	240	189	138	86	4.6	3.7	2.7	1.7	1.68	1.35	1.04	0.74	2.6	1.96	6.6	8.9	12.6
UBC-Comp2A1	241	189	138	86	4.7	3.7	2.7	1.8	1.77	1.42	1.09	0.78	2.6	1.96	6.2	8.9	13.3
UBC-Comp2A2	241	189	138	86	4.7	3.7	2.7	1.8	1.72	1.43	1.07	0.79	2.6	1.96	6.2	8.9	13.3
UBC-Comp2A	241	189	138	86	4.7	3.7	2.7	1.8	1.74	1.42	1.08	0.79	2.6	1.96	6.2	8.9	13.3
UBC-Comp2B1	240	189	138	86	4.6	3.7	2.7	1.7	1.75	1.45	1.07	0.75	2.6	1.96	6.1	8.9	13.9
UBC-Comp2B2	240	189	138	86	4.6	3.7	2.7	1.7	1.82	1.38	1.08	0.75	2.6	1.96	6.1	8.9	13.9
UBC-Comp2B	240	189	138	86	4.6	3.7	2.7	1.7	1.78	1.42	1.08	0.75	2.6	1.96	6.1	8.9	13.9
UBC-Comp3A1	240	189	138	86	4.7	3.7	2.7	1.8	1.81	1.38	1.06	0.80	2.6	1.96	6.3	8.9	13.1
UBC-Comp3A2	240	189	138	86	4.7	3.7	2.7	1.8	1.82	1.48	1.09	0.76	2.6	1.96	6.3	8.9	13.1
UBC-Comp3A	240	189	138	86	4.7	3.7	2.7	1.8	1.82	1.43	1.08	0.78	2.6	1.96	6.3	8.9	13.1
UBC-Comp3B1	240	189	138	86	4.7	3.7	2.7	1.8	1.74	1.38	1.08	0.73	2.6	1.96	6.0	8.9	13.8
UBC-Comp3B2	240	189	138	86	4.7	3.7	2.7	1.8	1.78	1.46	1.09	0.75	2.6	1.96	6.0	8.9	13.8
UBC-Comp3B	240	189	138	86	4.7	3.7	2.7	1.8	1.76	1.42	1.09	0.74	2.6	1.96	6.0	8.9	13.8
ALS-Feed-A	241	189	155	120	4.1	3.1	2.5	1.8	1.77	1.35	1.05	0.80	2.6	1.99	5.2	11.9	24.1
ALS-Feed-B	241	189	155	120	4.1	3.1	2.5	1.8	1.76	1.23	1.02	0.75	2.6	1.99	5.2	11.9	24.1
ALS-Feed-C	241	189	138	86	4.2	3.2	2.3	1.3	1.63	1.29	0.85	0.59	2.6	1.99	5.0	11.9	23.4
ALS-Comp-A	241	189	138	86	4.7	3.8	2.8	1.8	1.80	1.42	1.07	0.72	2.6	1.96	5.7	8.9	13.9
UBC-Feed-03A	240	189	138	86	4.2	3.2	2.3	1.3	1.65	1.35	0.91	0.61	2.6	1.99	4.9	11.9	24.1
UBC-Feed-03B	240	189	138	86	4.2	3.2	2.3	1.3	1.65	1.29	0.96	0.64	2.6	1.99	4.9	11.9	24.2

Appendix C HPGR Test Data

C.1 HPGR Pilot Operating Test Data

Press Constants	Roller Diameter (**D**)	[m]	1.000	HPGR Feed			Feed + (+ 2 mm Recycle)		
	Roller Width (**W**)	[m]	0.250						
Data	**Description**	**Test Number:**		**Feed 1**	**Feed 2**	**Feed 3**	**Comp 1**	**Comp 2**	**Comp 3**
Process Set Point	Specific Pressing Force	F_{SP}	[N/mm^2]	4.00	3.00	2.0	4.0	3.0	2.0
Process Data	**Average Actual Speed:**	ω_{AV}	[m/s]	0.75	0.75	0.75	0.75	0.75	0.75
	Standard Deviation	σ_ω		0.00	0.00	0.00	0.00	0.00	0.00
	Actual Roller gap (average)	X_{gAV}	**[mm]**	20.76	23.42	25.20	22.35	21.98	24.59
	Standard Deviation	σ_X		0.79	0.97	1.06	1.10	1.25	1.16
	Actual Hydraulic Pressure (average)	P_{AV}	**[bar]**	123.51	92.22	60.98	123.70	92.10	60.95
	Standard Deviation			0.49	0.61	0.69	0.82	0.61	0.73
	Actual Pressing Force (average)	F_{AV}	[kN]	993.36	741.66	490.40	994.86	740.71	490.21
	Actual Specific Pressure (average)	F_{SPAV}	**[N/mm^2]**	3.97	2.97	1.96	3.98	2.96	1.96
	Idle Power Draw	Pi	[kW]	4.49	5.25	5.32	5.08	5.16	5.33
	Power Draw	P	[kW]	100.72	91.82	64.67	101.81	76.89	58.94
	Total Specific Energy Consumption	E_{SP}	[kWh/t]	2.40	2.05	1.38	2.43	1.88	1.46
	Net Specific Energy Consumption	$E_{SP\ net}$	**[kWh/t]**	2.29	1.93	1.27	2.31	1.75	1.33
	Average torque floating		**[kNm]**	34.00	34.04	24.21	36.04	27.52	19.17
	Average torque fixed		**[kNm]**	32.86	26.91	18.72	31.54	23.52	19.95
	Press throughput	W	[t/h]	41.98	44.81	46.80	41.83	40.96	40.43
	Specific Throughput Constant	**m dot**	**[ts/hm^3]**	**222.96**	**237.98**	**248.56**	**222.1**	**217.5**	**214.7**

C.2 Pilot HPGR PSD Analysis

University of British Columbia													Edge	10%								
FSD & PSD																						
Sample		**Feed-Feed**			**Feed1**						**Feed2**						**Feed3**					
Force																						
Moisture		0.70	%			0.70	%					0.70	%					0.70	%			
Pressing Force		NA	kN			123.51	kN					92.22	kN					60.98	kN			
Pressure		NA	MPa			3.98	N/mm2					2.96	MPa					1.96	MPa			
Energy		NA	kWh/t			2.29	kWh/t					1.93	kWh/t					1.27	kWh/t			
Gap		NA	mm			2.29	mm					1.93	mm					1.27	mm			
Feed Density (loose)		0.00	g/cc			20.76	g/cc					23.42	g/cc					25.20	g/cc			
Feed Condensed (loose		1.68				NA						NA						NA				
Sieve #	**Size (mm)**	**Weight (g)**	**Cum. % passing**	**Size (mm)**	**Weight - Centre (g)**	**Weight - Edge (g)**	**Cum. % passing-Centre**	**Cum. % passing-Edge**	**Cum. % passing**	**Normalized**	**Weight - Centre (g)**	**Weight - Edge (g)**	**Cum. % passing-Centre**	**Cum. % passing-Edge**	**Cum. % passing**	**Normalized**	**Weight - Centre (g)**	**Weight -Edge (g)**	**Cum. % passing-Centre**	**Cum. % passing-Edge**	**Cum. % passing**	**Normalized**
	31.5	0.00	100.00	31.5	0.00	0.00	100.00	100.00	100.00	21.327	0	0	100.00	100.00	100.00	18.380	0	0	100.00	100.00	100.00	13.330
	26.5	1039.30	90.28	26.5	0.00	0.00	100.00	100.00	100.00	17.942	61.1	45.1	99.42	99.58	99.44	15.463	86.9	52.2	99.17	99.47	99.20	11.214
	19	2122.20	70.44	19	68.50	440.80	99.33	95.84	98.98	12.864	144.2	568.3	98.06	94.34	97.68	11.087	106.7	790.1	98.15	91.50	97.49	8.040
	16	959.00	61.48	16	136.70	683.70	97.99	89.38	97.13	10.833	259.9	660.6	95.59	88.24	94.86	9.336	345.5	771.3	94.85	83.72	93.74	6.771
	11.2	1447.10	47.95	11.2	639.60	1366.40	91.71	76.48	90.18	7.583	788.1	1508.8	88.13	74.31	86.75	6.535	1001	1373	85.28	69.87	83.74	4.739
	8	829.80	40.19	8	603.50	974.50	85.78	67.29	83.93	5.416	647.3	995.2	82.00	65.12	80.31	4.668	797.1	910.1	77.66	60.69	75.97	3.385
	5.6	666.10	33.96	5.6	1017.60	1251.00	75.79	55.47	73.76	3.792	1110.9	1214.1	71.48	53.92	69.72	3.268	1217	1136.4	66.03	49.22	64.35	2.370
	4	407.40	30.15	4	620.90	603.40	69.70	49.78	67.70	2.708	599.6	569	65.80	48.66	64.09	2.334	649	481.1	59.83	44.37	58.29	1.693
	2.8	352.40	26.86	2.8	638.90	533.60	63.42	44.74	61.56	1.896	588.1	512.7	60.23	43.93	58.60	1.634	573.2	437	54.35	39.96	52.91	1.185
	2.00	298.60	24.07	2	598.50	496.50	57.55	40.05	55.80	1.354	584.8	490.6	54.69	39.40	53.16	1.167	572.2	412.7	48.89	35.80	47.58	0.846
	1.4	267.50	21.56	1.4	694.90	543.60	50.73	34.92	49.15	0.948	719.5	537.7	47.88	34.44	46.53	0.817	688.6	465.5	42.31	31.10	41.18	0.592
	1	200.00	19.69	1	555.00	393.50	45.28	31.21	43.87	0.677	538.9	397	42.77	30.77	41.57	0.584	500.7	330	37.52	27.77	36.55	0.423
	0.71	190.00	17.92	0.71	471.90	328.80	40.65	28.10	39.39	0.481	441.8	320.8	38.59	27.81	37.51	0.414	406.7	264.9	33.63	25.10	32.78	0.300
	0.5	163.00	16.39	0.5	482.30	327.60	35.91	25.01	34.82	0.339	451.4	324.5	34.31	24.82	33.36	0.292	407.8	264.5	29.74	22.43	29.01	0.212
	0.355	141.50	15.07	0.355	398.70	268.00	32.00	22.48	31.05	0.240	365.7	260	30.85	22.41	30.01	0.207	322.8	212.1	26.65	20.29	26.02	0.150
	0.25	131.00	13.85	0.25	334.40	222.60	28.71	20.38	27.88	0.169	323.5	224.5	27.79	20.34	27.04	0.146	280.7	187.8	23.97	18.39	23.41	0.106
	0.18	109.50	12.82	0.18	271.60	188.40	26.05	18.60	25.30	0.122	268.4	186.8	25.24	18.62	24.58	0.105	234.2	157.8	21.73	16.80	21.24	0.076
	0.125	106.50	11.83	0.125	240.00	155.90	23.69	17.13	23.04	0.085	219.2	152.6	23.17	17.21	22.57	0.073	189.6	129.7	19.92	15.49	19.48	0.053
	0.09	87.00	11.01	0.09	205.80	136.00	21.67	15.84	21.09	0.061	189.2	132	21.38	15.99	20.84	0.053	162.4	110.3	18.37	14.38	17.97	0.038
	0.063	72.50	10.34	0.063	183.30	118.10	19.87	14.73	19.36	0.043	165	116	19.81	14.92	19.32	0.037	142.8	98.6	17.00	13.39	16.64	0.027
	0.045	52.50	9.84	0.045	156.30	104.60	18.34	13.74	17.88	0.030	142.7	101.5	18.46	13.98	18.01	0.026	124.2	84.7	15.82	12.53	15.49	0.019
	0.038	30.00	9.56	0.038	51.80	38.20	17.83	13.38	17.38	0.026	45.6	32.2	18.03	13.69	17.60	0.022	36.7	26.2	15.47	12.27	15.15	0.016
	Pan	1023.0		Pan	1816.10	1417.50		0.00	0.00		1903.8	1482.5		0.00	0.00		1618.3	1215.9		0.00	0.00	
	Total wt.	10695.90	F50		10186.3	10592.7			P50		10558.7	10832.5			P50		10464.1	9911.9			p50	
	Initial wt.		11.93						1.48						1.71						2.36	
	Delta		F80						P80						P80						p80	
	Delta %		22.61						7.07						7.93						9.66	
	Reduction Ratio								8.08						6.96						5.05	
	PP 1 mm		**17.918**												**53.162**							
			17.918																			

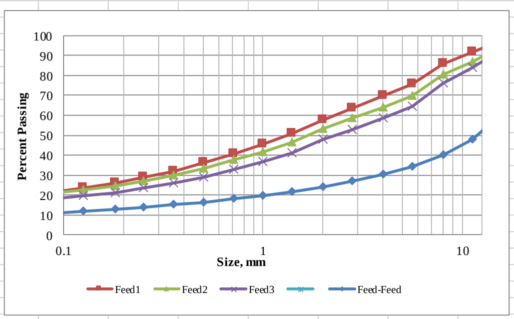

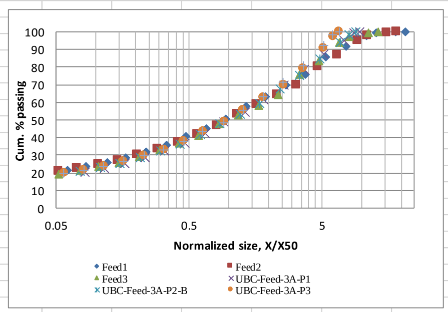

University of British Columbia													Edge	10%								
FSD & PSD																						
Sample	**Comp-Feed**				**Comp1**						**Comp2**						**Comp3**					
Force																						
Moisture		2.50	%			2.50	%					2.50	%					2.50	%			
Force		NA	kN			123.70	kN					92.10	kN					60.95	kN			
Pressure		NA	MPa			3.98	N/mm2					2.96	MPa					1.96	MPa			
Energy		NA	kWh/t			2.31	kWh/t					1.75	kWh/t					1.33	kWh/t			
Thickness		NA	mm			2.31	mm					1.75	mm					1.33	mm			
Feed Density (loose)		NA	g/cc			22.35	g/cc					21.98	g/cc					24.59	g/cc			
Feed Condensed (loose		NA				NA						NA						NA				
Sieve #	**Size (mm)**	**Weight (g)**	**Cum. % passing**	**Size (mm)**	**Weight - Centre (g)**	**Weight - Edge (g)**	**Cum. % passing-Centre**	**Cum. % passing-Edge**	**Cum. % passing**	**Normalized**	**Weight - Centre (g)**	**Weight - Edge (g)**	**Cum. % passing-Centre**	**Cum. % passing-Edge**	**Cum. % passing**	**Normalized**	**Weight - Centre (g)**	**Weight -Edge (g)**	**Cum. % passing-Centre**	**Cum. % passing-Edge**	**Cum. % passing**	**Normalized**
1/2 inch	31.5	0.00	100.00	31.5	0.00	0.00	100.00	100.00	100.00	17.792	0	0	100.00	100.00	100.00	14.847	0	0	100.00	100.00	100.00	13.336
7/16 inch	26.5	1117.30	94.31	26.5	0.00	0.00	100.00	100.00	100.00	14.968	0	0	100.00	100.00	100.00	12.490	0	79.3	100.00	99.25	99.93	11.219
3/8 inch	19	2747.90	80.33	19	40.80	315.70	99.63	96.81	99.34	10.732	97.9	287.2	99.03	97.20	98.85	8.955	106.5	720	99.04	92.46	98.38	8.044
1/4 inch	16	1287.10	73.78	16	107.40	436.00	98.64	92.41	98.02	9.037	135.7	598.9	97.70	91.35	97.06	7.541	344.7	712.7	95.95	85.73	94.93	6.774
4 Mesh	11.2	2956.20	58.74	11.2	704.90	1384.50	92.17	78.44	90.79	6.326	636.6	1335.1	91.42	78.31	90.11	5.279	817.8	1555.4	88.60	71.05	86.85	4.742
6 Mesh	8	2394.00	46.55	8	647.80	939.40	86.22	68.95	84.49	4.519	752	1086	84.00	67.70	82.37	3.771	790	1106.4	81.51	60.61	79.42	3.387
8 Mesh	5.6	2416.00	34.26	5.6	1227.70	1445.80	74.95	54.36	72.89	3.163	1264.7	1547.7	71.52	52.59	69.63	2.639	1359.6	1554.4	69.30	45.93	66.96	2.371
10 Mesh	4	1568.60	26.27	4	734.60	724.30	68.21	47.05	66.09	2.259	671.5	776.6	64.90	45.01	62.91	1.885	761.8	700.3	62.46	39.32	60.14	1.693
14 Mesh	2.8	1522.10	18.53	2.8	700.30	643.70	61.78	40.55	59.65	1.582	721.9	729.5	57.78	37.88	55.79	1.320	723.9	607.9	55.96	33.59	53.72	1.185
	2	1170.80	12.57	2	746.70	609.80	54.92	34.39	52.87	1.130	699.9	627.3	50.87	31.76	48.96	0.943	771.3	592.6	49.03	27.99	46.93	0.847
	1.4	720.10	8.91	1.4	837.60	572.00	47.23	28.62	45.37	0.791	759.6	564.3	43.38	26.24	41.67	0.660	839.5	551.2	41.49	22.79	39.62	0.593
	1	397.40	6.88	1	636.80	401.10	41.39	24.57	39.70	0.565	571.3	384.5	37.75	22.49	36.22	0.471	604.2	356.1	36.06	19.43	34.40	0.423
	0.71	282.00	5.45	0.71	520.20	301.40	36.61	21.53	35.10	0.401	463	286.9	33.18	19.69	31.83	0.335	472.5	264.9	31.82	16.93	30.33	0.301
	0.5	221.30	4.32	0.5	527.40	289.50	31.77	18.60	30.45	0.282	464.7	273	28.59	17.02	27.44	0.236	647.5	247.4	26.01	14.59	24.86	0.212
	0.355	173.60	3.44	0.355	416.70	217.60	27.94	16.41	26.79	0.201	362.5	205.8	25.02	15.01	24.02	0.167	358.3	185	22.79	12.85	21.79	0.150
	0.25	155.20	2.65	0.25	353.90	184.70	24.69	14.54	23.68	0.141	307.2	173.4	21.99	13.32	21.12	0.118	305.1	153.5	20.05	11.40	19.18	0.106
20 Mesh	0.18	125.40	2.01	0.18	311.20	151.10	21.84	13.02	20.95	0.102	260.3	143.1	19.42	11.92	18.67	0.085	253.3	118.8	17.77	10.28	17.02	0.076
28 Mesh	0.125	121.20	1.39	0.125	250.00	122.10	19.54	11.78	18.77	0.071	211.2	113.7	17.34	10.81	16.68	0.059	201.9	89.9	15.96	9.43	15.31	0.053
35 Mesh	0.09	97.80	0.90	0.09	204.00	104.30	17.67	10.73	16.98	0.051	175.7	97.1	15.60	9.86	15.03	0.042	169	74.8	14.44	8.72	13.87	0.038
48 Mesh	0.063	81.90	0.48	0.063	197.10	92.70	15.86	9.80	15.25	0.036	161.5	86.6	14.01	9.02	13.51	0.030	150.2	63.2	13.09	8.13	12.60	0.027
65 Mesh	0.045	60.90	0.17	0.045	161.40	80.70	14.38	8.98	13.84	0.025	138.8	75.8	12.64	8.28	12.20	0.021	129.4	53.4	11.93	7.62	11.50	0.019
100 Mesh	0.038	33.30	0.00	0.038	46.00	29.40	13.96	8.68	13.43	0.021	47.9	27.9	12.17	8.00	11.75	0.018	40.9	14.7	11.56	7.48	11.16	0.016
	Pan			Pan	1520.10	860.20		0.00	0.00		1233.6	819.7		0.00	0.00		1287.7	793		0.00	0.00	
	Total wt.	19650.10	F50		10892.6	9906.0			P50		10137.5	10240.1			P50		11135.1	10594.9			p50	
	Initial wt.		8.91						1.77						2.12						2.36	
	Delta		F80						P80						P80						p80	
	Delta %		18.85						7.07						7.55						8.25	
	Reduction Ratio								5.03						4.20						3.77	
	PP 1 mm		**5.448**																			
	PP 2 mm		**12.570**												**48.962**